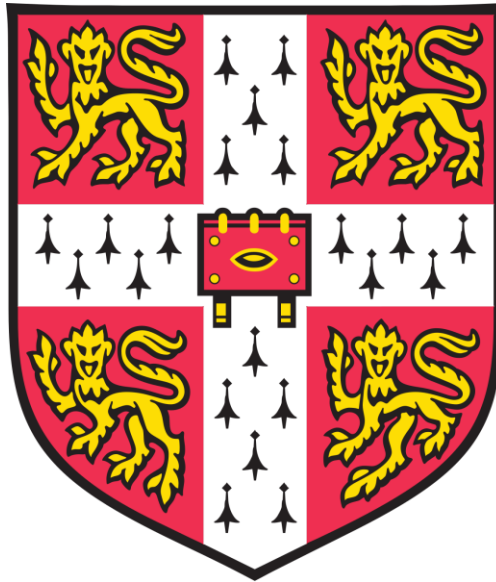


**A KLF6-driven transcriptional network links
lipid homeostasis and tumour growth in
clear cell renal cell carcinoma**



Saiful Effendi Bin Syafruddin

St Edmund's College

University of Cambridge

This dissertation is submitted for the degree of Doctor of Philosophy

January 2019

PREFACE

This dissertation is the result of my own work and includes nothing which is the outcome of work done in collaboration except as declared in the Preface and specified in the text. It is not substantially the same as any that I have submitted, or, is being concurrently submitted for a degree or diploma or other qualification at the University of Cambridge or any other University or similar institution except as declared in the Preface and specified in the text. I further state that no substantial part of my dissertation has already been submitted, or, is being concurrently submitted for any such degree, diploma or other qualification at the University of Cambridge or any other University or similar institution except as declared in the Preface and specified in the text. It does not exceed the prescribed word limit for the relevant Degree Committee.

Saiful Effendi Bin Syafruddin

A KLF6-driven transcriptional network links lipid homeostasis and tumour growth in clear cell renal cell carcinoma

ABSTRACT

Clear cell renal cell carcinoma (ccRCC) is characterised by frequent inactivation of the VHL tumour suppressor gene and consequent accumulation of HIF2A that drives tumourigenesis. The current clinically-approved therapies for ccRCC are those targeting the angiogenesis and mTOR signalling pathways, however, the overall patients' objective response rates are still low, and patients rapidly develop resistance towards the administered therapies. An incomplete understanding of the underlying molecular mechanisms that support ccRCC progression has contributed to the lack of effective diagnostic and/or therapeutic strategies developed, especially for the highly mortal advanced stage ccRCC. Thus, the identification of cellular networks on which ccRCC cells are highly dependent would facilitate the development of better diagnostic and/or therapeutic approaches for ccRCC.

Super enhancers have been reported to drive the expression of critical transcription regulators in various biological contexts including the regulation of cancer phenotypes. Previously generated H3K27ac ChIP-Seq data from several ccRCC cell lines has identified KLF6, a zinc finger DNA-binding transcription factor, to be associated with one of the strongest super enhancers in ccRCC, which could signify a biological relevance to KLF6 in supporting ccRCC pathogenesis. Thus, the purpose of this present study was to interrogate the role of KLF6 in ccRCC, and dissect the KLF6-regulated transcriptional networks and how they can contribute in supporting ccRCC pathogenesis.

It was discovered that *KLF6* expression was supported by a robust super enhancer that integrates signals from multiple pathways, including the ccRCC-initiating VHL-HIF2A pathway. In line with its regulation by the super enhancer, CRISPR-Cas9 and CRISPRi-mediated perturbation of *KLF6* led to impaired ccRCC cells growth *in vitro* and *in vivo* as well as reducing the cells metastatic lung colonisation capability. *KLF6* inhibition led to the deregulation of lipid homeostasis pathways in ccRCC cells. A dual *KLF6* role was identified in modulating lipid homeostasis pathways in ccRCC: First, *KLF6* directly regulates the expression of several important lipid homeostasis genes. Second, *KLF6* promotes *PDGFB* expression, which activates the mTORC1 signalling pathway and the key lipid metabolism transcriptional regulators SREBF1 and SREBF2. *KLF6* and mTORC1 thus co-regulate lipid homeostasis, consequently supporting ccRCC cell growth. Furthermore, findings from this study also reveal a molecular link between the PDGF and mTORC1 signalling pathways, which are the clinically relevant therapeutic targets in ccRCC. In general, the link between super enhancer-driven transcriptional networks and essential metabolic pathways described herein may provide clues to the mechanisms that maintain the stability of cell identity-defining transcriptional programmes in cancer.

*“.....to those who have resiliently fought cancer but lost their fight,
to those who are still battling and suffering from this debilitating disease,
may one day we could put an end to cancer once and for all.....”*

DEDICATION

The works in this thesis are specifically dedicated to my wife and daughter, Fateen Farhana and Maryam Delilah, and my late mother, Upik Yusnita, who are the most important people in my life. There are significant portions of this thesis were written while newly born Maryam was sleeping in my arm. Maryam Delilah, the princess and jewel of our heart, was born on the November 27th 2018, after more than five years of tireless waiting. The night that Maryam was born was an eventful night and I will clearly remember it forever. After Maryam was safely delivered, Fateen had a severe postpartum haemorrhage where she lost half of her blood and I honestly thought that I would lose my wife forever. Thanks to God the Almighty and the incredibly talented teams at the Rosie Hospital for saving her life and thus has allowed me to still be with her until today. Taking care both of Fateen and Maryam while writing this thesis as well as performing additional experiments for the Nature Communication revision and packing stuffs for shipment back to Malaysia were thus far the hardest challenges in my life.

Thinking about it now I am still surprised how I was able to juggle between everything. It is most likely due to my passion in doing science, faith in God, and importantly the fighting spirit and positive attitude of my late mother that have always inspired and driven me forward. My late mother had bravely fought against breast cancer between 2006 and 2011 but she lost the gruelling fight against advanced ovarian cancer that she was diagnosed in 2014, eight months before I started my PhD in Cambridge. I always remember she said that if she ever got treated she would like to come and visit Cambridge. I regret to see that her wish was not being fulfilled. I know that she are always by my side and I will always remember her in my pray and eternally be grateful to her because she has moulded me into what I am today. For my daughter Maryam, I pray that you will grow up well and be a successful person even more than what I have achieved today. Follow your dream and be passionate in what you will be doing. Nothing is impossible and you could go beyond the sky because the sky is unlimited. Only you could set the limit for yourself. I love you so much and you are worth the wait.

ACKNOWLEDGEMENT

All the praise to God the Almighty, the most beneficent and the most merciful, for blessing me with the strength and perseverance to not only complete my PhD study successfully but also fulfil the requirements set by the University of Cambridge and my funding body, Ministry of Higher Education Malaysia and National University of Malaysia.

My deepest gratitude to my PhD supervisor, Dr. Sakari Vanharanta whom I will be indebted forever, for providing his heartfelt support and invaluable teaching and guidance on the research project and also in my career development to be a well-trained researcher in the field of cancer biology. To study and be trained at one of the best universities in the world has always been one of my many dreams. This dream has come true when Sakari was very kind to give me the opportunity to pursue my PhD degree in his newly-established group in January 2015. My sincere appreciation to the Vanharanta lab family, Paulo Rodrigues, Saroor Patel, Nazhif Zaini, Erika Vojtasova, Emma Richardson, Ludo Wesolowski and Jianfeng Ge, for their help in my research. Also for the constant motivation and emotional support to help me get back on my feet whenever I felt down and keep me driven to complete my PhD project successfully. It has been a great pleasure to know each one of these guys and be part of a dynamic and proactive research group. Thank you very much for being my lovely brothers, sisters and little family in Cambridge. I will cherish all of our memories forever.

Without the total understanding and never-ending support and caring from the lovely lady who I married in 2013, Fateen Farhana, completing and publishing this PhD project would not have been possible. She has been very instrumental from the beginning and always by my side to hold my hand and guide me through thick and thin. There would be nothing I could do to repay her big sacrifice when she left everything behind and come to Cambridge with me in the end of 2014. I have to admit that in these past years my focus has drifted towards my PhD study where a lot of times were spent thinking and doing experiments in the laboratory. I know that there are

times that she would feel lonely and neglected. Yet she has never complained or even whispered a thing about it, instead she has continued to give her full and undivided support and encourage me to work harder and strive for excellence. I love her so much and if there is a way, I would like to rewind the time and make up for the lost time with her. I promise that from now on I will give everything to make her happy and be the best husband and companion ever.

Special thanks to my father (Syafuddin), sister (Nor Syafiqah), brother (Ahmad Fuad Afnan) and all of my family members for their continuous support. As the eldest in the family, I am really sorry for not always being around the family in Malaysia. I really appreciate their understanding to let me spend many years in the United States and United Kingdom so that I can pursue my dream to become a cancer researcher. I would also like to extend my sincere gratitude to all MRC Cancer Unit group leaders, MRC Cancer Unit lab management and administration staffs, CIMR flow cytometry core facility staffs, CRUK-CI BRU and University of Cambridge CBS animal facility staffs, Addenbrooke's Hospital Human Research Tissue Bank staffs and people at the University of Cambridge who have either directly or indirectly helped me with my PhD research or any other study/student-related matters.

Also, thank you very much to my previous primary and secondary school teachers, my lecturers at the Rochester Institute of Technology and University of Pennsylvania and all of my friends for making this journey possible and successful. Last but not least, to the Public Service Department Malaysia, Ministry of Higher Education Malaysia and National University of Malaysia, without your generous scholarship and fellowship program, I could only daydream of going overseas and studying at the best universities in the world.

*“It is not the knowledge which should come to you,
It is you who should come to the knowledge”*

MALIK IBN ANAS

*“All humans are dead except those who have knowledge;
and all those who have knowledge are asleep,
except those who do good deeds;
and those who do good deeds are deceived,
except those who are sincere;
and those who are sincere are always in a state of worry”*

MUHAMMAD IBN IDRIS AL-SHAFI'I

TABLE OF CONTENTS

| | |
|---|--------------|
| Preface | ii |
| Abstract | iii |
| Dedication | vi |
| Acknowledgement | vii |
| List of figures | xiv |
| List of tables | xvii |
| List of abbreviations | xviii |
| Chapter 1 Introduction | 1 |
| 1.1 Kidney and urinary system | 2 |
| 1.2 Kidney cancer overview | 4 |
| 1.3 Types of kidney cancer | 4 |
| 1.4 Overview of clear cell renal cell carcinoma | 5 |
| 1.5 The VHL-HIF pathway in cellular adaptation to hypoxic condition | 7 |
| 1.6 The VHL-HIF pathway, gatekeeper in renal tumourigenesis | 10 |
| 1.7 ccRCC genetic heterogeneity and mutational landscape | 12 |
| 1.8 mTOR signalling pathway overview | 13 |
| 1.9 mTORC1 complex upstream activators | 16 |
| 1.10 The cellular function of mTORC1 complex | 18 |
| 1.11 Hyper-activation of mTORC1 signalling pathway in ccRCC | 19 |
| 1.12 Increased mTORC1 activity in ccRCC mouse model | 21 |
| 1.13 ccRCC therapeutic strategies | 24 |
| 1.14 Transcriptional deregulation in cancer | 28 |
| 1.15 Super enhancer and cancer | 32 |
| 1.16 Problem statement and objectives | 36 |
| Chapter 2 Materials & methods | 40 |
| 2.1 Cell lines, plasmids and reagents | 41 |
| 2.2 Genomic DNA and plasmid extraction | 48 |
| 2.3 Sanger sequencing | 48 |
| 2.4 Production of chemically competent E.coli | 48 |
| 2.5 Bacteria transformation | 49 |
| 2.6 Lentiviral production and transduction | 49 |
| 2.7 Generation of stable Cas9 and dCas9-expressing ccRCC cell lines | 50 |
| 2.8 Construction of the pKLV-U6-gRNA(BbsI)-PGKhygro2AmCherry | 50 |
| 2.9 Construction of the pKLV-U6-gRNA(BbsI)-PGKhygro2AeGFP | 52 |

| | |
|---|-----------|
| 2.10 Cloning single sgRNA construct into the sgRNA expression vector | 53 |
| 2.11 Cloning tandem sgRNAs construct into the sgRNA expression Vector | 55 |
| 2.12 Cloning shRNA construct into the shRNA expression vector | 57 |
| 2.13 Expressing exogenous KLF6 | 58 |
| 2.14 TOPO-TA cloning | 61 |
| 2.15 RNA extraction and cDNA synthesis | 61 |
| 2.16 Quantitative real-time PCR (qPCR) | 61 |
| 2.17 RNA-Seq library preparation and analyses | 63 |
| 2.18 Protein extraction and quantification | 63 |
| 2.19 Western blotting | 64 |
| 2.20 Chromatin Immunoprecipitation (ChIP) | 65 |
| 2.21 ChIP-qPCR | 67 |
| 2.22 ChIP-Seq library preparation | 67 |
| 2.23 In vitro competitive proliferation assay | 68 |
| 2.24 Drug treatment proliferation assay | 68 |
| 2.25 Animal studies | 69 |
| 2.26 Histology and immunohistochemistry | 70 |
| 2.27 Total cholesterol quantification | 71 |
| 2.28 Statistical analyses | 71 |
| Chapter 3 Investigating the functional relevance of KLF6 on ccRCC Growth | 73 |
| 3.1 Introduction | 74 |
| 3.2 Results | 79 |
| 3.2.1 ccRCC cell lines identity validation | 79 |
| 3.2.2 KLF6 is expressed in ccRCC cell lines | 81 |
| 3.2.3 High efficiency of CRISPR-Cas9-mediated KLF6 targeting | 82 |
| 3.2.4 Development of competitive proliferation assay | 85 |
| 3.2.5 Competitive proliferation assay (CRISPR-Cas9-mediated KLF6 inhibition) | 87 |
| 3.2.5.1 786-M1A cells | 87 |
| 3.2.5.2 Rescuing the KLF6-targeted 786-M1A cells with exogenous KLF6 | 91 |
| 3.2.5.3 Targeting KLF6 in other ccRCC cell lines | 93 |
| 3.2.6 Competitive proliferation assay (CRISPRi-mediated KLF6 inhibition) | 96 |
| 3.2.6.1 CRISPRi-mediated KLF6 depletion in 786-M1A cells | 96 |
| 3.2.6.2 KLF6 CRISPRi rescue competitive proliferation assay | 101 |
| 3.2.7 Investigating the effect of KLF6 inhibition <i>in vivo</i> | 103 |
| 3.2.7.1 KLF6-targeted 786-M1A tumour formation assay | 103 |
| 3.2.7.2 KLF6-targeted OS-LM1 tumour formation assay | 107 |
| 3.2.7.3 Genetic analysis of the KLF6-targeted 786-M1A tumours | 109 |

| | |
|---|------------|
| 3.2.7.4 <i>KLF6</i> -targeted 786-M1A lung colonisation assay | 110 |
| 3.3 Summary | 113 |
| Chapter 4 Interrogating the role of super enhancer in driving <i>KLF6</i> expression | 114 |
| 4.1 Introduction | 115 |
| 4.2 Results | 116 |
| 4.2.1 CRISPRi-mediated super enhancer inactivation | 116 |
| 4.2.2 Combinatorial enhancers targeting | 120 |
| 4.2.3 CRISPR-Cas9 mediated deletion of the super enhancer region | 124 |
| 4.2.4 HIF2A modulates <i>KLF6</i> expression in ccRCC | 130 |
| 4.2.5 HIF2A acts through the super enhancer to support <i>KLF6</i> expression | 133 |
| 4.3 Summary | 135 |
| Chapter 5 Dissecting the transcriptional network regulated by <i>KLF6</i> that supports ccRCC growth | 137 |
| 5.1 Introduction | 138 |
| 5.2 Results | 138 |
| 5.2.1 Assessing the global effect of <i>KLF6</i> inhibition | 138 |
| 5.2.2 <i>KLF6</i> modulates a part of HIF2A-driven transcriptional Program | 140 |
| 5.2.3 Deregulation of lipid homeostasis pathways in <i>KLF6</i> -targeted cells | 143 |
| 5.2.4 Lipid homeostasis perturbation impairs ccRCC cells growth | 146 |
| 5.2.5 Co-regulation of lipid homeostasis by <i>KLF6</i> and mTORC1 | 149 |
| 5.2.6 Impaired mTORC1 activity in the <i>KLF6</i> -targeted ccRCC cell Lines | 154 |
| 5.2.7 mTORC1 activity supports ccRCC growth <i>in vitro</i> and <i>in vivo</i> | 156 |
| 5.2.8 <i>KLF6</i> modulates mTORC1 activity via transcriptional regulation of <i>PDGFB</i> | 157 |
| 5.2.9 <i>PDGFB</i> activates mTORC1 signalling pathway in ccRCC | 161 |
| 5.3 Summary | 164 |
| Chapter 6 Discussion | 167 |
| 6.1 Introduction | 168 |
| 6.2 <i>KLF6</i> expression regulation by a robust super enhancer | 168 |
| 6.3 Identification of <i>KLF6</i> upstream transcriptional regulators | 170 |
| 6.4 The pro-tumourigenic role of <i>KLF6</i> in ccRCC | 172 |
| 6.5 Dual <i>KLF6</i> roles in modulating lipid homeostasis pathways in ccRCC | 174 |

| | |
|--|------------|
| 6.6 Cholesterol biosynthesis role in supporting cells fitness and survival | 176 |
| 6.7 Cytoplasmic lipid accumulation and ccRCC clear cell phenotype | 178 |
| 6.8 KLF6 and the mTORC1 signalling pathway in ccRCC | 180 |
| 6.9 Targeting KLF6 as a novel ccRCC treatment strategy | 183 |
| 6.10 Summary and model | 184 |
| REFERENCES | 186 |
| APPENDICES | 205 |

LIST OF FIGURES

| Figure | | Page |
|---------------|---|-------------|
| 1 | The human urinary system | 2 |
| 2 | Structure of nephron, the functional unit of the kidneys | 3 |
| 3 | Clear cell histology of the human ccRCC cell line xenograft | 6 |
| 4 | HIF1A, HIF2A and HIF1B protein structure | 8 |
| 5 | VHL complex recognition and proteosomal degradation of HIF1A subunit | 9 |
| 6 | The structure of mTOR protein | 14 |
| 7 | The mTORC1 and mTORC2 protein complex | 15 |
| 8 | The mechanism of growth factor-mediated activation of mTORC1 signalling pathway | 17 |
| 9 | Strategy to construct pKLV-U6-gRNA(BbsI)-PGKhygro2AmCherry sgRNA expression vector. | 52 |
| 10 | Strategy to clone single sgRNA construct into the pKLV-U6-gRNA(BbsI)-PGKhygro2ABFP. | 54 |
| 11 | Strategy to clone single sgRNA construct into the pKLV-U6-gRNA(BbsI)-PGKhygro2AmCherry. | 55 |
| 12 | Strategy to clone tandem sgRNAs construct into the sgRNA expression vector | 57 |
| 13 | Strategy to clone shRNA construct into the sGEP shRNA expression vector. | 58 |
| 14 | Strategy to clone exogenous KLF6 CDS into the expression vector | 60 |
| 15 | Super enhancer profiling in ccRCC | 75 |
| 16 | KLF6 is highly expressed in ccRCC clinical samples | 76 |
| 17 | KLF6 structure and isoforms. | 77 |
| 18 | Validation of the ccRCC cell lines identity | 80 |
| 19 | Characterisation of KLF6 expression in ccRCC cell lines | 81 |
| 20 | CRISPR-Cas9-mediated KLF6 targeting | 82 |
| 21 | High efficiency of the sgKLF6 constructs in targeting KLF6 | 84 |
| 22 | The <i>in vitro</i> competitive proliferation assay | 86 |

| | | |
|----|---|-----|
| 23 | Competitive proliferation assay of the CRISPR-Cas9 KLF6-targeted 786-M1A cells | 89 |
| 24 | Exogenous KLF6 rescue competitive proliferation assay of the CRISPR-Cas9 KLF6-targeted 786-M1A cells | 93 |
| 25 | Competitive proliferation assay of the CRISPR-Cas9 KLF6-targeted OS-LM1, UOK101 and RCC-MF cells | 95 |
| 26 | Regions targeted by the CRISPRi iKLF6 tandem constructs | 97 |
| 27 | High efficiency of the CRISPRi approach in repressing KLF6 expression | 98 |
| 28 | Competitive proliferation assay of the CRISPRi <i>KLF6</i> -depleted 786-M1A cells | 100 |
| 29 | Exogenous KLF6 rescue competitive proliferation assay of the CRISPRi <i>KLF6</i> -depleted 786-M1A cells | 102 |
| 30 | Bioluminescence reads of the CRISPR-Cas9 KLF6-targeted 786-M1A cells <i>in vivo</i> | 105 |
| 31 | Tumours size of the CRISPR-Cas9 KLF6-targeted 786-M1A cells | 106 |
| 32 | Tumour formation assay of the CRISPR-Cas9 KLF6-targeted OS-LM1 cells | 108 |
| 33 | Genetic analysis of the KLF6-targeted 786-M1A tumours | 110 |
| 34 | Lung colonisation assay of the CRISPRi <i>KLF6</i> -depleted 786-M1A cells | 112 |
| 35 | Strategy for the CRISPRi-mediated inactivation of the <i>KLF6</i> -associated super enhancer | 117 |
| 36 | CRISPRi high efficiency in repressing the activity of constituent enhancers | 118 |
| 37 | Strategy for the CRISPRi-mediated inactivation of the <i>KLF6</i> -associated super enhancer | 119 |
| 38 | Combinatorial enhancers targeting | 121 |
| 39 | Simultaneous inactivation of all five enhancer regions | 123 |
| 40 | CRISPR-Ca9-mediated deletion of the large enhancers cluster in the population of 786-M1A and OS-LM1 cells | 125 |
| 41 | Large enhancers cluster deletion in the single cell-derived clones of the Del_SE_3-transduced 786-M1A cells | 128 |
| 42 | The expression level of genes that are located within a 5Mb window flanking the 113kb deletion of the super enhancer region | 129 |
| 43 | Correlation analysis of <i>EPAS1</i> and <i>KLF6</i> expression in ccRCC TCGA cohort | 130 |

| | | |
|----|--|-----|
| 44 | Expression of HIF2A downstream targets in HA-VHL reintroduced cells | 131 |
| 45 | shRNA-mediated <i>EPAS1</i> inhibition | 132 |
| 46 | HIF2A binds the <i>KLF6</i> super enhancer locus | 134 |
| 47 | Volcano plot of the differentially expressed genes in <i>KLF6</i> -targeted versus control 786-M1A CRISPRi cells | 139 |
| 48 | Significant association between <i>KLF6</i> depletion and the hypoxia-response gene signature | 141 |
| 49 | <i>KLF6</i> modulates the expression of <i>BHLHE40</i> | 142 |
| 50 | Deregulation of lipid homeostasis pathway in the <i>KLF6</i> -depleted 786-M1A cells | 144 |
| 51 | Targeting <i>SREBF1</i> and <i>SREBF2</i> reduced ccRCC cells growth | 147 |
| 52 | Chemical inhibition of the lipid homeostasis pathway impaired ccRCC cells growth | 149 |
| 53 | The mTORC1 complex regulates SREBF1 and SREBF2 activity in ccRCC | 151 |
| 54 | Reintroduction of flag- <i>KLF6</i> and flag-eGFP into the <i>KLF6</i> -depleted cells | 152 |
| 55 | Genomic regions bound by the flag- <i>KLF6</i> | 153 |
| 56 | Impaired mTORC1 activity in <i>KLF6</i> -depleted ccRCC cell lines | 155 |
| 57 | mTORC1 complex perturbation impairs ccRCC cells growth <i>in vitro</i> and <i>in vivo</i> | 157 |
| 58 | Downregulation of mTORC1 agonist <i>PDGFB</i> in the <i>KLF6</i> -depleted ccRCC cell lines | 159 |
| 59 | <i>KLF6</i> directly regulates the expression of <i>PDGFB</i> in ccRCC | 160 |
| 60 | <i>PDGFB</i> regulates mTORC1 signalling pathway in ccRCC | 162 |
| 61 | Recombinant <i>PDGFB</i> supplementation re-stimulates mTORC1 activity in the <i>KLF6</i> -depleted cells | 163 |
| 62 | FOXJ3 DNA binding motif at the iSE-2 enhancer region | 171 |
| 63 | <i>KLF6</i> and <i>E2F1</i> expression in <i>KLF6</i> -targeted 786-M1A CRISPRi cells | 173 |
| 64 | Increased <i>KLF6</i> -depleted 786-M1A CRISPRi cells sensitivity towards camptothecin-induced apoptosis | 177 |
| 65 | The model of lipid metabolism modulation by the super enhancer-driven <i>KLF6</i> in supporting ccRCC growth and survival. | 185 |

LIST OF TABLES

| Table | | Page |
|--------------|---|-------------|
| 1 | sgRNAs and shRNAs sequence | 43 |
| 2 | PCR and ChIP-qPCR primers sequence | 45 |
| 3 | Sequencing primers | 47 |
| 4 | TaqMan probes | 62 |
| 5 | Primary and secondary antibodies | 65 |
| 6 | Antibodies used for ChIP experiment | 67 |
| Supp. 1 | PCR conditions for amplifying the tandem oligonucleotides | 205 |
| Supp. 2 | PCR conditions for amplifying the shRNA oligonucleotides | 205 |
| Supp. 3 | PCR conditions for amplifying the <i>KLF6</i> coding sequence | 205 |
| Supp. 4 | PCR conditions for generating flag-tagged KLF6 | 206 |
| Supp. 5 | PCR conditions for generating flag-tagged eGFP | 206 |
| Supp. 6 | PCR conditions for TOPO-TA cloning | 206 |
| Supp. 7 | Recipe for SDS-PAGE resolving gel | 207 |
| Supp. 8 | Recipe for SDS-PAGE stacking gel | 207 |
| Supp. 9 | Recipe for resolving gel buffer | 207 |
| Supp. 10 | Recipe for stacking gel buffer | 208 |
| Supp. 11 | Recipe for 10x running buffer | 208 |
| Supp. 12 | Recipe for 10x transfer buffer | 208 |

LIST OF ABBREVIATIONS

| | |
|----------------|---|
| 4E-BP1 | Eukaryotic translation initiation factor 4E-binding protein 1 |
| ADP | Adenosine diphosphate |
| AMPK | AMP-activated protein kinase |
| ATP | Adenosine triphosphate |
| BAP1 | BRCA1-associated protein 1 |
| BCL3 | B-cell lymphoma-encoded protein |
| BCL-xL | B-cell lymphoma-extra large |
| BFP | Blue fluorescent protein |
| bHLH | basic helix-loop-helix |
| BHLHE40 | basic helix-loop-helix family member e40 |
| BNIP3 | BCL2/adenovirus E1B 19 kDA protein-interacting 3 |
| BRD4 | Bromodomain-containing protein 4 |
| CAIX | Carbonic anhydrase 9 |
| CAS9 | CRISPR-associated protein 9 |
| ccRCC | Clear cell renal cell carcinoma |
| CCND1 | Cyclin D1 |
| CCND2 | Cyclin D2 |
| CDH16 | Cadherin-16 |
| CDK7 | Cyclin-dependent kinase 7 |
| CDS | Coding sequence |
| ChIP | Cyclin-dependent kinase 7 |
| CRISPR | Clustered regularly interspaced short palindromic repeats |
| C-TAD | C-terminal transactivation domain |
| CTCF | CCCTC-binding factor |
| CXCR4 | C-X-C chemokine receptor type 4 |
| DEPTOR | DEP domain-containing mTOR-interacting protein |
| DMEM | Dulbecco's modified eagle's media |
| DMSO | Dimethyl sulfoxide |
| DNMT | DNA methyltransferases |

| | |
|----------------|---|
| E2F1 | E2F transcription factor 1 |
| eGFP | Enhanced green fluorescent protein |
| EPAS1 | Endothelial PAS domain-containing protein 1 |
| EPO | Erythropoietin |
| EWS | Ewing sarcoma |
| FACS | Fluorescence-activated cell sorting |
| FBS | Fetal bovine serum |
| FIMO | Finding individual motif occurrences |
| FLI1 | Friend leukaemia integration transcription factor |
| FOXO1 | Forkhead box protein O1 |
| GAP | GTPase-activating protein |
| GATA3 | GATA-binding protein 3 |
| GBM | Glioblastoma multiforme |
| GLUT | Glucose transporter |
| GSEA | Gene set enrichment analysis |
| H3K27AC | Histone 3 lysine 27 acetylation |
| HAT | Histone acetyltransferase |
| HDAC | Histone deacetylase |
| HDM | Histone demethylase |
| HIFA | Hypoxia inducible factor alpha subunit |
| HIFB | Hypoxia inducible factor beta subunit |
| HMG-CoA | Hydroxy-3-methyl-glutaryl-coenzyme A reductase |
| HMT | Histone methyltransferases |
| HRE | Hypoxia response element |
| IGF-1 | Insulin-like growth factor 1 |
| IFN-A | Interferon alpha |
| IL-2 | Interleukin 2 |
| INDELS | Insertions and/or deletions |
| KLF | Kruppel-like factors |
| LHDA | Lactate dehydrogenase A |
| LSS | Lanosterol synthase |

| | |
|------------------------|--|
| MEME | Multiple EM for motif elicitation |
| mLST8 | Mammalian lethal with SEC13 protein 18 |
| MM | Multiple myeloma |
| mTOR | Mechanistic target of rapamycin |
| mTORC | Mechanistic target of rapamycin complex |
| NHEJ | Non-homologous end joining |
| N-TAD | N-terminal transactivation domain |
| ODD | Oxygen dependent domain |
| PAX3 | Paired box gene 3 |
| PAX8 | Paired box gene 8 |
| PBRM1 | Protein polybromo-1 (BRG1-associated factor 180) |
| PBS | Phosphate-buffered saline |
| PCR | Polymerase chain reaction |
| PD-1 | Programmed cell death protein 1 |
| PDGFB | Platelet-derived growth factor beta subunit |
| PDGFR | Platelet-derived growth factor receptor |
| PKD1 | Phosphoinositide-dependent kinase 1 |
| PD-L1 | Programmed death-ligand 1 |
| PDPK1 | 3-phosphoinositide-dependent protein kinase 1 |
| PEPCK | Phosphoenolpyruvate carboxykinase |
| PHD | Prolyl hydroxylase |
| PI3K | Phosphoinositide 3-kinase |
| PIP₂ | Phosphatidylinositol 4,5-biphosphate |
| PIP₃ | Phosphatidylinositol 3,4,5-triphosphate |
| PLIN2 | Perilipin 2 |
| PTEN | Phosphatase and tensin homolog |
| PPARG | Peroxisome proliferator-activated receptor gamma subunit |
| PRDM1 | PR domain zinc finger protein 1 |
| RAPTOR | Regulatory-associated protein of mTOR |
| RBX1 | RING-box protein 1 |
| RCC | Renal cell carcinoma |

| | |
|----------------|--|
| RICTOR | Rapamycin-insensitive companion of mTOR |
| RHEB | RAS homolog enriched in brain |
| RPMI | Roswell Park Memorial Institute |
| RTK | Receptor tyrosine kinase |
| RUNX1 | Runt-related transcription factor 1 |
| SCD | Stearoyl-CoA Desaturase |
| SCLC | Small cell lung cancer |
| SEM | Standard error of mean |
| SETD2 | SET domain containing 2 |
| sgRNA | Single guide RNA |
| shRNA | Short hairpin RNA |
| SNP | Single nucleotide polymorphism |
| SREBF | Sterol regulatory element-binding protein 1 |
| STR | Short tandem repeat |
| SWI/SNF | SWItch/sucrose non-fermentable |
| TAL1 | T-cell acute lymphocytic leukaemia protein 1 |
| T-ALL | T-cell acute lymphoblastic leukaemia |
| TBP | TATA-binding protein |
| TCGA | The Cancer Genome Atlas |
| TET | Ten-eleven translocation |
| TF | Transcription factor |
| TIAM2 | T-cell lymphoma invasion and metastasis 2 |
| TP53 | Tumour protein p53 |
| TSC | Tuberous sclerosis |
| VEGFA | Vascular endothelial growth factor alpha subunit |
| VEGFR | Vascular endothelial growth factor receptor |
| VHL | von-Hippel-Lindau |
| XBPI | X-box binding protein 1 |

Chapter 1

Introduction

1.1 Kidney and urinary system

Kidneys are part of the urinary system which is also comprised of ureter, bladder, prostate (in man) and urethra (Figure 1)¹. The urinary system main function is to filter and excrete excess water and metabolic waste from the body. These excessive products are filtered out from the blood in kidneys and eliminated from the body in the form of urine. The urine is transported from kidneys to bladder for storage and excreted from the body via ureter and urethra, respectively^{1,2}. In addition to filtration and excretion functions, kidneys also play a role as a hormone secretion organ. Kidneys secrete hormones such as erythropoietin to stimulate the production of red blood cells in the bone marrow and calcitriol, an activated form of Vitamin D, which increases the calcium uptake in the intestine². Renin, another hormone secreted by kidneys, involves in maintaining the blood pressure via renin-angiotensin-aldosterone axis². Thus, the urinary system function is vital to maintain the body homeostasis by regulating the water and electrolytes balance, blood pH and pressure as well as removing waste products from the body. Impaired in kidney functions due to injury or diseases such as cancer may pose serious health problems and could be fatal.

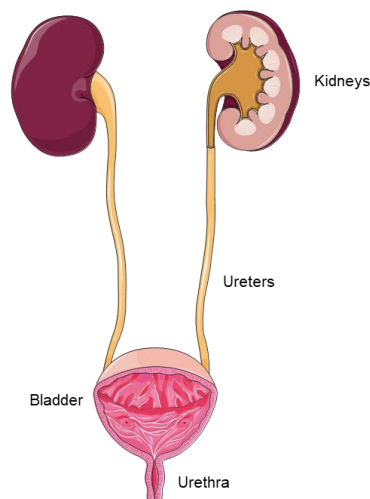


Figure 1: The human urinary system. Source: <https://smart.servier.com>

Blood filtration and reabsorption of necessary metabolites and waters take place in the nephron which is the kidneys “functional unit”³. There are approximately one million nephrons in each of human kidney, looping between the renal cortex and renal medulla. The nephron consists of two components, (1) the renal corpuscle that comprised of glomerulus and Bowman’s capsule, and (2) the renal tubules. The components of renal tubules are proximal convoluted tubule, loop of Henle, distal convoluted tubule and collecting duct³. The blood filtration takes place in the renal corpuscle. The filtrate that passes into the Bowman’s capsule from the glomerulus will travel through the renal tubules. The reabsorption of essential metabolites as well as water occurs along the renal tubules before the final filtered waste is emptied into the collecting duct and subsequently transported to bladder³. The structure of nephron is depicted in figure 2.

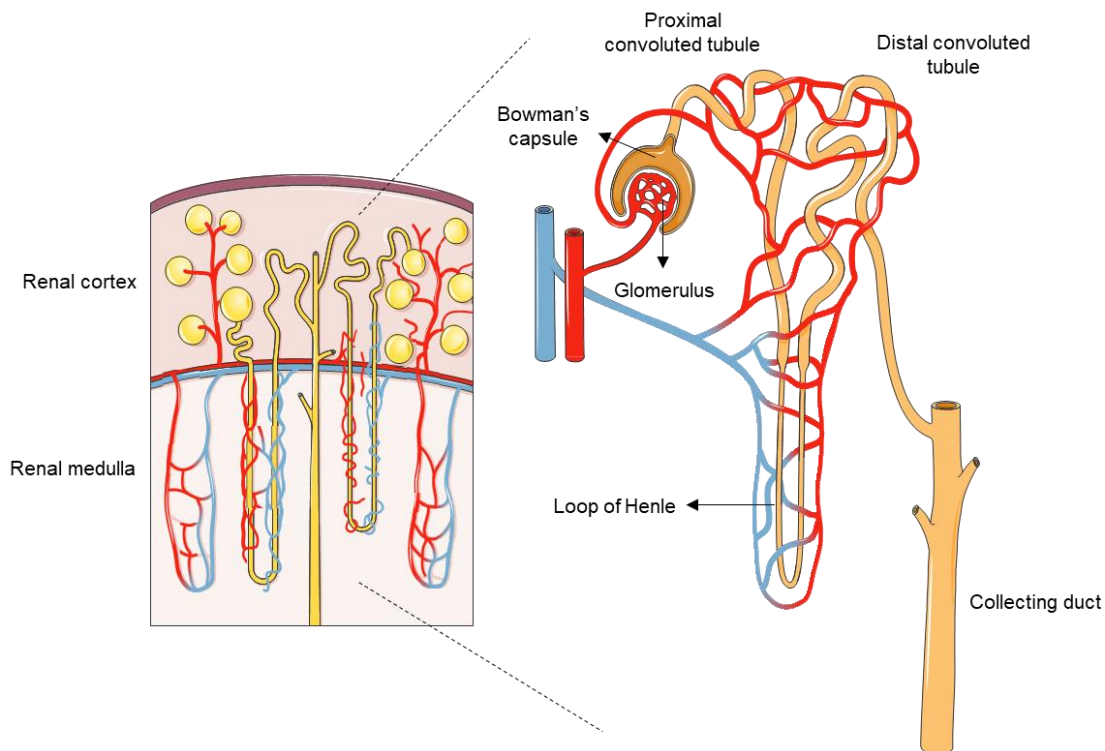


Figure 2: Structure of nephron, the functional unit of the kidneys. Source: <https://smart.servier.com>

1.2 Kidney cancer overview

Like any other major organs in human, cancer can arise in the kidney due to uncontrolled cells growth, which is largely caused by genetic and epigenetic alterations that occur inside the kidney cells. There is approximately 400,000 new kidney cancer cases and 144,000 deaths from kidney cancer reported annually worldwide⁴, making kidney cancer as the 12th most common cancer in the world⁵. As the seventh most prevalent cancer in the United Kingdom, there were about 12,500 new kidney cancer incidences and ~4,400 kidney cancer-related deaths recorded in the UK in 2015⁶. The American Cancer Society has recently estimated that there will be 63,000 new kidney cancer cases and projected 15,000 deaths from kidney cancer in the United States⁷. This figure is expected to steadily rise in the coming years due to lack of effective treatments especially against the advanced stage kidney cancer^{6,7}. Kidney cancer patients are usually diagnosed after the primary tumour has metastasised to the secondary sites where at this stage, the tumour is highly aggressive and normally irresponsive towards conventional chemo- and radiotherapies⁸. If the disease is detected at the early stage, the primary tumour can be removed, thus preventing it from spreading to the distant sites⁸. However, surgical resection might reduce the renal function which could possibly lead to chronic renal diseases as well as affecting the body biological processes and homeostasis.

1.3 Types of kidney cancer

Kidney cancer can be classified into two types; the renal cell carcinoma and transitional cell carcinoma. Renal cell carcinoma (RCC) originates from the cells that form the lining of the renal tubules. It is the most common type of kidney cancer that accounts for approximately 90% of all kidney cancer diagnosed worldwide. Transitional cell carcinoma on the other hand, arises in the renal pelvis and makes up about 5-10% of all kidney cancer cases⁹. RCC can be further

classified into several subtypes based on the histological appearance and genetic alterations that are associated with that specific subtypes¹⁰. The most prevalent RCC subtype is the clear cell or commonly known as the clear cell renal cell carcinoma which accounts for ~75% of all kidney cancer incidences. Other RCC subtypes are papillary renal cell carcinoma and chromophobe renal cell carcinoma in which each accounts for about 10% and 5% of all kidney cancer cases, respectively¹¹. In addition to these existing subtypes, there are emergence of novel, pathologically-distinct RCC subtypes such as the hereditary leiomyomatosis and renal cell carcinoma syndrome-associated RCC and succinate dehydrogenase-deficient renal cell carcinoma⁹. This present study focuses on clear cell renal cell carcinoma, the predominant type of kidney cancer that contributes to the most kidney cancer-related deaths.

1.4 Overview of clear cell renal cell carcinoma

As previously described, 75% of all kidney cancer incidences are of the clear cell subtype. The clear cell renal cell carcinoma (hereinafter referred to as ccRCC) originates in the proximal convoluted tubule lining of the renal cortex⁸. The term “clear cell” arises from the ccRCC distinctive clear, glass-like cytoplasm, which is due to the accumulation of cytoplasmic lipids and glycogen^{12,13}. Figure 3 shows the example of clear cell histology of the human ccRCC cell line xenograft. Alterations in the lipid and glucose metabolism have been observed in ccRCC whereby this metabolic rewiring plays a crucial role in supporting ccRCC pathogenesis¹⁴⁻¹⁶. This metabolic rewiring may contribute to the accumulation of cytoplasmic lipid and glycogen and consequent formation of the clear cell phenotype. Nonetheless, it still remains less understood on the molecular mechanism underpinning the cytoplasmic lipid accumulation in ccRCC. In addition, ccRCC is highly vascularized due to the upregulation of pro-angiogenic factors such as VEGFA and PDGFB in this tumour type⁸.

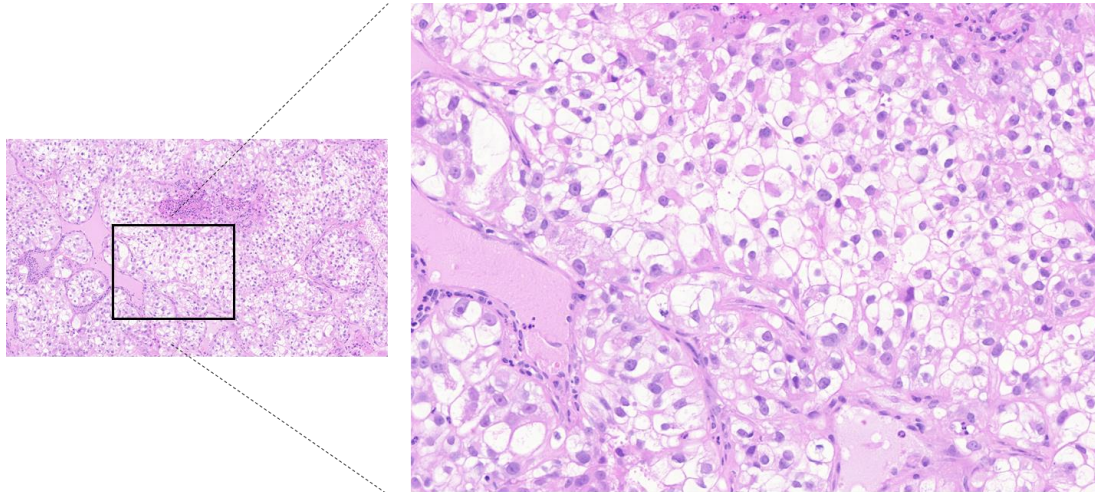


Figure 3: Clear cell histology of the human ccRCC cell line xenograft.

ccRCC is well-characterised by the bi-allelic inactivation of the *von-Hippel-Lindau* (*VHL*) tumour suppressor gene. *VHL* inactivation, either due to somatic alterations or epigenetic silencing, is the hallmark gatekeeper event in ccRCC pathogenesis, contributing to approximately 90% of sporadic ccRCC cases^{17,18}. On top of this, inactivation of *VHL* is also implicated in the von-Hippel-Lindau syndrome, a familial form of ccRCC¹⁹. Recent multi-region sequencing efforts revealed intratumoural heterogeneities in ccRCC in which the ubiquitous *VHL* mutations are predicted to be the truncal event in ccRCC pathogenesis^{17,20,21}. The widespread genetic heterogeneities in ccRCC has been the stumbling block in the development of efficient therapeutic strategy for ccRCC. Also, incomplete understanding on the underlying molecular mechanisms that support ccRCC pathogenesis especially the advanced-stage ccRCC contributes to the lack of effective treatments developed for ccRCC. Advanced-stage ccRCC is highly metastatic, predominantly to the lung and bones, and associated with high mortality due to the tumour irresponsiveness towards conventional therapies. This poses a major problem because

significant fraction of ccRCC patients already manifest the metastatic disease at the time of diagnosis due to lack of early symptoms.

1.5 The VHL-HIF pathway in cellular adaptation to hypoxic condition

VHL gene is located on the short arm of chromosome 3 (3p25) and comprises of 3 exons. This gene encodes for pVHL, which along with elongin B, elongin C, cullin-2 and RBX1, forms the ubiquitin-mediated proteosomal degradation complex²². This complex functions as an E3 ubiquitin ligase (hereinafter referred to as VHL complex) that tags its targeted protein for proteosomal degradation. The hypoxia-inducible factor alpha subunit (HIF α) is the well-characterised target of this VHL complex¹⁹. To date, there are three HIF α isoforms identified, HIF1A, HIF2A and HIF3A²³. Out of these three, the HIF1A and HIF2A are the well-studied isoforms. Both HIF1A and HIF2A have a similar structure that comprised of (1) N-terminus bHLH domain that mediates the DNA binding, (2) protein-protein interaction PAS (Per-ARNT-Sim) domain (3) oxygen-dependent degradation domain (ODD) and (4) C-terminus transactivation domain (N-TAD and C-TAD)^{24,25}. In addition to these HIF α subunits, there is also the presence of one beta subunit (HIF1 β). The HIF1 β subunit has the bHLH and the dimerization PAS domains but lack the ODD and NTAD²⁵. The HIF1A, HIF2A and HIF1 β protein structures are illustrated in figure 4.

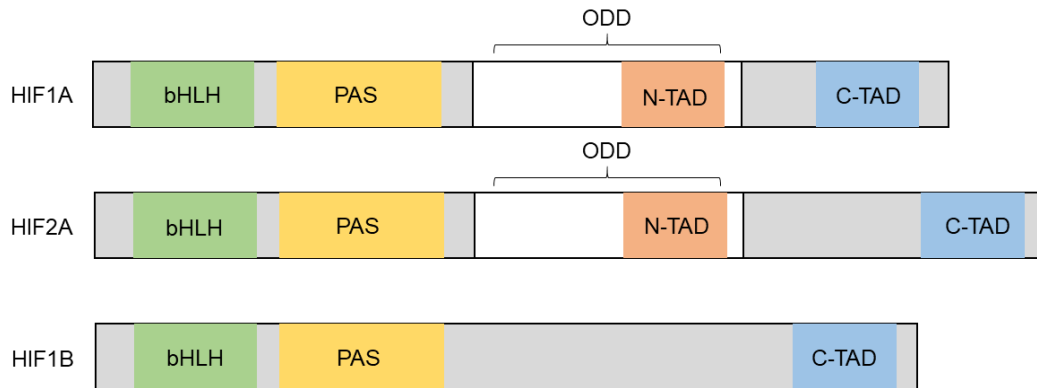


Figure 4: HIF1A, HIF2A and HIF1B protein structure. Adopted from Chen *et al.*²⁵

The HIF1A forms a heterodimer with HIF1B to drive the transcriptional programmes that facilitate cellular adaptation and survival under the hypoxic condition^{23,26,27}. The dimerization of these two subunits to form functionally active HIF transcription factor only occurs under the hypoxic condition due to HIF1A instability and is proteasomal-degraded in the normal oxygen level²⁸. The HIF1B on the other hand is constitutively expressed regardless the oxygen level. Hence, the hypoxia-responsive transcriptional programmes is driven and highly dependent on HIF1A availability, thus making this subunit the indispensable component of HIF transcription factor complex. Under the normoxic condition where the HIF-driven transcriptional programmes are not necessary, the proline residues within the HIF1A oxygen-dependent degradation domain are hydroxylated by the prolyl hydroxylases. This reaction only occurs in the normal oxygen level because the conversion of proline to hydroxyl-proline requires oxygen molecule^{29,30}. The VHL complex will then recognise the prolyl-hydroxylated HIF1A and subsequently ubiquitin-tagged it for proteasomal degradation. The VHL complex recognition and proteasomal degradation of the prolyl-hydroxylated HIF1A under the normoxic condition is illustrated in figure 5.

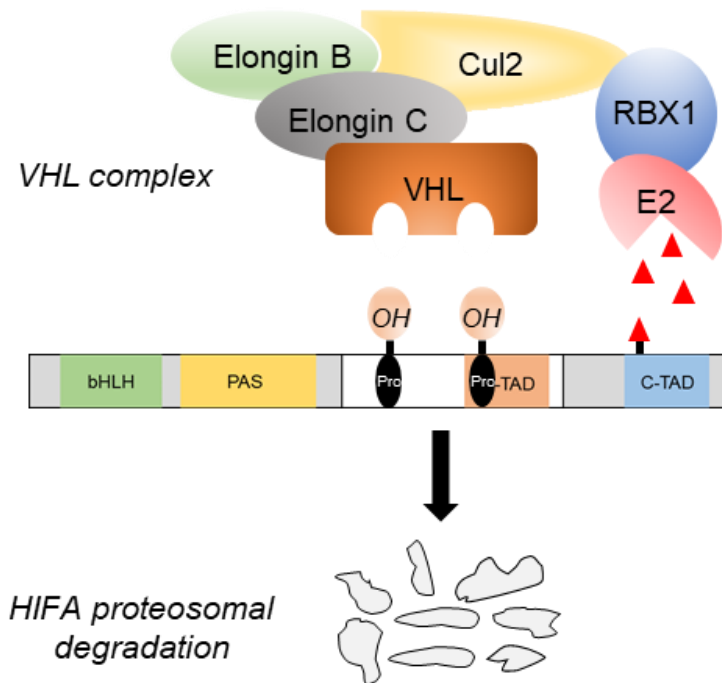


Figure 5: VHL complex recognition and proteosomal degradation of HIF1A subunit. Adopted from Chen *et al*²⁵

The heterodimer HIF1A/B transcription factor (hereinafter referred to as HIF1A) recognises the hypoxia-responsive element (5'–[A/G] CGTG–3') located within the regulatory region of its downstream targets³¹. Several well-characterised HIF1A downstream targets are the pro-angiogenic factors such as *vascular endothelial growth factor alpha (VEGFA)*, enzymes involved in glucose metabolism reprogramming such as *glucose transporter 1 (GLUT1)*, *lactate dehydrogenase A (LDHA)* and *pyruvate dehydrogenase kinase 1 (PDK1)* as well as *erythropoietin (EPO)* that play roles in regulating red blood cells production³². The expression of these hypoxia-associated genes facilitates the cellular adaptation and increase survival in the low oxygen environment. For example, the increase formation of new blood vessels and red blood cells will increase the supply of oxygen as well as nutrients to the hypoxic cells. The glucose

metabolism reprogramming will lead to efficient utilisation of oxygen by shifting the energy production from the high oxygen-dependence oxidative phosphorylation towards glycolysis.

1.6 The VHL-HIF pathway, gatekeeper in renal tumorigenesis

VHL is a classic two-hit tumour suppressor gene³³ that conforms to the Knudson hypothesis on cancer formation³⁴. In the sporadic ccRCC cases, bi-allelic inactivation of *VHL* normally occurs through acquisition of somatic mutations in one of the allele followed by deletion or loss of heterozygosity of the other wild-type allele^{17,35,36}. Hyper-methylation of the *VHL* promoter region, which silences the *VHL* expression, has also been reported in ccRCC patients^{35,37}. Patients with the von-Hippel-Lindau syndrome could also develop ccRCC. This is the hereditary form of ccRCC in which the affected individuals inherit one mutated *VHL* allele from either father or mother and usually followed by deletion/loss of heterozygosity in the other wild-type allele later in their life¹⁹. Other than ccRCC, patients with VHL syndrome could also develop hemangioblastoma which is a type of tumour that forms in the blood vessels of retinal and central nervous system.

The bi-allelic VHL inactivation in ccRCC leads to continuous HIF1A accumulation that will in turn aberrantly activate the hypoxic-response transcriptional programmes even in the normal oxygen level. The upregulation of these transcriptional programmes in this context could promote the formation of tumour. In fact, several of HIF1A downstream targets are known to be pro-tumourigenic^{32,38}. The angiogenic regulator *VEGFA* for instance has been implicated in the tumourigenesis of many cancer types³⁹. Upregulation of glycolytic enzymes and the glucose metabolism reprogramming from the oxygen dependent-oxidative phosphorylation to aerobic glycolysis (known as the Warburg effect) are essential to support the tumour cells rapid

proliferation⁴⁰. Despite the inefficient ATP production, intermediates of this aerobic glycolysis are utilised for the biosynthesis of macromolecules such as lipid, amino acid and nucleotide that are required for cells growth and expansion⁴⁰. Other well-studied HIFA downstream targets that involve in promoting tumourigenesis are *cyclin D1 (CCND1)*⁴¹ and *C-X-C chemokine receptor type 4 (CXCR4)*⁴². The CCND1 activates cyclin-dependent kinase 4/6 to promote cell cycle progression through the G1 phase and G1/S phase transition. The chemokine receptor CXCR4 is one of many factors that mediate the metastatic process.

As discussed in the previous section, dimerization of either HIF1A or HIF2A with the constitutively expressed HIF1B activates the HIFA downstream targets. However, there are set of genes that are exclusively regulated by each of this HIFA subunit⁴³. Several evidences have shown that HIF2A functions as an oncogene in ccRCC whereas the HIF1A may have the opposite growth suppressive function⁴⁴⁻⁴⁶. For instance, HIF2A regulates the expression of pro-tumourigenic genes such as *C-MYC*⁴⁶, *VEGFA* and *CCND1*⁴³ whereas HIF1A antagonises *C-MYC* expression⁴⁷ as well as positively regulating the expression of the pro-apoptotic *BNIP3*⁴³. The VHL-deficient ccRCC cell lines as well as the ccRCC clinical samples either co-expressed HIF1A and HIF2A or solely the HIF2A^{28,48}. shRNA-mediated HIF2A knockdown suppresses ccRCC tumour growth *in vivo*⁴⁹. The reintroduction of VHL-resistant exogenous HIF2A (mutated VHL-binding site) into the VHL-restored ccRCC cells was able to promote tumour growth *in vivo*⁴⁹, whereby the re-expression of VHL-resistant exogenous HIF1A was not sufficient to promote tumourigenesis⁵⁰. In fact, a recent study showed that wild-type HIF1A suppressed ccRCC growth⁴⁵. Due to HIF2A pro-tumourigenic role in ccRCC, several small molecule inhibitors targeting HIF2A have been developed and tested in ccRCC patients which will be discussed in details in section 1.13.

1.7 ccRCC genetic heterogeneity and mutational landscapes

Comprehensive ccRCC molecular analyses were performed via large scale, high-throughput sequencing efforts with the aim to identify the relevance and critical drivers of ccRCC pathogenesis. A better understanding on the molecular mechanisms governing ccRCC growth and progression will facilitate the development of novel and efficient diagnostic and/or therapeutic strategies for ccRCC. Two independent studies conducted by The Cancer Genome Atlas Networks (TCGA) and Sato *et al.* identified *VHL* as the most frequently altered gene in their ccRCC patient cohort^{35,36}. Mutations in tumour suppressor gene *polybromo-1 (PBRM1)* were the second most prevalent genetic alterations in ccRCC patients^{35,36,51}. This gene encodes for BRG1-associated factor 180 (BAF180), a subunit of the SWI/SNF chromatin remodelling. Also, loss of *PBRM1* was correlated with higher ccRCC tumour grade and poor prognosis⁵².

Moreover, other frequently reported genetic alterations in ccRCC are mutations in *SET domain containing 2 (SETD2)*⁵³ and *BRCA1 associated protein 1 (BAP1)*⁵⁴. *SETD2* and *BAP1* encode for histone methyltransferase and histone deubiquitinase, respectively, in which both of these genes are tumour suppressor that conform to the Knudson's two-hit hypothesis. In addition, *BAP1* mutations are observed in the high-grade ccRCC⁵⁴. The high prevalence of mutations observed in the component of chromatin remodelling complex as well as in chromatin-modifying enzymes suggest that epigenetic deregulations along with *VHL* alterations are among the important drivers of ccRCC pathogenesis^{35,53}. Interestingly, *PBRM1*, *SETD2* and *BAP1* genes are all located on the chromosome 3 short arm in the vicinity of the *VHL* locus, thus making the loss of heterozygosity of this region accounts for 90% of all ccRCC cases³⁵. In addition, low percentage of genetic alterations (<10%) were also observed in the following genes; *phosphatase and tensin homolog (PTEN)*, *mechanistic target of rapamycin (mTOR)* and *p53*³⁵.

The ccRCC molecular characterisations discussed above were performed via high-throughput sequencing analyses of bulk ccRCC samples. Hence, in order to examine the genomic landscape of ccRCC evolution, multi-regions high-throughput sequencing were carried out^{17,20,21,55,56}. Remarkably, these analyses revealed high intratumour genetic heterogeneities in ccRCC. Furthermore, construction of predicted ccRCC driver mutations phylogenetic trees revealed that ccRCC evolution followed the branched evolutionary pattern instead of linear pattern. Due to these high intratumour heterogeneities, it would be more challenging to efficiently treat ccRCC patients especially when the therapeutic approaches are designed to target a specific driver mutation. Despite these “branching” intratumour heterogeneities, *VHL* inactivation and the chromosome 3p loss of heterozygosity are the truncal events that drive ccRCC pathogenesis^{17,21,56}. Most of other predicted ccRCC driver mutations are subclonal. This seems to suggest that the opportunity for mutation-based therapeutic approaches in ccRCC are limited to dependencies resulting from *VHL* inactivation.

1.8 mTOR signalling pathway overview

The mTOR signalling pathway promotes cells growth and survival by regulating cellular metabolism processes as well as the biosynthesis of macromolecules which are the essential building blocks for the cells^{57,58}. In addition to driving these processes, the autophagy-mediated organelles degradation and protein turnover have been demonstrated to be negatively regulated by the mTOR signalling pathway^{57,58}. This signalling cascade can be activated by various intra- and extracellular signals such as growth factors, nutrients availability and cellular energy status⁵⁹. Thus, in response to these environmental cues, the mTOR signalling pathway will coordinate and tightly regulate the cellular metabolism processes that are required by the cells to proliferate and/or survive in that particular environment.

Gene encodes for mTOR protein is located on chromosome 1. Function as a serine/threonine protein kinase, mTOR is comprised of several domains; the HEAT repeat, focal adhesion kinase targeting domain (FAT), FKB12-Rapamycin binding domain (FRB) and the catalytic kinase domain⁶⁰. The simplified structure of mTOR protein is depicted in figure 6. mTOR forms complex with a defined set of proteins in order to regulate/phosphorylate its downstream targets. To date, there are two distinct mTOR protein complexes identified, the mTORC1 and mTORC2⁶¹. The protein components that constitute these complexes are exemplified in figure 7. The mTORC1 complex is sensitive to rapamycin. In contrast, the mTORC2 complex is characterised to be insensitive towards acute rapamycin treatment^{62,63}. Binding of allosteric inhibitor rapamycin-FKB12 (FK506-binding protein) complex at the mTOR FRB domain hinders the substrates recruitment to the mTORC1 complex as well as inhibiting the access to its catalytic kinase domain⁶⁰.



Figure 6: The structure of mTOR protein. Adopted from Laplante and Sabatini⁵⁹

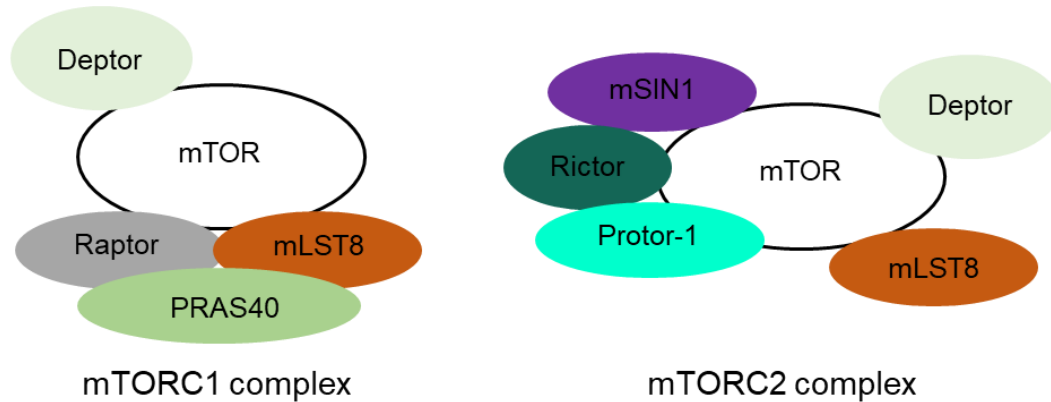


Figure 7: The mTORC1 and mTORC2 protein complex. Adopted from Zoncu *et al*⁶¹

The mTOR protein is the core and catalytic subunit of these mTORC1 and mTORC2 protein complex. Some components are shared between these complexes which are the mammalian lethal with SEC13 protein 8 (mLST8)⁶⁴ and DEP domain-containing mTOR-interacting protein (Deptor)⁶⁵. There are also components that exclusive to either mTORC1 or mTORC2 complex. For example, the regulatory-associated protein of mTOR (Raptor) is part of the mTORC1 complex⁶⁶ whereas the rapamycin-insensitive companion of target of rapamycin (Rictor) makes up the mTORC2 complex⁶⁷. Out of these two complexes, the mechanisms of activation and roles of mTORC1 complex have been well-characterised. Nonetheless, there have been also plenty of discoveries made in understanding the role of mTORC2 complex. In brief, the mTORC1 complex functions as the central regulator of cellular metabolism processes which have been described previously. The mTORC2 complex has been identified to be involved in cytoskeleton remodelling^{62,67}. Nonetheless, the processes regulated by these mTORC1/2 complexes are important in order to promote cells growth as well as increasing the cells survival in response to the environmental cues. Whilst the mTORC1 signalling pathway can be activated

by the environmental cues outlined above, the mTORC2 complex is only responsive towards the growth factors activation⁵⁸.

1.9 mTORC1 complex upstream activators

Different environmental cues employ distinct mechanisms in activating the mTORC1 complex. Herein, the growth factors-mediated mTORC1 complex activation is discussed. Growth factors such as insulin/insulin-like growth factor 1 (IGF-1)⁶⁸ and platelet-derived growth factor subunit B (PDGFB)^{69,70} binds to their respective receptor tyrosine kinase (RTK) and subsequently induces the RTK dimerization. This activates the RTK, followed by the phosphorylation of phosphoinositide 3-kinase (PI3K) which is the RTK downstream effector⁵⁹. The function of PI3K is to integrate and transduce the environmental cues into intracellular signalling cascade. Mechanistically, PI3K catalyses the phosphorylation of phosphatidylinositol (4, 5)-biphosphate (PIP₂) to phosphatidylinositol (3, 4, 5)-triphosphate (PIP₃) in which PIP₃ is a secondary messenger that relays the intracellular signal to the subsequent downstream effectors and finally activates the mTORC1 complex⁷¹.

PIP₃ modulates the PDK1-mediated phosphorylation and activation of AKT⁷¹. This process is negatively regulated by PTEN which mediates dephosphorylation of PIP₃⁷². Upon activation, AKT will in turn phosphorylate the tuberous sclerosis complex (TSC), a GTPase activating protein (GAP). AKT-mediated phosphorylation of TSC will result in its inactivation^{68,73}. Since TSC function is to convert the active GTP-RHEB (Ras homolog enriched in brain) to its inactive GDP-RHEB form, TSC phosphorylation will result in RHEB remains in its active form⁷⁴. This will allow it to subsequently activate the mTORC1 complex which is its downstream effector. Thus, TSC serves as the negative regulator of the mTORC1 signalling

pathway. The mechanism of growth factor-mediated activation of mTORC1 signalling pathway is simplified in figure 8.

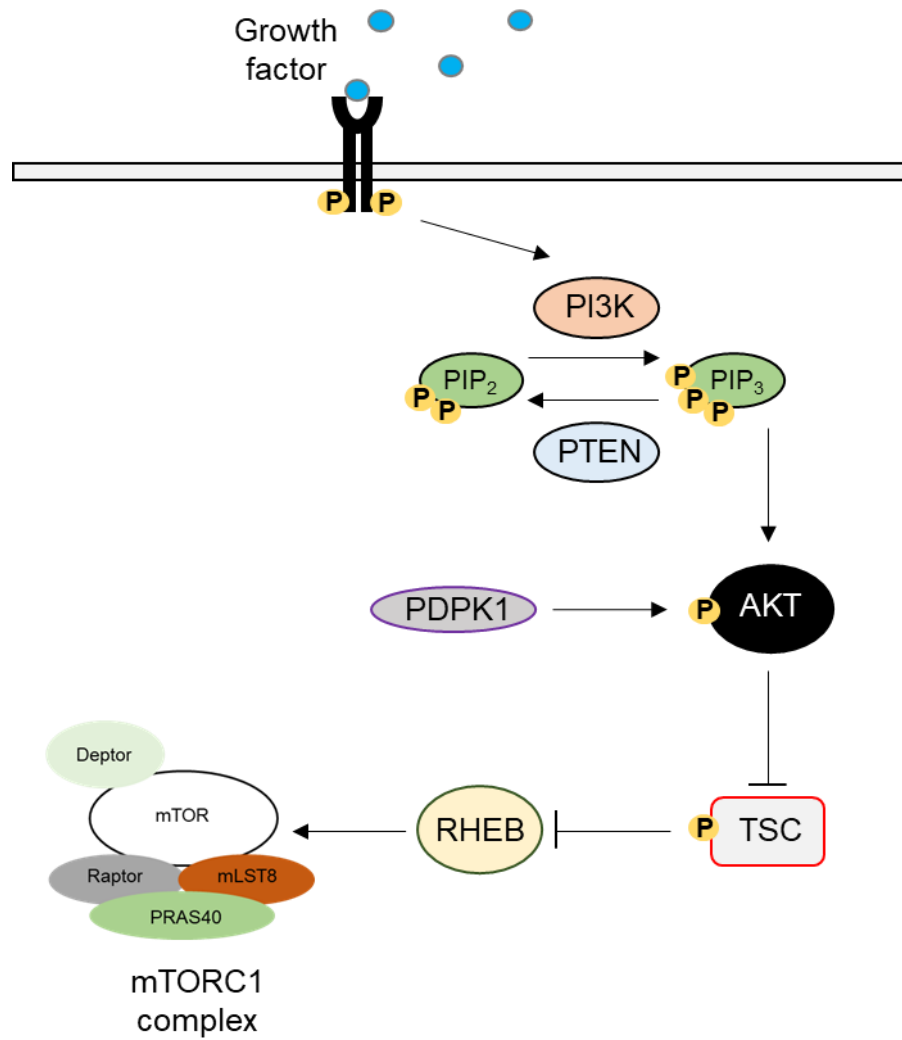


Figure 8: The mechanism of growth factor-mediated activation of mTORC1 signalling pathway. Adopted from Yu *et al*⁷⁵

1.10 The cellular functions of mTORC1 complex.

The mTORC1 complex modulates cellular metabolism processes by regulating the expression or activity of the upstream regulators of these processes, depending on the type of cues received from the environment^{58,59,76}. For instance, growth factors stimulation or abundant nutrients availability promotes the protein and lipid biosynthesis whilst inhibiting the autophagy processes. However, in the low cellular energy state marked by a low ATP to ADP ratio, AMP-activated protein kinase (AMPK) will phosphorylate and activate the TSC complex, negative regulator of mTORC1 complex. Therefore, the energy-demanding anabolic processes such as the macromolecules biosynthesis will be negatively regulated in the low ATP condition⁷⁷. The mTORC1 complex promotes protein biosynthesis by modulating the mRNA translation process and ribosome biogenesis via the phosphorylation of eukaryotic initiation factor 4E (eIF-4E)-binding protein 1 (4E-BP1) and p70-ribosomal S6 kinase (p70 S6 kinase), respectively. Phosphorylated 4E-BP1 will not be able to bind to eIF-4E, thus enabling the eIF-4E to promote the 5'cap-dependent translation initiation^{78,79}. The mTORC1-mediated phosphorylation of p70 S6 kinase will subsequently activates multiple downstream effectors that involve in 5'cap-dependent translation initiation and elongation, and ribosome biogenesis⁸⁰.

The mTORC1 complex regulates the lipid biosynthesis by mediating SREBFs activation⁸¹⁻⁸³, which is the key regulator of lipid homeostasis pathways. There are three SREBF isoforms, the SREBF-1a, SREBF-1c and SREBF2. Inactive form of SREBFs are retained in the endoplasmic reticulum membrane. The activation of mTORC1 signalling pathway by the corresponding cues will result in the translocation of this inactive SREBF into the Golgi apparatus where it will undergo proteolytic cleavage and maturation process⁸⁴. The activated

SREBFs are then translocated into the nucleus where they will bind to the sterol-binding element of their target genes that participate in lipid biosynthesis and homeostasis pathways⁸⁵.

1.11 Hyper-activation of mTORC1 signalling pathway in ccRCC

As a central regulator of various key biological processes, deregulations of the mTORC1 signalling pathway have been implicated in diseases such as cancer, type II diabetes and obesity^{57,61}. Aberrant activation by its upstream regulators or genetic alterations that perturb the function of this signalling pathway components can contribute to its deregulation, which are frequently observed in many cancer types⁸⁶⁻⁸⁸. For example, gene encoding for PI3K, *PIK3CA*, is commonly mutated in the breast cancer luminal A (45%) and luminal B subtype (29%) in the TCGA breast cancer cohort⁸⁹. Furthermore, comprehensive molecular characterisation of endometrial cancer revealed that *PIK3CA* were among the most frequently mutated genes in this cancer types⁹⁰. In addition, mutations in *PTEN* are also frequently observed in many cancer types⁹¹. The aberrant activation or deregulation of mTORC1 signalling pathway would thus lead to either disruption of cellular homeostasis or upregulation of those biological processes that could facilitate uncontrolled cells growth and expansion, thus driving the formation of cancer.

The mTORC1 signalling pathways is frequently observed to be hyper-activated in ccRCC patients^{92,93}. Pantuck *et al.* performed phosphorylated ribosomal S6 protein (P-S6) immunohistochemical staining on 375 ccRCC tissue microarray samples and found that 85% of the analysed ccRCC samples were positively stained for this phosphorylated protein⁹². Ribosomal S6 is the substrate of p70 S6 kinase that play a role in ribosomal biogenesis during protein biosynthesis. Activated mTORC1 complex phosphorylates the p70 S6 kinase which will in turn phosphorylate its substrate, the ribosomal S6 protein^{94,95}. Thus, both phosphorylated p70

S6 kinase and phosphorylated S6 proteins are used as the read-out for mTORC1 activity. Moreover, the expression of P-S6 positively correlated with the tumour grades and was significantly higher in the patients with the metastatic disease⁹². Nevertheless, the mechanisms that drive mTORC1 pathway hyper-activation in ccRCC are yet to be fully elucidated.

Like many other cancer types, hyper-activation of mTORC1 signalling pathway in ccRCC has been associated with genetic alterations in the components of this pathway. The large scale sequencing efforts on ccRCC samples conducted by TCGA networks and Sato *et al.* have identified that *PIK3CA* and *PTEN* were mutated in approximately 2%-5% of ccRCC cases^{35,36}. This mutation fraction, however, was significantly lower when compared to the alterations observed in the endometrial cancer cases for instance⁹⁰. Furthermore, mutations in the *mTOR* gene are found in approximately 6% of ccRCC cases in which the majority of these alterations are clustered within the FAT and catalytic kinase domains^{35,96}. A small fraction of mutations is also identified in *tuberous sclerosis 1 (TSC1)* which encodes for the component of the tuberous sclerosis complex, the negative regulator of mTORC1 signalling pathway⁹⁷.

Collectively, genetic alterations along this signalling axis are thus likely to contribute to mTORC1 hyper-activation in ccRCC. However, only a small fraction of ccRCC patients actually harboured these mutations which seems to suggest the involvement of another molecular players in driving mTORC1 hyper-activation in this cancer type. In fact, a previous study has reported an increased in mTORC1 activity in metastatic renal cancer despite the absence of *PTEN* deletion⁹⁸, indicating that upstream activating signals and/or regulators are still required in some cases. In line with this finding, Xu *et al.* has shown that in HeLa cells that harboured the mTOR-activating mutations, the mTORC1 activity in these cells remained dependent on the activation by its

upstream regulator RHEB⁹⁶. Moreover, shRNA-mediated RHEB knockdown significantly reduced the mTORC1 activity of all mTOR-activating mutations tested⁹⁶.

1.12 Increased mTORC1 activity in ccRCC mouse model

There have been plenty of efforts to improve the currently available ccRCC mouse model in order to accurately mimic ccRCC pathogenesis *in vivo*⁹⁹. Having a robust mouse model for ccRCC would give us a valuable experimental tool to better understand this disease and could also be used for testing the newly-developed therapies for ccRCC pre-clinically. The early approach employed to engineer ccRCC mouse model was based on knocking out the *VHL* gene alone. The rationale of this strategy was VHL inactivation is the truncal event of the renal tumorigenesis and found in majority of ccRCC sporadic cases. Also, *VHL* germline mutation is observed in the VHL syndrome patients who are predisposed to hereditary ccRCC. Nonetheless, the germline homozygous *VHL* knockout in mice (*VHL*^{-/-}) led to embryonic lethality, demonstrating that VHL functions are essential during embryogenesis¹⁰⁰. To circumvent this issue, the Cre-lox-based conditional *VHL* knockout is employed. By using this approach, *VHL* inactivation can be controlled and carried out only in the tissue of interest at a specific time.

Since ccRCC arises from the epithelium of the proximal tubules, *VHL* has been conditionally inactivated in this tissue as well as in other tissues of the renal tubule system. The *VHL* conditional knockout is achieved by using the renal tubule-specific promoter, such as phosphoenolpyruvate carboxykinase (*PEPCK*)¹⁰¹, cadherin 16 (*CDH16*)¹⁰² and paired box gene 8 (*PAX8*)¹⁰³, to drive the expression of CRE-recombinase and knockout *VHL* specifically in this tissue. Nonetheless, conditional *VHL* targeting alone was not sufficient to induce tumour formation, indicating the requirements of additional genetic/epigenetic alterations or oncogenic

drivers to promote tumour formation in this ccRCC mouse model. Hence, the strategy to engineer ccRCC mouse model was improvised by conditionally co-inactivating *VHL* with other tumour suppressor genes such as *PBRM1* and *BAP1*. These are the two most recurrently mutated genes in ccRCC after *VHL*, identified in the recent ccRCC molecular characterisation studies^{35,36}. Moreover, *PBRM1* and *BAP1* are located on the chromosome 3p arm in which this region loss of heterozygosity was also identified as the truncal event in renal tumourigenesis¹⁷. Based on these evidences, inactivating either of these genes along with *VHL* could possibly mimic ccRCC pathogenesis and drive the tumour formation in this mouse model.

Recent study by Gu *et al.* generated the *VHL*^{-/-}; *Bap1*^{-/-} double knockout ccRCC mouse model using the PAX8-Cre system. Conditional inactivation of these genes in the renal tubules was able to initiate ccRCC formation, which recapitulated several important human ccRCC features such as the presence of the prominent clear cell cytoplasm and increased in the expression of HIF1A downstream targets and mTORC1 activity¹⁰⁴. In line with the observation in ccRCC clinical samples that *BAP1* mutations were associated with aggressive phenotype and high tumour grade, tumours that arised in this *VHL*^{-/-}; *BAP1*^{-/-} mouse model were found to be the high-grade subtype^{54,104}. In parallel, the group also tested the effect of conditionally knocking out *PBRM1* in combination with *VHL* using the PAX8-Cre system. The *VHL*^{-/-}; *PBRM1*^{-/-} ccRCC mouse model was able to form tumours that exhibited the human ccRCC phenotypes. However, the developed tumours were low grade the which were in contrast to the higher grade tumours observed in the other *VHL*^{-/-}; *BAP1*^{-/-} ccRCC mouse model¹⁰⁴. Nonetheless, these phenotypes were in agreement with the prognosis status and tumour grades of the human *BAP1*-deficient and *PBRM1*-deficient ccRCC samples¹⁰⁵.

An independent parallel study conducted by Nargund *et al.* also developed the *VHL*^{-/-}; *PBRM1*^{-/-} ccRCC mouse model. However, in contrast to the Gu *et al.*, this group employed the KSP-Cre system instead of the PAX8-Cre system. Regardless, conditional double inactivation of *VHL* and *PBRM1* using this KSP-Cre system also led to the tumour development in this mouse model. Histologically, the tumours had the distinct human ccRCC clear cell morphology and positively stained for carbonic anhydrase 9 (CAIX), a marker of HIF1A activity, indicating upregulation of HIF1A in these tumours¹⁰⁶. mTORC1 hyper-activation was also observed in this KSP-driven *VHL*^{-/-}; *PBRM1*^{-/-} ccRCC mouse model. The hyper-activation of this mTORC1-signalling pathway was deemed to be third event that further drove the tumour progression after a long latency period¹⁰⁶.

Increased in mTORC1 activity was consistently observed in the course of tumour development in these ccRCC mice models^{104,106}. This observation recapitulated the mTORC1 hyper-activation that is prevalent in ccRCC clinical samples^{92,93}. Interestingly, the studies described above did not report any genetic alterations along the mTORC1 signalling pathway that might contribute to the increased in mTORC1 activity in their ccRCC mice models. This may suggest that the increased in mTORC1 activity in ccRCC could be the consequence of *VHL* and/or *PBRM1* loss-of-function. Further investigations to elucidate the link between *VHL* and/or *PBRM1* loss with mTORC1 hyper-activation are thus warranted whereby these mice models would be the perfect platform to address this question. Overall, the success in generating novel ccRCC mice models that closely mimic the human ccRCC pathogenesis will significantly transform the field of renal cancer research. In turn, better insights on renal tumourigenesis can be gained in which the ultimate goal is to translate this valuable knowledge clinically for the benefit of ccRCC patients.

1.13 ccRCC therapeutic strategies

Radical or partial nephrectomy is the standard treatment for the early stage or localized ccRCC cases which is also depending on the location and size of the effected tissues^{8,9}. Radical nephrectomy is the removal of the whole kidney whereas in the partial nephrectomy, only the cancerous regions get surgically resected. Overall, the prognosis of patients with stage 1 and stage 2 disease, where tumour is only localized to the kidney, is good with five-year survival rate of more than 70%. Thus, ccRCC early detection followed by curative surgery could significantly improve the overall patients' survival and also vital in order to prevent the tumour from spreading to the distant organs. Nonetheless, disease relapse at the secondary sites have often been seen in patients with localized disease who had undergone the curative surgery¹⁰⁷.

ccRCC is classified at the advanced stage (stage III and IV) when the tumours have already spread beyond the kidney to the nearby tissues or lymph nodes, or metastasise to the distant organs⁹. As discussed previously, patients with the advanced diseases have poor prognosis and are associated with high mortality. Unfortunately one-third of ccRCC patients have the metastatic disease in which the five-year survival rate of this stage is less than 10%. It is a great challenge to efficiently treat advanced stage ccRCC due to disease aggressiveness and its irresponsiveness towards conventional chemo- and radiotherapies. Nevertheless, substantial efforts have been put in to improve the current therapeutic strategies especially for the advanced stage ccRCC.

About two decades ago, the cytokines-based immunotherapy was the only viable option to treat the metastatic ccRCC. These included administering ccRCC patients with interferon alpha (IFN-A) and high dose of interleukin 2 (IL-2). Despite this being the preferred therapeutic

strategy back then, the IFN-A and IL2-based therapies had poor overall patients' response rates, which was less than 20%¹⁰⁸⁻¹¹⁰. This treatment strategy was also associated with high toxicity and several adverse effects. The inefficiency of this cytokines-based immunotherapy had prompted researchers and clinical scientists to come up with novel and more effective strategies to treat ccRCC patients. Thus, two novel therapeutic strategies were developed to target the receptor tyrosine kinases and mTOR-signalling pathway. These novel treatment options were licensed to use in the clinic in mid 2000s to treat advanced stage ccRCC.

Upregulation of pro-angiogenic factors such as *VEGFA* which is the downstream target of VHL-HIFA contributes to the ccRCC hyper-vascular nature²⁴. Thus, inhibiting angiogenesis by targeting RTKs VEGFR and PDGFR was then one of the attractive therapeutic strategies to treat ccRCC patients. Sunitinib¹¹¹, sorafenib¹¹² and pazopanib¹¹³ were among the anti-angiogenic drugs developed to target the RTKs and clinically approved for treating ccRCC patients. Sunitinib is the first-line treatment for metastatic ccRCC and has shown better objective response rate and longer progression-free survival as compared to the IFN-A treatment¹¹¹. In addition to targeting the RTKs, treatment option of bevacizumab, a monoclonal antibody against *VEGFA*, plus IFN-A has also been clinically approved as a first-line treatment for metastatic ccRCC¹¹⁴.

Due to the high prevalence of mTORC1 hyper-activation in ccRCC, inhibitors targeting the mTOR have also been developed. These inhibitors such as temsirolimus¹¹⁵ and everolimus¹¹⁶ have already been approved for use in the clinic for treating advanced ccRCC. Temsirolimus and everolimus are the rapamycin derivatives which is also known as rapalogs. Rapalogs forms a protein complex with FKB12 that binds to the mTOR FRB domain. The rapalog-FKB12 complex is an allosteric inhibitor that prevent the substrates recruitment and phosphorylation by the mTOR catalytic kinase domain⁶⁰. Both of these mTOR inhibitors have shown promising

effects in the clinic. Temsirolimus, for instance, is among the first-line treatments for metastatic ccRCC and has shown better efficacy in term of progression-free survival and overall response rates than IFN- α treatment¹¹⁵. However, one limitation with this therapeutic approach is that the rapalogs only target the mTORC1 complex. It has been demonstrated that the inhibition of mTORC1 complex could result in mTORC2-mediated negative feedback loop of AKT activation that would increase cells survival¹¹⁷. In order to address this, there is a second class of mTOR inhibitor currently being developed targeting both mTORC1 and mTORC2 complex. The mechanism of its inhibition is by competing with ATP for binding site in the mTOR catalytic kinase domain^{118,119}.

Despite the superior efficacy over their predecessors IFN-A and IL2, the overall patients' response rates of these anti-angiogenic agents and mTOR inhibitors are yet to reach the satisfactory level¹²⁰. Importantly, significant fractions of ccRCC patients develop intrinsic resistance towards these inhibitors¹²¹. In order to improve the treatment strategies for ccRCC patients, several clinical trials have been conducted to test the efficacy and safety of combinatorially treating ccRCC patients with both anti-angiogenic and mTOR inhibitors. Unfortunately, increased in drugs-related adverse effects with no added efficacy was observed in some of these trials^{122,123}. However, a phase II randomised clinical trial testing a combined treatment of everolimus and lenvatinib on advanced ccRCC patients who have progressed after one previous anti-VEGFR treatment showed an improved median progression-free and overall survival compared to this drug single treatment¹²⁴. This promising result indicates that the combinatorial targeting approach can still be potentially further developed as the treatment option for advanced stage ccRCC patients who have disease progression after the first-line treatments.

The immune checkpoint inhibitors have recently drawn a great interest to be developed as a novel therapeutic strategy for several type of cancers including the renal cancer¹²⁵. One way cancer cells could evade the immune responses is by inhibiting the cytotoxic T-cell function. Cancer cells release a protein called *program death ligand 1* (PD-L1) that binds to the *programmed cell death protein* (PD-1) on the surface of cytotoxic T-cells that will switch off the T-cells, thus preventing these immune cells from attacking the cancer cells¹²⁶. Targeting either PD-1 or PD-L1 would keep the T-cells active and be able to recognise and kill the cancer cells. Nivolumab is a monoclonal antibody developed against PD-1 in ccRCC. Several phase III clinical trials are currently on going to assess the efficacy of treating advanced ccRCC patients with several immune checkpoint inhibitors including nivolumab in combination with the current clinically-approved drugs described above¹²⁰. The primary end point of these clinical trials is to determine whether the patients who have received the combo treatment would have a significantly improved progression-free and overall survival.

Another strategy employed to treat ccRCC patients is by directly inhibiting the pro-tumourigenic HIF2A. HIF2A is a relevant and attractive target due to VHL-HIF2A axis role as the hallmark gatekeeper of renal tumourigenesis. Also, due to ccRCC high intratumour heterogeneities, targeting this truncal event of renal tumourigenesis could potentially be a viable option and may provide a therapeutic advantage for ccRCC patients. Despite transcription factor is typically deemed to be difficult to drug, recent studies have succeeded in developing HIF2A small molecule inhibitors, namely the PT2399¹²⁷ and PT2385¹²⁸, which bind to a cavity within the HIF2a PAS-B domain¹²⁹. This will consequently prevent HIF2A dimerization with the HIF1B to form the functionally active transcription factor. PT2399 has been demonstrated to confer anti-tumour activity in both pre-clinical ccRCC models and ccRCC patient-derived

xenografts^{127,130}. However, variable degrees of sensitivity towards PT2399 were observed in both studies in which PT2399 sensitivity is correlated with HIF2A expression level. Prolong treatment resulted in the tumour developing resistance to this HIF2A inhibitor which has always been the recurrent problem in ccRCC treatments¹³⁰. A phase I dose-escalation clinical trial with PT2385 revealed the safety of the drug with mixed patients' response¹³¹.

1.14 Transcriptional deregulation in cancer

Eukaryotic gene expression programs are tightly controlled by gene regulatory elements that consist of promoters, enhancers and insulators¹³². Promoters are located in the proximity of the transcription start site and bound by RNA polymerase II, general transcription factors and co-factors. These components, known as the basal transcription apparatus, initiate the transcription process. Recruitment of the basal transcription apparatus at the promoter region to promote the transcription initiation generally depends on the activities or cues from the nearby enhancer regions¹³². Enhancers are stretches of DNA sequences, located either upstream or downstream of the transcription start site, which are bound by transcription activators and co-activators that function to regulate the expression of a particular gene. The eukaryotic transcriptional processes are precisely controlled especially the cell-type-specific transcriptional programs, developmental and cell fate determination processes as well as transcriptional programs that respond to the environmental cues such as hypoxic or stress conditions. In the regulation of cell-type-specific transcriptional programs for instance, multiple cell-type-specific TFs co-ordinately bind to these enhancer regions, recruit transcription co-factors such as mediator and p300/CBP, and subsequently perform a loop to interact with promoter region of the nearby genes^{133,134}. This enhancer-promoter/genes looping interaction only occurs within the insulated neighbourhoods, which are bound by the CTCF proteins and the cohesin complex¹³⁵.

The transformation of normal cells into malignant, neoplastic cells is accompanied by the acquisition of several capabilities that enable the cells to undergo such transformation process. These phenotypic changes are essential in facilitating both tumour formation and its progression into the more advanced stages. Hanahan and Weinberg have described these acquired traits as the hallmarks of cancer that include; (1) infinite replicative potential, (2) capable of stimulating its own proliferation and angiogenesis, (3) irresponsiveness towards growth suppressor signals, (4) apoptosis and immune destruction evasiveness, (5) metabolic and energy production rewiring, and (6) capable of invading and colonising the distant sites¹³⁶. The ability of normal cells to acquire the cancer-associated traits outlined above could be the consequence of transcriptional deregulations that occur within the cells. Aberrant transcriptional networks or gene expression programs would result in the cells overexpressing particular pro-tumourigenic and/or repressing genes with tumour suppressive function, in which both attributes if not the main, is among the important factors that drive tumourigenesis¹³⁷.

In general, dysregulated transcriptional regulators due to genetic alterations could contribute to the aberrant gene expression programs observed in many cancer types¹³⁷. In fact, several frequently mutated oncogenes and tumour suppressor genes in human cancers are transcription factors such as *MYC* and *TP53*, respectively, which play vital roles in regulating cells growth. For instance, *MYC* activation is implicated in several cancer types, which is the result of amplification or chromosomal translocation^{138,139}. *TP53*, on the other hand, is a tumour suppressor gene and somatic mutations in this gene commonly lead to loss-of-functions. Deemed as the guardian of the genome, *TP53* have various physiological roles which some of them are anti-tumourigenic such as the regulation of cell cycle, DNA repair mechanisms and apoptosis¹⁴⁰. Moreover, chromosome translocation can result in the formation of fusion transcription factors

that would have pro-tumourigenic properties or drive the high expression of this transcription factor if it is translocated into the active regulatory region of other genes¹⁴¹. For example, the translocation of *EWS* gene transactivation domain to the *FLI1* transcription factor resulted in the formation of highly active, pro-tumourigenic chimeric EWS-FLI1 transcription factor that drives the tumour formation and progression in Ewing Sarcoma¹⁴². Also, translocation of *MYC* locus to the IgH enhancer locus drives the high expression of *MYC* in Burkitt's lymphoma¹⁴³.

Also, transcription factors are the common terminal effectors of many oncogenic signalling pathways such as the PI3K-AKT, RTK-RAS, and WNT signalling pathways¹⁴⁴. Aberrant activity of these signalling pathways agonists or activating mutations in the components of these signalling cascades have frequently been reported in human cancers such as the *PIK3CA* mutations in breast cancer, *BRAF* mutations in melanoma and *KRAS* mutations in the colorectal and lung cancer¹⁴⁴. Since these oncogenic signalling pathways converged on the transcription factors, deregulation of these pathways would consequently lead to aberrant gene expression programs that confer for tumour growth advantage and promote its progression. In addition, dysregulated transcription factors activity could also be contributed by the loss-of-function of their upstream regulators. An example of this is the stabilisation and accumulation of HIF2A transcription factor and subsequent upregulation of the pro-tumourigenic gene expression programs upon VHL inactivation in ccRCC^{35,36}. As a result, the cancer cells would develop “*addiction*” and high dependencies on these transcription factors that drive the gene expression programs, which favour the tumour growth and progression¹³⁷. In addition, aberrant enhancer activities have also been demonstrated to play an important role in driving tumour formation and progression¹⁴⁵. Mutations or the presence of single nucleotide polymorphisms within the enhancer sequences would generate a novel binding site for transcription factors that would in

turn drive the aberrant gene expression programs, in which some of these programs could be pro-tumourigenic. Also, in the case of *c-MYC* described above, chromosome translocation would locate a pro-tumourigenic transcription factor (or other oncogenes) in the vicinity of active enhancers which may drive the high expression of these transcription factors and subsequently promote tumourigenesis^{137,145}.

Furthermore, epigenetic regulations such as DNA methylation and histone modifications have also been shown to play a critical role in controlling genes activation and expression in eukaryotic cells¹⁴⁶. DNA hypo- and hyper-methylation at the CpG islands is associated with transcriptional activation and silencing, respectively. Abnormal DNA methylation have been implicated in several cancer types in which hypo-methylation of an oncogene regulatory region would activate and drive its expression whereas tumour suppressor genes hyper-methylation will lead to its silencing¹⁴⁷. For example, *VHL* promoter region hyper-methylation been observed in ccRCC that result in *VHL* repression and subsequent HIF2A accumulation³⁷. Moreover, dysregulated DNA methylation process is generally due to genetic alterations in the enzymes that involve in adding (DNA methyltransferases, DNMT) or removing (ten eleven translocation, TET) the methyl group at this CpG islands¹⁴⁷.

DNA is tightly packed and wrapped around core histone octamers called nucleosome. Nucleosomes are connected to each other via histone 1 tail (H1) and linker DNA and compacted together to form chromatin. Since chromatin is a highly compact structure, chromatin “*opening/relaxing*” so that the DNA regions are accessible by the transcriptional and replication machineries as well as “*closing/condensing*” largely depends on the chemical modifications of the core histone octamers residues¹⁴⁶. The methylation and acetylation of the histone 3 (H3) residues are critical in the gene expression regulation. The acetylation of lysine 27 (H3K27ac)

and tri-methylation of lysine 4 (H3K4me1) marks for opened accessible chromatin and associated with active transcription¹⁴⁸. Also, these chromatin modifications such as the H3K27ac for instance is widely used in the ChIP experiments as the surrogate marker for active enhancer regions¹⁴⁹. On the other hand, methylation of lysine 27 (H3K27me) as well as lysine 9 (H3K9me) marks for close inactive chromatin and transcription repression¹⁴⁶. Epigenetic regulation of transcriptional activation/repression via precise histone modifications-mediated “*opening*” and “*closing*” of the chromatin structures, respectively, are vital to ensure normal transcriptional programs and biological processes are taken place. Nevertheless, genes encoding for the family members of the histone-modifying enzymes such as the histone acetyltransferases (HATs)/deacetylase (HDACs) and histone methyltransferases (HMTs)/demethylases (HDMs) are also targets for genetic alterations and in fact, mutations in these genes have been frequently observed in several cancer types¹⁴⁷. For examples, mutations in SETD2, a H3 lysine 36-specific methyltransferases, and KDM5C, a lysine demethylase, were found in a fraction of ccRCC patients^{35,36}. Overall, precise regulation of gene expression programs are vital whereby perturbations of these finely-tuned transcriptional networks have been demonstrated as one of the important factors that drive cancer formation and progression.

1.15 Super enhancer and cancer

As previously described, enhancer is a DNA regulatory element that serves as the binding site for transcription factors and co-activators and plays a crucial role in activating the transcription process. Recent studies have shown that enhancers could form a large cluster of enhancers or commonly known as super enhancer^{149,150}. Unlike typical enhancer, super enhancer could span across large DNA region and be bound by several master transcription factors and co-activators such as the mediators and bromodomain-containing protein 4 (BRD4). Also, super

enhancers are enriched with H3K27ac signals, marker for active enhancer region¹⁴⁹⁻¹⁵². Super enhancer was first identified in murine embryonic stem cells which function was to regulate the expression of master transcription factors that involve in maintaining the cells pluripotency¹⁵³. It has then been demonstrated that super enhancer is an important regulator of cell identity, cell fate determination and also the lineage- or cell-type-specific gene expression programs¹⁴⁹. Super enhancer drives the expression of cell-type-specific transcription factors or known as master transcription factors. They typically auto-regulate their own expression as well as regulating each other expression to form an interconnected auto-regulatory loop. These master transcription factors will co-ordinately bind and activate the expression of their downstream targets¹⁵⁴. This precise and tight regulation of the expression of these master transcription factors as well as their downstream targets is vital in defining the “correct” cell identity and fate and also ensuring the activation of “*necessary*” gene expression programs in specific cells at a given time.

In addition to driving the expression of critical transcriptional regulators that define cells identity, super enhancer have also been implicated in regulating several cancer phenotypes¹⁵⁵. In multiple myeloma (MM), high densities of mediator and BRD4 binding was found in the super enhancer regions that were associated with key genes that promote MM pathogenesis such as *MYC*, *XBPI* and *PRDMI* as well as other pro-tumourigenic genes such as *CCND2* and *BCL-xL*¹⁵¹. Mediator, BRD4 and H3K27ac ChIP-Seq was performed to identify super enhancer region in glioblastoma multiform (GBM) and small-cell lung cancer (SCLC)¹⁵¹. Super enhancer was found to associate with prominent genes in GBM biology such as *RUNX1*, *BHLHE40* and *BCL3*. *RUNX1* and *BHLHE40* are important transcription factors that mediate the mesenchymal transformation of brain tumour. In SCLC, super enhancer was identified in the vicinity of *INSM2* and *ID2*, two important oncogenes that were highly expressed in this tumour type.

Super enhancer profiling in adult T-cell leukaemia (ATL) revealed the presence of super enhancer regions at the genes that involve in T-cell activation pathway and known oncogenes¹⁵⁶. Interestingly, through this profiling study, a novel critical driver of ATL, *TIAM2*, was discovered to be associated with super enhancer and highly expressed in this tumour type. Knocking down the expression of this gene in ATL cell lines induced apoptosis whereas overexpression of *TIAM2* promoted cells growth. Furthermore, super enhancer profiling in several squamous cell carcinomas identified the long non-coding RNA *CCAT1* to be super enhancer-associated¹⁵⁷. The expression *CCAT1* was co-activated by the super enhancer-regulated master transcription factors, TP63 and SOX2. Knocking down either one of *CCAT1*, *TP63* and *SOX2* impaired cells growth *in vitro* and *in vivo*. Further analyses found that *CCAT1* forms a complex with *TP63* and *SOX2* to activate *EGFR* expression, which was also associated with super enhancer itself, to promote SCC pathogenesis via the activation of MEK/ERK1/2 and PI3K/AKT signalling pathways.

Cancer cells could acquire oncogenic super enhancer via several mechanisms. In a fraction of T-cell acute lymphoblastic leukaemia (T-ALL) patients, insertion of few nucleotides in the regulatory element upstream of oncogene *TALI* generated a *de-novo* binding site for transcription factor MYB¹⁵⁸. MYB binding to this region recruited other transcription factors, *RUNX1*, *GATA-3* as well as *TALI*, which made up the core components of major leukaemogenic transcriptional complex. The binding of this core regulatory complex created the super enhancer landscape that are important in driving T-ALL pathogenesis. Key oncogenic drivers can acquire super enhancer via chromosomal rearrangement that results in the relocation of these oncogenes near the super enhancer of other gene, or *vice-versa*. For example, in adenoid cystic carcinoma, the translocation of the *TGFB3* super enhancer locus to the proximity of *MYB* oncogene drove the high expression of *MYB* and subsequent activation of MYB-dependent oncogenic

transcriptional program¹⁵⁹. In addition, focal amplification of the *cis*-regulatory element of several oncogenes such as *MYC* can also lead to the formation of super enhancer that drives the high expression of these oncogenes and promotes tumourigenesis¹⁶⁰. Furthermore, generation of novel oncogenic fusion transcription factor could also establish a super enhancer landscape. For instance, in alveolar rhabdomyosarcoma, chimeric transcription factor PAX3-FOXO1 generated a *de novo* super enhancer landscape in collaboration with myogenic master transcription factors MYOG, MYOD and MYCN in driving this cancer type tumourigenesis¹⁶¹. Furthermore in Ewing sarcoma, super enhancer were found within the target genes of EWS-FLI1 chimeric transcription factor and several of these super enhancer-driven genes play important role in promoting the development and survival of Ewing sarcoma¹⁶²⁻¹⁶⁴.

Due to cancer cells high dependencies or addiction towards these super enhancer-driven genes, targeting the super enhancer has become an attractive therapeutic option for cancer. In fact, small molecule inhibitors have been developed to perturb the cancer associated-super enhancers that include the BRD4 inhibitor JQ1 and THZ1 which is the inhibitor of cyclin-dependent kinase 7 (CDK7)^{151,165-170}. BRD4 interacts with the Mediator to activate transcription process via regulating the RNA polymerase II-mediated transcriptional elongation. CDK7 is a component of general transcription factor IIIH (TFIIH) that involves in the regulation of RNA polymerase II initiation pausing. Treating cancer cells with these small molecules inhibitors led to the downregulation of the super enhancer-driven genes prominently the key oncogenic driver *MYC* and also in some cases could affect the general super enhancer landscape¹⁵⁵. These data demonstrated that cancer-associated super enhancers are sensitive to perturbation, thus making them an appealing therapeutic target for cancer.

1.16 Problem statement and objectives

Within these past decades, plenty of significant progresses have been made in understanding ccRCC pathogenesis. The gained knowledge have been translated into the development of diagnostic and therapeutic strategies for ccRCC. This includes the development of therapeutic agents targeting angiogenesis and mTOR signalling pathways which are frequently upregulated in ccRCC patients. Despite these agents are being widely used in the clinic, the overall patients' objective response rates are yet to reach the satisfactory level and the patients often develop resistance towards the administered therapies. Thus, there is a pressing need for efficient ccRCC diagnostic and/or therapeutic strategies especially for the advanced stage ccRCC patients due to their poor prognosis with the five-year survival rate is less than 10%. The fact that a significant fraction of ccRCC patients have already exhibited the metastatic disease at the time of diagnosis further exacerbating and posing a major challenge to treat this disease.

One factor that contributes to the lack of efficient therapies developed for ccRCC is the incomplete understanding on the underlying mechanisms that support ccRCC progression. Tumourigenesis is a complex evolutionary process facilitated by series of genetic and epigenetic alterations that confer for selective growth advantage and acquisition of cancer-associated traits^{136,171}. Cancer cells have to regularly rewire themselves and are sometimes highly dependent on certain genes or pathways in order to maintain the cancer phenotypes as well as adapting to various cellular stresses¹⁷². In ccRCC, aberrant upregulation of hypoxia-responsive gene expression program due to VHL inactivation if not the main is among important drivers of ccRCC pathogenesis¹⁹. In addition to this, we hypothesised the involvement of other transcriptional networks in which ccRCC cells are highly addicted to in order to support its

growth and survival. Hence, the **general objective** of this present study was **to identify novel transcriptional dependencies in ccRCC and to interrogate how they support ccRCC progression**. A better insight into ccRCC transcriptional dependencies could be a promising avenue for the development of efficient diagnostic and/or therapeutic strategies for ccRCC.

As discussed in the previous section, recent reports have demonstrated that critical transcriptional regulators that drive tumourigenesis in many cancer types are regulated by super enhancers. Therefore, to identify important ccRCC transcriptional regulators, previous works in the lab conducted by Paulo Rodrigues have performed H3K27ac ChIP-Seq in several ccRCC cells line to profile the super enhancer regions in ccRCC and look for super enhancer-associated transcription factors. The ChIP-Seq data were analysed by Sakari Vanharanta in which *Kruppel-like factor 6 (KLF6)* was found to be in the proximity of one of the strongest super enhancer in ccRCC, thus could signify its biological relevance in supporting ccRCC pathogenesis. The background of this transcription factor KLF6 will be briefly discussed in the Chapter 3 (section 3.1).

Stemming from the previous finding, the specific objective of my PhD project was therefore **to interrogate the roles of KLF6 and its regulated transcriptional program in supporting ccRCC growth**. In order to attain this objective, this present study was structured to consist of **three main aims** in which several research questions would be specifically addressed under each aims.

Aim 1: Assessing KLF6 functional relevance in supporting ccRCC growth

KLF6 was found to be in the proximity of one of the strongest super enhancer in ccRCC. It has been widely demonstrated that super enhancer drives the expression of genes that are

important in regulating cancer phenotypes in many cancer types^{150,151}. Therefore, the first aim of this study was to functionally test whether KLF6 has any biological relevance in supporting ccRCC growth. By utilizing the CRISPR-Cas9 and CRISPRi tools to target KLF6 in several VHL-deficient ccRCC cell lines, I subsequently investigated specific questions below which were important to achieve the main objective of this aim 1:

- a) **Does targeting KLF6 affects ccRCC cells proliferation *in-vitro*?**
- b) **Would the reintroduction of exogenous KLF6 into the KLF6-targeted ccRCC cells rescue the cells growth defect?**
- c) **Does targeting KLF6 impairs ccRCC cells growth and tumour forming capability *in-vivo*?**
- d) **What is the effect of targeting KLF6 on the ccRCC cells capability to metastasize and colonize the lung?**

Aim 2: Investigating the super enhancer role in regulating KLF6 expression

Regular enhancer as well as super enhancer can drive the expression of their downstream targets that are located thousands of base pairs away. Therefore, one of the questions that would be addressed in this aim 2 was **(a) whether this large super enhancer spanning the KLF6 locus actually drives *KLF6* expression in ccRCC**. In addition, I would also examine **(b) whether this super enhancer region is sensitive to the perturbation in the activity of its constituent enhancers**. This is because several studies have demonstrated that cancer-associated super enhancers could be sensitive to the perturbation of its constituent enhancers or regulatory components that maintain the super enhancer landscape^{165,169}. Both CRISPRi-mediated enhancer inactivation and CRISPR-Cas9-mediated super enhancer deletion would be utilized in order to address these two important questions.

Moreover, multiple transcription factors and co-activators can bind to the large super enhancer region and co-regulate the expression of their downstream targets. Therefore, in this aim 2, I would also try to identify the KLF6 upstream regulator which I specifically interested in investigating **(c) whether the transcription factor HIF2A binds to the super enhancer region and drives *KLF6* expression in ccRCC.**

Aim 3: Dissecting the mechanisms through which KLF6 supports ccRCC growth

The KLF6 biological relevance and its upstream regulator were investigated in aim 1 and 2, respectively. Next, in this aim 3, I tried to elucidate the transcriptional program regulated by *KLF6* and understand how KLF6 perturbation led to impaired ccRCC cells growth and fitness. The following are questions that I would specifically interrogate which would in turn contribute to attaining the main objective of this aim 3:

- a) What are the differentially expressed genes between the KLF6-targeted and control ccRCC cells?**
- b) Are there any significantly deregulated pathways in the KLF6-targeted ccRCC cells?**
- c) Does directly perturbing this pathway (identified in b) reduces ccRCC cells growth and fitness?**
- d) How does KLF6 involve in regulating this deregulated pathway and subsequently supports ccRCC cells growth and fitness?**

Collectively, the findings and observations obtained from these three main aims would be utilised to propose a model of KLF6-mediated transcriptional dependency that supports ccRCC cells growth and fitness.

Chapter 2

Materials and Methods

2.1 Cell lines, plasmids and reagents

The human ccRCC cell lines; 786-O, 786-M1A, OS-RC2, OS-LM1 and RCC-MF, were obtained from J. Massagué (Memorial Sloan Kettering Cancer Center, NY). The 786-M1A and OS-LM1 are the metastatic derivative of 786-O and OS-RC2 cells, respectively, which were established and described previously¹⁷³. The UOK101 cell line was obtained from Marston Linehan (National Cancer Institute, MD). The A549 lung cancer cell line was obtained from C. Martins (MRC Cancer Unit). The identity of all cell lines used in this study was confirmed by STR analysis. Additionally, the identity of ccRCC cell lines were also validated via Sanger sequencing-based detection of known VHL mutations that are unique to each of these cell lines. MycoAlert™ Mycoplasma Detection Kit (Lonza LT07-318) was used for mycoplasma screening. All ccRCC cell lines and the A549 cell line were cultured in RPMI-1640 medium (R8758 Sigma) supplemented with 10% FBS, penicillin (100U mL⁻¹) and streptomycin (μg mL⁻¹). HEK293T cells were used for lentivirus production and cultured in DMEM (Invitrogen), supplemented with 10% FBS, penicillin (100U mL⁻¹) and streptomycin (μg mL⁻¹).

The doxycycline-inducible Cas9 plasmid, pCW-Cas9, was a gift from Eric Lander and David Sabatini (Addgene plasmid #50661)¹⁷⁴. The constitutive Cas9 plasmid, lentiCas9-Blast, was a gift from Feng Zhang (Addgene plasmid #52962)¹⁷⁵. The constitutive dCas9 plasmid, pHR-SFFV-KRAB-dCas9-P2A-mCherry, was a gift from Jonathan Weissman (Addgene plasmid #60954)¹⁷⁶. The sgRNA expression vector, pKLV-U6-gRNA(BbsI)-PGKpuro2ABFP, was a gift from Kosuke Yusa (Addgene plasmid #50946)¹⁷⁷. This vector was modified to generate the following variants: 1) pKLV-U6-gRNA(BbsI)-PGKhygro2ABFP, 2) pKLV-U6-gRNA(BbsI)-PGKhygro2AmCherry 3) pKLV-U6-gRNA(BbsI)-PGKhygro2AeGFP. The strategy to generate

these mCherry and eGFP variants are described in details in section 2.8 and 2.9 below. The pLVX-Puro (Clontech #632164) and pLVX-Hygro (modified by Paulo Rodrigues) were used to express the exogenous cDNA constructs. For lentivirus production, the packaging plasmids psPAX2 (Addgene plasmid #12260) and pMD2.G (Addgene plasmid #122259) were gifts from Didier Trono. The shRNA expression vector, sGEP and LT3-GEPIR, were gifts from Johannes Zuber. All sgRNA and shRNA constructs, and primers used in this study were purchased from Sigma-Aldrich and these sequences are listed in Table 1 - 3 of this chapter.

Simvastatin (S6196), fatostatin (F8932), propylene glycol (W294004) and Tween-80 (P1754) were purchased from Sigma-Aldrich. Everolimus was purchased from APEX BIO (A8169). The recombinant human PDGF-BB was purchased from Peprotech (#100-14B). D-Luciferin was purchased from Syd Labs (MB000102-R70170).

Table 1. sgRNAs and shRNAs sequence

| Construct | Sequence (5'-3') |
|----------------------|--|
| sgNTC | GAGTGTCTGTCGTTGCTCCTA |
| sgKLF6_4 | TCGCCAGGGAAGGTGCGCAG |
| sgKLF6_5 | CCCACTTGAAAGCACACCAG |
| Control (Tandem) | ATCGAAGACAACACCCGGAGTGTCTGTCGTTGCTCCTAGTTTTAGAGCGC AGGTGTCTGCCACCTGCGAAACACCCGGGATACGGTGCCTCAATCTAGTT TTACAGTCTTCTCG |
| iKLF6_2 | ATCGAAGACAACACCCGGCTCGCAGAGACGCCCGGCGTTTTAGAGCGC AGGTGTCTGCCACCTGCGAAACACCCGGGCGAGGCGCGCGGTGGGAGC GTTTTACAGTCTTCTCG |
| iKLF6_3 | ATCGAAGACAACACCCGGCTCGCAGAGACGCCCGGCGTTTTAGAGCGC AGGTGTCTGCCACCTGCGAAACACCCGGTTACGTTTGCAGTCAGTCGTT TTACAGTCTTCTCG |
| iPDGFB_1 | CCTCCCCCGCTGCCTCCCTA |
| iPDGFB_2 | GGAGCCCTAGGGAGGCAGCG |
| iSREBF1/2 combo 1 | ATCGAAGACAACACCCGCAGGACACGAACGCGCGGAGTTTTAGAGCG CAGGTGTCTGCCACCTGCGAAACACCCGCGGGCGCAACGCAAAACATGGG TTTTACAGTCTTCTCG |
| iSREBF1/2 combo 2 | ATCGAAGACAACACCCGGTGTCTGCTGCCCTGGCCTCAGGTTTTAGAGCG CAGGTGTCTGCCACCTGCGAAACACCCGCGCAACGCAAAACATGGCGGCG TTTTACAGTCTTCTCG |
| iSE_1 | ATCGAAGACAACACCCGAGAATCGCTGAAGAAACGCGGTTTTAGAGCG CAGGTGTCTGCCACCTGCGAAACACCCGACTGCACTGAAGACTCGGAG TTTTACAGTCTTCTCG |
| iSE_2 | ATCGAAGACAACACCCGACCAGCACAATTTGTCACCGGTTTTAGAGCGC AGGTGTCTGCCACCTGCGAAACACCCGTTGAAAAAAACCTATCACAGTT TTACAGTCTTCTCG |
| iSE_3 | ATCGAAGACAACACCCGATGTGGCTCTGAATCACCATGTTTTAGAGCGC AGGTGTCTGCCACCTGCGAAACACCCGAACGGTGAGTTCCCGGTACAGT TTTTACAGTCTTCTCG |

| | |
|--------------------------|---|
| iSE_4 | ATCGAAGACAACACCCGAGTTGGAAAGTTGCATGCTGGTTTTAGAGCG CAGGTGTCGCCACCTGCGAAACACCGTTACACCAACAGATAAATATGT TTTACAGTCTTCTCG |
| iSE_5 | ATCGAAGACAACACCCGATAAAGCCTGTTATTACCAAGTTTTAGAGCGC AGGTGTCGCCACCTGCGAAACACCGTTAGCTAATGCTGAACAGAGGTT TTACAGTCTTCTCG |
| Del SE_2 | ATCGAAGACAACACCCGTAGAATGTATTAGTCTTGTGGTTTTAGAGCGC AGGTGTCGCCACCTGCGAAACACCGTGGGGTCTTAGGTACCCGAAGT TTTACAGTCTTCTCG |
| Del SE_3 | ATCGAAGACAACACCCGTGGATCCATGATTGATGCATGTTTTAGAGCGC AGGTGTCGCCACCTGCGAAACACCGACAGCTAGTTAGTGACACGAGT TTTACAGTCTTCTCG |
| iHIF2a binding site_1 | ATCGAAGACAACACCCGTCACTCATCTCAGAGAAATGGTTTTAGAGCGC AGGTGTCGCCACCTGCGAAACACCGTCTGTGTTGCTAAATCCCGAGTT TTACAGTCTTCTCG |
| iHIF2a binding site_2 | ATCGAAGACAACACCCGACTGGATACGTGGAGTTATGGTTTTAGAGCGC AGGTGTCGCCACCTGCGAAACACCGATTTCAAAACACATTTCACGTT TTACAGTCTTCTCG |
| shREN 713 | TGCTGTTGACAGTGAGCGCAGGAATTATAATGCTTATCTATAGTGAA GCCACAGATGTATAGATAAGCATTATAAT TCCTATGCCTACTGCCTCGGA |
| shEPAS1_4 | TGCTGTTGACAGTGAGCGACCAGGTGAAAGTCTACAACAATAGTGAA GCCACAGATGTATTGTTGTAGACTTTCACCTGGCTGCCTACTGCCTCG GA |
| shEPAS1_9 | TGCTGTTGACAGTGAGCGCCCAGCAGATGGACAACCTGTATAGTGAA GCCACAGATGTATACAAGTTGTCCATCTGCTGGTTGCCTACTGCCTCG GA |

Table 2. PCR and ChIP-qPCR primers sequence

| Construct | Sequence (5'-3') |
|-------------------------|--|
| KLF6 cDNA PCR F | ATGGACGTGCTCCCCATGTG |
| KLF6 cDNA PCR R | ACATGAAGAGGCACCTCTGA |
| Flag KLF6 cDNA PCR F | ATGGACTATAAGGACCACGACGGAGACTACAAGGATCATGATA TTGATTACAAAGACGATGACGATAAGGGCTCCGGAGACGTGCT CCCCATGTGCAG |
| Flag eGFP cDNA PCR F | ATGGACTATAAGGACCACGACGGAGACTACAAGGATCATGATA TTGATTACAAAGACGATGACGATAAGGGCTCCGGAGTGAGCAA GGGCGAGGAGCT |
| Flag eGFP cDNA PCR R | TTACTTGTACAGCTCGTCCA |
| Tandem oligo PCR F | TAGACATCGAAGACAACACCG |
| Tandem oligo PCR R | GCGACGAGAAGACTGTAAAAC |
| shRNA PCR F | TGAACTCGAGAAGGTATATTGCTGTTGACAGTGAGCG |
| shRNA PCR R | TCTCGAATTCTAGCCCCTTGAAGTCCGAGGCAGTAGGC |
| PGKhygro-2A PCR F | ATCGGGATCCAATTCTACCGGGTAGGGGAG |
| 2A-PCR R | TGGGCCAGGATTCTCCTCCACG |
| 2A-mCherry PCR F | GTGACGTGGAGGAGAATCCTGGCCCAATGGTGAGCAAGGGCG AGGAGG |
| 2A-mCherry PCR R | ATCGCGGCCGCTTACTTGTACAGCTCGTCCA |
| 2A-eGFP PCR F | GTGACGTGGAGGAGAATCCTGGCCCAATGGTGAGCAAGGGCG AGGAGC |
| 2A-eGFP PCR R | CCTAGCGGCCGCTTACTTGTACAGCTCGTCCATGCC |
| SE del. PCR screening F | CTAGTGGACGAAGGGTTGGA |
| SE del. PCR screening R | AACAACCGGAATCTCCACTG |
| EPAS1 locus PCR F | GGATTTTCAGACTGTTGAAT |
| EPAS1 locus PCR R | CCTACAGAAGAACAGACATG |

| | |
|-------------------------------|-----------------------------|
| Flag KLF6 ChIP qPCR (PDGFB) F | ATTCCGGGTAGACTTGCCAA |
| Flag KLF6 ChIP qPCR (PDGFB) R | GCACGGGAGATGGGGTATAA |
| Flag KLF6 ChIP qPCR (PDGFB) R | GCACGGGAGATGGGGTATAA |
| ChIP qPCR iSE-1 F | GAAGTTGAGTCCCGGTGAAA |
| ChIP qPCR iSE-1 R | ATACCCGTCCTGGGAAAATC |
| ChIP qPCR iSE-2 F | TCTGTAGCTGCTGAGGCTGA |
| ChIP qPCR iSE-2 R | CACGGTGACAAATTGTGCTG |
| ChIP qPCR iSE-3 F | CAGGGAGTGGAAGCTGATGT |
| ChIP qPCR iSE-3 R | CACGCTTGCTGATTTCAAAG |
| ChIP qPCR iSE-4 F | CACAGATTTAAGGTGGCTGTCA |
| ChIP qPCR iSE-4 R | CAAAAGCCAAAATGATGGA |
| ChIP qPCR iSE-5 F | GCGCTTTTCCAATCAGAGTC |
| ChIP qPCR iSE-5 R | CTGAAACCTCCTCTTCAAACAA |
| ChIP-qPCR Ctrl 1 F | TGCGTATTAATGCTTTTCATTCC |
| ChIP-qPCR Ctrl 1 R | TCAATTAGTAAAGAATGATGCTTGAAA |
| ChIP-qPCR Ctrl 2 F | CTGCTGTTTGGGGAGCTTAC |
| ChIP-qPCR Ctrl 2 | CTGCCTCCTGAATGATGACA |

Table 3. Sequencing primers

| Construct | Sequence (5'-3') |
|---|--|
| sgKLF6_4 targeted region F | P5- <i>Read1 sequencing template</i> -TTGCGTGCCCCGGGGAGCT |
| sgKLF6_4 targeted region R | P7- <i>Index-Index sequencing template</i> -CAAGTGGGAGCTTTTGGTGT |
| sgKLF6_5 targeted region F | P5- <i>Read1 sequencing template</i> -GGAAAGTTTACACCAAAGCT |
| sgKLF6_5 targeted region R | P7- <i>Index-Index sequencing template</i> -CTTTGGTGGAAAACATCTGA |
| M13 F (TOPO cloning) | GTAAAACGACGGCCAGT |
| M13 R (TOPO cloning) | CAGGAAACAGCTATGAC |
| U6 Promoter F (single sgRNA cloning) | GAGGGCCTATTTCCCATGATTCC |
| Tandem pKLV F (tandem sgRNA cloning) | AGTACCGGGCCCTACG |
| Tandem pKLV R (tandem sgRNA cloning) | GGAAAAGCGCCTCCCCT |
| miR-Seq 5 F (shRNA cloning) | TGTTTGAATGAGGCTTCAGTAC |
| pCEP F (CDNA cloning) | AGAGCTCGTTTAGTGAACCG |
| 786-M1A VHL validation F | CTCCCAGGTCATCTTCTGCAA |
| 786-M1A VHL validation R | AGTTCCCCGTCTGCAAAATG |
| OS-LM1 VHL validation F | AGTACGGCCCTGAAGAAGAC |
| OS-LM1 VHL validation R | CGTCGAAGTTGAGCCATACG |
| RCC-MF VHL validation F | AGTACGGCCCTGAAGAAGAC |
| RCC-MF VHL validation R | AGTTCCCCGTCTGCAAAATG |

2.2 Genomic DNA and plasmid extraction

Genomic DNA was extracted by using the QIAamp DNA mini kit (Qiagen #51304) according to the manufacturer's protocol. For the midi and miniprep plasmids extraction, the PureYield™ Plasmid Midiprep System (Promega A2492) and Quick Clean II Plasmid miniprep kit (GenScript L00420) were used, respectively, by following the manufacturer's recommendations. The yield and purity of the extracted materials were determined by using NanoDrop™ 1000 Spectrophotometer (Thermo).

2.3 Sanger sequencing

The Mix2Seq Kit (Eurofins Genomics) was used for Sanger sequencing. The samples were prepared according to the manufacturers recommendations.

2.4 Production of chemically competent *E.coli*

The NEB5α competent *E.coli* (NEB C2987H) was cultured in LB broth overnight. On the following day, the bacteria culture was diluted 1:100 in fresh LB broth and grown until the optical density (600nm) reached between 0.6-0.65. The optical density was measured using the Eppendorf Biophotometer plus. The bacteria culture was incubated on ice for 30 minutes, followed by spinning down at 3500 rpm for 10 minutes at 4°C. The bacteria pellets were gently resuspended in 50mM ice-cold CaCl₂ and incubated on ice for another 15 minutes. The bacteria suspension was spun down at 3500 rpm at 4°C for 15 minutes. The bacteria pellets were gently resuspended in 17mL 50mM ice-cold CaCl₂ and 3mL 100% glycerol was added into the solution. The chemically competent bacteria were aliquoted and stored in the -80°C freezer.

2.5 Bacteria transformation

The *to-be-transformed* plasmids were added onto the chemically competent *E.coli* and mixed by gentle flicking. The bacteria-plasmid mix was incubated on ice for 30 minutes, followed by heat-shocking at 42°C for 1 minute and incubation on ice for another 5 minutes. After adding the SOC recovery media, the bacteria culture was incubated on shaking incubator at 37°C for an hour. The transformed bacteria were then plated on LB + ampicillin plate and incubated at 37°C overnight.

2.6 Lentiviral production and transduction

The plasmid of interest (1.5µg) was mixed with the lentiviral packaging plasmids, psPAX2 (1.3µg) and pMD2.G (0.5µg), in the Opti-MEM™ I Reduced-Serum Medium (Gibco LS31985062). The FuGENE 6 transfection reagent (Promega E269A) was also diluted in the Opti-MEM™ I Reduced-Serum Medium and added dropwise onto the plasmids mixture, followed by incubation at the room temperature for 30 minutes. The FuGENE 6-plasmids mixture was gently added onto the HEK293T cells (seeded onto the 6-wells plate a day prior to the transfection). The media containing lentivirus were collected 72-hours post-transfection. Briefly, the media containing the lentivirus were spun down at 1000 RPM for 5 minutes to pellet any cells or cellular debris. The supernatant was transferred into a syringe and filtered through a 0.45µM PVDF sterile filter (Elkay Laboratory E25-PV45-50S). The lentivirus containing supernatant was either directly used for cells transduction or stored in the -80°C freezer.

Cells were seeded onto the 6-wells plate at a density of 250000–300000 cells/well 24 hours before the transduction. The lentivirus supernatant was added onto the cells in the presence of 8µg/mL Polybrene (Merck Millipore TR-1003). After overnight incubation, media containing

the lentivirus supernatant was removed, followed by washing the transduced cells with 1x PBS twice. Fresh media was added onto the cells. The positively transduced cells were either antibiotic selected or sorted by using FACS. The antibiotic selection was started 48-hours post-transduction whereas the cells sorting was performed by the Flow Cytometry Core Facility, Cambridge Institute for Medical Research (CIMR) at least a week post-transduction.

2.7 Generation of stable Cas9 and dCas9-expressing ccRCC cell lines

To generate stable Cas9-expressing ccRCC cell lines, the cells were transduced with lentivirus carrying either the lentiCas9-Blast or pCW-Cas9 plasmid. The lentiCas9-Blast and pCW-Cas9 plasmid encode for constitutive and doxycycline-inducible human codon-optimized *S. pyogenes* Cas9 protein, respectively. The lentiCas9-Blast- and pCW-Cas9-transduced cells were selected with 30µg/mL blasticidin (Invivogen ant-bl) and 4µg/mL puromycin (Invivogen ant-pr), respectively. Cells were transduced with the pHR-SFFV-KRAB-dCas9-P2A-mCherry plasmid to generate stable dCas9-KRAB-expressing cells (CRISPRi cells). The positively transduced cells were sorted based on the expression of mCherry fluorescent protein.

2.8 Construction of the pKLV-U6-gRNA(BbsI)-PGKhygro2AmCherry

The pKLV-U6-gRNA(BbsI)-PGKhygro2AmCherry sgRNA expression vector was constructed by first generating the PGKhygro2AmCherry fragment. The *BamHI*-PGKhygro2A fragment (hereinafter referred to as 5' fragment) was amplified from the pKLV-U6-gRNA(BbsI)-PGKhygro2ABFP plasmid. The mCherry-*NotI* fragment (hereinafter referred to as 3' fragment) was amplified from the pHR-SFFV-KRAB-dCas9-P2A-mCherry plasmid and complementary 2A overhang sequences were incorporated into the 5' end of this mCherry-*NotI* fragment. The PCR amplification was performed using the 2x Accuzyme™ Mix (Bioline Bio-

25028) according to the manufacturer's protocols. Gradient temperature PCR was performed to determine the optimum annealing temperature to amplify each of these 5' and 3' fragments. These amplified fragments were purified using the Quick Clean II Gel Extraction Kit (GenScript L00418) and fused together via two rounds of PCR amplification.

Briefly, the first round of PCR was performed without adding the primers. These 5' and 3' fragments annealed to each other at the complementary 2A sequences that resulted in self-amplification. The self-amplified, fused product was then amplified using the forward and reverse primers used to initially amplify the 5' fragment and 3' fragment, respectively. The fused PGKHygro2AmCherry fragment was double-digested with 10 unit/ μ g *Bam*HI (NEB R0136) and 10 unit/ μ g *Not*I (NEB R0189) according to manufacturer's recommendations and ligated into the *Bam*HI and *Not*I-double digested pKLV-U6-gRNA(BbsI)-PGKhygro2ABFP plasmid. The ligation was performed at room temperature for at least 30 minutes using the T4 ligase (Thermo EL0011) at a ratio of insert to vector 5:1 (<https://nebiocalculator.neb.com>), followed by bacteria transformation. The strategy to construct the pKLV-U6-gRNA(BbsI)-PGKhygro2AmCherry plasmid is illustrated in figure 9.

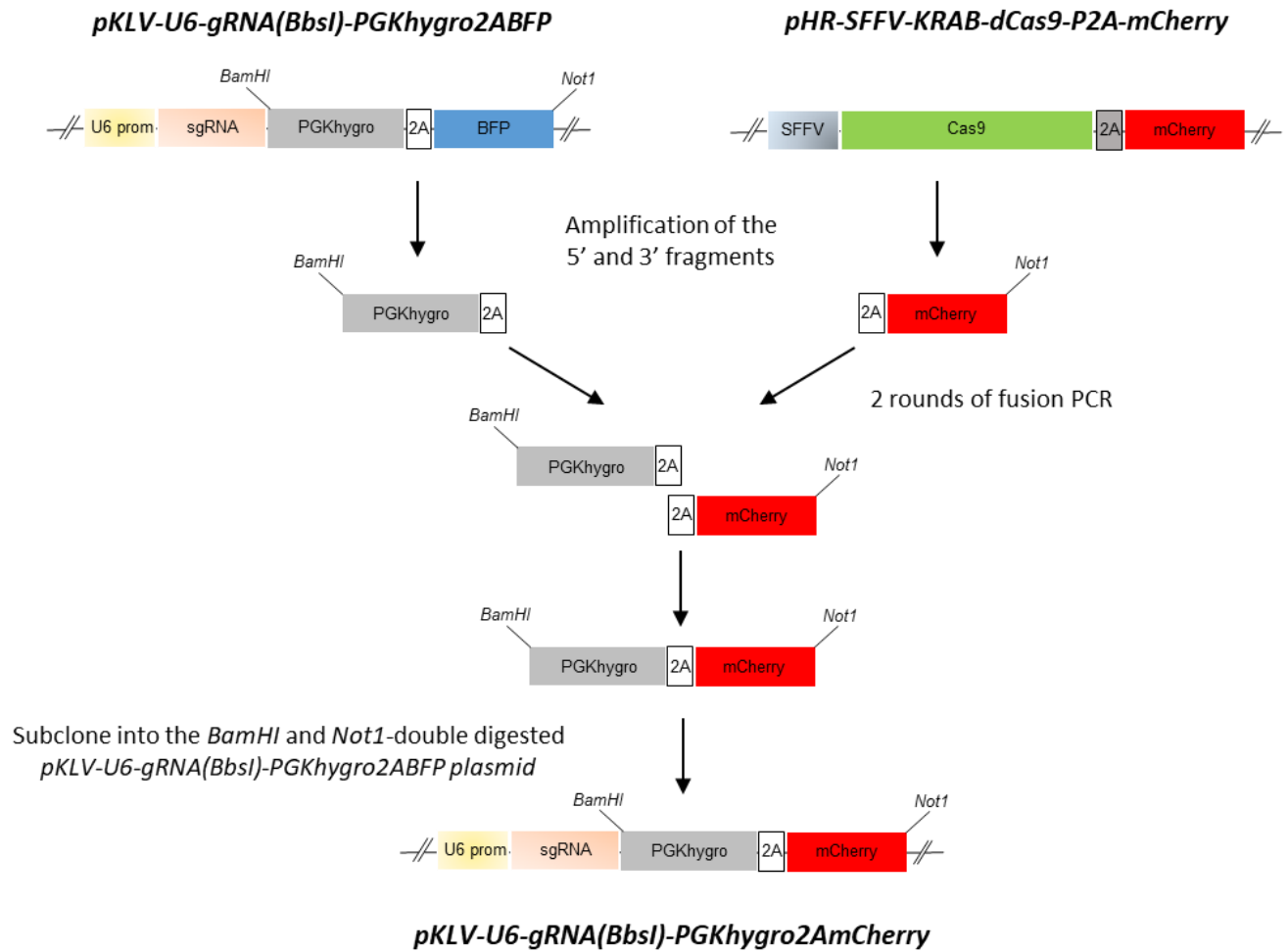


Figure 9: Strategy to construct pKLV-U6-gRNA(BbsI)-PGKhygro2AmCherry sgRNA expression vector.

2.9 Construction of the pKLV-U6-gRNA(BbsI)-PGKhygro2AeGFP

Similar strategy to construct the pKLV-U6-gRNA(BbsI)-PGKhygro2AmCherry was employed to generate the pKLV-U6-gRNA(BbsI)-PGKhygro2AeGFP sgRNA expression vector. The only modification was the 2AeGFP-*NotI* fragment (3' fragment) was amplified from the LT3-GEPIR plasmid.

2.10 Cloning single sgRNA construct into the sgRNA expression vector

The pKLV-U6-gRNA(BbsI)-PGKhygro2ABFP was digested with 10 unit/ μ g *BbsI* (NEB R0539), followed by treatment with 5 unit/ μ g Antarctic Phosphatase (NEB M0289) according to the manufacturer's protocol. The sgRNA construct sense and anti-sense strands were purchased separately from Sigma-Aldrich. *BbsI* restriction site overhang was incorporated into the 5' end of these sense and anti-sense strands as exemplified in figure 10. Both strands were annealed together and phosphorylated by using T4 Polynucleotide Kinase (NEB M0201) and T4 ligation buffer (Thermo EL0011). The reaction was incubated at 37°C for 30 minutes, followed by heat-inactivation at 95°C for 5 minutes. The annealed sgRNA construct was diluted 1/200 in DNase/RNase-free water and ligated into the sgRNA expression vector. The ligation was performed using the T4 ligase as described previously, followed by transformation into the chemically competent *E.coli*. The presence of the ligated sgRNA construct was confirmed and sequence-verified via Sanger sequencing. Cells that were transduced with this sgRNA expression vector were either selected with 90 μ g/mL hygromycin (Invivogen ant-hg) or sorted based on the expression of BFP fluorescent protein.

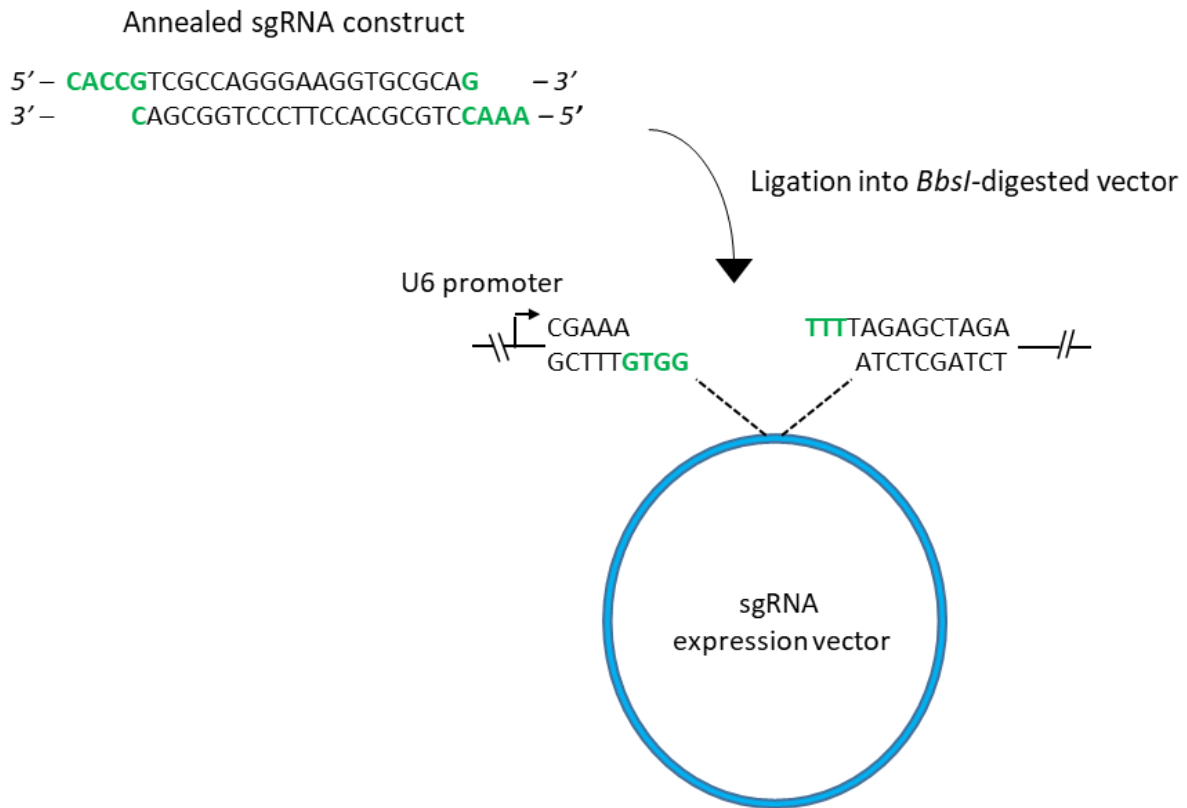


Figure 10: Strategy to clone single sgRNA construct into the pKLV-U6-gRNA(*BbsI*)-PGKhygro2ABFP.

Different strategy was employed for cloning the single sgRNA construct into the pKLV-U6-gRNA(*BbsI*)-PGKhygro2mCherry due to the presence of additional *BbsI* restriction site within the mCherry fluorescent DNA sequence. To overcome this, the sgRNA construct was first cloned into the BFP sgRNA expression vector as described previously. This was followed by double digesting the sgRNA construct-ligated BFP sgRNA expression vector with 10 unit/ μ g *XhoI* (NEB R0146) and *BamHI* to release the *U6 promoter-sgRNA construct-sgRNA scaffold* fragment. The released fragment was gel purified and sub-cloned into the AnP treated, *XhoI* and

BamHI double-digested the pKLV-U6-gRNA(*BbsI*)-PGKhygro2mCherry. The strategy employed to clone single sgRNA construct into the mCherry sgRNA expression vector is simplified in figure 11. Cells that were transduced with this mCherry sgRNA expression vector were either selected with 90µg/mL hygromycin (Invivogen ant-hg) or sorted based on the expression of mCherry fluorescent protein.

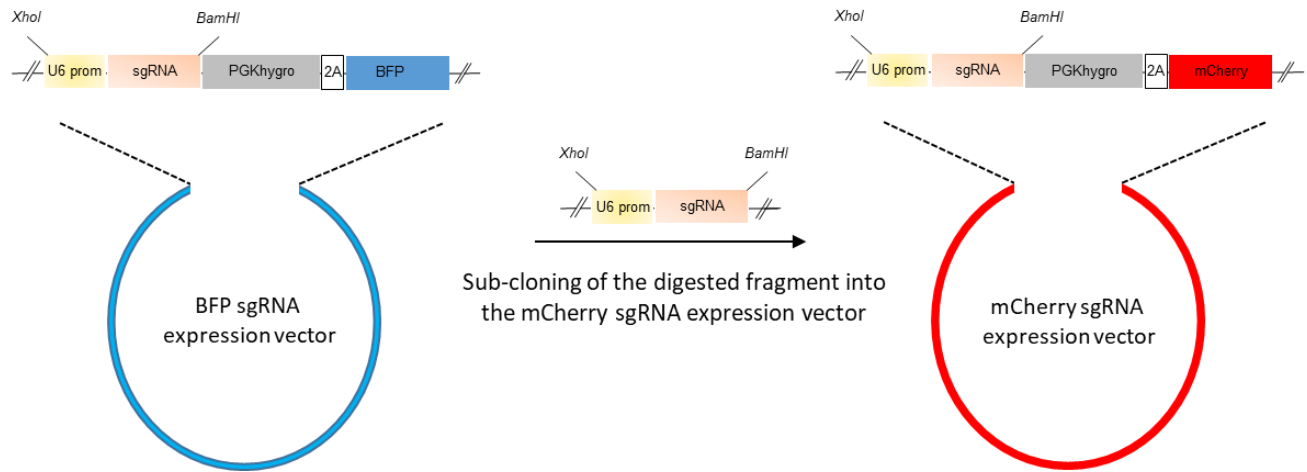


Figure 11: Strategy to clone single sgRNA construct into the pKLV-U6-gRNA(*BbsI*)-PGKhygro2AmCherry.

2.11 Cloning tandem sgRNAs construct into the sgRNA expression vector

The tandem sgRNAs construct was designed to express two independent sgRNAs. *AarI* restriction site was incorporated between these sgRNAs sequences with *BbsI* restriction sites flanking the constructs. The *BbsI* restriction sites were utilised to clone the tandem sgRNAs construct into the sgRNA expression vector. The *AarI* restriction site was used to clone an additional sgRNA scaffold-U6 promoter fragment into the tandem sgRNAs construct-ligated sgRNA expression vector.

In brief, the tandem sgRNAs construct was first amplified using the AccuPrime™ PFX supermix (Thermo #12344040) according to the manufacturer's protocol. The PCR primers and conditions used to amplify this tandem sgRNAs construct are listed in table 2 of this chapter and supplementary table 1 in the appendices, respectively. The amplified tandem sgRNAs construct was gel purified and digested with *BbsI* restriction enzyme. This was followed by ligation into the AnP treated, *BbsI*-digested sgRNA expression vector and transformation into the chemically competent *E.coli*. The presence of the ligated tandem sgRNAs construct was confirmed and sequence-verified via Sanger sequencing. The sequence-verified plasmid was subsequently digested with 1 unit/μg *AarI* restriction enzyme (Thermo ER1581) according to the manufacturer's recommendations and AnP-treated.

The *to-be-cloned* additional sgRNA scaffold-U6 promoter fragment was previously cloned into the pBigT plasmid. This plasmid was digested with *AarI* restriction enzyme to release the sgRNA scaffold-U6 promoter fragment. This released fragment was gel purified and subsequently cloned into the AnP treated, *AarI*-digested plasmid described above. The ligated plasmid was transformed into the chemically competent *E.coli* and the presence of the ligated sgRNA scaffold-U6 promoter fragment was confirmed via Sanger sequencing. Figure 12 shows schematic of the tandem sgRNAs construct and strategy to clone this construct into the sgRNA expression vector.

and sequence-verified via Sanger sequencing. The shRNA construct cloning strategy into the sGEP expression vector is illustrated in figure 13.

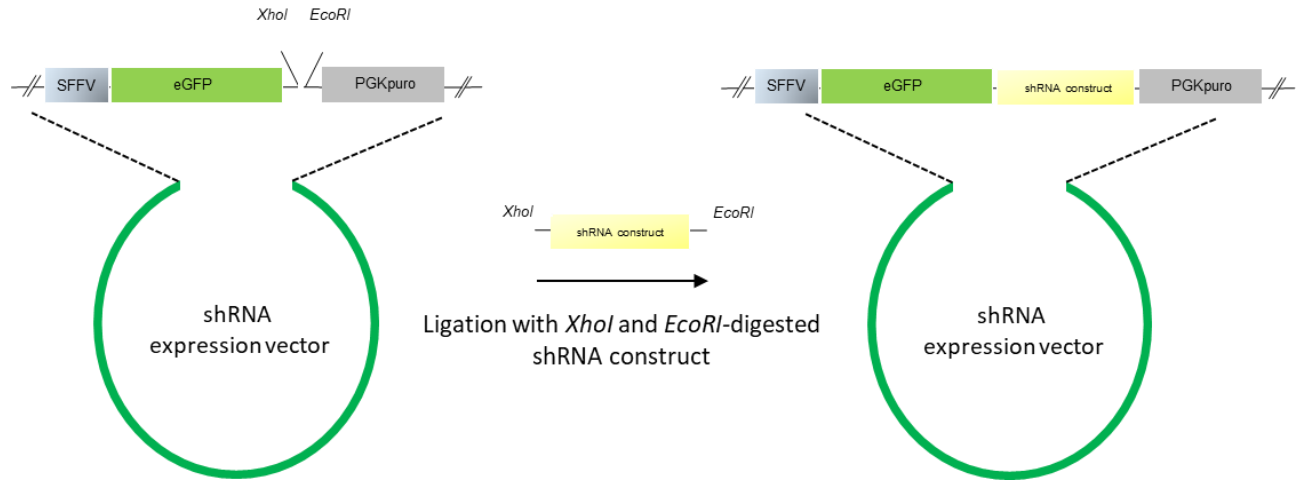


Figure 13: Strategy to clone shRNA construct into the sGEP shRNA expression vector.

2.13 Expressing exogenous KLF6

Either pLVX-Puro or pLVX-Hygro expression vector was used to express the exogenous *KLF6*. The *KLF6* coding sequence (CDS) was amplified from cDNA synthesized from the 786-M1A cells. The *EcoRI* restriction site was incorporated before the start codon whereas *BamHI* restriction site was incorporated after the stop codon, in which these restriction sites were utilised for cloning the *KLF6* CDS into the expression vector multiple cloning site. The PCR primers and conditions used to amplify *KLF6* CDS are listed in table 2 of this chapter and supplementary table 3 in the appendices, respectively. The amplified *KLF6* CDS was sequence-verified via Sanger sequencing, followed by double digestion with *EcoRI* and *BamHI* restriction enzymes and ligation into the AnP treated, *EcoRI* and *BamHI*-digested expression vector. The ligated

plasmids were transformed into the chemically competent *E.coli*. The presence of the ligated transgene was confirmed and sequence-verified via Sanger sequencing.

Prior to reintroducing exogenous KLF6 into the CRISPR-Cas9 sgKLF6_4 786-M1A cells, the region targeted by this sgRNA in the exogenous KLF6 CDS was modified using the site-directed mutagenesis approach. Briefly, this was performed by amplifying the KLF6 CDS-ligated expression vector (described above) using primers that bound to the sgKLF6_4 target region. These primers harboured the *to-be-introduced* synonymous mutations. The amplified plasmids were subsequently treated with *DpnI* restriction enzyme (NEB R0176) which would only digest the methylated parental plasmid, not the site-directed mutagenised plasmids. After the *DpnI* treatment, the plasmids were transformed into the chemically competent *E.coli*. Several colonies were picked for plasmid extraction, followed by sending these plasmids for Sanger sequencing to validate the presence of the reintroduced synonymous mutations.

For the Flag ChIP experiment, the 5' end of KLF6 and eGFP CDS was tagged with Flag. To generate the Flag-KLF6, 3x Flag sequences were incorporated into the 5' end of the previously used KLF6 CDS forward primer. The constructed pLVX-Puro_KLF6 CDS plasmid was used as the template to amplify the Flag-KLF6 CDS in which the cloning was performed as described above. The pKLV-U6-gRNA(BbsI)-PGKhygro2AeGFP was used as the template to amplify the Flag-eGFP. The forward primer was designed to contain the 3x Flag sequences and *EcoRI* restriction site whereas *BamHI* restriction site was incorporated into the reverse primer. Similar cloning strategy as described above was employed to construct the pLVX-Puro_Flag-eGFP. Both engineered plasmids were sequence-verified via Sanger sequencing before using them in the subsequent ChIP experiments. The primers and PCR conditions used to construct these plasmids are listed in table 2 of this chapter and supplementary table 4-5 in the appendices,

respectively. Figure 14 shows the cloning strategies to generate the pLVX-Puro_KLF6 CDS and pLVX-Puro_Flag-KLF6 CDS plasmids.

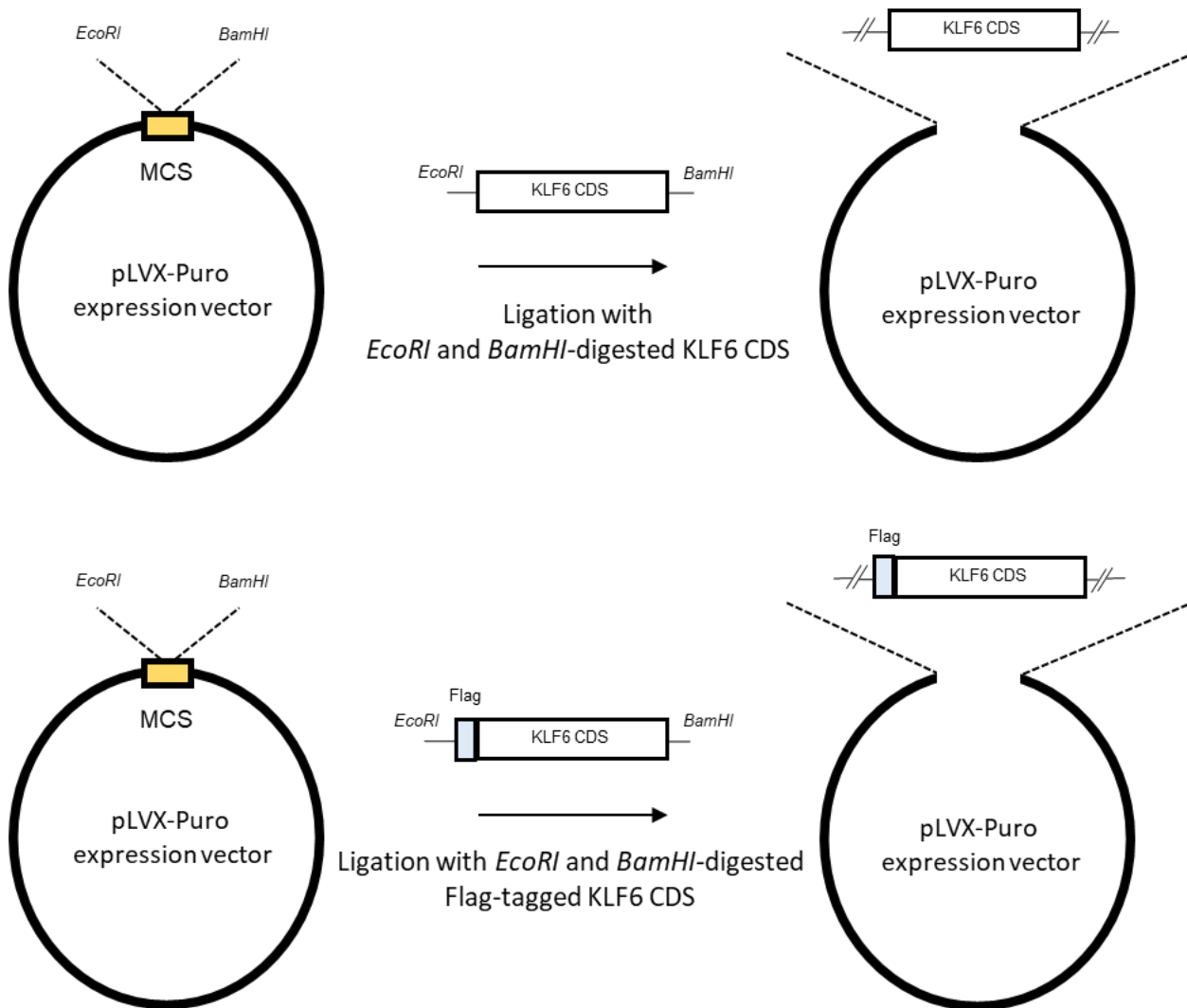


Figure 14: Strategy to clone exogenous KLF6 CDS into the expression vector. (Top) pLVX-Puro-KLF6 CDS and (Bottom) pLVX-Puro_Flag-KLF6 CDS.

2.14 TOPO-TA cloning

Genomic DNA was extracted from the sgKLF6₄-transduced 786-M1A cells. Region targeted by the sgKLF6₄ was amplified using the AccuzymeTM Mix (Bioline) according to the manufacturer's recommendations, followed by gel purification. The 3'A overhang was incorporated into the gel purified amplicons using the BIOTAQTM DNA polymerase (Bioline BIO-21040). The product was cloned into the PCR 4-TOPO vector (Thermo #450071) according to the manufacturer's protocol and subsequently transformed into the chemically competent *E.coli*. The recipes and PCR conditions used for incorporating the 3' overhang and cloning into the TOPO vector are listed in supplementary table 6 in the appendices. Several individual colonies were picked for plasmids extraction and sent for Sanger sequencing.

2.15 RNA extraction and cDNA synthesis

Total RNA was extracted from the cells using the RNAzol[®]RT (Sigma-Aldrich R4533) by following the manufacturer's protocols. The concentration and purity of the extracted RNA were determined by using the NanoDropTM 1000 Spectrophotometer (Thermo). 1µg of total RNA were converted into cDNA using the High-Capacity cDNA Reverse Transcription Kit (Thermo #4368814) according to the manufacturer's protocol.

2.16 Quantitative real-time PCR (qPCR)

The gene expression analyses were performed using the 2x Taqman Fast Advanced master mix (Thermo #4444557) and 20x pre-designed Taqman gene expression probes (Thermo) on the StepOnePlusTM Real Time PCR instrument (Thermo). The default settings for running the

Taqman qPCR were used. The TaqMan probes used in this study are listed in table 4 of this chapter.

Table 4. TaqMan probes

| Probe | Assay ID |
|--------------|-----------------|
| KLF6 | Hs00810569_m1 |
| EPAS1 | Hs01026149_m1 |
| PDGFB | Hs00966522_m1 |
| CXCR4 | Hs00607978_s1 |
| CCND1 | Hs00765663_m1 |
| VEGFA | Hs00900055_m1 |
| BHLHE40 | Hs01041212_m1 |
| SREBF1 | Hs01088679_g1 |
| SREBF2 | Hs01081784_m1 |
| SCD | Hs01682761_m1 |
| LSS | Hs01552331_m1 |
| TBP | Hs00427620_m1 |

The gene of interest Ct value were normalised to the Ct value of the housekeeping gene, *TBP*. The gene expression fold change was calculated using the $2^{-\Delta\Delta Ct}$ method as described previously¹⁷⁸.

2.17 RNA-Seq library preparation and analyses

Total RNA was extracted from the cells in four replicates using the RNeasy Mini Kit (Qiagen #74104) according to the manufacturer's protocols. The quality and concentration of the extracted RNA were determined using the Agilent RNA Nano 6000 kit (Agilent #5067-1511) on the Agilent Bioanalyzer 2100 instrument. The RNA-Seq libraries were prepared using the SENSE mRNA-Seq Library Prep Kit V2 (Lexogen) by following the manufacturer's recommendations with 1µg of total RNA was used as the starting material. The size and quality of the final library products were determined using the Agilent High Sensitivity DNA Kit (Agilent #5067-4626) on the Agilent Bioanalyzer 2100 instrument. The library concentration was determined using the KAPA Library Quantification Kit (KR0405) according to manufacturer's recommendations. The prepped RNA-Seq library from each sample was pooled in equimolar concentrations and sent for Illumina high-throughput sequencing. The RNA-Seq data were analysed by Sakari Vanharanta. Gene set enrichment analysis and pathway analysis were performed by Dora Bihary and Shamith Samarajiwa using the analysed RNA-Seq data.

2.18 Protein extraction and quantification

Cells were either trypsinized or scraped on ice, followed by washing the pelleted cells with 1x ice-cold PBS once. The cells were lysed on ice for 30 minutes in RIPA buffer (Sigma-Aldrich R0278) containing 1:100 protease inhibitor cocktail (Sigma-Aldrich) and 1:100 phosphatase inhibitor cocktail (Sigma-Aldrich). The lysate was vortexed vigorously for 15 seconds and spun down at 4°C for 20 minutes at 14000 RPM. The protein lysates were quantified using the Pierce BCA Protein Assay Kit (Thermo #23225) according to

manufacturer's protocol whereby the absorbance (562nm) was measured by using the Tecan infinite M200 pro plate reader.

2.19 Western blotting

The protein samples were mixed with 4x TruPAGE LDS sample buffer (Sigma-Aldrich PCG3009) and 1:20 B-mercaptoethanol (Sigma M6250), followed by boiling at 95°C for 5 minutes. The protein samples were separated either using 8% or 10% home-made SDS-PAGE gels. The Precision Plus Protein™ Kaleidoscope™ Pre-Stained Protein Standards (BioRad #1610375) was used as the molecular weight marker. The separated proteins were transferred onto Immobilon PVDF transfer membrane (Millipore) for 2 hours. The membrane was blocked at room temperature for 1 hour with either 5% non-fat dry milk in 0.1% PBS-Tween or 5% BSA in 0.1% TBS-Tween. The membrane was incubated with the blocking buffer-diluted primary antibody at 4°C overnight. The primary antibodies and respective dilution used in this study are listed in table 5.

On the following day, the membrane was washed three times with either 0.1% PBS-Tween or 0.1% TBS-Tween (5 minutes/wash), followed by incubation with secondary antibody at room temperature for an hour. The secondary antibodies and respective dilution used in this study are listed in table 5. The secondary antibodies used were polyclonal goat anti-mouse IgG/HRP (Dako, P0447 1:10000) and polyclonal goat anti-rabbit IgG/HRP conjugated (Dako, P0448 1:5000). After washing the membranes three times (5 minutes/wash), the Luminata Classico Western HRP substrate (Millipore WBLUC0500) was added onto the membrane, followed by incubation at room temperature for 5 minutes. The membrane was exposed onto the WB X-ray film (SLS MOL7016) and developed using the film processor machine. The recipes

to prepare the SDS-PAGE gels and buffers for running the Western blotting are listed in supplementary table 7-12 in the appendices.

Table 5. Primary and secondary antibodies

| Antibodies | Catalog number and dilution |
|-------------------------------------|--|
| KLF6 | Santa Cruz Biotech, sc-7158, 1:1000 |
| HIF2A | Novus Biologicals, NB100-122, 1:1000 |
| VHL | BD Biosciences, #564183, 1:1000 |
| P-p70 S6-kinase | Cell Signaling Technology, #9205, 1:1000 |
| p70-S6-kinase | Cell Signaling Technology, #9292, 1:1000 |
| P-S6 ribosomal | Cell Signaling Technology, #4857, 1:3000 |
| S6 ribosomal | Cell Signaling Technology, #2317, 1:1000 |
| SREBP1 | Santa Cruz Biotech, sc-13551, 1:100 |
| SREBP2 | Santa Cruz Biotech, sc-13552, 1:100 |
| FLAG | Sigma-Aldrich, F1804, 1:500 |
| B-actin | Sigma-Aldrich, A1978, 1:20000 |
| Polyclonal goat anti-mouse IgG/HRP | Dako, P0447 1:10000 |
| polyclonal goat anti-rabbit IgG/HRP | Dako, P0448 1:5000 |

2.20 Chromatin Immunoprecipitation (ChIP)

The trypsinized cells were pelleted and crosslinked with 1% formaldehyde diluted in 1x PBS. The crosslinking reaction was performed by incubating the 1% formaldehyde-resuspended cells at the room temperature for 10 minutes. The reaction was quenched with 0.125M glycine,

followed by incubation at the room temperature for 5 minutes. The crosslinked cells were pelleted and washed with 1x PBS twice. After the final wash, the cells were pelleted and then either stored at -80°C or directly used for chromatin immunoprecipitation (ChIP) experiment.

For ChIP, the protein A/G magnetic beads (Thermo #26162) were first equilibrated by washing the beads with 0.5% BSA in 1x PBS three times. After the final wash, the beads were resuspended with 0.5% BSA in 1x PBS. Antibody was subsequently added and conjugated onto the resuspended beads by rotating the tube on a rotating shaker at 4°C for at least 4 hours. The antibodies used in the ChIP experiment are listed in table 6 of this chapter: The crosslinked cells were resuspended and dounced in lysis buffer (20 mM Tris-HCl pH8.0, 150 mM NaCl, 2mM EDTA pH 8.0, 0.1% SDS and 1% Triton X-100), followed by sonication using the Bioruptor (Diagenode) for 14 cycles, 30" on / 30" off. The lysates were spun down at 4°C for 20 minutes at 14000 rpm and the supernatants were collected. The antibody-conjugated beads were washed with 0.5% BSA in 1x PBS three times and after the final wash, the beads were resuspended in 0.5% BSA in 1x PBS. The collected supernatants were added into the antibody-conjugated beads and incubated overnight at 4°C on the rotating shaker.

On the following day, the beads were washed three times with low salt buffer (50 mM HEPES pH 7.5, 140 mM NaCl, 1% Triton) and once with high salt buffer (50 mM HEPES pH 7.5, 500 mM NaCl, 1% Triton). DNA that bound to the antibody-conjugated beads was eluted with the elution buffer (50 mM NaHCO₃, 1% SDS). De-crosslinking was performed by incubating the eluted DNA at 65°C, 1000 rpm for 3 hours. The de-crosslinked DNA was purified using the QuickClean II PCR Extraction Kit (Genescript L00419) according to the manufacturer's recommendations and eluted with DNase/RNase free water.

Table 6. Antibodies used for ChIP experiment

| Antibodies | Catalog number and dilution |
|-----------------------|------------------------------------|
| H3K27ac | Abcam ab4729 |
| FLAG | Sigma-Aldrich F1804 |
| Rabbit polyclonal IgG | Abcam ab27478 |

2.21 ChIP-qPCR

The ChIP-qPCR was performed by adding the purified ChIP DNA into the reaction mix that consisted of 2x PowerUp SYBR Green Master Mix (Thermo A25742), 10 μ M forward and 10 μ M reverse primers to amplify the region of interest. The ChIP-qPCR was run on the StepOnePlusTM Real Time PCR instrument (Thermo) using the default setting for running SYBR green qPCR.

2.22 ChIP-Seq library preparation

The ChIP-Seq library was prepared by Paulo Rodrigues. In brief, the libraries were prepared from the purified ChIP DNA using the KAPA Hyper Prep Kit (KR0961) according to the manufacturer's recommendations. The sequencing libraries were ligated with adapter, followed by size selection using the Agencourt AmPure XP beads (Beckman Coulter A63880) to obtain fragments with the size of 150-350 base pairs. The size-selected fragments were amplified using the KAPA HiFi HotStart ReadyMix PCR Kit (KR0370). The amplified libraries were pooled in equimolar concentration and sent for Illumina high-throughput sequencing. The ChIP-Seq data were analysed by Sakari Vanharanta.

2.23 *In vitro* competitive proliferation assay

For the CRISPR-Cas9 competitive proliferation assay, the Cas9-expressing ccRCC cell lines were transduced with either non-targeting control (sgNTC) or sgRNAs targeting the gene of interest constructs. The sgNTC and sgRNA constructs were initially cloned into the BFP and mCherry variant of the sgRNA expression vector, respectively, or *vice versa* for the fluorescent-swapped experiment. The control and targeted cells were mixed at a 1:1 ratio and plated onto 6-wells plate. The assay was performed for at least 2 weeks or up to 1 month. The percentage of each cell population was analysed at the plating day (T=0) and at multiple time points throughout the assays by flow cytometry on the LSR Fortessa (BD Biosciences). The following gating approaches were used: FSC-A / SSC-A, and FSC-H / SSC-A to select for live and single cells, respectively, and then mCherry (561nm/610nm) / BFP (383nm/445nm) channels for discriminating these two cells populations. Similar strategy was employed for the CRISPRi competitive proliferation assay with slight modification; the BFP⁺ / mCherry⁺ sgRNA-expressing CRISPRi cells were mixed with the mCherry⁺ / BFP⁻ parental CRISPRi cells at a 1:1 ratio. Both CRISPR-Cas9 and CRISPRi competitive proliferation assay strategies are discussed in details in Chapter 3.

2.24 Drug treatment proliferation assay

The drug treatment proliferation assay was performed using the IncuCyte[®] Zoom System (Essen Bioscience). The cells were seeded onto 24-wells plate at a density of 8000 cells / well and transferred into the Incucyte. After overnight incubation, the media was removed and fresh media containing either drug or vehicle was added onto the cells. For the fatostatin treatment proliferation assay, the drug was dissolved in DMSO to make a 20mM stock solution, followed

by further diluting this stock solution with DMSO to make 10mM, 1mM and 0.5mM working solutions. These working solutions were diluted 1:1000 in media to achieve the final concentration of 10 μ M, 1 μ M and 0.5 μ M, respectively, and subsequently added onto the cells.

For the simvastatin treatment proliferation assay, the drug was dissolved and activated according to the manufacturer's protocol. The stock concentration of the activated simvastatin was 10mM. This activated simvastatin was diluted in media to achieve the following final concentrations; 10 μ M, 1 μ M and 0.5 μ M, and added onto the cells. For the everolimus treatment proliferation assay, the drug was dissolved in DMSO to make a 10mM stock solution, followed by further diluting this stock solution with DMSO to make 10 μ M and 1 μ M working solutions. These working solutions were diluted 1:1000 in media to achieve the final concentration of 10nM and 1nM, respectively, and subsequently added onto the cells

2.25 Animal studies

All animal experiments were performed in accordance with protocols approved by the Home Office (UK) and the University of Cambridge Animal Welfare and Ethical Review Body (PPL 70/7990). For subcutaneous tumour growth assay, cells were pelleted and resuspended in PBS/Matrigel Matrix (BD) mix at a 1:1 ratio. 1×10^5 cells in 100 μ L solution were injected into each flank of 5-8 weeks old athymic male nude mice (Charles River Laboratories). The cells proliferation rate and tumour growth were assessed by IVIS bioluminescence imaging (Perkin Elmer) and calliper measurement, respectively. For the bioluminescence imaging, 100 μ L luciferin was injected intraperitoneally into the mice and the imaging was performed 10 minutes post-injection. The cells used in this assay expressed firefly luciferase that catalysed the

oxidation of luciferin to oxyluciferin in the reaction that produced bioluminescence as the by-product.

The calliper measurement was performed after the subcutaneous tumours became palpable. Tumour volume (V) was calculated using the equation $V = (\text{length} \times \text{width}^2) \times 0.5$. At the end of the assay, the mice were euthanized and the subcutaneous tumours were extracted and weighed. For the lung colonisation assay, cells were pelleted and resuspended in 1x sterile PBS. 3×10^5 cells in 100 μ L solution were inoculated into the lateral tail vein of 5-8 weeks old NOD/SCID mice (Charles River Laboratories) and bioluminescence imaging was performed as described above. At the end of the experiment, lungs were extracted from the euthanized mice and processed for immunohistochemistry.

For the *in vivo* everolimus treatment experiment, everolimus was dissolved in 30% propylene glycol and 5% Tween-80 in sterile water. Cells were pelleted and resuspended in PBS/Matrigel Matrix (BD) mix at a 1:1 ratio. 5×10^5 cells in 100 μ L solution were subcutaneously injected into each flank of 5-8 weeks old athymic male nude mice (Charles River Laboratories). After the tumours became palpable, the mice were separated into two groups with equal average tumour size and treated orally with either everolimus (5mg/kg/daily) or vehicle for 3 weeks. The tumour growth was monitored by calliper measurement.

2.26 Histology and immunohistochemistry

The extracted lungs were fixed in 10% formalin in PBS overnight. On the following day, the formalin-fixed samples were washed with 1x PBS twice and stored in 70% ethanol. The formalin-fixed samples were sent to the Cambridge University Hospital Human Research Tissue Bank for paraffin-embedding and sectioning. Human vimentin (Cell Signaling Technology,

#5741 1:100) staining was performed on the Bond-Max instrument (Leica) using Bond Polymer Refine Detection reagents (Leica) according to the manufacturer's protocol (IHC Protocol F).

2.27 Total cholesterol quantification

Lipids were extracted from the cells using the chloroform-free lipid extraction kit (Abcam ab211044) according to the manufacturer's recommendation. In brief, cells were pelleted and washed with 1x PBS once. The cells were resuspended in 1 x PBS, followed by adding the lipid extraction buffer onto the cells. The cell suspension was vortexed vigorously for 1 minute and agitated on see-saw rocker at room temperature for 20 minutes. The cells were spun down at 10 000 RPM for 5 minutes. The supernatant was collected and dried overnight at 37°C. On the following day, the lipid extract was resuspended in suspension buffer and sonicated for 20 minutes followed by agitation 37°C for 20 minutes. The total cholesterol was quantified using the Amplex Red Cholesterol Assay Kit (Invitrogen A12216) according to the manufacturer's protocol. The quantified total cholesterol was normalised to the total protein amount of each samples.

2.28 Statistical analysis

Statistical analyses were performed either in R or GraphPad Prism (Version 5). *P*-values lower than 0.05 were considered statistically significant. For competitive proliferation assays, *in vitro* drug treatment proliferation assays and *in-vivo* subcutaneous tumour formation assays, two-way ANOVA with Tukey's range test was used. On the other hand, one-way ANOVA with Tukey's range test was used for *in-vivo* photon flux analysis, *in-vivo* tumour weight and lung colonization assays, *in-vivo* everolimus treatment subcutaneous tumour formation assay and *in-vivo* total cholesterol quantification assay. For qPCR, three independent experiments are shown

unless stated otherwise in the figure legend, each of the experiment is the average of three technical replicates. The qPCR statistical significance was determined by using either one-way ANOVA with Dunnett's test or two-tailed unpaired Student's t-test depending on the assays. Boxplots represent median, 25th and 75th percentiles, the whiskers extend to data extremes.

Chapter 3

Investigating the functional relevance of
KLF6 on ccRCC growth

3.1 Introduction

Acetylation of histone H3 at the lysine 27 residue (H3K27ac) is associated with active gene regulatory elements. Within some genomic loci, multiple enhancers cluster together to form a large enhancer domain, also known as super enhancers, with enriched H3K27ac signals. Super enhancers have been widely reported to support the expression of critical transcriptional regulators in various biological contexts such as the cell-type-specific gene expression programmes. In addition, several lines of evidence have demonstrated that super enhancers play an important role in regulating cancer phenotypes which this has been discussed in Chapter 1 (section 1.16).

As highlighted in Chapter 1 (section 1.17), H3K27ac ChIP-Seq was previously performed on several VHL-deficient ccRCC cell lines by Paulo Rodrigues in order to profile the enhancers/super enhancers regions in ccRCC cell lines. The aforementioned work had also utilised these H3K27ac ChIP-Seq data to identify transcription factors that were associated or located in the vicinity of super enhancer region. It was postulated that these transcription factors could potentially have important roles in supporting ccRCC pathogenesis based on the growing evidences demonstrating the link between super enhancers and regulation of many critical genes that include transcription factors.

The H3K27ac ChIP-Seq data were analysed by Sakari Vanharanta in which the identified enhancers were ranked based on their H3K27ac signals. *Kruppel-like factor 6 (KLF6)*, a zinc finger DNA-binding transcription factor, was found to be in the vicinity of one of the strongest super enhancers in ccRCC cells (Figure 15A). Figure 15B shows the H3K27ac ChIP-Seq track of the ccRCC cells *KLF6* locus where there was large cluster of active enhancers with high

H3K27ac signals in the proximity of this *KLF6* locus. To confirm this observation, previous works by Paulo Rodrigues had also performed H3K27ac ChIP-Seq on several human ccRCC clinical samples as well as ccRCC xenograft samples. There was also a large cluster of active enhancers observed nearby the *KLF6* locus in these analysed samples (Figure 15B).

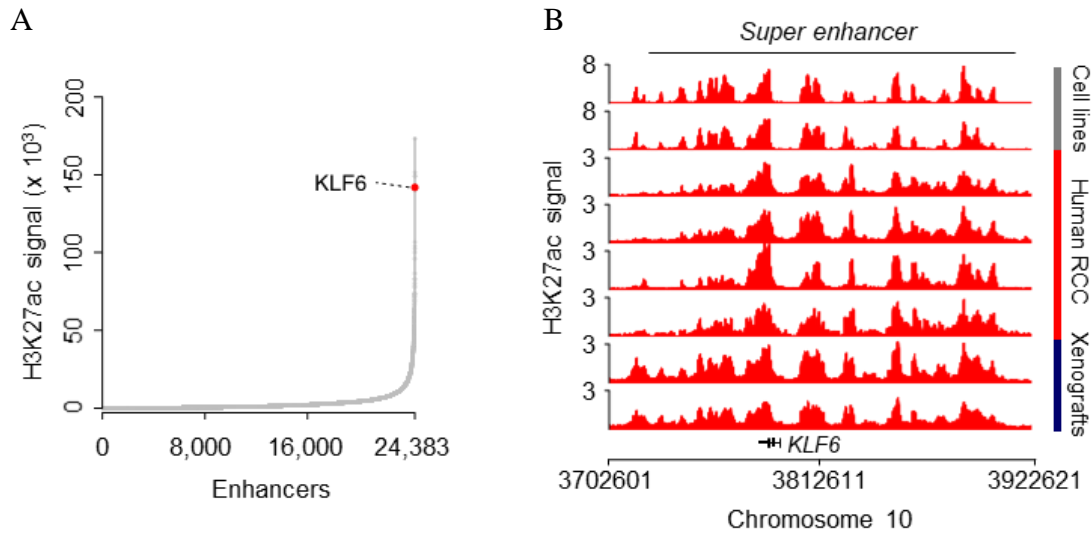


Figure 15: Super enhancer profiling in ccRCC. **(A)** *KLF6* is associated with one of the strongest super enhancer in ccRCC. **(B)** H3K27ac ChIP-Seq signal at the large enhancer cluster in the proximity of the *KLF6* locus in ccRCC cell lines, ccRCC clinical samples and tumour xenografts.

Super enhancers-regulated genes are typically highly expressed and in some cases, the expression of these genes can be cell-type-specific. Analysis of the large TCGA RNA-Seq data by Sakari Vanharanta revealed high and specific expression of *KLF6* in ccRCC compared to other tumour types in the large TCGA cohort (Figure 16A). This observation was in line with the possibility that *KLF6* expression in ccRCC could be super enhancer driven. Furthermore, the expression of *KLF6* was significantly upregulated in ccRCC samples as compared to the normal

kidney tissues (Figure 16B). This observation seemed to suggest that KLF6 might be pro-tumourigenic and involved in supporting ccRCC pathogenesis.

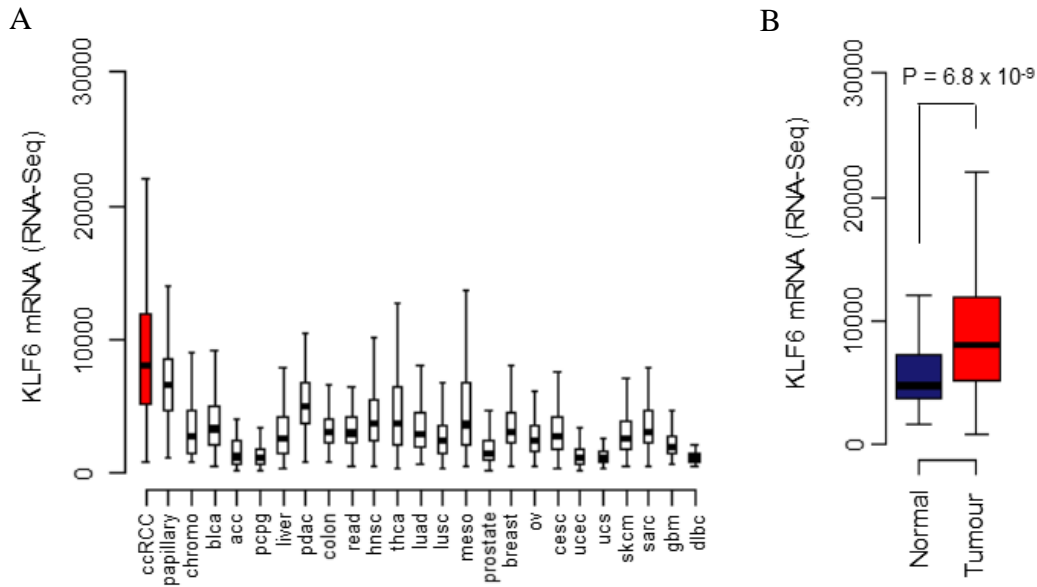
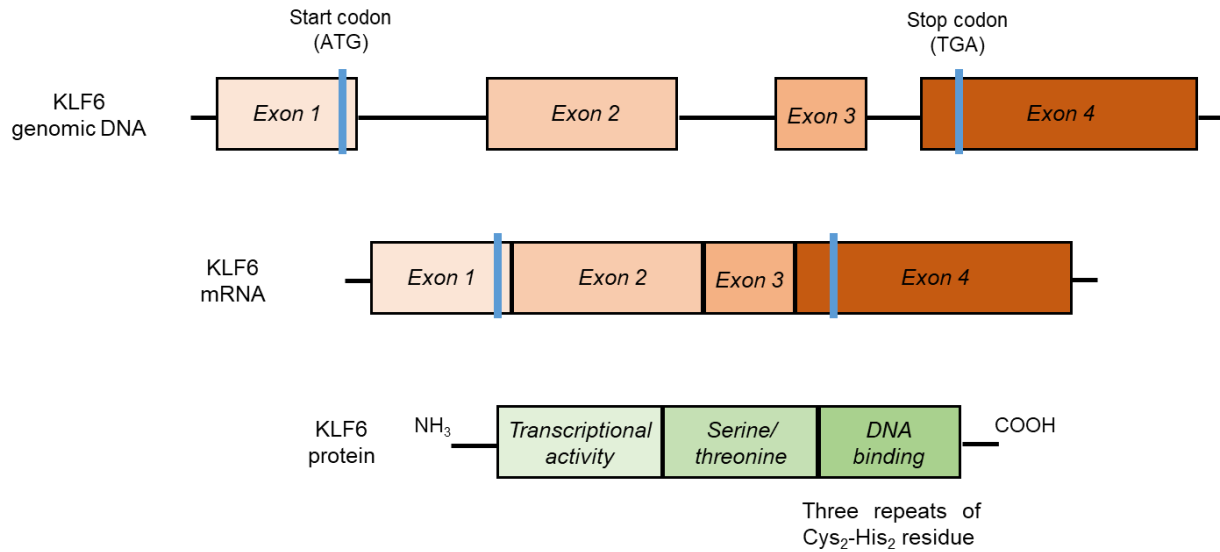


Figure 16: KLF6 is highly expressed in ccRCC clinical samples. **(A)** *KLF6* expression, RSEM normalised count, in ccRCC and other tumour types from the TCGA cohort. Mann-Whitney U test. **(B)** *KLF6* expression, RSEM normalised count, in ccRCC and normal kidney tissues in the TCGA cohort. Mann-Whitney U test.

In brief, KLF6 belongs to the *Kruppel*-like factors family and to date, there are seventeen members of this family discovered. KLFs are the mammalian orthologs of *Drosophila melanogaster* gene, Kruppel, in which mutations in this gene disrupt the fly segmentation pattern at the early stage of embryogenesis¹⁷⁹. As a zinc finger DNA binding protein, KLFs can either function as transcriptional activator or repressor and members of human KLF family have been shown to play important roles in various biological processes and also in disease pathogenesis¹⁷⁹. *KLF6* is located on chromosome 10p15 and contains 4 exons. The KLF6 protein consists of 3 domains; activation domain, serine threonine domain and the DNA binding domain (Figure

17A). The C-terminal DNA binding domain is composed of three repeats of cysteine₂-histidine₂ (cys₂-his₂) zinc finger and this domain is highly conserved among the 17 members of the KLF family¹⁸⁰. In addition, there had been reports on the presence of three *KLF6* transcript isoforms namely *KLF6-SV1*, *KLF6-SV2* and *KLF6-SV3*. The presence of these isoforms was due to the alternative splicing that resulted from germline mutations in the *KLF6* exon 2 (Figure 17B). Both *KLF6-SV1* and *KLF6-SV2* isoforms lack the nuclear localization signal sequences whereas the *KLF6-SV3* isoform does not have exon 3¹⁸¹.

A



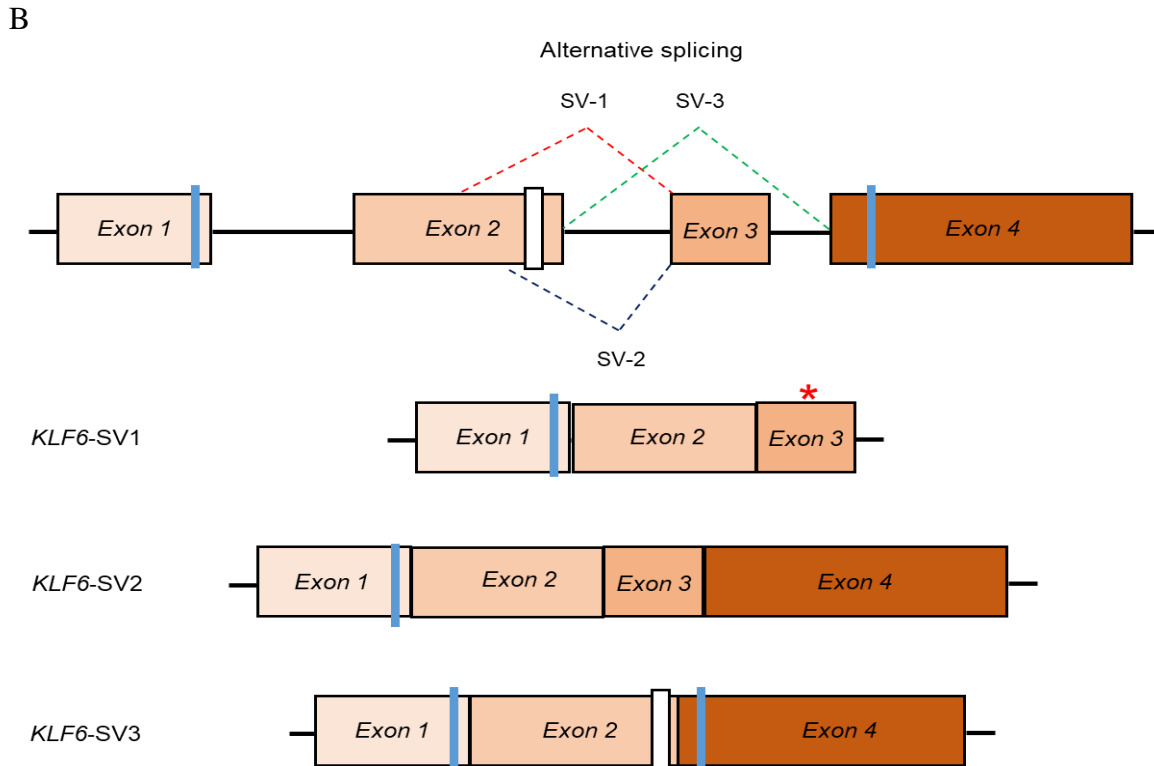


Figure 17: KLF6 structure and isoforms. (A) Schematic illustrating the KLF6 genomic DNA, mRNA and proteins domains. (B) The presence of *KLF6* transcript isoforms due to the alternative splicing. Adopted from Andreoli *et al*¹⁸⁰

There have been contradictory reports on the functions of KLF6 in cancers. Several early studies have described KLF6 to have growth suppressive function due to their observations that KLF6 was frequently inactivated or downregulated in the analysed cancer types¹⁸²⁻¹⁸⁴. However, recent large-scale genome re-sequencing efforts reveal that *KLF6* is rarely inactivated via genetic alterations^{185,186}. There were also studies that showed KLF6 supports cancer growth¹⁸⁷⁻¹⁸⁹. Furthermore, the spliced-variants of *KLF6*, particularly the *KLF6*-SV1 isoform, has been associated with cancer progression and poor prognosis in prostate, breast and ovarian cancer¹⁹⁰⁻¹⁹². Based on these contradictory reports, I was therefore interested to further understand the role

of KLF6 in ccRCC. It was hypothesised that KLF6 could involve in supporting ccRCC pathogenesis based on the observation that *KLF6* is located in the vicinity of one of the strongest super enhancers in ccRCC. This was supported by the fact that super enhancers have been widely shown to regulate the expression of important genes in various biological processes as well in supporting cancer phenotypes. Also, it was observed that *KLF6* expression was higher in ccRCC samples as compared to the normal kidney tissues. Thus, the focus of this chapter was to test the hypothesis presented above by investigating whether KLF6 plays a role in supporting ccRCC growth. To attain this, the *state-of-the-art* CRISPR-Cas9 and CRISPRi gene editing tools were employed to target KLF6 in several VHL-mutant ccRCC cell lines, followed by assessing the effect of KLF6 inhibition on ccRCC growth via *in vitro* and *in vivo* functional assays.

3.2 Results

3.2.1 ccRCC cell lines identity validation

The effect of KLF6 inhibition was tested on several VHL-deficient ccRCC cell lines; 786-M1A, OS-LM1, RCC-MF and UOK101. Prior to performing the *in-vitro* functional assays, it was crucial to validate the identity of each of these cell lines in order to ensure the cells were what they were supposed to be and no cross-contamination had happened. As described in Chapter 2 (section 2.1), each of this ccRCC cell line harbours a unique homozygous *VHL* mutations that can be directly detected via Sanger sequencing. Thus, the identity of these cells was authenticated by confirming their corresponding *VHL* mutation. There is a deletion of guanine at position 310 and 173 in the *VHL* exon 1 of the 786-M1A and OS-LM1 cells, respectively. In the RCC-MF cell line, there is a cytosine to thymine substitution at position 256

in the *VHL* exon 1 as well. There is a deletion of cytosine in the *VHL* exon 3 of UOK101 cells. PCR primers were designed to amplify region encompassing the mutated site in each of this cell line and the amplicons were sent for Sanger sequencing. Figure 18 shows the sequencing electropherograms that highlighted the *VHL* mutation in (A) 786-M1A, (B) OS-LM1, and (C) RCC-MF cells. Each of this cell line harboured their respective unique *VHL* mutations, thus validating the identity of these cell lines. The identity of UOK101 cells was successfully authenticated by Nazhif Zaini, a member of the lab.

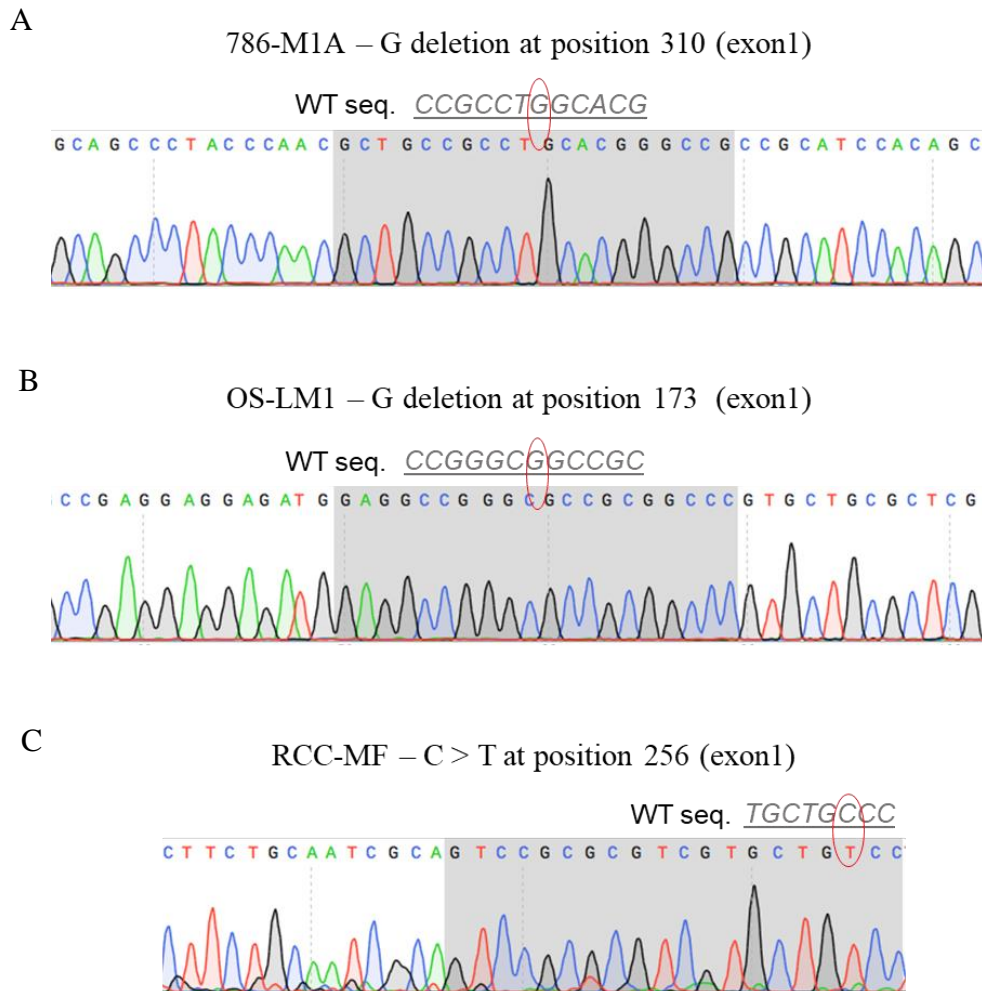


Figure 18: Validation of the ccRCC cell lines identity. (A-C) Sequencing electropherogram highlighting the *VHL* mutation in (A) 786-M1A, (B) OS-LM1 and (C) RCC-MF.

3.2.2 KLF6 is expressed in ccRCC cell lines

Next, the expression of KLF6 protein was assessed in the cell lines described previously and in the parental 786-O and OS-RC2 cells as well. For comparison, KLF6 expression was also assessed in the A549 lung cancer cell line. The ccRCC cell lines expressed higher level of KLF6 as compared to the A549 lung cancer cell line (Figure 19A). This was in agreement with the analyses of TCGA RNA-Seq data set that revealed higher and specific expression of *KLF6* in ccRCC clinical samples compared to other tumour types (Figure 16A). As highlighted in the introduction section 3.1, several studies have reported the presence of three additional *KLF6* transcript isoforms, KLF6-SV1, SV2 and SV3, due to the alternative splicing. Thus, it was important to determine the predominantly expressed *KLF6* isoform in our model system. Analysis of the previously generated RNA-Seq data from several ccRCC cell lines confirmed that the full-length *KLF6* was the predominantly expressed isoform in ccRCC cell lines with little evidence showing the other transcript isoforms being expressed in these cells (Figure 19B).

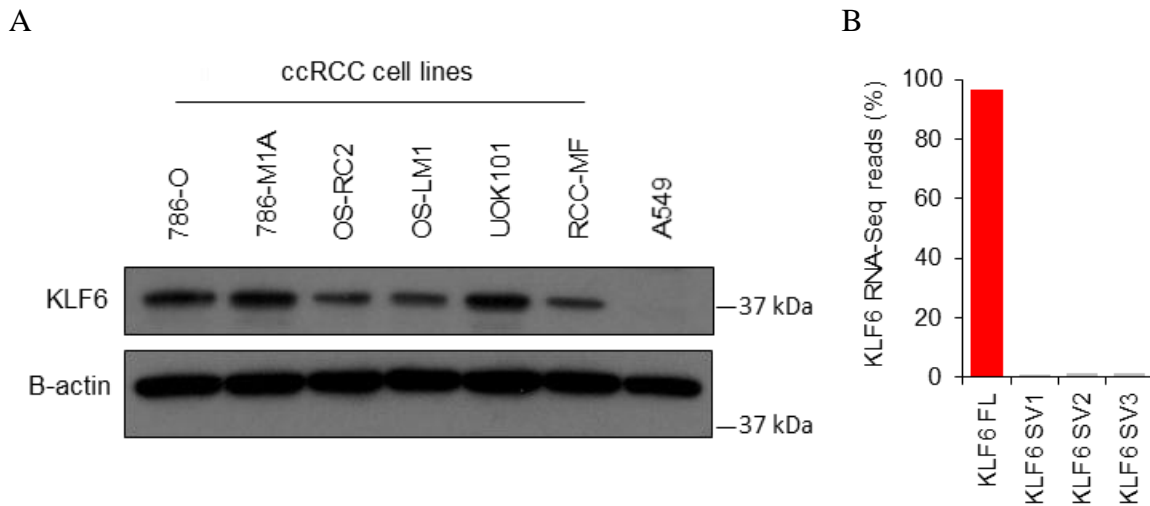
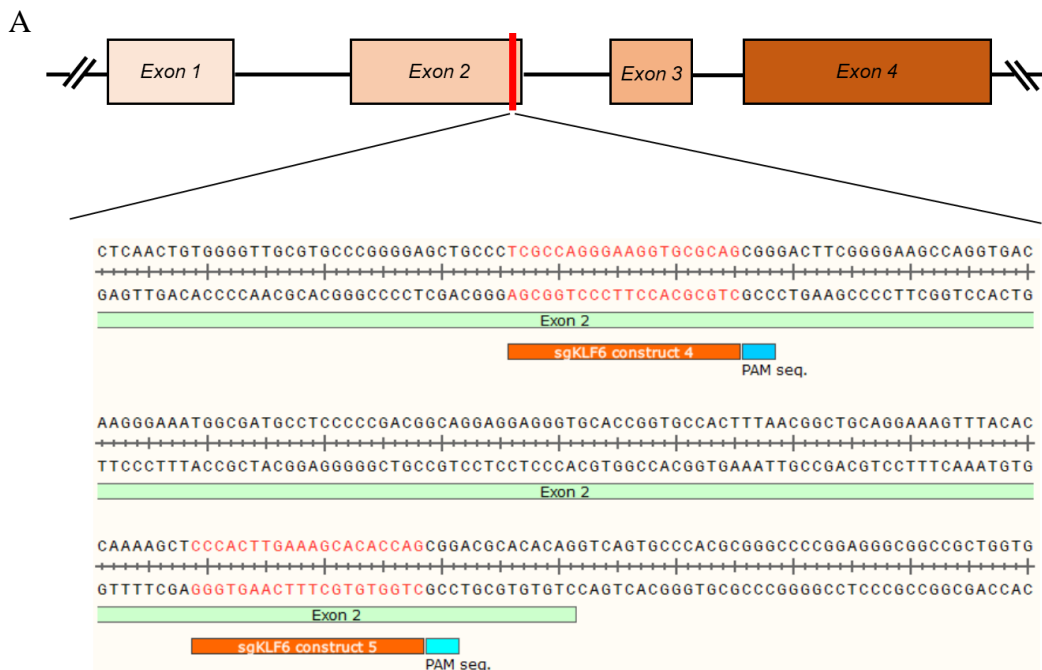


Figure 19: Characterisation of KLF6 expression in ccRCC cell lines. **(A)** KLF6 protein expression in a panel of ccRCC cell lines and A549, a lung cancer cell line. **(B)** Transcript reads of the full length and alternatively spliced *KLF6* variants as measured by RNA-Seq in ccRCC cell lines.

3.2.3 High efficiency of CRISPR-Cas9-mediated KLF6 targeting

As described previously, the CRISPR-Cas9 gene editing tool was employed to perturb KLF6 function in the ccRCC cell lines. The *KLF6*-targeting sgRNAs were designed using the Broad Institute sgRNA design tool. Based on the prediction algorithm, two sgRNAs were chosen, sgKLF6_4 and sgKLF6_5, in which each of this sgRNA targeted two independent regions within the *KLF6* exon 2 (Figure 20A). The Cas9 protein would be recruited and cleaved these sgRNAs-targeted sites where in the absence of repair template, the error-prone NHEJ would take place that subsequently resulted in the introduction of mutations¹⁹³. In addition, the non-targeting control construct, sgNTC, was also designed. The sgKLF6 and sgNTC constructs were cloned into the pKLV-U6-gRNA(BbsI)-PGKhygro2ABFP sgRNA expression vector, followed by transduction into the 786-M1A cells expressing the doxycycline-inducible Cas9. The targeting efficiency of these sgKLF6 constructs was assessed by performing genetic analysis on their respective targeted regions and checking the KLF6 expression level in these cells. The workflow for assessing the sgKLF6 targeting efficiency is exemplified in figure 20B.



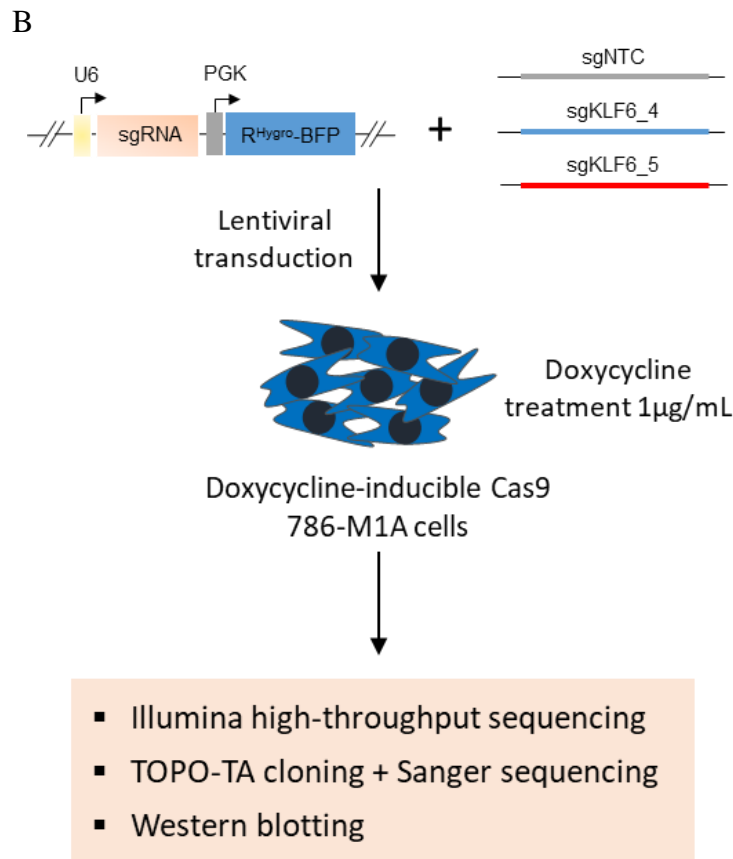


Figure 20: CRISPR-Cas9-mediated KLF6 targeting. (A) Regions targeted by sgKLF6_4 and sgKLF6_5 constructs within the *KLF6* exon 2. (B) Experimental workflow to assess the sgKLF6 constructs targeting efficiency.

The most common type of mutations induced by the CRISPR-Cas9 gene editing tool are insertions and/or deletions (INDELS). INDELS result in either frameshift or introduction of nonsense mutations, which could be deleterious¹⁹⁴. However, there is a possibility that the induced mutations are synonymous or in-frame mutations, which could retain the KLF6 wild-type functions. To examine the targeting efficiency of both sgKLF6 constructs, the sgKLF6_4 and sgKLF6_5-targeted regions were amplified from the transduced 786-M1A cells and the amplicons were sent for Illumina high throughput sequencing. About 98% of the sequencing

reads analysed from both sgKLF6-targeted sites were mutated sequences (Figure 21A). In addition, the TOPO-TA cloning was also performed on the sgKLF6_4-targeted site. Out of fifteen TOPO-TA clones sent for Sanger sequencing, ten clones had six different types of deletion, all resulting in frameshift mutation. Two clones had same one nucleotide insertion; also resulting in frameshift mutation, while three other clones had failed sequencing reads (Figure 21B). Importantly, there was no wild-type sequence detected. Next, the KLF6 protein level in the sgKLF6_4 and sgKLF6_5-transduced 786-M1A cells was assessed and it was observed that KLF6 expression was significantly depleted in these cells (Figure 21C). Collectively, these finding confirmed the high efficiency of sgKLF6_4 and sgKLF6_5 constructs in targeting KLF6 and be used in the subsequent functional assays.

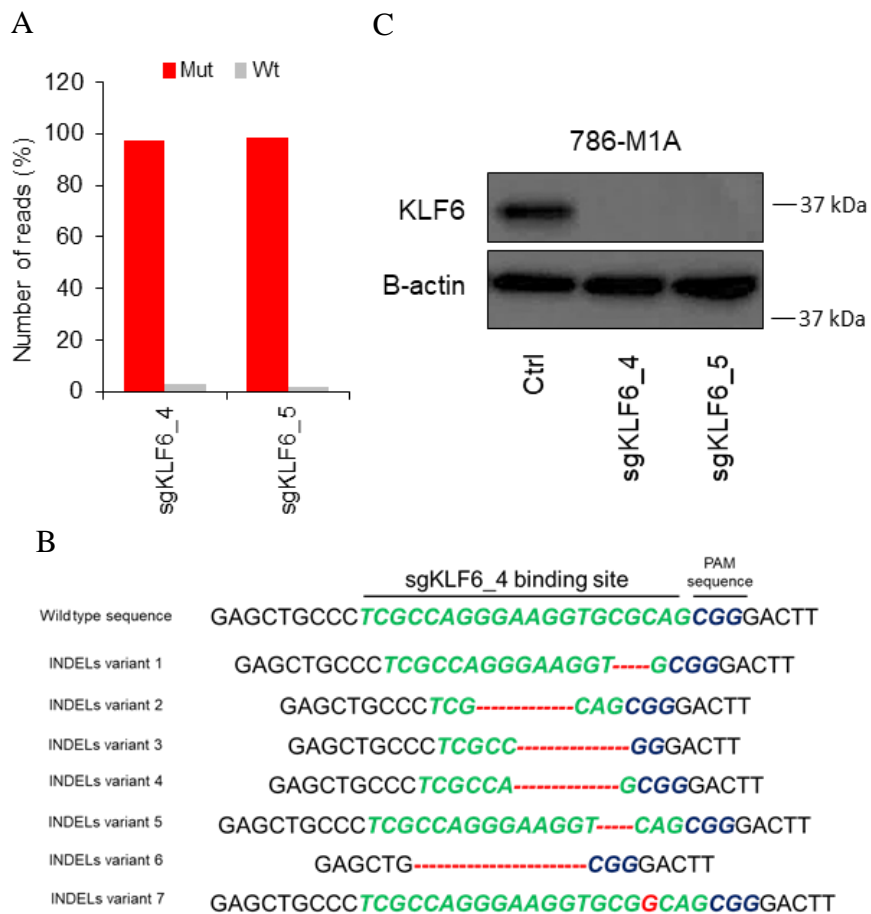


Figure 21: High efficiency of the sgKLF6 constructs in targeting KLF6. **(A)** Fraction of wild type and mutant KLF6 genomic DNA in cells targeted by sgKLF6_4 and sgKLF6_5 constructs. **(B)** Genetic analysis of the sgKLF6_4-targeted region TOPO-TA clones. **(C)** KLF6 expression in 786-M1A cells transduced with sgKLF6_4, sgKLF6_5 and non-targeting control constructs.

3.2.4 Development of competitive proliferation assay

The phenotypic effect upon KLF6 inhibition in the ccRCC cell lines was assessed using the competitive proliferation assay which I developed in the lab. The basis of this assay was to mix the KLF6-targeted and control cells at a 1:1 ratio, followed by assessing the percentage of each cells population over time using FACS. By employing this strategy, the cells growth was able to be assessed for an extended period of time, thus ensuring a small or delayed effect in cell proliferation could be observed. As discussed in Chapter 2, several variants of the sgRNA expression vector were generated and one of them was the pKLV-U6-gRNA(BbsI)-PGKhygro2AmCherry. These BFP and mCherry variant of the sgRNA expression vectors were utilised to distinguish between the pooled KLF6-targeted and control cell populations. In brief, the sgKLF6 and sgNTC constructs were cloned into the BFP and mCherry sgRNA expression vectors, respectively, followed by transducing the cells with either of these constructs. As a result, the sgKLF6-transduced cells population would be BFP⁺ whereas the control cell population would be mCherry⁺. These BFP⁺ KLF6-targeted and mCherry⁺ control cells were co-cultured according to the condition described above.

If KLF6 does play a role in supporting ccRCC pathogenesis, targeting KLF6 would impair ccRCC cells growth. Therefore, in the competitive proliferation assay, the BFP⁺ KLF6-targeted cell population would be depleted from the assay and outgrown by the mCherry⁺ control

cells population. However, if the KLF6 role in ccRCC is dispensable, it was predicted that this BFP⁺ cell population would proliferate at the same rate as the mCherry⁺ control cell population. Thus, the percentage of each cell population at the end of the assay would be similar to their respective percentage on the plating day, T=0. Figure 22 simplifies the competitive proliferation assay strategy along with the expected observations for the control and experimental conditions. The experimental condition consisted of a mixture of BFP⁺ KLF6-targeted and mCherry⁺ control cell population. In addition, BFP⁺ control cells were also generated in which this cell population was co-cultured with the mCherry⁺ control cell population that served as the control condition for this competitive proliferation assay.

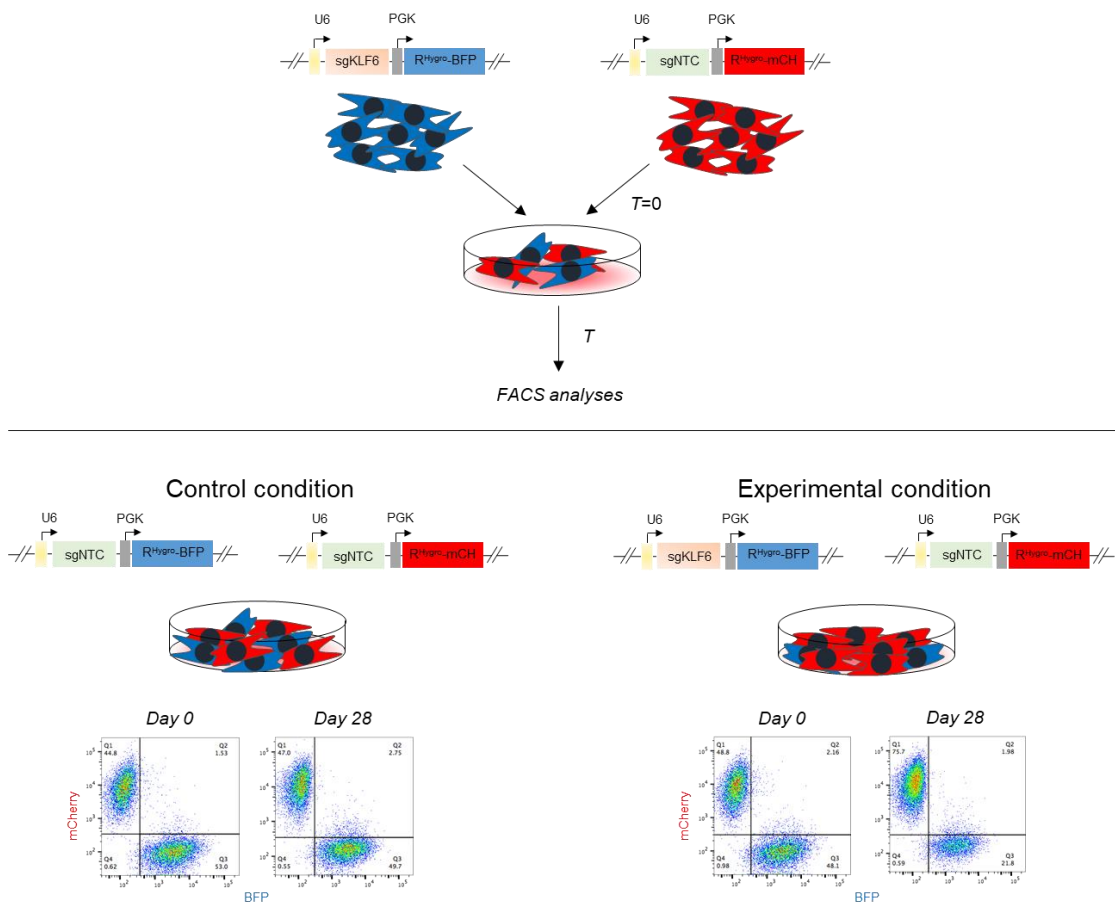


Figure 22: The *in-vitro* competitive proliferation assay. **(Top)** A Simplified diagram of the competitive proliferation assay strategy. **(Bottom)** The observations in the control and experimental conditions of the competitive proliferation assay.

3.2.5 Competitive proliferation assay (CRISPR-Cas9-mediated KLF6 inhibition)

3.2.5.1 786-M1A cells

The 786-M1A cells expressing the doxycycline-inducible Cas9 were first transduced with either sgKLF6-BFP or sgNTC-mCherry constructs. Three different conditions were set up in this competitive proliferation assay. The first condition was the control condition which has been described previously. The second and third conditions were the mCherry⁺ control cells mixed with the BFP⁺ sgKLF6_4 and sgKLF6_5 cells, respectively. The assay was performed for 28 days where the percentage of BFP⁺ and mCherry⁺ cell populations in each condition was assessed weekly by FACS.

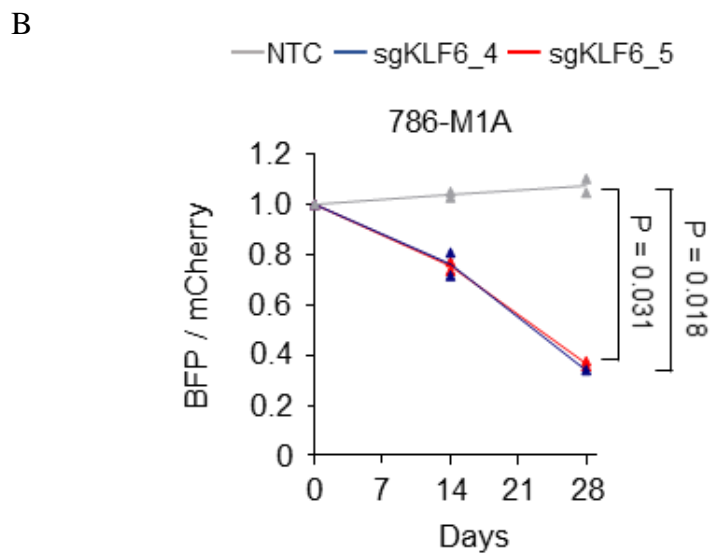
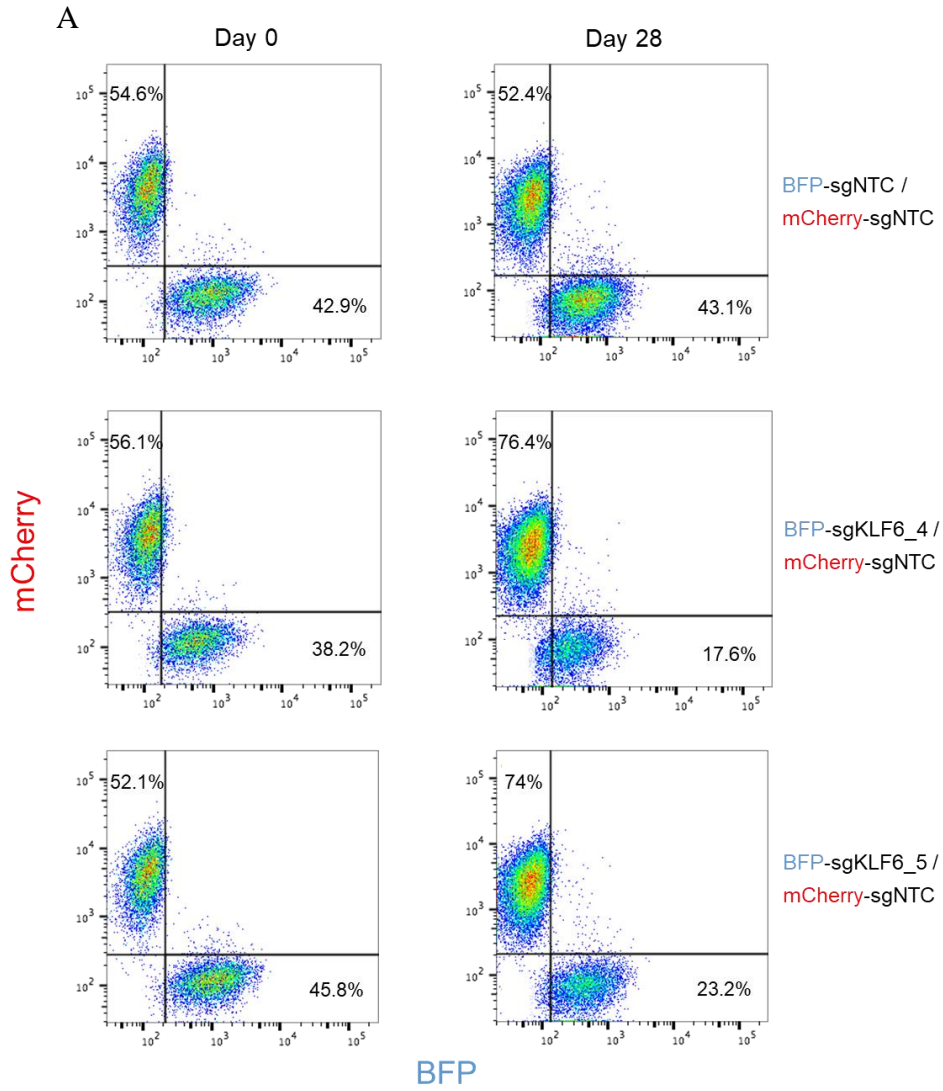
Figure 23A shows the percentage of BFP⁺ and mCherry⁺ cell populations in each condition at the beginning and end of the assay. The x-axis and y-axis show the excitation/detection wavelength used to detect the BFP and mCherry fluorescents, respectively. For the control condition (top panel), as compared to day 0, there was no significant change in the percentage of BFP⁺ and mCherry⁺ cell populations at the end of the assay. For example, the percentage of BFP⁺ control cell population at the start and end of the assay was 42.9% and 43.1%, respectively. This was in line with the initial expected result for this control condition. This was due to both cell populations were transduced with non-targeting control construct which in theory should not have any effect the cells growth.

The middle panel shows the condition of the mixed BFP⁺ sgKLF6_4/mCherry⁺ control cell populations. The percentage of BFP⁺ KLF6 targeted-cells was 38.2% at the start of the assay and significantly decreased to 17.6% after 28 days in culture. In contrast, the percentage of the mCherry⁺ control cell population increased from 56.1% to 76.4% at the end of the assay. Similar

result was observed when I mixed the BFP⁺ sgKLF6_5 cells with the mCherry⁺ control cells (last panel). The population of BFP⁺ KLF6-targeted cells decreased from 45.8% to 23.2% whereas the mCherry⁺ cell population increased from 52.1% to 74% at the end of the assay.

These competitive proliferation assay data were analysed by normalising the percentage of cell populations in each week to their respective percentage at the beginning of the assay. After normalising the percentage of each week to the plating day, the relative fraction of BFP⁺ KLF6-targeted and mCherry⁺ control cells was determined. The graph in figure 23B shows the analysed data for all three set-up conditions for this assay. The relative fraction of BFP⁺ and mCherry⁺ cells populations in the control condition remained unchanged throughout the assay. However, in both KLF6 targeting conditions, the relative fraction of BFP⁺ KLF6 targeted-cell and mCherry⁺ control cell populations continuously decreased throughout the assay where at the end of the assay, the ratio between BFP⁺ and mCherry⁺ cells was about 0.3.

To confirm that the observed phenotype was not confounded by the fluorescent proteins, the sgRNA expressing vectors were swapped by cloning the sgKLF6 and sgNTC constructs into mCherry and BFP backbones, respectively. It was then observed that the KLF6-targeted cells which in this “*fluorescent markers-swapped*” experiment expressed the mCherry fluorescent protein got depleted from the assay and outgrown by the BFP⁺ control cells population (Figure 23C). The relative fraction of mCherry⁺ KLF6-targeted and BFP⁺ control cell populations was 0.44 for the sgKLF6_4 construct and 0.29 for the sgKLF6_5 (Figure 23D). Collectively, the observations from these competitive proliferation assays suggested that KLF6 plays a role in supporting ccRCC growth, at least in the 786-M1A cell line. The KLF6-targeted 786-M1A cells grew slower that resulted in the depletion of this cell population in the competitive proliferation assay.



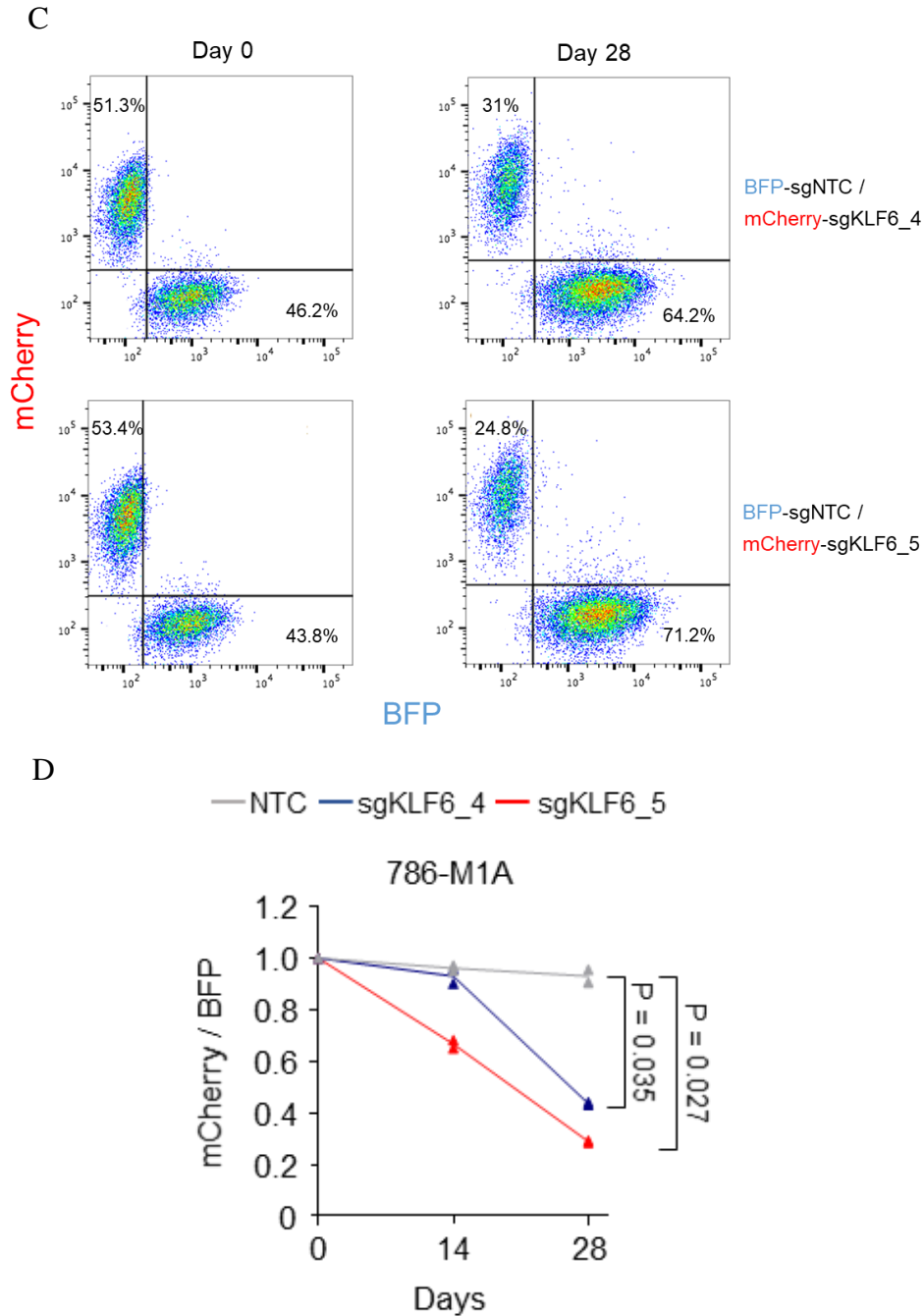


Figure 23: Competitive proliferation assay of the CRISPR-Cas9 KLF6-targeted 786-M1A cells. **(A)** FACS plots of each of the set-up condition at the start and end of the assay. **(B)** Analysis of the experiment shown in A. Graph shows the relative fraction of BFP⁺ KLF6-targeted and mCherry⁺ control cells, normalised to day 0. Two-way ANOVA with Tukey's range test. **(C)** FACS plot of the swapped fluorescent markers experiment. **(D)** Analysis of the experiment

shown in C. Graph shows the relative fraction of mCherry⁺ KLF6-targeted and BFP⁺ control cells, normalised to day 0. Two-way ANOVA with Tukey's range test.

3.2.5.2 Rescuing the KLF6-targeted 786-M1A cells with exogenous KLF6

In order to validate the previous findings, a rescue experiment was performed by reintroducing exogenous KLF6 into the KLF6-targeted 786-M1A cells, followed by assessing the effect of this KLF6 reintroduction on cells growth. This rescue experiment would confirm that the observed growth defect was actually the result of KLF6 inhibition, not due to unexpected *off-target* effect. KLF6 coding sequence (CDS) was amplified from the cDNA of 786-M1A cells and the amplified KLF6 CDS was sequence-verified via Sanger sequencing. The sequence-verified KLF6 CDS was cloned into the pLVX-Hygro expression vector which was modified by Paulo Rodrigues from the commercially available pLVX-Puro expression vector. Since the rescue experiment was performed in the sgKLF6₄-transduced cells, several synonymous mutations were reintroduced within the sgKLF6₄ target site of the exogenous KLF6 using the site-directed mutagenesis tool. This was to prevent the reintroduced exogenous KLF6 from being targeted by the sgKLF6₄ construct.

Next, the 786-M1A cells expressing the doxycycline-inducible Cas9 were transduced with either pLVX-Hygro empty vector (hereinafter referred to as EV cells) or pLVX-Hygro KLF6 CDS (hereinafter referred to as KLF6 CDS cells). These EV and KLF6 CDS cells were subsequently transduced with either sgKLF6₄-mCherry or sgNTC-BFP constructs depending on the competitive proliferation assay conditions. Figure 24A shows the KLF6 immunoblot of the sgNTC + EV cells, sgKLF6₄ + EV cells and sgKLF6₄ + KLF6 CDS cells. KLF6 protein expression was significantly depleted in the sgKLF6₄ transduced-EV cells (*lane 2*). KLF6

expression was detected in the sgKLF6_4-transduced KLF6 CDS cells; this supposed to be from the reintroduced exogenous KLF6 since the endogenous KLF6 was targeted by sgKLF6_4 (*lane 3*).

Three different conditions were set up for this rescue competitive proliferation assay where in the first condition, the mCherry⁺ sgNTC + EV and BFP⁺ sgNTC + EV cells were competed against each other. This served as the control condition. The second condition was the mixture of mCherry⁺ sgKLF6_4 + EV and BFP⁺ sgNTC + EV cells and this condition mimicked the experimental conditions of the previous competitive proliferation assay. The last condition was the rescue condition that consisted of a mixture of mCherry⁺ sgKLF6_4 + KLF6 CDS and BFP⁺ sgNTC + EV cell populations.

The results of this rescue competitive proliferation assay are shown in figure 24B. The relative fraction of the mCherry⁺ and BFP⁺ sgNTC + EV cell populations in the control condition remained unchanged throughout the assay. This was expected because both of these cell populations proliferated normally at a similar rate. The relative fraction of the mCherry⁺ sgKLF6_4 + EV and BFP⁺ sgNTC + EV cells decreased over time due to KLF6 inhibition in these mCherry⁺ sgKLF6_4 + EV cells. This result was consistent with the previous competitive proliferation assay observations that targeting KLF6 led to impaired cells growth. However, in the rescue condition, the reintroduction of exogenous KLF6 into the sgKLF6_4-targeted cells (mCherry⁺ sgKLF6_4 + KLF6 CDS) alleviated the proliferative defect. It can be observed from the graph that these cells (*orange line*) grew better compared to the KLF6-targeted cells that did not carry the exogenous KLF6 (*red line*). The findings of this rescue competitive proliferation assay confirmed that the previously observed growth defect in KLF6-targeted 786-M1A cells was indeed due to KLF6 inhibition.

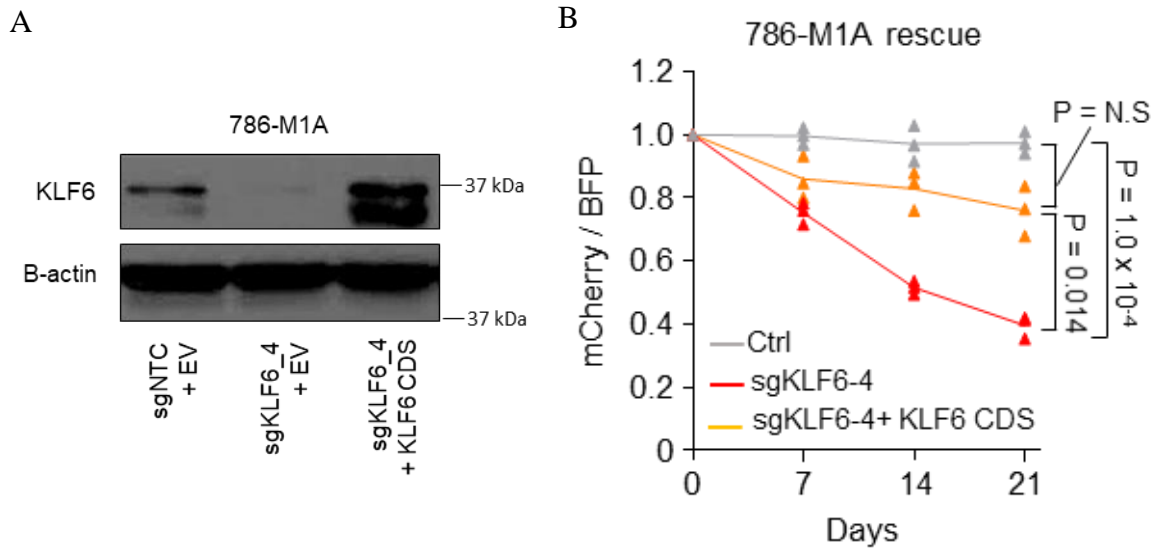


Figure 24: Exogenous KLF6 rescue competitive proliferation assay of the CRISPR-Cas9 KLF6-targeted 786-M1A cells. **(A)** KLF6 expression in the cells used in the KLF6 CRISPR-Cas9 rescue competitive proliferation assay. **(B)** Analysis of the rescue competitive proliferation assay. Graph shows the relative fraction of mCherry⁺ sgKLF6_4 + EV cells and mCherry⁺ sgKLF6_4 cells reintroduced with exogenous KLF6 compared to BFP⁺ control cells. Two-way ANOVA with Tukey's range test.

3.2.5.3 Targeting KLF6 in other ccRCC cell lines

Next was to investigate whether KLF6 inhibition would also affect the growth of several other VHL-deficient ccRCC cell lines. To test this, the constitutively-expressing Cas9 OS-LM1, RCC-MF and UOK101 cells were generated, followed by transducing these cells with either sgKLF6_4, sgKLF6_5 or sgNTC constructs. As expected, a reduction in the KLF6 protein level was observed in the cells that were transduced with the sgKLF6_4 and sgKLF6_5 constructs (Figure 25A). The previously described competitive proliferation assay was employed to assess the effect of KLF6 inhibition in these OS-LM1, RCC-MF and UOK101 cells. Results of the competitive proliferation assay are shown in figure 25B where in this experiment, the BFP⁺

KLF6-targeted cells were competed against the mCherry⁺ control cells. The CRISPR-Cas9-mediated KLF6 targeting in these cells resulted in impaired cells growth, indicated by the decreased relative fraction of the BFP⁺ KLF6 targeted and mCherry⁺ control cell populations over times. This was due to the depletion of these BFP⁺ cells from the assay and consequent increased in the population of mCherry⁺ cells.

The sgRNA expression vectors were also swapped in order to ensure the observed growth defect was not confounded by the fluorescent proteins. Consistent results were observed where the swapped mCherry⁺ KLF6-targeted cells grew slower compared to the BFP⁺ control cells that resulted in the depletion of these mCherry⁺ cells from the assay. This was reflected by the decreased relative fraction of the mCherry⁺ KLF6 targeted and BFP⁺ control cell populations over times (Figure 25C). Collectively, these observations corroborated the hypothesis that KLF6 plays important role in supporting ccRCC cells growth.

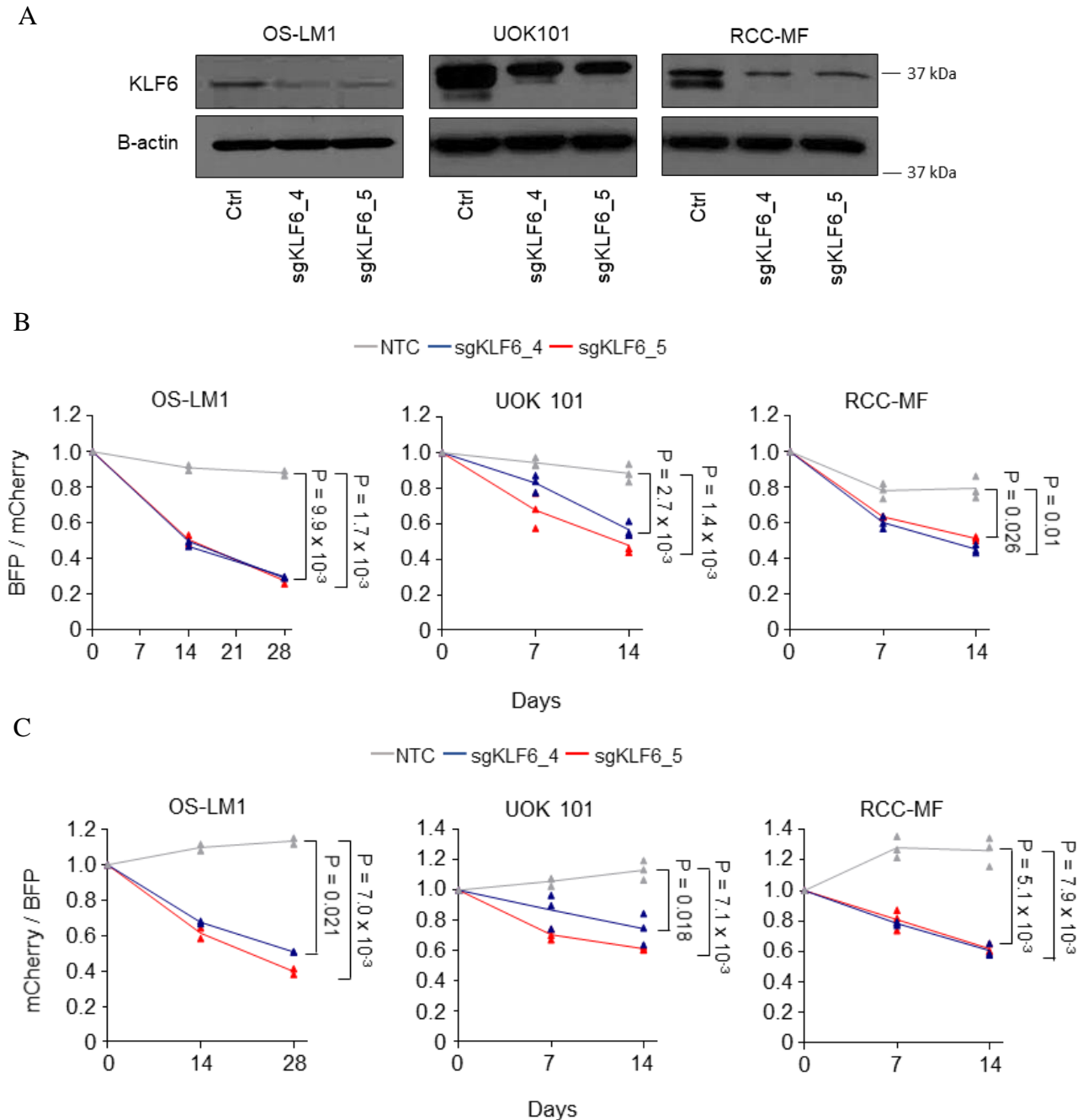


Figure 25: Competitive proliferation assay of the CRISPR-Cas9 KLF6-targeted OS-LM1, UOK101 and RCC-MF cells. **(A)** KLF6 expression in the KLF6-targeted OS-LM1, UOK101 and RCC-MF cells. **(B)** Graph shows the relative fraction of BFP⁺ KLF6-targeted and mCherry⁺ control cells, normalised to day 0. Two-way ANOVA with Tukey's range test. **(C)** Graph shows the relative fraction of mCherry⁺ KLF6-targeted and BFP⁺ control cells, normalised to day 0. Two-way ANOVA with Tukey's range test.

3.2.6 Competitive proliferation assay (CRISPRi-mediated *KLF6* inhibition)

The induction of double-strand break by the CRISPR-Cas9 mutagenesis tool could put the cells under stress and consequently reduced the cells fitness. Hence, it was also important to confirm that the previously observed impaired cells growth was not contributed by the CRISPR-Cas9-mediated double-strand break. To address this, CRISPRi approach was employed to inhibit *KLF6* in ccRCC cell line and the cells proliferation rate upon CRISPRi-mediated *KLF6* depletion was assessed. CRISPRi is a non-mutational approach to target protein that employs catalytically-inactivated Cas9 (dCas9) fused with transcriptional repressor domain KRAB¹⁹⁵. Unlike the wild-type Cas9 that induces the double-strand break and INDELS, the catalytically-inactivated dCas9 will only sit at the targeted site whereby the fused KRAB domain will repress the expression of gene encoding the protein of interest.

3.2.6.1 CRISPRi-mediated *KLF6* depletion in 786-M1A cells

In the CRISPR-Cas9 system, the sgRNAs are designed to target the protein coding sequences, normally the early exons. This is because INDELS and frameshift mutations in these early exons would be deleterious and result in non-functional protein. In the case of *KLF6*, the sgRNAs targeted regions were in exon 2. In contrast, there is a difference in the CRISPRi system where the targeted region is within -300 to +50 base pairs of the transcription start site. In order to increase the CRISPRi inhibition efficiency, the tandem sgRNAs approach was utilised which has been described in Chapter 2 (section 2.11). Two independent constructs, iKLF6_2 and iKLF6_3, were designed based on the prediction made in Gilbert *et al*¹⁷⁶. These iKLF6 constructs targeted the *KLF6* 5' untranslated region. The regions targeted by iKLF6_2 and iKLF6_3 within the *KLF6* 5' untranslated region are shown in figure 26.

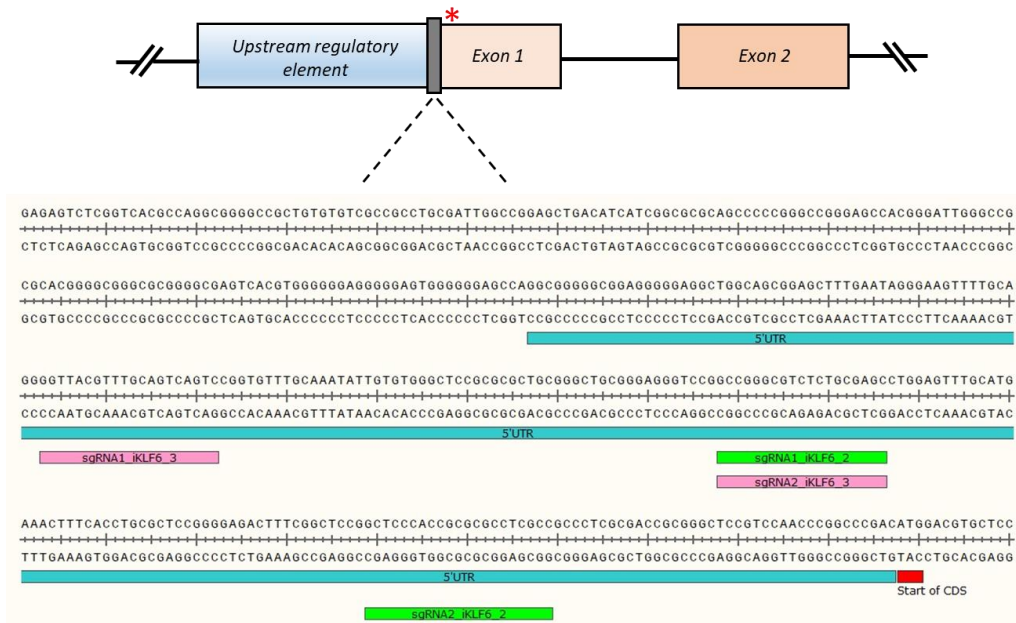


Figure 26: Regions targeted by the CRISPRi iKLF6 tandem constructs.

The 786-M1A cells were transduced with KRAB-dCas9-mCherry plasmid, hereinafter referred to as 786-M1A CRISPRi cells. These mCherry⁺ 786-M1A CRISPRi cells were then transduced with either iKLF6 or non-targeting control tandem constructs. These constructs were previously cloned into the BFP sgRNA expression vector. The KLF6 repressing efficiency of this CRISPRi approach was assessed at both mRNA and protein level. As compared to the control cells, there was about 90% reduction in KLF6 mRNA level in the iKLF6-transduced cells (Figure 27A). In agreement with the qPCR data, the expression of KLF6 protein was significantly depleted in these cells (Figure 27B). These observations confirmed the high efficiency of this CRISPRi tool along with the utilisation of the tandem sgRNAs targeting approach in knocking down *KLF6* expression in these 786-M1A cells.

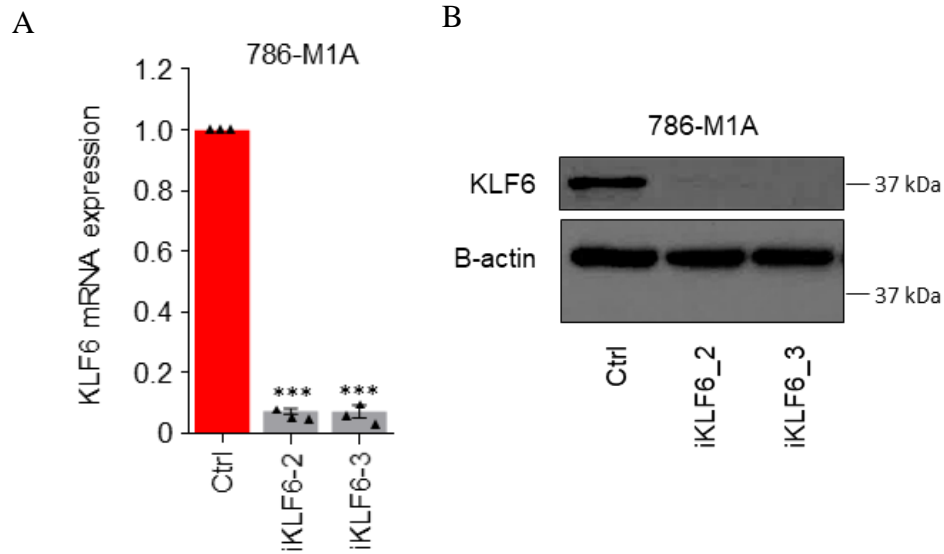
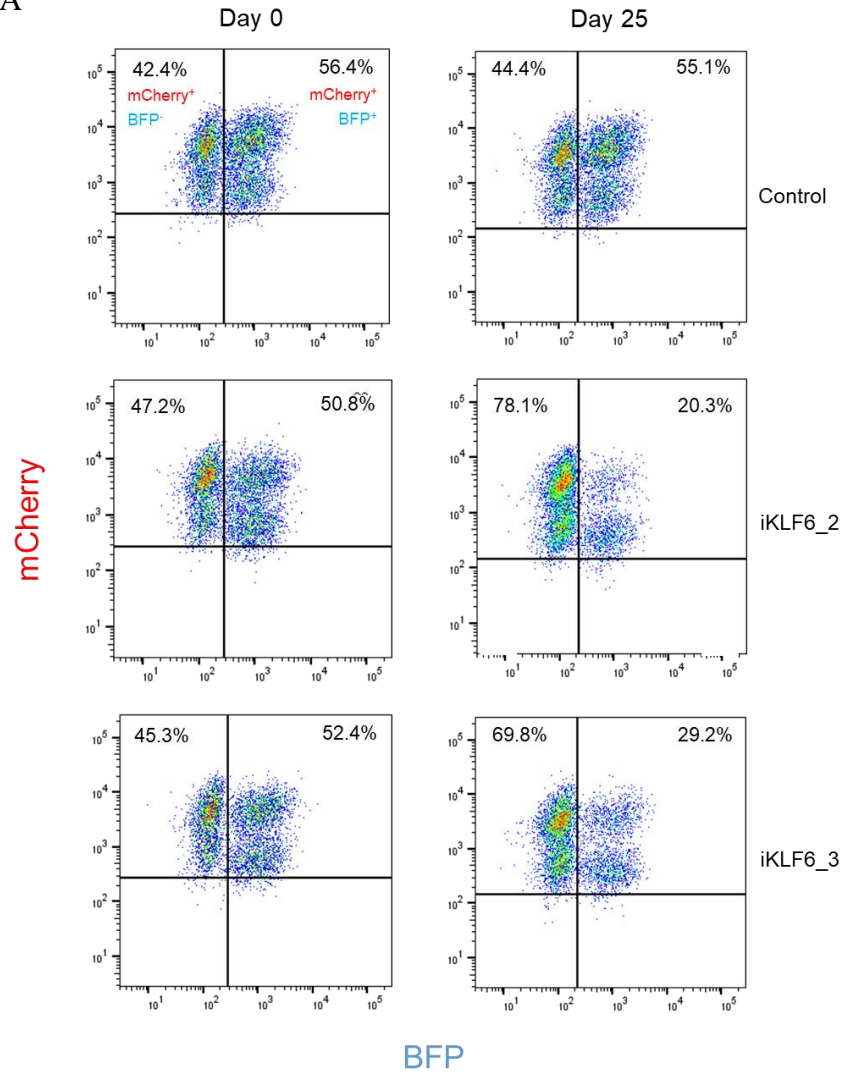


Figure 27: High efficiency of the CRISPRi approach in repressing KLF6 expression. **(A)** KLF6 mRNA expression in the *KLF6*-targeted 786-M1A CRISPRi cells. Average of three experiments. Error bars, SEM. One-way ANOVA with Dunnett's test. * $P < 0.05$, ** $P < 0.005$ and *** $P < 0.0005$. **(B)** KLF6 protein expression in the *KLF6*-targeted and control 786-M1A CRISPRi cells.

The phenotypic effect of CRISPRi-mediated *KLF6* inhibition was assessed using the competitive proliferation assay with slight modification. The double $mCherry^+/BFP^+$ iKLF6 or control 786-M1A CRISPRi cells were competed against the $mCherry^+/BFP^-$ 786-M1A CRISPRi parental cells. Similar to the previous assay, three conditions were set up. The first condition was the competition between the $mCherry^+/BFP^+$ control 786-M1A CRISPRi cells and $mCherry^+/BFP^-$ 786-M1A CRISPRi parental cells. This condition served as control condition. The second and third condition were the mixture of $mCherry^+/BFP^-$ 786-M1A CRISPRi parental with either $mCherry^+/BFP^+$ iKLF6_2 or iKLF6_3 786-M1A CRISPRi cells, respectively. The FACS plots in figure 28A show the percentage cell populations in each condition at the start and end of the competitive proliferation assay.

In the control condition (*top panel*), there was no significant difference in the percentage of both cell populations at the beginning and end of the assay. However, for the iKLF6_2 and iKLF6_3 conditions (*middle and bottom panel*), both mCherry⁺/BFP⁺ iKLF6_2 and iKLF6_3 786-M1A CRISPRi cells grew slower compared to the mCherry⁺/BFP⁻ 786-M1A CRISPRi parental cells that resulted in the depletion of these double positive cells at the end of the assay. For instance, the population of mCherry⁺/BFP⁺ iKLF6_2 cells decreased from 50.8% to 20.3% whereas the mCherry⁺/BFP⁻ cell population increased from 47.2% to 78.1% at the end of the assay. These competitive proliferation assay results were analysed by normalising the percentage of each cell populations in each week to their respective percentage at the beginning of the assay. Then, the relative fraction of the mCherry⁺/BFP⁺ (iKLF6_2, iKLF6_3 or control) 786-M1A CRISPRi cells and mCherry⁺/BFP⁻ 786-M1A CRISPRi parental cells was determined and the analysed data are shown in figure 28B.

A



B

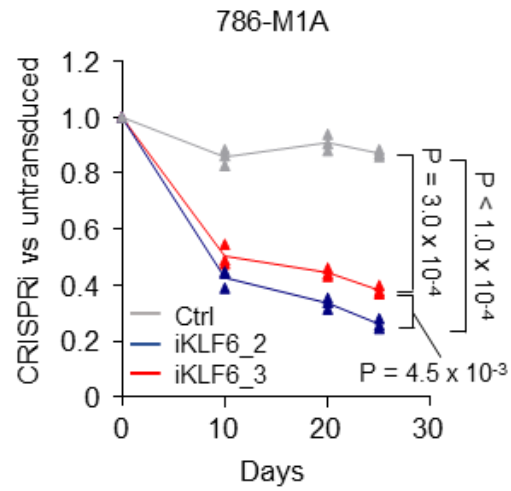


Figure 28: Competitive proliferation assay of the *KLF6*-depleted 786-M1A CRISPRi cells. **(A)** FACS plot of the CRISPRi *KLF6* targeting competitive proliferation assay. **(B)** Analysis of the experiment shown in A. Relative fraction of the *KLF6*-targeted and control 786-M1A CRISPRi cells, normalised to day 0, compared to 786-M1A CRISPRi parental cells. Two-way ANOVA with Tukey's range test.

3.2.6.2 *KLF6* CRISPRi rescue competitive proliferation assay

KLF6 CRISPRi rescue experiment was also performed by reintroducing exogenous *KLF6* into the *KLF6*-depleted 786-M1A CRISPRi cells. In contrast to the *KLF6* CRISPR-Cas9 rescue experiment (section 3.2.6.2), the exogenous *KLF6* CDS was not subjected to any nucleotides substitution because the i*KLF6* tandem constructs target sites resided outside this transgene. The *KLF6* CDS was cloned into the pLVX-Puro expression vector. The 786-M1A CRISPRi cells were transduced with either pLVX-Puro empty vector (hereinafter referred to as EV cells) or pLVX-Puro *KLF6* CDS (hereinafter referred to as *KLF6* CDS cells). This was followed by transducing these EV and *KLF6* CDS cells with either the non-targeting control or i*KLF6_2* construct to generate the following cell lines; 1) non-targeting control + EV cells, 2) i*KLF6_2* + EV cells and 3) i*KLF6_2* + *KLF6* CDS cells.

The non-targeting control + EV cells were used in the control condition. The i*KLF6_2* + EV cells and i*KLF6_2* + *KLF6* CDS cells were used in the *KLF6* inhibition and rescue conditions, respectively. *KLF6* expression in these cells were confirmed by Western blotting (Figure 29A). In each condition, the mCherry⁺/BFP⁺ cells were competed against the mCherry⁺/BFP⁻ 786-M1A CRISPRi parental cells. Figure 29B shows the result of the *KLF6* CRISPRi rescue experiment, represented by the relative fraction of the mCherry⁺/BFP⁺ cells and the mCherry⁺/BFP⁻ cell populations. Consistent with the previous findings, *KLF6* inhibition

resulted in impaired cells growth (*red line*). However, the presence of exogenous KLF6 in the *KLF6*-targeted cells was able to mitigate the proliferative defect caused by the *KLF6* inhibition (*orange line*). Collectively, using two independent approaches to target KLF6 (CRISPR-Cas9 and CRISPRi), I have robustly demonstrated that KLF6 involved in supporting ccRCC cells growth *in vitro*. KLF6 inhibition reduced ccRCC cells growth *in vitro* whilst the reintroduction of exogenous KLF6 was able to alleviate this proliferative defect.

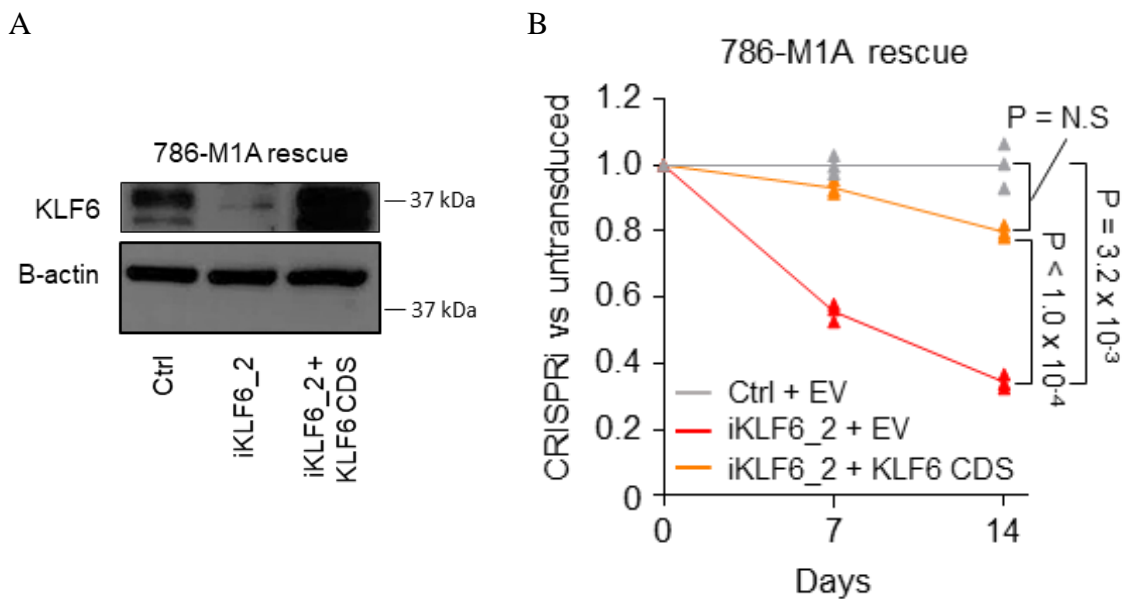


Figure 29: Exogenous KLF6 rescue competitive proliferation assay of the CRISPRi *KLF6*-depleted 786-M1A cells. **(A)** KLF6 expression in the cells used in the *KLF6* CRISPRi rescue competitive proliferation assay. **(B)** Analysis of the rescue competitive proliferation assay. Graph shows the relative fraction of the *KLF6*-targeted, *KLF6*-targeted with the reintroduction of exogenous KLF6 and control 786-M1A CRISPRi cells, normalised to day 0, compared to 786-M1A CRISPRi parental cells. Two-way ANOVA with Tukey's range test.

3.2.7 Investigating the effect of KLF6 inhibition *in vivo*

Next, I investigated the effect of targeting KLF6 on ccRCC cells growth and tumour-forming capability *in vivo*. To test this, CRISPR-Cas9 KLF6-targeted and control 786-M1A as well as the OS-LM1 cells were subcutaneously injected into the athymic nude mice by Sakari Vanharanta. As an additional information, Sakari Vanharanta performed the cells injection for all *in vivo* experiments in the lab to ensure consistencies across the experiments. The cells growth was assessed by measuring the bioluminescence signals weekly until the signals had saturated. Both 786-M1A and OS-LM1 cells harboured the TGL reporter transgene that encodes for luciferase, an enzyme that catalyses the oxidization of D-Luciferin in a reaction that produces bioluminescence as by-product. Hence, to perform the bioluminescence imaging experiment, D-luciferin was injected into the mice intraperitoneally. The bioluminescence signals positively correlate with the cells abundance. For instance, cells that are rapidly growing would have high bioluminescence signals due to the presence of more cells whereas the slow proliferating cells would have lower bioluminescence signals. Once the subcutaneous tumours were palpable, the tumour volume was calliper measured until the end of the assay.

3.2.7.1 KLF6-targeted 786-M1A cells tumour formation assay

Figure 30A illustrates the experimental set-up for the CRISPR-Cas9 KLF6-targeted 786-M1A *in vivo* tumour formation assay. Three animal groups were set up in which each group consisted of five mice. The mice in each group were fed with doxycycline-supplemented food to induce the Cas9 expression. After the cells inoculation, the bioluminescence signals in each mice were measured which are shown in figure 30B. The average bioluminescence signals in each group were relatively similar, demonstrating consistencies in cells preparation and injection.

The bioluminescence imaging was performed for three weeks before the signals had saturated. Figure 30C shows the bioluminescence signals in each mice three weeks post-inoculation. Overall, the mice in control group had higher bioluminescence signals than the mice in sgKLF6_4 and sgKLF6_5 groups, indicating that the KLF6-targeted 786-M1A cells grew slower than the control cells. To ensure that the difference between these KLF6-targeted and control groups was not due to variation in the initially inoculated cells, I normalised the week 3 bioluminescence reads of each mice to their corresponding inoculation day signals. The relative to day 0 photon flux of the mice in control group was significantly higher compared to the mice in both KLF6-targeted groups (Figure 30D). This data demonstrated that KLF6 perturbation reduced the 786-M1A cells proliferation *in vivo*, which was in concordant with the *in vitro* observations.

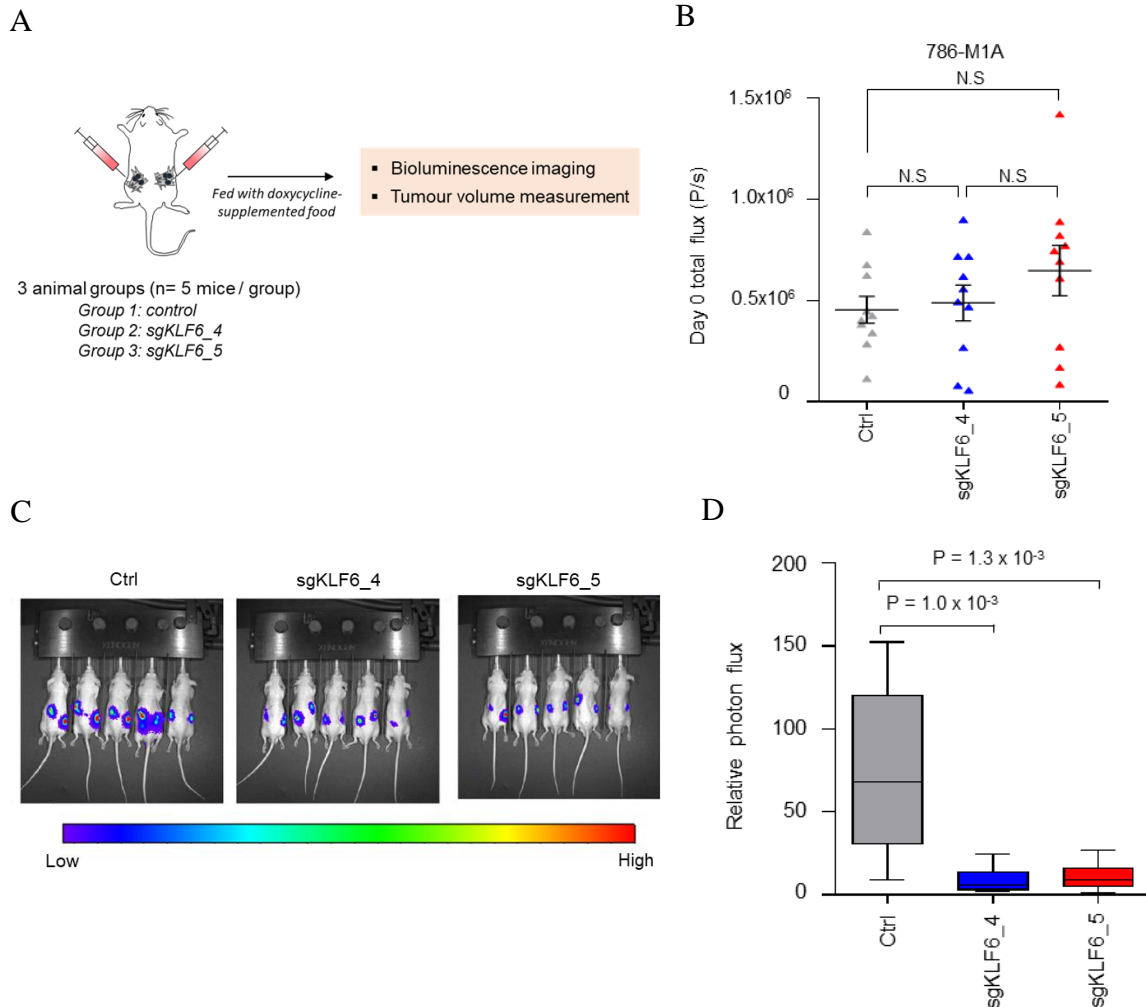


Figure 30: Bioluminescence reads of the CRISPR-Cas9 KLF6-targeted 786-M1A cells *in vivo*. **(A)** Schematic illustrating the experimental design for KLF6-targeted 786-M1A cells tumour formation assay. **(B)** Bioluminescence reads of the KLF6-targeted and control cells at the inoculation day. N=10 injection sites / group. One-way ANOVA with Tukey's range test. **(C)** Bioluminescence images of mice in the KLF6-targeted and control groups three weeks post-inoculation. **(D)** Normalised to day 0 bioluminescence reads in week 3 of each animal group. One-way ANOVA with Tukey's range test.

The tumour volume was determined by calliper measurement after the tumours became palpable. It was observed that the KLF6-targeted 786-M1A cells were still able to form tumours.

Nevertheless, due to these cells impaired growth, the formed tumours were much smaller compared to the tumours of the control cells. At the end of the experiment, the average tumour volume in the control group was 480 mm³ whereas the average tumours volume of the sgKLF6_4 and sgKLF6_5 groups were 155 mm³ and 177 mm³, respectively (Figure 31A). The subcutaneous tumours were extracted and weighed in order to validate these observations. In line with the tumour volume data, the average control group tumour weight was about 300 mg whereas the average tumour weight of the KLF6-targeted groups was around 100 mg (Figure 31B).

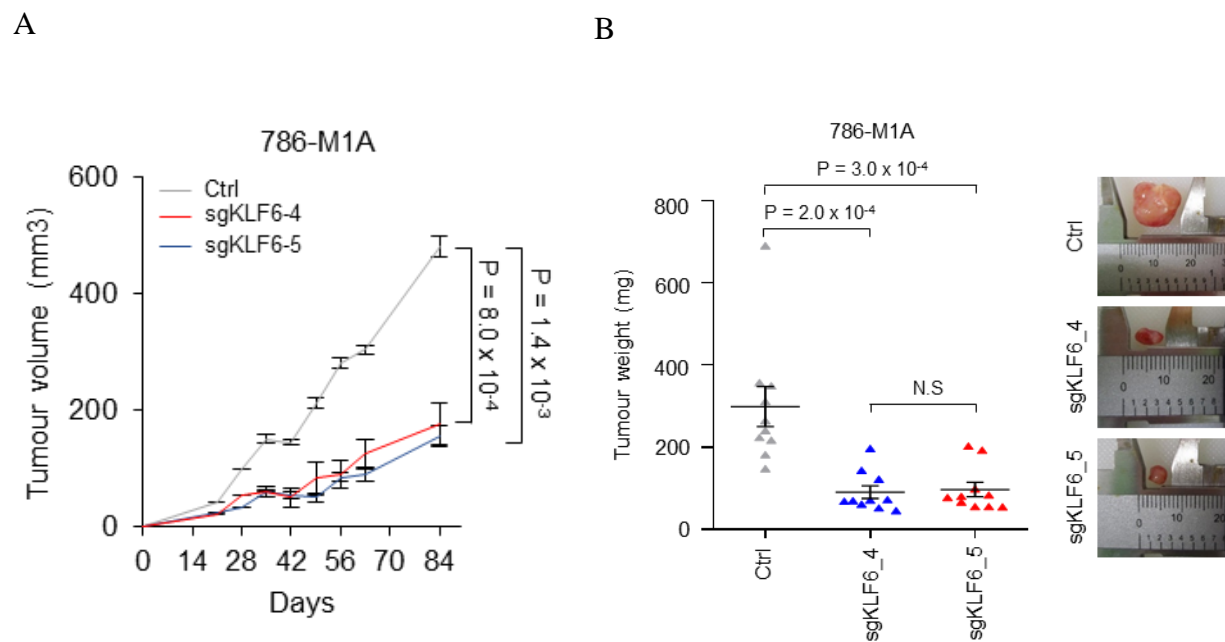


Figure 31: Tumours size of the CRISPR-Cas9 KLF6-targeted 786-M1A cells. **(A)** The average tumours volume of the KLF6-targeted and control groups at the indicated time points. N=10 tumours /group. Error bars, SEM. Two-way ANOVA with Tukey’s range test. **(B)** The weight of tumours in each group at the end of the experiment shown in A. One-way ANOVA with Tukey’s range test.

3.2.7.2 KLF6-targeted OS-LM1 tumour formation assay

The tumour formation assay was also performed on the CRISPR-Cas9 KLF6-targeted OS-LM1 cells. There were 6 mice in the control group whereas the sgKLF6_4 and sgKLF6_5 group consisted of 7 mice / group. Figure 32A shows the bioluminescence read of the inoculated cells in each group at day 0. The bioluminescence reads of each mice at day 21 were normalised to their respective day 0 signals. These normalised bioluminescence reads are shown in figure 32B. The sgKLF6_4 and sgKLF6_5 groups had lower normalised to day 0 bioluminescence reads than the control group, consistent with the observations that targeting KLF6 in ccRCC cells resulted in impaired cells proliferation. This consequently led to the formation of smaller tumours compared to tumours of the control cells (Figure 32C). The average tumour volume of the control group was 472.5 mm³ whereas the average tumour volume of the sgKLF6_4 and sgKLF6_5 group was 194.3 mm³ and 235.5 mm³, respectively.

In sum, targeting KLF6 in the 786-M1A and OS-LM1 cells reduced the cells growth *in vivo*. Both of these KLF6-targeted cells were still capable to form tumours. Nonetheless, in line with these cells impaired growth, the formed tumours were smaller compared to the tumours of the control cells. For instance, in the 786-M1A experiment, there was about three-fold difference between the average tumour size of the control and KLF6-targeted groups. These findings further corroborated the role of KLF6 in supporting ccRCC cells growth both *in vitro* and *in vivo*.

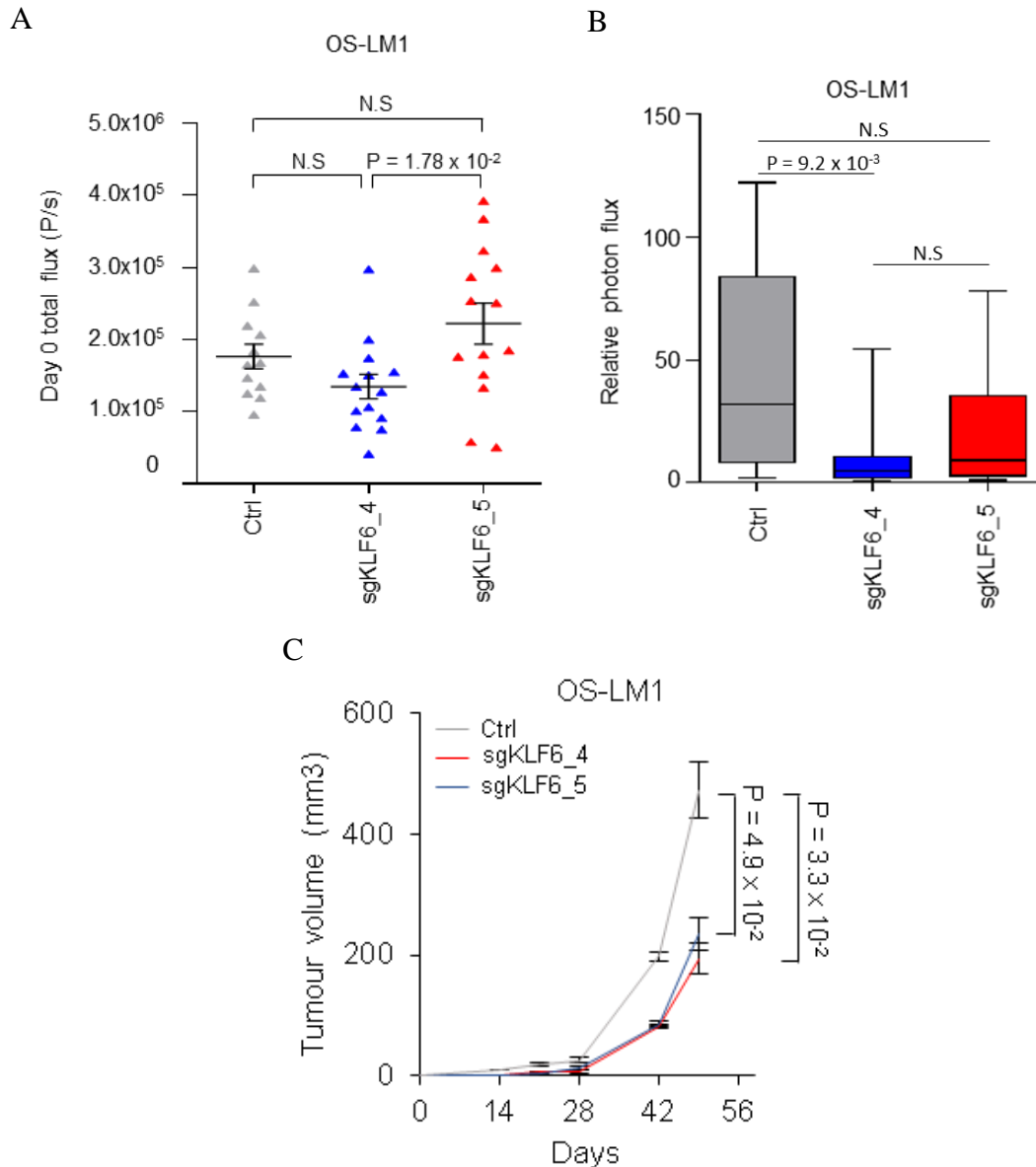


Figure 32: Tumour formation assay of the CRISPR-Cas9 KLF6-targeted OS-LM1 cells. **(A)** Bioluminescence reads of the KLF6-targeted and control OS-LM1 cells at the inoculation day. N=12 injection sites for control group. N = 14 injection sites for sgKLF6_4 and sgKLF6_5 groups. One-way ANOVA with Tukey's range test. **(B)** Normalised to day 0 bioluminescence reads in week 3 of each animal group. One-way ANOVA with Tukey's range test. **(C)** The average tumours volume of the KLF6-targeted and control groups at the indicated time points. N= 10 tumours for the control group. N = 14 tumours for the sgKLF6_4 and sgKLF6_5 groups. Error bars, SEM. Two-way ANOVA with Tukey's range test.

3.2.7.3 Genetic analysis of the KLF6-targeted 786-M1A tumours

As demonstrated in the previous sections, the CRISPR-Cas9 KLF6-targeted cells were still capable to form tumours. Since the mutations induced by the CRISPR-Cas9 approach were random, it was postulated that these KLF6-targeted 786-M1A and OS-LM1 cell populations might consist of cells that retained the KLF6 activity as well as wild-type escaper cells. Furthermore, there might be selective growth advantage on the escaper clones especially since the subcutaneous tumour formation assays were performed for an extended period of time. Thus, to directly test this possibility, genetic analysis was performed on the KLF6-targeted 786-M1A subcutaneous tumours. These tumours were harvested at the end of the assay which was 84 days (12 weeks) post-cells inoculation.

Genomic DNA was extracted from tumours of the sgKLF6_4 (n=2) and control group (n=1). The sgKLF6_4 targeted region was amplified and the amplicons were sent for Illumina high-throughput sequencing in order to assess the percentage of mutated and wild-type *KLF6* alleles in these extracted tumours. As expected, it was found that 99.6% of reads in the control tumour were wild-type *KLF6*. However, in the two tumours targeted by sgKLF6_4, I found that the wild-type *KLF6* alleles in each of this tumour were 18% and 66%, respectively (Figure 33). The fraction of *KLF6* wild-type allele in these sgKLF6_4 targeted tumours was significantly higher compared to the KLF6-targeted 786-M1A cells *in vitro*, in which < 3% of the *KLF6* alleles were wild-type (Figure 21A). This finding confirmed the speculation that due to the selective growth advantage, at least a fraction of tumours formed by the KLF6-targeted cells contained the wild-type escaper clones.

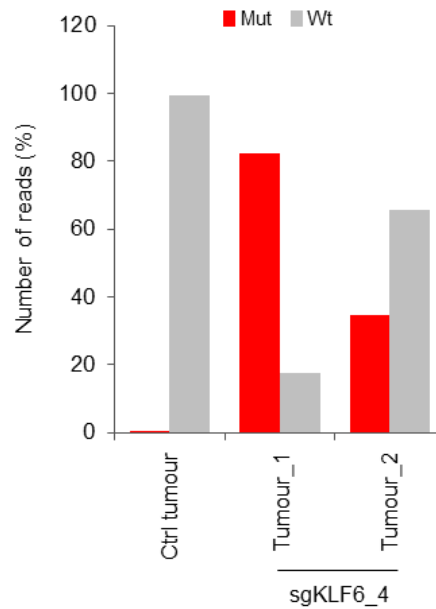


Figure 33: Genetic analysis of the KLF6-targeted 786-M1A tumours. Fraction of wild-type and mutant *KLF6* allele at the sgKLF6_4 target region in the control and KLF6-targeted subcutaneous tumours harvested 84 days (12 weeks) post-cell inoculation.

3.2.7.4 *KLF6*-targeted 786-M1A lung colonisation assay

Advanced stage ccRCC is highly aggressive which predominantly metastasises to the lung or liver. The main ccRCC cell line used in this study was the 786-M1A, a metastatic derivative of 786-O cells. Vanharanta *et al.* have demonstrated that these 786-M1A cells are aggressive and have a significantly higher lung colonisation capability as compared to its parental 786-O cell line. Thus, I next sought to investigate whether KLF6 inhibition would have any effect on the 786-M1A cells lung colonisation capability.

To perform the lung colonisation assay, the CRISPRi *KLF6*-targeted 786-M1A cells were used. *KLF6* expression in these cells was first assessed prior to using them in the *in vivo* lung

colonisation assay. Strong and stable *KLF6* repression was observed in these *KLF6*-targeted cells as compared to the control cells (Figure 34A). The *KLF6*-depleted and control 786-M1A CRISPRi cells were inoculated into the lateral tail vein of the NOD/SCID mice (N=5 mice/group). The lung bioluminescence signals were measured right after the cells inoculation (day 0 measurement), followed by performing the bioluminescence imaging weekly until the end of the assay. The mice lung bioluminescence signals in each week were normalised to their respective signals at the day 0. The average normalised to day 0 bioluminescence signals for each animal group is shown in figure 34B. It was observed that the *KLF6*-deficient cells had a profound reduced lung colonisation capacity compared to the control 786-M1A CRISPRi cells, which was in line with the previous observations that *KLF6* inhibition led to reduced ccRCC growth *in vitro* and *in vivo*. Nonetheless, the difference in the average normalised photon flux between these groups did not reach statistical significance. This was possibly due to the high variability in the bioluminescence signals of the mice in the control group.

The lungs were extracted at the end of the assay and processed for human vimentin IHC staining. This was to confirm that the lung metastatic foci were formed by the inoculated ccRCC cells which were of human origin. Figure 34C shows the representative mice lung bioluminescence images from each group along with their respective human vimentin-stained histological lung sections. The vimentin-stained lung metastatic foci of the animal in each group were quantified in which the quantification data are shown in figure 34D. Four out of five mice in the control group had significantly higher overall tumour load in their lungs compared to the mice in the *KLF6*-targeted groups.

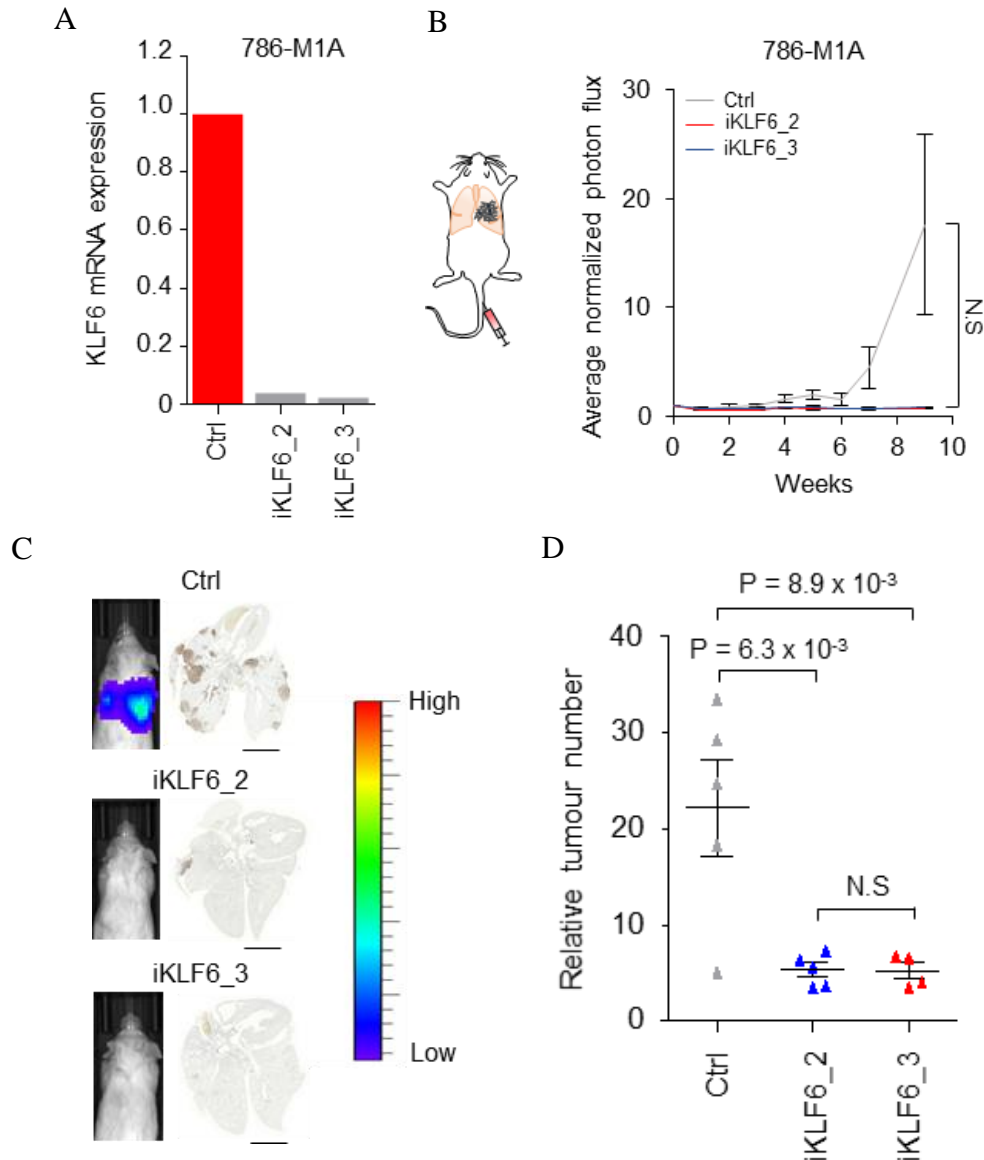


Figure 34: Lung colonisation assay of the CRISPRi *KLF6*-depleted 786-M1A cells. **(A)** *KLF6* expression in *KLF6*-targeted and control 786-M1A CRISPRi cells prior to tail vein inoculation. **(B)** Average normalised to day 0 lung photon flux of the *KLF6*-targeted and control 786-M1A CRISPRi cells at the indicated time points. N=5 mice/group. Error bars, SEM. Two-way ANOVA with Tukey's range test. **(C)** Representative bioluminescence images and the respective lung sections stained with human vimentin. Scale bar, 5mm. **(D)** Quantification of vimentin-stained lung metastatic foci of each animal group. N= 5 lung sections for control and iKLF6_2 groups. N= 4 lung sections for iKLF6_3 group. One-way ANOVA with Tukey's range test.

3.3 Summary

Through active chromatin profiling, KLF6 was identified in a previous study in the lab to be in the vicinity of one of the strongest super enhancer in ccRCC. In line with the possibility that *KLF6* expression in ccRCC could be super enhancer-driven, *KLF6* expression was found to be high and relatively specific to ccRCC as compared to other tumour types. Importantly, in comparison to normal kidney tissues, *KLF6* expression was significantly upregulated in ccRCC clinical samples, suggesting the pro-tumourigenic role of this transcription factor KLF6 in supporting ccRCC pathogenesis.

In contrast to several studies that have suggested the growth suppressive function of KLF6, KLF6 was found to have a growth promoting role in ccRCC. CRISPR-Cas9 and CRISPRi-mediated KLF6 targeting in ccRCC cell lines resulted in impaired cells growth *in vitro*. This was demonstrated through the competitive proliferation assay where the KLF6-targeted cell population was depleted from the assay and outgrown by the control cell population. The reduced rate of proliferation was confirmed to be the consequence of KLF6 inhibition in these cells because the reintroduction of exogenous KLF6 into the KLF6-targeted cells was able to alleviate this proliferative defect. Consistent with the phenotypic effect *in vitro*, CRISPR-Cas9-mediated KLF6 inhibition reduced the ccRCC cells growth *in vivo* which subsequently resulted in the formation of smaller subcutaneous tumours compared to tumours of the control cells. Furthermore, targeting *KLF6* using the CRISPRi approach in the 786-M1A cells, which had enhanced metastatic capabilities, significantly reduced the cells lung colonisation capability. Overall, these data indeed supported the hypothesis that this super enhancer-associated transcription factor KLF6 plays an important role in supporting ccRCC pathogenesis.

Chapter 4

Interrogating the role of super enhancer in
driving *KLF6* expression

4.1 Introduction

In the previous chapter 3, it was demonstrated that *KLF6* was an important transcriptional regulator that involved in supporting ccRCC growth both *in vitro* and *in vivo*. This was well-aligned with its high expression and association with one of the strongest super enhancer in ccRCC. Whether this adjacent super enhancer locus actually drove *KLF6* expression in ccRCC remained to be investigated. Enhancer/super enhancer can activate the expression of distant genes that are located thousands of base pairs away. Therefore, it was crucial to test and confirm whether this super enhancer region plays a role in supporting *KLF6* expression in ccRCC which was the main focus of this chapter. To functionally investigate the link between this super enhancer and regulation of *KLF6* expression in ccRCC, CRISPRi tool was employed to inactivate several constituent enhancers within the super enhancer locus. This was followed by assessing the *KLF6* expression level upon repressing the activity of these enhancers. In addition, the CRISPR-Cas9 mediated deletion of large segment of the super enhancer region was also performed in order to test the role of this super enhancer in driving *KLF6* expression.

As discussed in Chapter 1 (section 1.16), cancer-associated super enhancers can be sensitive to perturbation of its constituent enhancers or regulatory components that maintain the super enhancer landscape such as the BRD4 and CDK7. Repressing the activity of the constituent enhancers can disrupt the super enhancer and in some cases, even would result in the super enhancer complete inactivation. Thus, targeting super enhancer has been widely explored as an alternative treatment option for cancer due to its sensitivity to perturbation as well as the cancer cells high dependency towards the super enhancer-driven genes. Therefore, it was interesting to examine whether this *KLF6*-associated super enhancer would also be sensitive to

perturbation in the activity of its constituent enhancers, or perhaps this super enhancer locus acts in a robust fashion to drive *KLF6* expression in ccRCC.

Multiple transcription factors can bind the super enhancer region to co-regulate the expression of their downstream targets. Given the prominent role of the transcription factor HIF2A in driving ccRCC pathogenesis, works in this chapter also focused on investigating whether there was any link between the ccRCC-initiating VHL-HIF2A pathway and the modulation of *KLF6* expression in ccRCC. This was initially done by examining the correlation between the *EPAS1*-encoded HIF2A and *KLF6* expression in the ccRCC RNA-Seq TCGA data set which will be discussed in further details in the results section below.

4.2 Results

4.2.1 CRISPRi-mediated super enhancer inactivation

The CRISPRi and tandem sgRNAs approaches were employed to inactivate several distinct enhancers within the *KLF6* super enhancer locus in the 786-M1A cells. Previous study in the lab has demonstrated that these strategies were highly efficient and specific in targeting the distal enhancer regions¹⁹⁶. The H3K27ac ChIP-Seq track in figure 35A shows the targeted regions in which these regions were named as iSE-1 – iSE-5. In order to design the sgRNAs targeting these regions, the p300 ChIP-Seq data, previously generated by Paulo Rodrigues, were used as a guide¹⁹⁶. As a transcriptional co-factor, p300 is a marker for enhancer region. p300 peaks are found in the valley of H3K27ac signals in which this region is considered to be the transcription factors binding site¹⁴⁸. In total, five independent tandem sgRNAs targeting the iSE-

1 – iSE-5 regions were designed. Figure 35B exemplified the tandem sgRNAs construct targeting the p300 peak in the valley of H3K27ac iSE-2 region. Also shown is the dCas9-KRAB protein recruitment to the p300 region bound by the two sgRNAs construct.

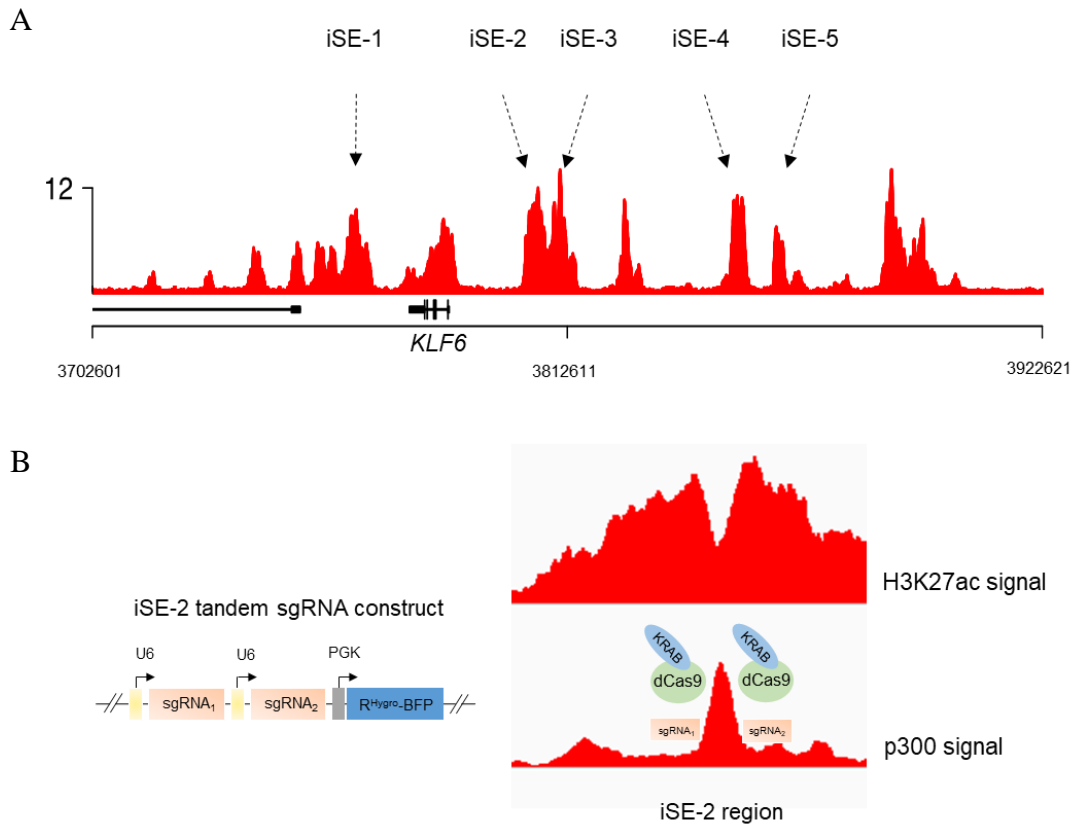


Figure 35: Strategy for the CRISPRi-mediated inactivation of the *KLF6*-associated super enhancer. **(A)** Several constituent enhancer regions, iSE-1 – iSE-5, targeted by CRISPRi. **(B)** Tandem sgRNAs approach targeting the p300 peak in the valley of H3K27ac iSE-2 region.

The 786-M1A CRISPRi cells were transduced with either one of the iSE-1–iSE-5 tandem sgRNAs construct. For control, the 786-M1A CRISPRi cells were transduced with the tandem non-targeting control construct. I subsequently performed the H3K27ac chromatin immunoprecipitation on each of these cells. The ChIP-Seq libraries were prepared by Paulo

Rodrigues whereby the sequencing data were subsequently analysed by Sakari Vanharanta. In agreement with previous study in the lab, the combination of CRISPRi and tandem sgRNAs targeting approaches were efficient in specifically repressing the activity of their respective targeted region. This was marked by a complete loss of H3K27ac signals, marker for an active enhancer, at each of this targeted region (Figure 36A). In parallel, I also performed ChIP-qPCR on the purified H3K27ac ChIP DNA above and found profound reduction in H3K27ac occupancy at each of the inactivated enhancer region, thus validating the ChIP-Seq data (Figure 36B).

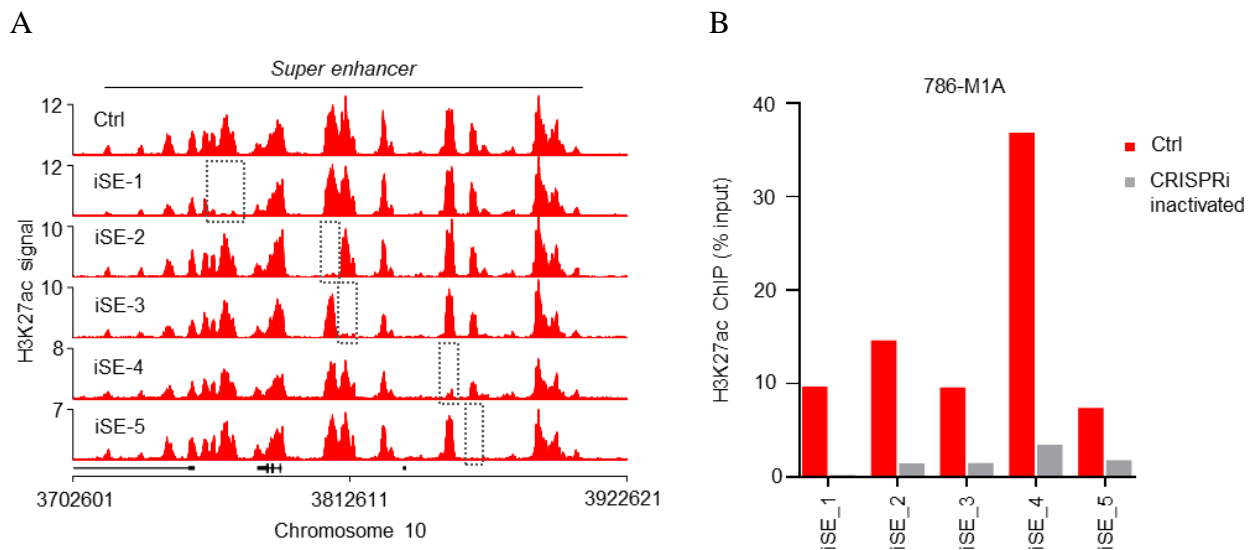


Figure 36: CRISPRi high efficiency in repressing the activity of constituent enhancers. **(A)** H3K27ac ChIP-Seq signal in the *KLF6* locus. The CRISPRi-targeted enhancer regions, iSE-1 – iSE-5, are indicated by the boxes. **(B)** H3K27ac ChIP-qPCR of the CRISPRi-inactivated iSE-1 – iSE-5 enhancers regions.

In contrast to the previous reports that cancer-associated super enhancers can be sensitive to perturbation of their constituent enhancers, there was no interdependency observed between individual enhancers within this *KLF6*-associated super enhancer locus (Figure 36A). Rather,

this super enhancer remained strongly active, demonstrating the robustness of this *KLF6*-associated super enhancer landscape. Next was to examine whether inactivating these enhancer regions would have any effect on the expression of nearby *KLF6*. There was no massive *KLF6* downregulation by the repression each of this constituent enhancer individually (Figure 37). For instance, there was only about 25% and 10% reduction in the *KLF6* mRNA level upon inactivating the iSE-2 and iSE-3 enhancer region, respectively. Furthermore, inhibiting the iSE-1, iSE-4 and iSE-5 enhancer regions did not result in *KLF6* downregulation, yet the *KLF6* expression level remained similar to the level seen in control cells. These observations seemed to suggest that this super enhancer locus operated in a modular fashion to drive *KLF6* expression in ccRCC. This could possibly explain why inactivating one individual enhancer within this super enhancer locus was not sufficient to significantly reduce *KLF6* expression in these cells.

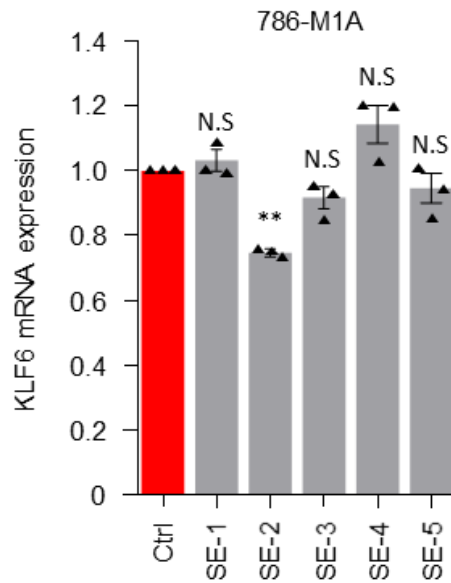


Figure 37: *KLF6* expression in the individually inactivated iSE-1 – iSE-5 region in 786-M1A CRISPRi cells. Average of three experiments. Error bars, SEM. One-way ANOVA with Dunnett’s test. * P < 0.05, ** P < 0.005 and *** P < 0.0005.

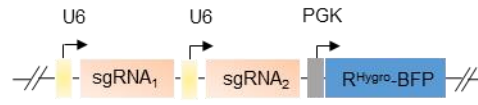
4.2.2 Combinatorial enhancers targeting

It was speculated in the previous section that this super enhancer locus acted in a modular manner in driving the expression of *KLF6* in these cells. Thus, to test this possibility, I attempted to inactivate two constituent enhancer regions simultaneously and assessed whether this combinatorial targeting approach would lead to further reduction in the *KLF6* mRNA level. As demonstrated in figure 37, targeting of these enhancers individually did not affect the *KLF6* mRNA level apart from the iSE-2 inactivation where 25% reduction in *KLF6* expression level was observed. Hence, I chose to inactivate the iSE-2 region in combination with either iSE-3 or iSE-4 region. The combinatorial enhancers targeting strategy is illustrated in figure 38A.

In brief, the 786-M1A CRISPRi cells were first transduced with the iSE-2-BFP-hygromycin vector. The positive cells were hygromycin-selected, followed by second round of transduction with either iSE-3 or iSE-4-eGFP-hygromycin vector. Then, I sorted for the double BFP⁺ and eGFP⁺ cell populations and subsequently assessed the expression of *KLF6* in these cells. In line with the hypothesis, combinatorial iSE-2 and iSE-3 inactivation resulted in 40% reduction in the *KLF6* mRNA level, indicating that there was some additive effect when these two enhancers were targeted simultaneously (Figure 38B). Moreover, compared to the effect of individual iSE-2 and iSE-4 targeting, simultaneous iSE-2 and iSE-4 inactivation also resulted in a slightly better reduction in the expression of *KLF6* (Figure 38B). Despite the observed additive effect upon combinatorial enhancer targeting, *KLF6* expression in these cells remained fairly strong.

A

1st round



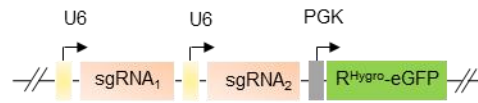
iSE-2_BFP

*Transduced with iSE-2_BFP and
selected with hygromycin*



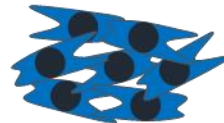
Hygromycin resistant, iSE-2_BFP
transduced 786-M1A cells

2nd round



iSE-3_eGFP

Transduced with iSE-3 eGFP



*Sorting for double positive
BFP and eGFP cells*



iSE-2_BFP and iSE-3_eGFP
transduced 786-M1A cells

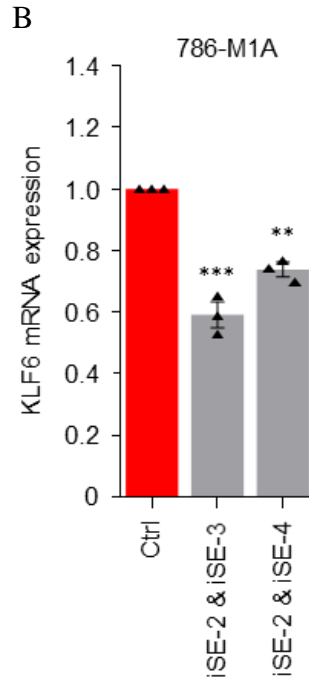
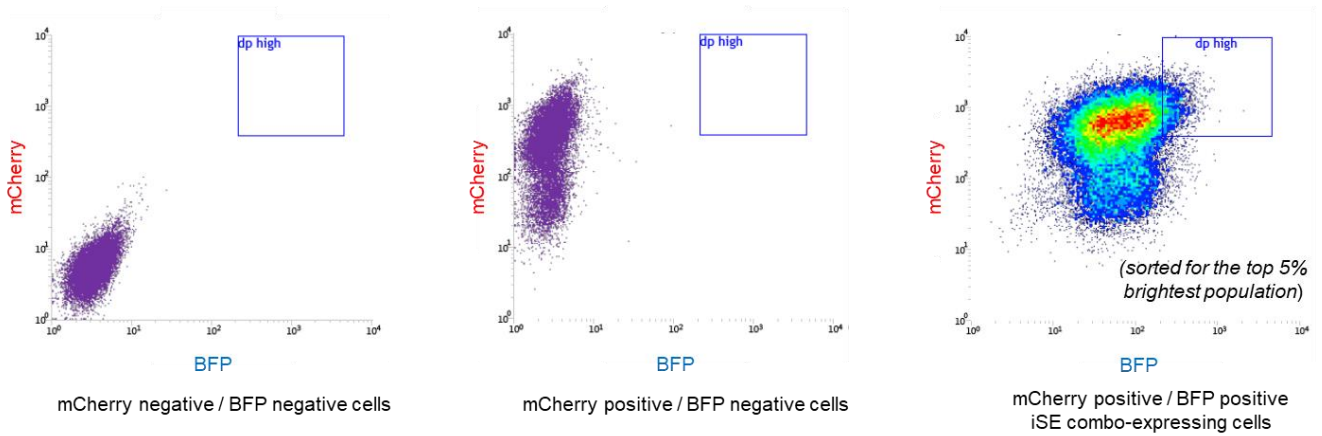


Figure 38: Combinatorial enhancers targeting. **(A)** Schematic illustrating the combinatorial enhancer targeting strategy. **(B)** *KLF6* expression in the 786-M1A cells with combinatorial enhancer targeting. Average of three experiments. Error bars, SEM. One-way ANOVA with Dunnett’s test. * $P < 0.05$, ** $P < 0.005$ and *** $P < 0.0005$.

The additive effect observed when two enhancers were simultaneously inactivated had prompted me to test the effect of targeting all five enhancers at once. The following strategy was employed where the 786-M1A CRISPRi cells were lentivirally-transduced with iSE-1, iSE-2, iSE-3, iSE-4, and iSE-5-targeting constructs simultaneously, followed by sorting for the top 5% BFP⁺ cell population. The rationale of sorting the population of cells with the brightest BFP expression was that these cells could express all five tandem sgRNAs constructs (hereinafter referred to as iSE combo-expressing 786-M1A cells). Figure 39A shows the FACS gating strategy used to sort for these iSE combo-expressing cells. It was observed that concurrent inactivation of these five enhancers resulted in about 60% reduction in the *KLF6* mRNA level

(Figure 39B), further corroborating the hypothesis that this super enhancer region operates in a modular fashion to drive *KLF6* expression in ccRCC.

A



B

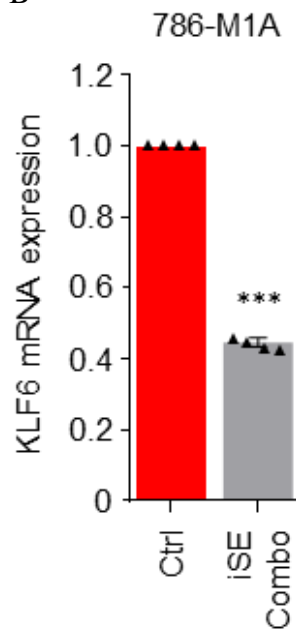


Figure 39: Simultaneous inactivation of all five enhancer regions. (A) The gating strategy to sort for the iSE combo-expressing 786-M1A cells. (B) KLF6 mRNA expression in the 786-M1A cells that had simultaneous inactivation of all five enhancer regions. Average of four experiments. Error bars, SEM. Two-tailed Student's t-test. * $P < 0.05$, ** $P < 0.005$ and *** $P < 0.0005$.

4.2.3 CRISPR-Cas9 mediated deletion of the super enhancer region

By employing the CRISPRi-based enhancer inactivation, I have demonstrated that this super enhancer functions in a modular fashion to drive *KLF6* expression. Inactivating individual enhancer did not significantly affect the expression of *KLF6*. However, there was a progressive depletion in the *KLF6* expression level upon repressing several enhancers simultaneously. To further consolidate these findings, I next attempted to delete the entire enhancers cluster upstream of *KLF6* locus using the CRISPR-Cas9 approach and assessed the *KLF6* expression level. In order to delete this 113Kb large enhancer region, two independent tandem sgRNAs constructs were designed, namely the Del_SE_2 and Del_SE_3. Each of this tandem sgRNAs construct expressed two sgRNAs; the first sgRNA was designed to target the 5' end whereas the second sgRNA targeted the 3' end of this large enhancers cluster. Simultaneous Cas9 recruitment and cleavage of its targeted sites could potentially result in large deletion of this enhancers cluster. Figure 40A illustrates the strategy employed to delete this enhancer cluster as well as the Del_SE_2 tandem sgRNAs construct. .

The Cas9-expressing 786-M1A and OS-LM1 cells were transduced with either Del_SE_2 or Del_SE_3 tandem sgRNAs construct. For control, these cells were transduced with the tandem non-targeting control construct. This was then followed by assessing the expression of *KLF6* in all of the cells generated above. However, only relatively modest downregulation of *KLF6* was observed in the population of these Del_SE_2 and Del_SE_3-transduced 786-M1A (Figure 40B) and OS-LM1 cells (Figure 40C). For instance, I observed about 20% and 40% reduction in the expression of *KLF6* in the Del_SE_2 and Del_SE_3-transduced 786-M1A cells, respectively. In addition, the level of *KLF6* downregulation in the Del_SE_3-transduced cells

was similar to the effect seen when I concurrently inactivated the iSE-2 and iSE-3 enhancer regions in the 786-M1A cells (Figure 38B).

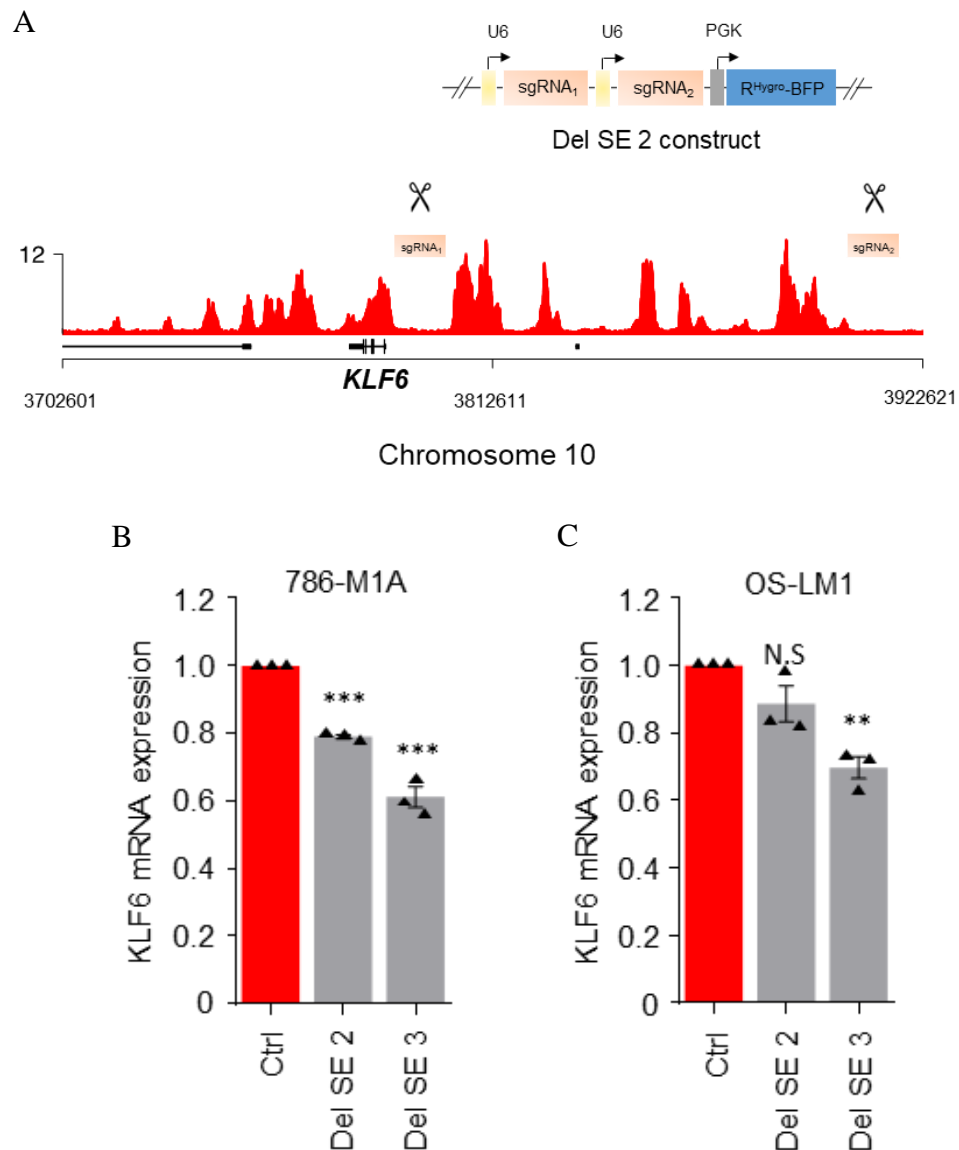


Figure 40: CRISPR-Cas9-mediated deletion of the large enhancers cluster in the population of 786-M1A and OS-LM1 cells. **(A)** Schematic of the tandem sgRNAs construct and strategy used for the CRISPR-Cas9-mediated deletion of the large enhancers cluster upstream of *KLF6*. **(B and C)** *KLF6* mRNA expression in the *enhancers-deleted* **(B)** 786-M1A and **(C)** OS-LM1 cells. Average of three experiments. Error bars, SEM. One-way ANOVA with Dunnett's test. * $P < 0.05$, ** $P < 0.005$ and *** $P < 0.0005$.

The modest reduction in the *KLF6* expression level observed in figure 40B-C could possibly be due to the heterogeneity in the CRISPR-Cas9 targeting efficiency in these cells. It was speculated that there was the presence of wild-type cell population as well as population of cells that did not harbour the desired homozygous large deletion of this targeted region. Also, it was important to point out that deleting such a large segment of DNA on both alleles was inefficient. Nonetheless, I decided to pursue this super enhancer deletion experiment in more detail by performing single-cell sorting of the Del_SE_3-transduced 786-M1A cells in order to identify clones that had a homozygous deletion of the region. The reason for using these Del_SE_3-transduced 786-M1A cells for single-cell sorting was that these cells had a better *KLF6* downregulation. Then I performed a PCR-based screening strategy to identify single cell-derived clones that would harbour a homozygous large deletion of this region. The basis of screening strategy was to amplify a small region in the middle of the deleted enhancers cluster (Figure 41A). In theory, there should not be any amplified product in the clones that harboured a homozygous large deletion of this region.

Several single cell-derived clones were screened using this approach. I identified clones with putative homozygous deletion (Del_SE_3_19), heterozygous deletion (Del_SE_3_15) as well as wild-type clone with no deletion (Del_SE_3_9) (Figure 41A). The Del_SE_3_19 clone could potentially possess the homozygous deletion of the entire enhancers region due to the absence of any amplified product. In contrast, the Del_SE_3_9 clone had a strong amplified product band, indicating that the targeted enhancers cluster was still intact. The Del_SE_3_15 clone, on the other hand, could possibly harbour the heterozygous deletion because the intensity of the amplified product band appeared to be the intermediate of Del_SE_3_9 and Del_SE_3_19 clones. As a positive control, I performed PCR amplification of a region within

the *EPASI* locus using the same genomic DNA used in this deletion screening experiment. The respective *EPASI* region was able to be amplified in all of the screened clones, thus validating the quality of the genomic DNA templates.

Next, I performed H3K27ac ChIP-Seq on these Del_SE_3_9, Del_SE_3_15 and Del_SE_3_19 clones in order to assess the targeted region H3K27ac signals in each of this clone. Like the previous ChIP-Seq experiments, the sequencing libraries were prepared by Paulo Rodrigues whereby the ChIP-Seq data were analysed by Sakari Vanharanta. In agreement with the PCR screening data, there was no H3K27ac signal detected in the Del_SE_3_19 clone, thus confirming that this clone indeed harboured a homozygous large deletion of the enhancers cluster. There were reduction in H3K27ac signals in the Del_SE_3_15 clone and this was in line with the prediction that this clone might carry a heterozygous deletion. Moreover, there were high H3K27ac signals observed in the Del_SE_3_9 clone targeted region, consistent with the PCR screening data that suggested the enhancers cluster in this clone was still intact (Figure 41B). Next was to determine whether the *KLF6* expression level in these clones correlated with their enhancers cluster deletion status. In agreement, there was about 65% reduction in the expression of *KLF6* in the Del_SE_3_19 clone which carried the homozygous large deletion (Figure 41C). The magnitude of *KLF6* downregulation in this clone was similar to the effect of inhibiting all five enhancer regions simultaneously using the CRISPRi approach (Figure 39B). Moreover, there was ~50% reduction in the *KLF6* mRNA level in the Del_SE_3_15 clone. As expected, the *KLF6* expression level in the Del_SE_3_9 wild-type clone was similar to the level of the control clone (Figure 41C).

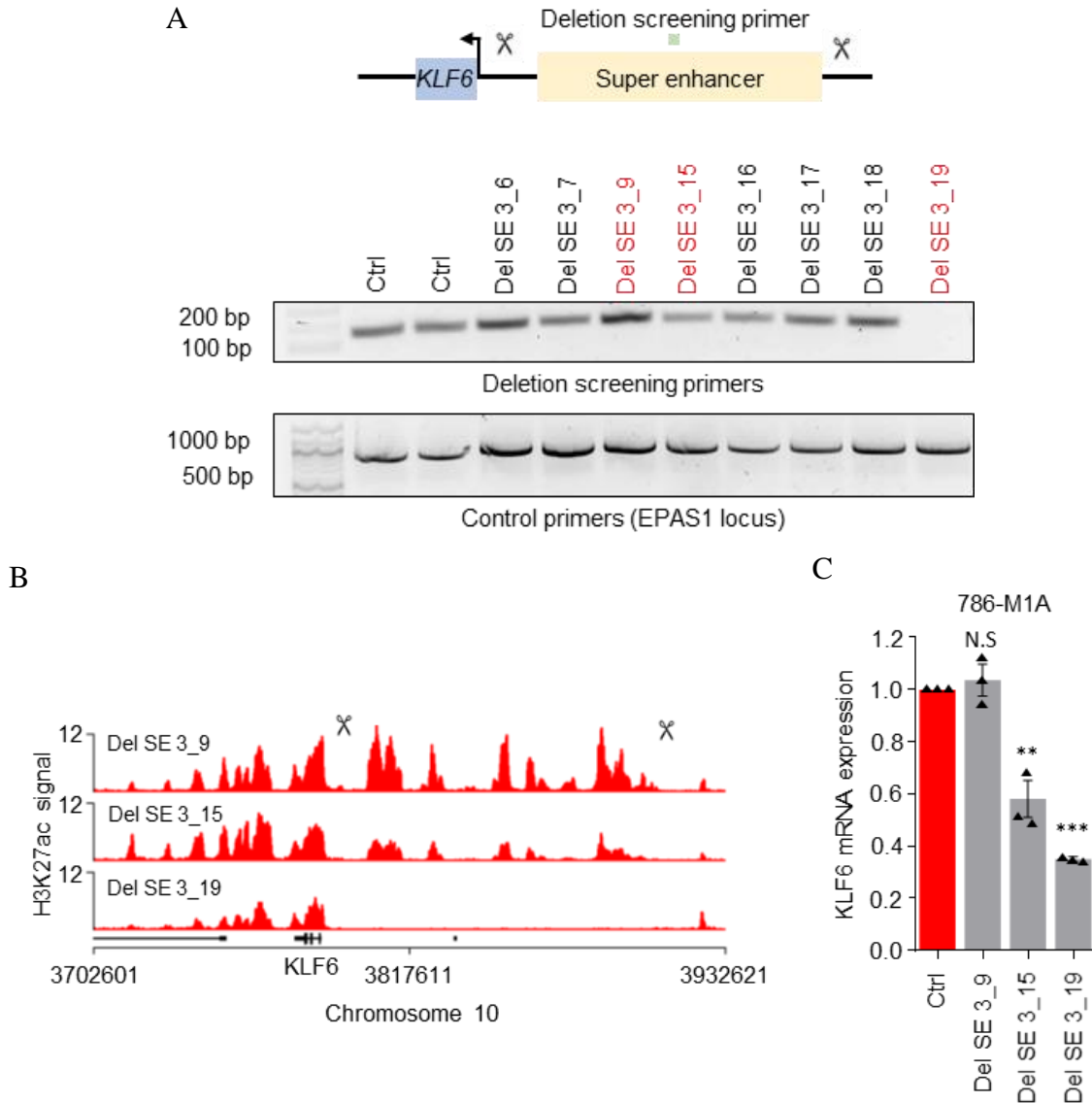


Figure 41: Large enhancers cluster deletion in the single cell-derived clones of the Del_SE_3-transduced 786-M1A cells. **(A)** PCR-based screening for single cell-derived clones that harboured deletion of the large enhancers cluster. Clones shown in red, Del_SE_3_9, Del_SE_3_15 and Del_SE_3_10, were selected for further analysis. Green bar shows the amplified region for the PCR screening strategy. The *EPAS1* locus was used as genomic control region. **(B)** H3K27ac ChIP-Seq signals of the *KLF6* locus in clones with no deletion (Del_SE_3_9), heterozygous deletion (Del_SE_3_15) and homozygous deletion (Del_SE_3_19). **(C)** Corresponding *KLF6* expression in the single cell-derived clones shown in B. Average of three experiments. Error bars, SEM. One-way ANOVA with Dunnett's test. * $P < 0.05$, ** $P < 0.005$ and *** $P < 0.0005$.

Collectively, these data demonstrated that *KLF6* expression in ccRCC was indeed supported by this nearby super enhancer in a modular fashion. As briefly highlighted in the previous introduction section, enhancers or super enhancer can drive the expression of distant genes that are located thousands base pairs away. Therefore, I was interested to check whether this super enhancer region also drives the expression of other genes along this chromosome 10 arm. To address this, I performed RNA-Seq on the wild-type Del_SE_3_9 clone that had no deletion and the enhancer cluster-deleted Del_SE_3_19 clone. The RNA-Seq data were analysed by Sakari Vanharanta in which he compared the expression level of genes that are located within the 5Mb window flanking the deleted enhancers cluster in these two clones. The RNA-Seq analysis revealed that *KLF6* was the most significantly downregulated gene within the 5Mb genomic region flanking the 113kb deleted region, further corroborating the previous observations that *KLF6* was the main target of this super enhancer (Figure 42).

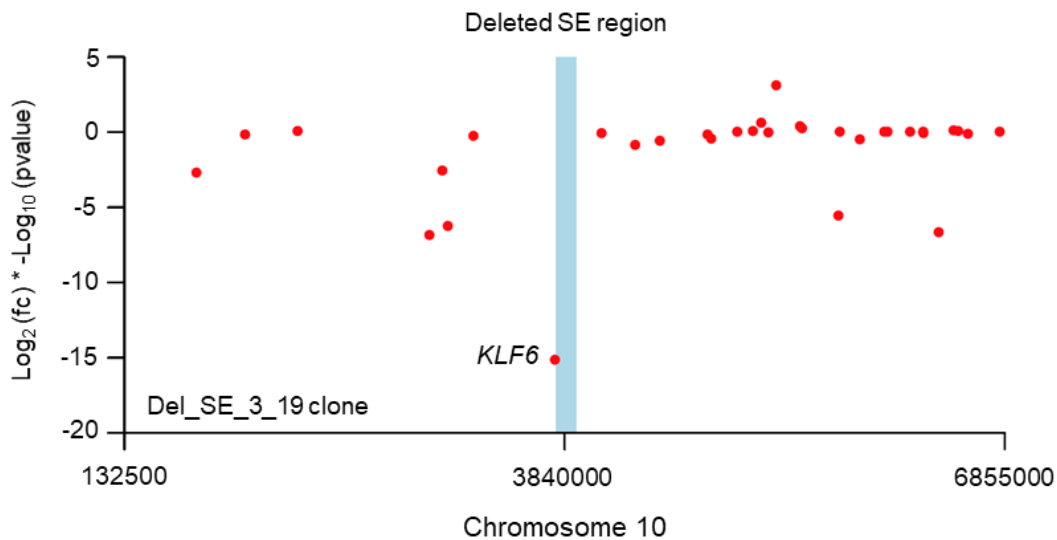


Figure 42: The expression level of genes that are located within a 5Mb window flanking the 113kb deletion of the super enhancer region. Del_SE_3_19 clone compared to Del_SE_3_9 clone by RNA-Seq. N=4 for both samples. Blue bar indicates the location of the 113kb deletion.

4.2.4 HIF2A modulates *KLF6* expression in ccRCC

Several transcription factors could bind to this super enhancer locus and co-regulate the expression of *KLF6* in ccRCC. Since the transcription factor HIF2A is a well-established oncogenic driver of ccRCC pathogenesis, Sakari Vanharanta and I were prompted to directly investigate whether there was any link between HIF2A and *KLF6* expression in ccRCC. We first began by utilising the publicly available ccRCC TCGA RNA-Seq data and examined whether there was any correlation between the expression of *EPAS1*-encoded HIF2A and *KLF6* in the ccRCC clinical samples. Interestingly, there was a positive correlation between *EPAS1* and *KLF6* expression in the ccRCC clinical samples in which the correlation value between these genes was fairly similar to the correlation value seen between *EPAS1* and its well characterised downstream target *CCND1* (Figure 43). The positive correlation observed between the expression of *EPAS1* and *KLF6* in ccRCC clinical samples might suggest that HIF2A could potentially play a role in modulating *KLF6* expression in ccRCC.

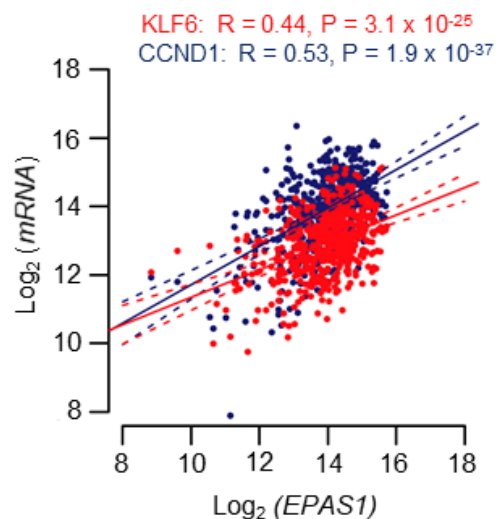


Figure 43: Positive correlation between the expressions of *EPAS1* with either *KLF6* (red) or *CCND1* (blue) in the clinical TCGA ccRCC data set.

To functionally test the link between HIF2A and KLF6, I checked the expression of *KLF6* in the HA-VHL reintroduced-786-M1A and OS-LM1 cells. In parallel, the expression of two well-characterised HIF2A downstream targets *CXCR4* and *CCND1* were also assessed in these HA-VHL reintroduced cells. VHL reintroduction will result in the proteosomal degradation of HIF2A that will consequently downregulate the expression of its downstream targets. As expected, *CXCR4* and *CCND1* expressions were significantly attenuated in the HA-VHL reintroduced-786-M1A and OS-LM1 cells. There was about 50% reduction in the *KLF6* mRNA level in both HA-VHL reintroduced-786-M1A and OS-LM1 cells (Figure 44A). In addition, I also checked the *KLF6* protein expression level in the HA-VHL-reintroduced 786-M1A cells by Western blotting. Firstly, the expression of reintroduced exogenous HA-VHL and consequent loss of HIF2A expression were confirmed in these cells. Then, in line with the qPCR results, I observed *KLF6* protein depletion in these HA-VHL reintroduced-786-M1A cells (Figure 44B).

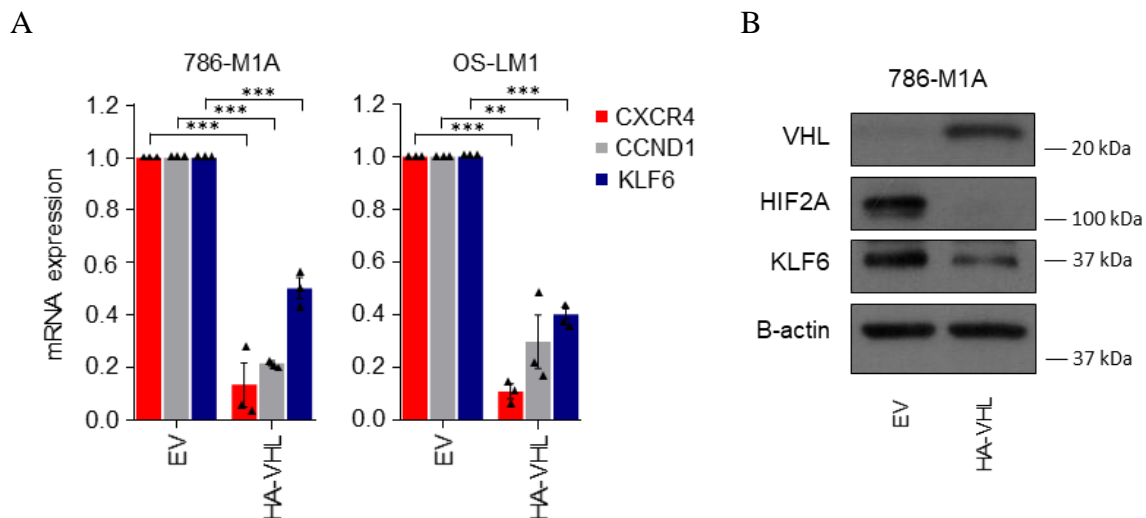


Figure 44: Expression of HIF2A downstream targets in HA-VHL reintroduced cells. **(A)** The expression of *KLF6*, *CXCR4* and *CCND1*, in the HA-VHL reintroduced-786-M1A and OS-LM1 cells. Average of three experiments. Error bars, SEM. Two-tailed Student's t-test. * $P < 0.05$, ** $P < 0.005$ and *** $P < 0.0005$. **(B)** *KLF6*, *HIF2A* and *VHL* immunoblot of 786-M1A cells transduced with either HA-VHL or empty vector.

To corroborate these findings, the RNAi approach as described by Fellmann *et al*¹⁹⁷ was additionally employed to knockdown *EPAS1* expression in the 786-M1A cells. The expression of *CCND1*, *KLF6* as well as the *EPAS1* itself were assessed in these cells. The shRNA-mediated *EPAS1* inhibition in these 786-M1A cells resulted in the downregulation of *CCND1* and *KLF6* expression by about 50% and 30%, respectively (Figure 45). However, the level of *CCND1* and *KLF6* downregulation in this *EPAS1* shRNA experiment was not as profound as compared to the effect of reintroducing VHL into this 786-M1A cell line (Figure 44A). This could be due to the magnitude of *EPAS1* knockdown in this RNAi experiment which was downregulated by only 60%. Hence, it was postulated that a much stronger *EPAS1* knockdown in these cells would result in more profound *CCND1* and *KLF6* downregulation. Nevertheless, the findings of HA-VHL reintroduced and RNAi experiments demonstrated that HIF2A does play a role in modulating *KLF6* expression in ccRCC.

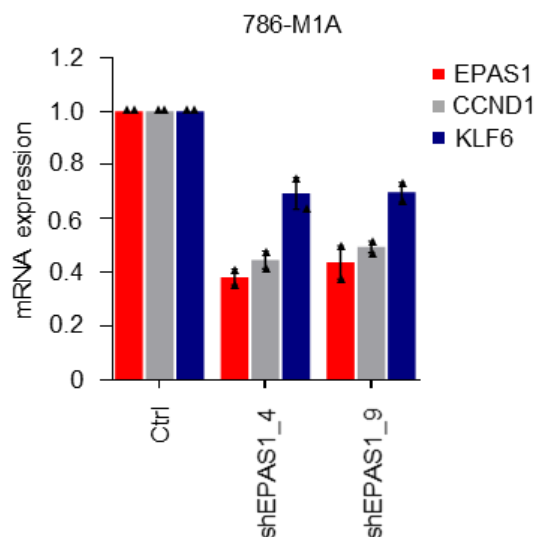


Figure 45: shRNA-mediated *EPAS1* inhibition. The expression of *EPAS1*, *CCND1* and *KLF6* in the *EPAS1* knockdown 786-M1A cells. Average of two experiments. Error bars, SEM.

4.2.5 HIF2A acts through the super enhancer to support *KLF6* expression

A recent study has linked HIF2A with the maintenance of super enhancer in ccRCC¹⁹⁸. In relation to this, I have demonstrated that *KLF6* expression in ccRCC was super enhancer-driven and modulated by HIF2A. Thus, to test whether these present findings were in line with the aforementioned study above, Sakari Vanharanta and I re-examined the H3K27ac ChIP-Seq data of the HA-VHL-reintroduced 786-M1A and OS-LM1 cells, previously generated in the lab by Paulo Rodrigues. We assessed the effect of VHL reintroduction and consequent HIF2A loss to the H3K27ac patterns of the *KLF6* super enhancer locus. There was a reduction in H3K27ac signal at one of the enhancer regions downstream of *KLF6* locus in both HA-VHL reintroduced-786-M1A and OS-LM1 cells (Figure 46A). Apart from this, there was no significant difference in the general H3K27ac signals pattern of this *KLF6* super enhancer locus between the control and VHL-reintroduced cells. This was consistent with the previous findings that demonstrated the robustness of this particular *KLF6*-associated super enhancer region (Figure 36A).

Moreover, examination of the previously generated and analysed 786-M1A and OS-LM1 HIF2A ChIP-Seq data revealed that HIF2A bound the same enhancer region that had the H3K27ac signal reduced upon VHL reintroduction (Figure 46B-C). Based on these HIF2A ChIP-Seq data, HIF2A might modulate *KLF6* expression in ccRCC by acting through the *KLF6* super enhancer locus. In order to test this possibility, the HIF2A binding site, shown in figure 46B, was CRISPRi-inactivated in combination with another enhancer region putatively bound by HIF2A in the 786-M1A cells. The combinatorial enhancers targeting strategy as described in section 4.2.2 above was employed to perform this iHIF2A binding site experiment. The CRISPRi-mediated inactivation of these HIF2A binding sites reduced the *KLF6* expression level by 40% (Figure 46D). This finding was relatively similar to the effect of reintroducing HA-VHL

into these 786-M1A cells (Figure 44A). Overall, these findings confirmed that HIF2A binds to this super enhancer locus to modulate the expression of *KLF6* in ccRCC.

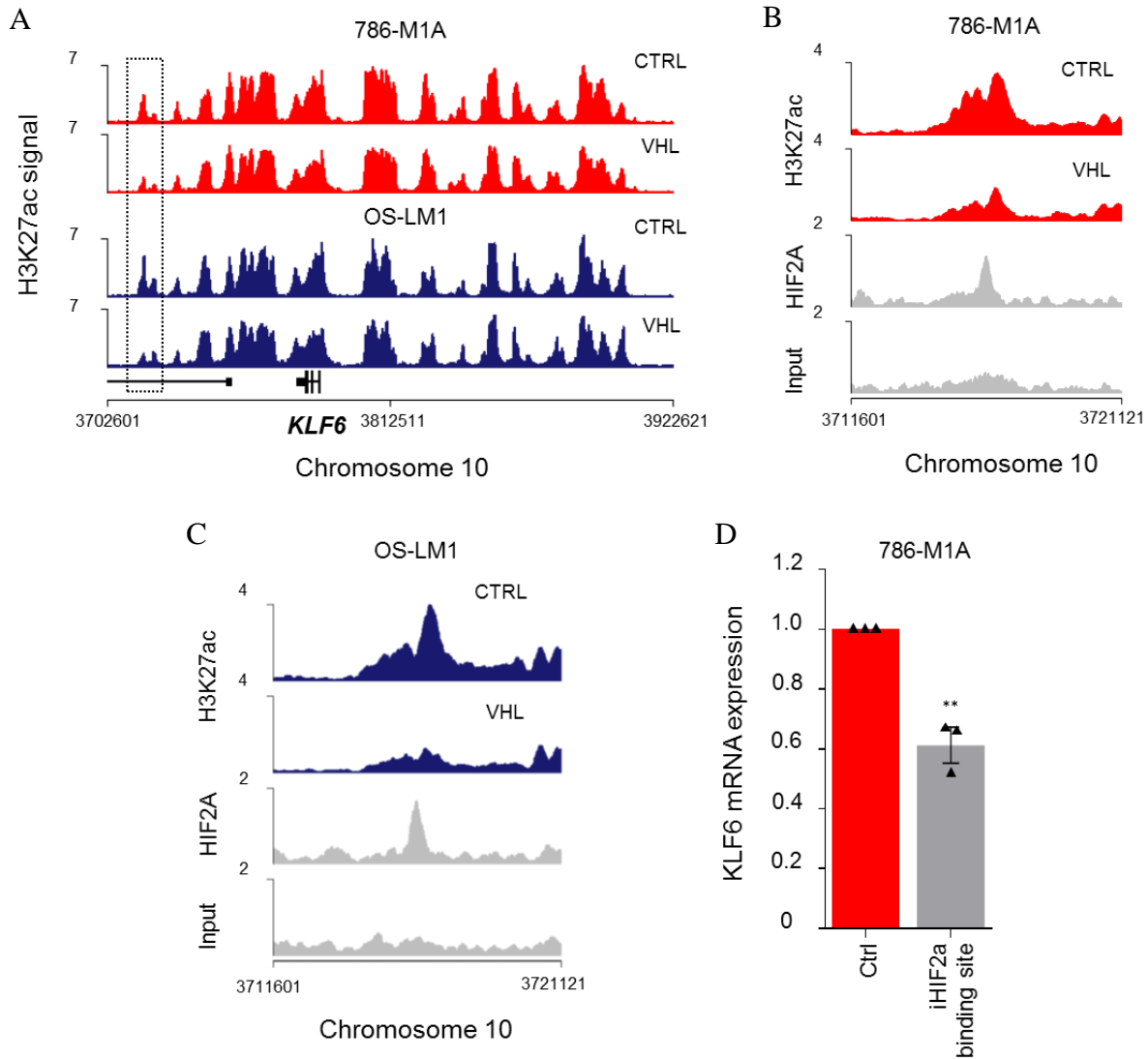


Figure 46: HIF2A binds the *KLF6* super enhancer locus. (A) H3K27ac ChIP-Seq signal of 786-M1A and OS-LM1 cells transduced with either empty vector or HA-VHL. A region significantly altered in both HA-VHL reintroduced cells when compared to the empty vector control highlighted by grey box. (B and C) A close up of the region highlighted in panel A together with HIF2a ChIP-Seq signals in (B) 786-M1A and (C) OS-LM1 cells. (D) *KLF6* expression in the 786-M1A cells in which two putative HIF2a binding sites were inactivated using CRISPRi. Average of three experiments. Error bars, SEM. Two-tailed Student's t-test. * $P < 0.05$, ** $P < 0.005$ and *** $P < 0.0005$.

4.3 Summary

One of the primary focus of this chapter was to investigate whether *KLF6* expression in ccRCC was supported by this nearby super enhancer locus. Using the CRISPRi-based enhancer inactivation approach, it was discovered that this super enhancer region drove the expression of *KLF6*. In addition, this super enhancer acted in a modular fashion to drive *KLF6* expression in ccRCC. Significant reduction in the expression of *KLF6* mRNA level was only achieved when either several constituent enhancers were inactivated concurrently or by genetic deletion of the large enhancers cluster, in which in this present study the CRISPR-Cas9 approach was used to delete 113Kb of the enhancers cluster upstream of *KLF6* locus.

Moreover, it was observed that this *KLF6* super enhancer was robust and insensitive to the perturbations in the activity of its constituent enhancers. There was no interdependency between these constituent enhancers. Inactivating one individual enhancer only resulted in the loss of H3K27ac signals at the specific targeted region without affecting the general H3K27ac signals pattern or the whole super enhancer landscape. This was in contrast to several recent studies that have demonstrated the cancer-associated super enhancers are sensitive to perturbation of its constituent enhancers or regulatory components that establish or maintain the super enhancer landscape. However, such redundancy and robustness are well-aligned with the fact that most critical biological processes and developmental transcriptional programmes are insensitive to environmental and other incoming variations.

Last but not least, the works in this chapter also revealed a link between the ccRCC-initiating VHL-HIF2A pathway and *KLF6* expression modulation in ccRCC. Through the previously generated VHL reintroduced-cells H3K27ac ChIP-Seq as well as the HIF2A ChIP-

Seq data, HIF2A was discovered to bind this *KLF6* super enhancer locus, in which the HIF2A binding sites were identified downstream of the *KLF6* locus. Collectively, these data suggested that HIF2A supports *KLF6* expression by acting through the large KLF6 super enhancer, potentially explaining the relatively high KLF6 levels in ccRCC when compared to other tumour types (Chapter 3, figure 16).

Chapter 5

Dissecting the transcriptional network
regulated by KLF6 that supports
ccRCC growth

5.1 Introduction

It has been demonstrated in previous chapter that *KLF6* expression in ccRCC is supported by a robust super enhancer that is partially activated by the ccRCC-initiating VHL-HIF2a axis. Consistent with the observation that *KLF6* is highly expressed in ccRCC clinical samples, which reflects its relevance in ccRCC pathogenesis, CRISPR-Cas9 and CRISPRi-mediated *KLF6* perturbation impaired ccRCC cells growth both *in-vitro* and *in-vivo*. Therefore, as an important transcriptional regulator, inhibition of *KLF6* could affect pro-tumourigenic transcriptional programs that are involved in supporting ccRCC growth and progression. Hence, the works described in this chapter primarily focus on further understanding how *KLF6* supported ccRCC pathogenesis and unravelling the transcriptional programmes regulated by this super enhancer-associated transcription factor. Understanding the functions of *KLF6* as well as its downstream targets/regulated transcriptional networks could be useful in further understanding ccRCC pathogenesis and paving the way for the development of better diagnostic and/or therapeutic strategies for ccRCC.

5.2 Results

5.2.1 Assessing the global effect of *KLF6* inhibition

In order to identify the *KLF6* downstream targets, I performed RNA-Seq on the *KLF6*-targeted and control 786-M1A CRISPRi cells and assessed the differentially expressed genes between these two cell populations at the genome wide level. Sequencing libraries were prepared from the total RNA of each cell line (four replicates/cell line) and subjected to Illumina high-

throughput sequencing. The RNA-Seq data were analysed by Sakari Vanharanta where he performed the differential gene expression analysis. The volcano plot in figure 47 shows the differentially expressed genes in the *KLF6*-targeted versus control 786-M1A CRISPRi cells. Genes that were significantly downregulated upon *KLF6* inhibition are represented in red circles whereas the blue circles represent genes that were significantly upregulated in the *KLF6*-targeted cells. As expected, *KLF6* was the top most significantly downregulated gene in the *KLF6*-targeted cells, thus validating the robustness of the CRISPRi *KLF6* targeting approach and most importantly the validity of the RNA-Seq data.

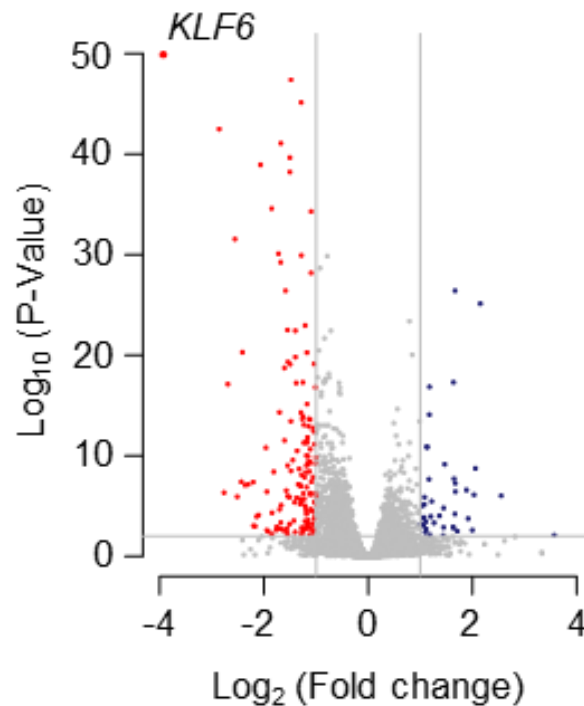


Figure 47: Volcano plot of the differentially expressed genes in *KLF6*-targeted versus control 786-M1A CRISPRi cells. Blue and red circles represent genes that were significantly upregulated and downregulated, respectively, in *KLF6*-targeted cells.

5.2.2 KLF6 modulates a part of HIF2A-driven transcriptional program

Our collaborator, Dora Bihary and Shamith Samarajiwa, assisted us in further analysing the RNA-Seq data where they performed the gene set enrichment (GSEA) and pathway analyses. The gene set enrichment analysis revealed a highly significant association between *KLF6* inhibition and downregulation of the canonical hypoxia-response gene set (Figure 48A). It has been previously demonstrated that HIF2A acted through the super enhancer region to partially activate *KLF6* expression in ccRCC. Thus, I hypothesised that some of these HIF2A downstream targets might be secondary targets activated by KLF6. To test this hypothesis, I reintroduced exogenous KLF6 into the VHL-expressing 786-M1A cells, followed by assessing the expression of several known HIF2A downstream targets *CCND1*, *VEGFA* and *BHLHE40* in these cells. Based on the hypothesis, reintroducing exogenous KLF6 into these cells might be able to rescue the expression of some of these genes. As expected, proteosomal degradation of HIF2A led to reduced expression of *CCND1*, *VEGFA* and *BHLHE40* in the VHL-reintroduced cells (Figure 48B). Interestingly, reintroduction of exogenous KLF6 into these cells completely restored *BHLHE40* expression to the level similar to the control cells. Moreover, there was also slight upregulation in the expression of *CCND1* and *VEGFA*, but overall the expression of these genes remained low.

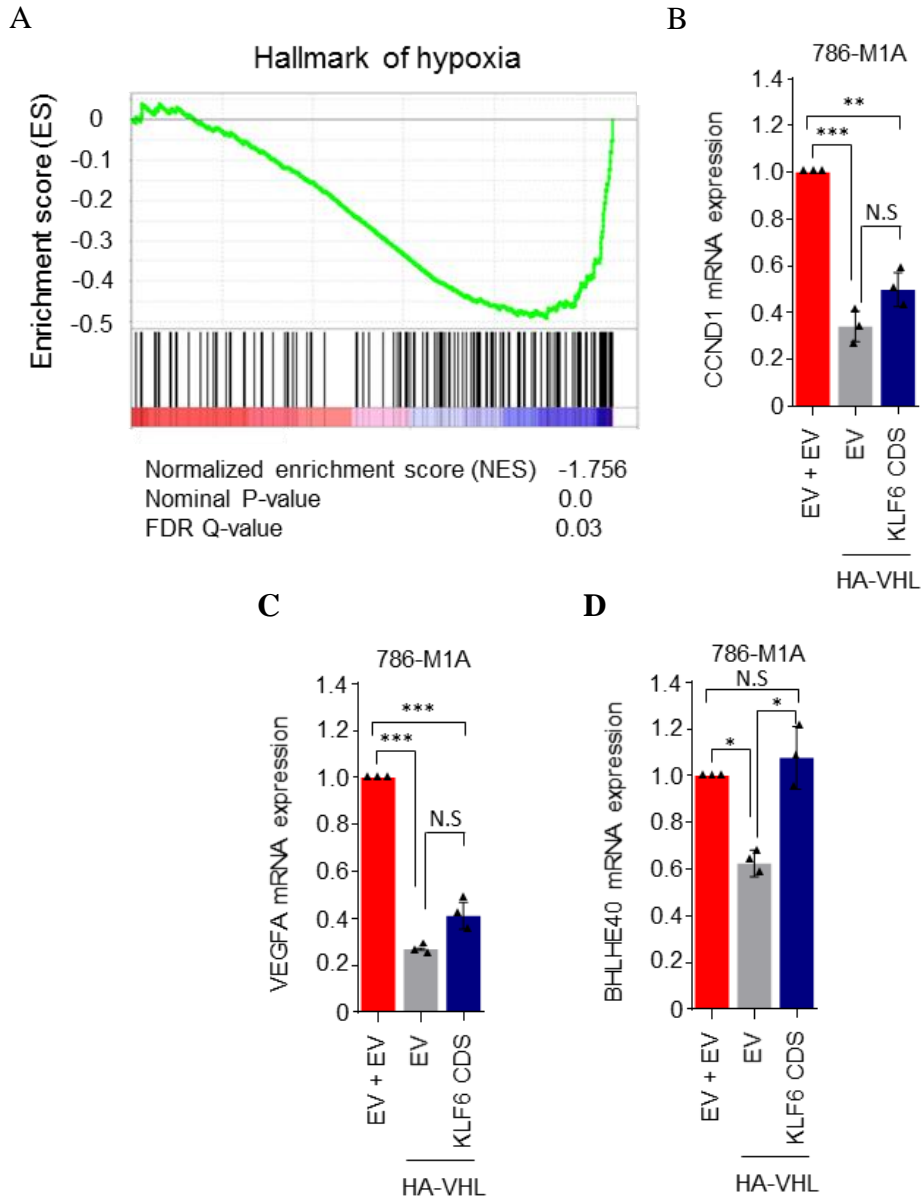


Figure 48: Significant association between *KLF6* depletion and the hypoxia-response gene signature. **(A)** Gene set enrichment analyses shows downregulation of the canonical hypoxia-response gene set in the *KLF6*-depleted 786-M1A cells. **(B-D)** Expression of HIF2A downstream targets, **(B)** *CCND1*, **(C)** *VEGFA* and **(D)** *BHLHE40*, in the VHL-expressing 786-M1A cells, reintroduced with either empty vector or exogenous *KLF6*. Average of three experiments. Error bars, SEM. One-way ANOVA with Tukey's range test. * $P < 0.05$, ** $P < 0.005$ and *** $P < 0.0005$.

The reintroduction of exogenous KLF6 was only able to completely restore *BHLHE40* expression in the VHL-expressing cells. Hence, I focused on further investigating KLF6 involvement in regulating the expression of this gene. I first checked the expression of *BHLHE40* in the *KLF6*-depleted 786-M1A CRISPRi using qPCR. It was observed that the expression of this gene was downregulated in these cells, consistent with the KLF6 possible role in modulating *BHLHE40* expression in ccRCC. Moreover, reintroduction of exogenous KLF6 into these *KLF6*-depleted 786-M1A CRISPRi cells was able to restore *BHLHE40* expression to the level seen in the control cells (Figure 49A-B), thus confirming that KLF6 operates upstream of *BHLHE40*. Taken these data together, a part of HIF2A downstream targets are secondary targets whose expression are regulated by the HIF2A transcriptional effector KLF6.

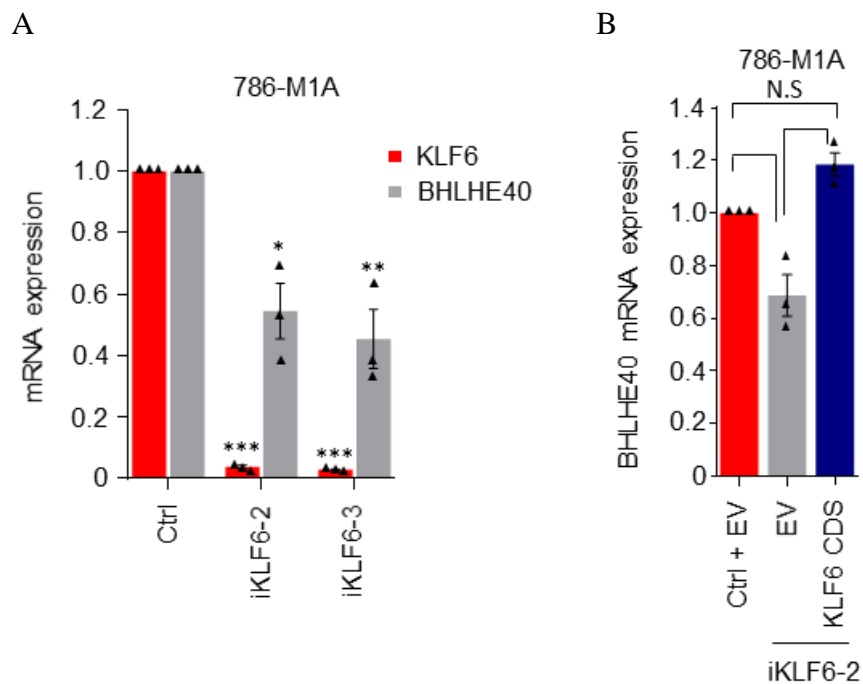


Figure 49: KLF6 modulates the expression of *BHLHE40*. (A) Expression of *KLF6* and *BHLHE40* in the *KLF6*-depleted 786-M1A cells. Average of three experiments. Error bars, SEM. One-way ANOVA with Dunnett's test. * P < 0.05, ** P < 0.005 and *** P < 0.0005. (B) *BHLHE40* expression in the *KLF6*-depleted 786-M1A cells reintroduced with either empty

vector or exogenous KLF6. Average of three experiments. Error bars, SEM. One-way ANOVA with Tukey's range test. * $P < 0.05$, ** $P < 0.005$ and *** $P < 0.0005$.

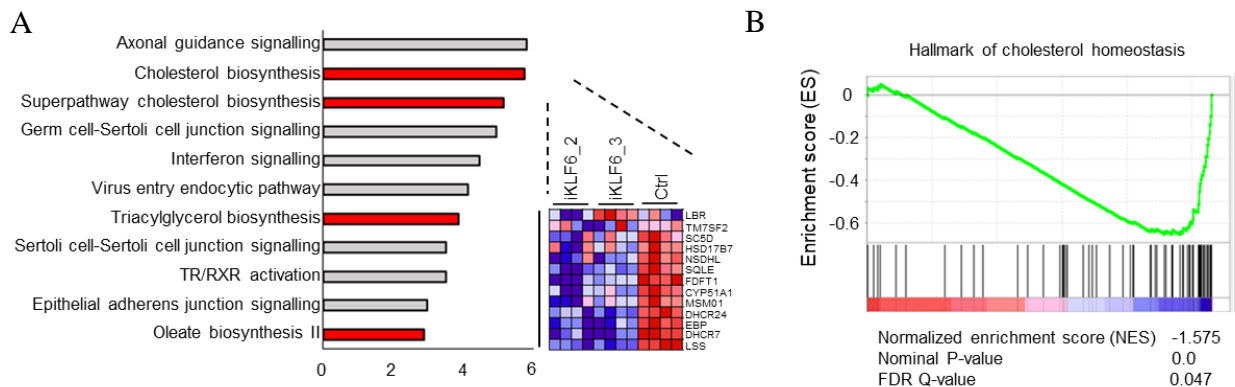
5.2.3 Deregulation of lipid homeostasis pathways in KLF6-targeted cells

Despite being a part of the VHL-HIF2a pathway, it was worth to note that the phenotype of KLF6-targeted cells differed from the VHL-reintroduced cells *in vitro*¹⁹. As demonstrated in Chapter 3, KLF6 inhibition resulted in impaired cells growth whereas the VHL-reintroduced cells, which have the HIF2A degraded, do not exhibit a proliferative defect under standard tissue culture conditions. Hence, it was postulated that the observed growth defect of the KLF6-inhibited cells could be due to the perturbation of “*unknown*” transcriptional programs that are directly regulated by the KLF6. To identify potential KLF6 downstream effectors that could explain the observed phenotypic effect, unbiased pathway analysis was performed on the RNA-Seq data by our collaborator in order to look for pathways that were significantly deregulated upon KLF6 inhibition. Pathways related to lipid homeostasis that include cholesterol, triacylglycerol and oleate biosynthesis were among the top most significantly deregulated pathways in these *KLF6*-depleted 786-M1A cells (Figure 50A). In addition, the heatmap in figure 50A highlights downregulation of several key genes that involve in the cholesterol biosynthesis pathway in these cells.

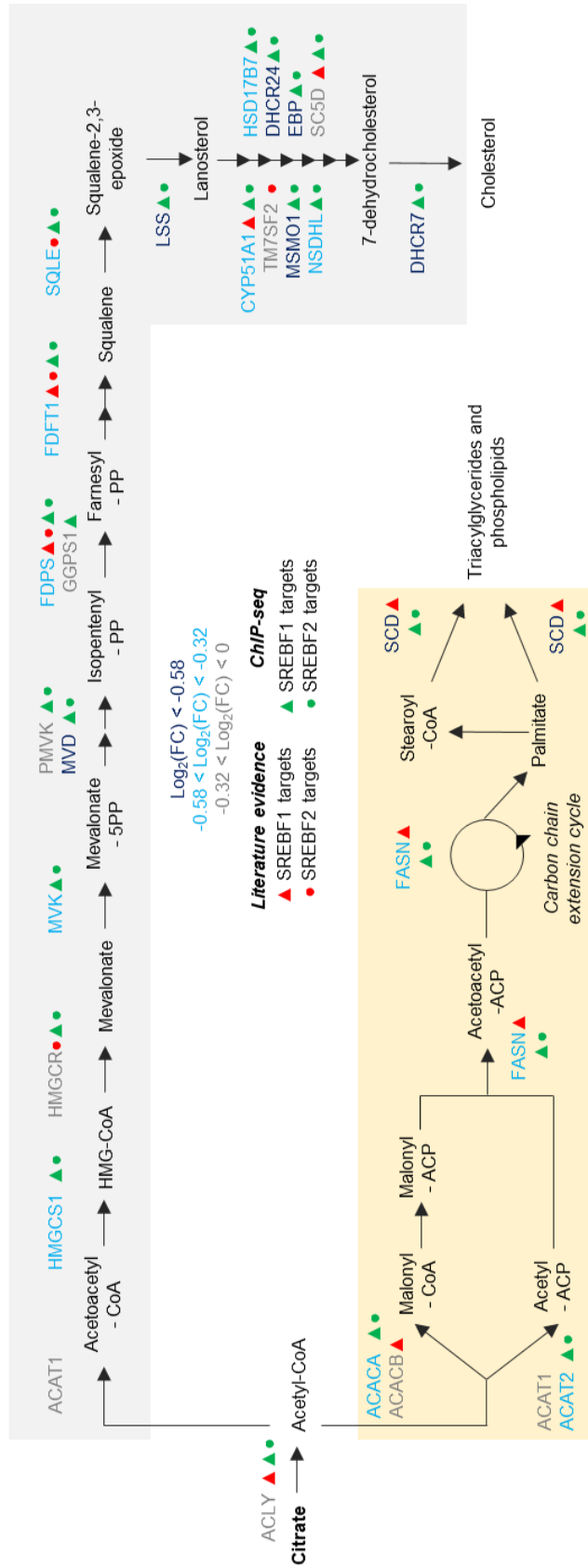
In agreement, the gene set enrichment analysis revealed a highly significant association between genes that were downregulated upon KLF6 depletion and those participated in cholesterol homeostasis (Figure 50B). I also checked the expression level of genes that participate in each intermediate steps of the triacylglycerol and cholesterol biosynthesis pathways in which these pathways are illustrated in figure 50C. This targeted analysis revealed

that most of these genes were downregulated in the *KLF6*-depleted cells. The fold change downregulation of these genes was represented in different shade of blue. Downregulation of *SREBF1* and *SREBF2*, two critical transcription factors that support the expression of many lipid homeostasis-associated genes, were also observed in the cells that had *KLF6* knockdown. Analysis of publicly available *SREBF1* and *SREBF2* ChIP-Seq datasets, as well as literatures search, by our collaborator Dora Bihary and Shamith Samarajiwa revealed that the regulatory region of these downregulated genes were bound by the transcription factor *SREBF1* and/or *SREBF2* (Figure 50C).

To validate these RNA-Seq findings, qPCR was performed in order to assess the expression level of *SREBF1* and *SREBF2* as well as *SCD* and *LSS* in these *KLF6*-targeted 786-M1A CRISPRi cells. *SCD* and *LSS* are among the key enzymes that are involved in the intermediate steps of triacylglycerol and cholesterol biosynthesis pathways, respectively. qPCR analysis confirmed the downregulation of these genes upon *KLF6* inhibition in these 786-M1A cells (Figure 50D). To determine whether these transcriptional changes were translated phenotypically, I quantified the total cholesterol level of the *KLF6*-depleted and control 786-M1A CRISPRi cells. Indeed, a significant reduction in the total cholesterol level was observed in the *KLF6*-depleted cells as compared to the control cells (Figure 50E). Collectively, these findings demonstrated that *KLF6* plays a role in modulating lipid homeostasis in ccRCC.



C



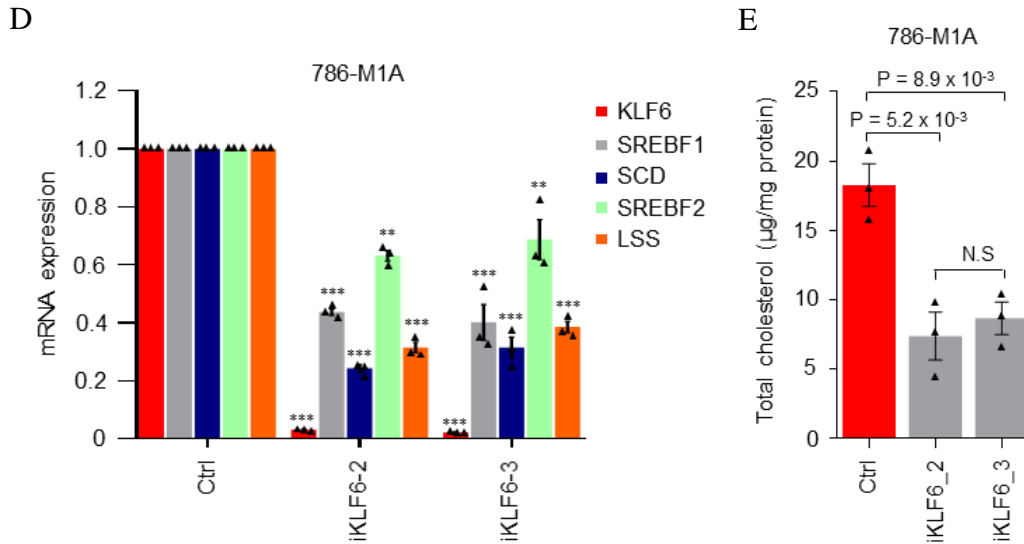


Figure 50: Deregulation of lipid homeostasis pathway in the *KLF6*-depleted 786-M1A cells. **(A)** Most significantly deregulated pathways upon *KLF6* depletion as determined by Ingenuity Pathway Analysis. Highlighted in red are pathways involved in lipid homeostasis. Heatmap (right) shows significant downregulation of several key genes in the cholesterol biosynthesis pathway. **(B)** Gene set enrichment analysis shows downregulation of cholesterol homeostasis-related genes in *KLF6*-depleted cells. **(C)** A simplified schematic of triacylglycerol and cholesterol biosynthesis pathways. Different shade of blue represents expression level fold change in the *KLF6*-targeted cells. *SREBF1* and *SREBF2* target genes determined by systematic literature analysis (red triangles and circles) and publicly available ChIP-Seq datasets analysis (green triangles and circles). **(D)** Validation of *SREBF1*, *SCD*, *SREBF2* and *LSS* expression using qPCR. Average of three experiments. Error bars, SEM. One-way ANOVA with Dunnett's test. * $P < 0.05$, ** $P < 0.005$ and *** $P < 0.0005$. **(E)** Total cholesterol level in the *KLF6*-targeted 786-M1A cells. Average of three experiments. Error bars, SEM. One-way ANOVA with Tukey's range test.

5.2.4 Lipid homeostasis perturbation impairs ccRCC cells growth

Lipid metabolism has been shown to play a role in promoting tumorigenesis of various cancer types¹⁹⁹. Hence, I next examined the effect of perturbing the lipid homeostasis pathways

on ccRCC cells growth. To test this, the CRISPRi combinatorial targeting approach was employed to simultaneously inhibit *SREBF1* and *SREBF2* expression in the 786-M1A cells. Two tandem sgRNAs constructs were designed, namely the iSREBF1/2 combo 1 and combo2. Each of these constructs expressed two independent sgRNAs, one targeting *SREBF1* while the other targeting *SREBF2*. There was downregulation in the expression of both *SREBF1* and *SREBF2* in these iSREBF1/2–transduced 786-M1A CRISPRi cells (Figure 51A). Then the total cholesterol level of these cells was determined. I found that there was a significant reduction in the total cholesterol level in these *SREBF1/2*-targeted 786-M1A cells (Figure 51B). This was indeed in line with the central role of transcription factor *SREBF1* and *SREBF2* in regulating the lipid homeostasis pathways. Next, the proliferation rate of these *SREBF1* and *SREBF2*-targeted cells was assessed using the previously described competitive proliferation assay. Simultaneous *SREBF1* and *SREBF2* targeting in the 786-M1A cells reduced the cells growth, which was in line with the phenotype of inhibiting *KLF6* in these cells (Figure 51C).

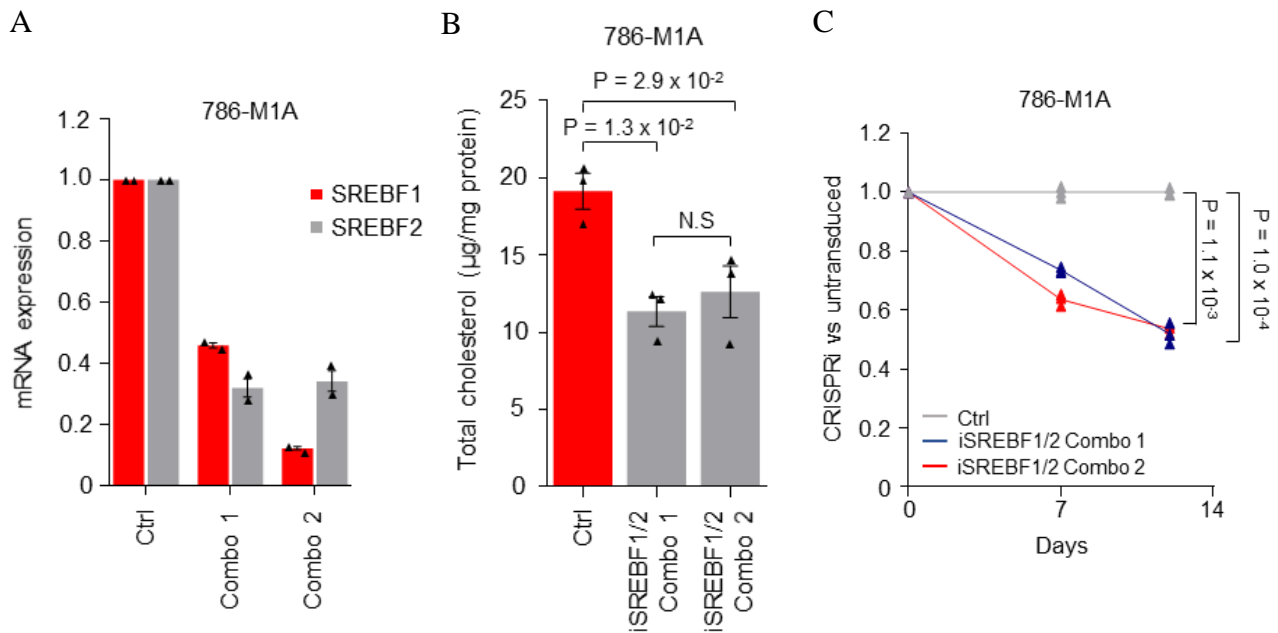


Figure 51: Targeting *SREBF1* and *SREBF2* reduced ccRCC cells growth. (A) (Top) Illustration of the tandem sgRNAs construct used for combinatorial targeting of *SREBF1* and *SREBF2* by

CRISPRi approach. (Bottom) *SREBF1* and *SREBF2* expression in *SREBF1* and *SREBF2*-targeted 786-M1A cells. Average of two experiments. Error bars, SEM. (B) Total cholesterol level in the *SREBF1* and *SREBF2*-targeted 786-M1A cells. Average of three experiments. Error bars, SEM. One-way ANOVA with Tukey's range test. (C) Competitive proliferation assay of the *SREBF1* and *SREBF2*-targeted 786-M1A cells. Relative fraction of iSREBF1/2 combo and NTC-transduced cells, normalised to day 0, compared to untransduced cells. Average of three replicates. Two-way ANOVA with Tukey's range test.

In addition to targeting *SREBF1* and *SREBF2* genetically, I also investigated the effect of treating ccRCC cells with fatostatin, a small molecule that inhibits SREBF1 and SREBF2 activation²⁰⁰, on the cells growth. Downregulation of *SCD* and *LSS*, downstream targets of SREBF1 and SREBF2, respectively, were observed after 48 hours of fatostatin treatment, indicating the inhibition of SREBF1 and SREBF2 activation in these fatostatin-treated cells (Figure 52A). The cells treated with fatostatin had slower growth compared to the vehicle-treated cells in a dose-dependent manner (Figure 52B). To consolidate these findings, I also examined the effect of treating 786-M1A cells with simvastatin which is the HMG-CoA reductase inhibitor. HMG-CoA reductase is one of the key enzymes that involve in the cholesterol biosynthesis pathway. Simvastatin-mediated inhibition of the cholesterol biosynthesis pathway impaired the cells growth (Figure 52C). It was also observed that treating the cells with higher concentration of simvastatin resulted in cell death. Collectively, these findings demonstrated the role of lipid metabolism in supporting ccRCC pathogenesis and revealed a link between KLF6, lipid homeostasis pathways and ccRCC cell growth. Inhibition of KLF6 led to the deregulation of lipid homeostasis pathways that consequently reduced the ccRCC cells rate of proliferation.

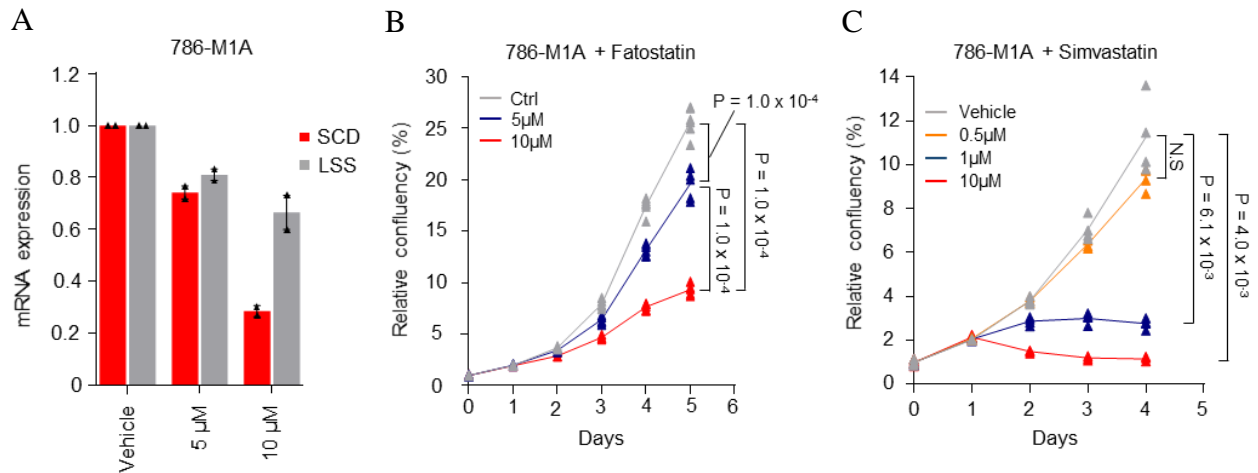


Figure 52: Chemical inhibition of the lipid homeostasis pathway impaired ccRCC cells growth. **(A)** Expression of *SCD* and *LSS* in 786-M1A cells treated with fatostatin for 48 hours as measured by qPCR. Average of two experiments. Error bars, SEM. **(B)** Proliferation of 786-M1A cells treated with either vehicle or indicated concentrations of fatostatin. Average of six technical replicates. Two-way ANOVA with Tukey’s range test. **(C)** Proliferation of 786-M1A cells treated with either vehicle or indicated concentrations of simvastatin. Average of four technical replicates. Two-way ANOVA with Tukey’s range test.

5.2.5 Co-regulation of lipid homeostasis by KLF6 and mTORC1

Next, I wanted to investigate the mechanism on how KLF6 would involve in modulating the lipid homeostasis pathways in ccRCC. The mTORC1 complex has been shown to modulate lipid metabolism by regulating the expression and activity of SREBF1 and SREBF2^{81,82}. Thus, I hypothesised that the coordinated downregulation of lipid homeostasis genes upon KLF6 inhibition could be the consequence of perturbed mTORC1 activity in these cells. In addition to this speculation, the previous findings also seemed to suggest that KLF6 could operate upstream and positively regulate the expression of these genes.

In order to distinguish between these two possibilities, I first tested whether the mTORC1 complex regulates SREBF1 and SREBF2 activity in ccRCC. The 786-M1A cells were treated with Torin1, a potent mTOR antagonist, followed by checking the expression of SREBF1 and SREBF2 matured form. As expected, Torin1 strongly inhibited mTORC1 activity that was demonstrated by the absence of phosphorylated p70 S6 kinase (P-p70 S6 kinase) and consequent loss of ribosomal S6 phosphorylation (P-S6), a substrate of the P-p70 S6 kinase (Figure 53A). As described in the Chapter 1 (section 1.11), P-p70 S6 kinase and P-S6 were used as the read-out for mTORC1 activity. I also observed the decreased expression of SREBF1 and SREBF2 active form in the Torin1-treated cells (Figure 53A), which was in line with the previous reports that have demonstrated mTORC1 role in regulating SREBF1 and SREBF2 activation. Additionally, inhibition of SREBF1 and SREBF2 activation was translated into a reduction in total cholesterol level in the Torin1-treated 786-M1A cells (Figure 53B).

I also assessed the SREBF1, SREBF2, SCD and LSS mRNA level in the Torin1-treated 786-M1A cells using qPCR. In line with the reduced SREBF1 and SREBF2 activity observed in figure 53A, the expression of their downstream targets *SCD* and *LSS* was also downregulated in a dose-dependent manner. In addition, I found that the Torin1 treatment also resulted in the downregulation of *SREBF1* expression (Figure 53C). However, an increase in the *SREBF2* expression level was observed, which was in contrast to the effect seen upon KLF6 inhibition where the *SREBF2* expression was downregulated in the *KLF6*-targeted cells (Figure 50D). Thus, while this data demonstrated that mTORC1 inhibition indeed phenocopied the effects of KLF6 depletion at the level SREBF1 and SREBF2 downstream targets, an increase in the SREBF2 mRNA level possibly suggested that KLF6 directly regulates the expression of this gene.

To test whether KLF6 directly regulates the expression of these lipid homeostasis genes, I reintroduced exogenous flag-KLF6 and flag-eGFP into the *KLF6*-depleted 786-M1A CRISPRi cells. This was followed by performing flag ChIP-Seq in order to identify regions that are bound by KLF6. This flag-KLF6 ChIP-Seq strategy was employed because there was no suitable KLF6 antibody for performing the KLF6 ChIP experiment. The expression of the reintroduced flag-KLF6 and flag-eGFP were confirmed in the respective cells by immunoblotting (Figure 54A). Then, I assessed the expression of *LSS* in these cells in order to test whether the exogenous flag-KLF6 construct was functional. Indeed, downregulation of *LSS* was observed in the *KLF6*-depleted cells that were reintroduced with flag-eGFP, which was consistent with both RNA-Seq and qPCR validation data. The reintroduction of flag-KLF6 into these *KLF6*-depleted cells was able to restore *LSS* expression to the level similar to flag-eGFP-transduced control cells, thus confirming the functionality of this exogenous flag-KLF6 construct (Figure 54B).

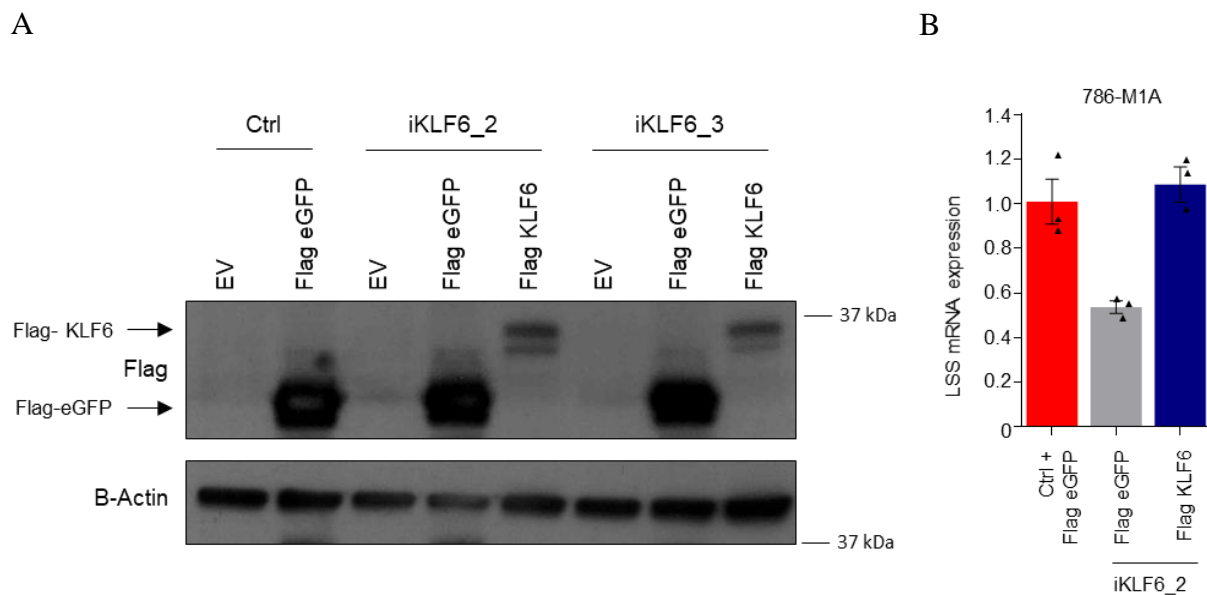


Figure 54: Reintroduction of flag-KLF6 and flag-eGFP into the *KLF6*-depleted cells. **(A)** Expression of flag-KLF6 and flag-eGFP in the respective cells. **(B)** *LSS* expression in the *KLF6*-depleted 786-M1A cells, transduced with either flag-KLF6 or flag-eGFP. Average of three technical replicates is shown. Error bars, SEM.

Analysis of the flag ChIP-Seq data by Sakari Vanharanta revealed about 11,000 KLF6 peaks in which these peaks were distributed across different genomic regions. The most prominent region was the promoter with an enrichment for a motif known to be bound by the members of KLF family (Figure 55A). In concordant with the RNA-Seq and qPCR validation data, the proximal regulatory regions of *SREBF1*, *SREBF2*, *SCD* and *LSS* were found to be bound by KLF6, which was indicated by the presence of KLF6 peaks at these regions (Figure 55B –E). Thus, these ChIP-Seq data confirmed the hypothesis that KLF6 directly regulates the expression of these genes in ccRCC.

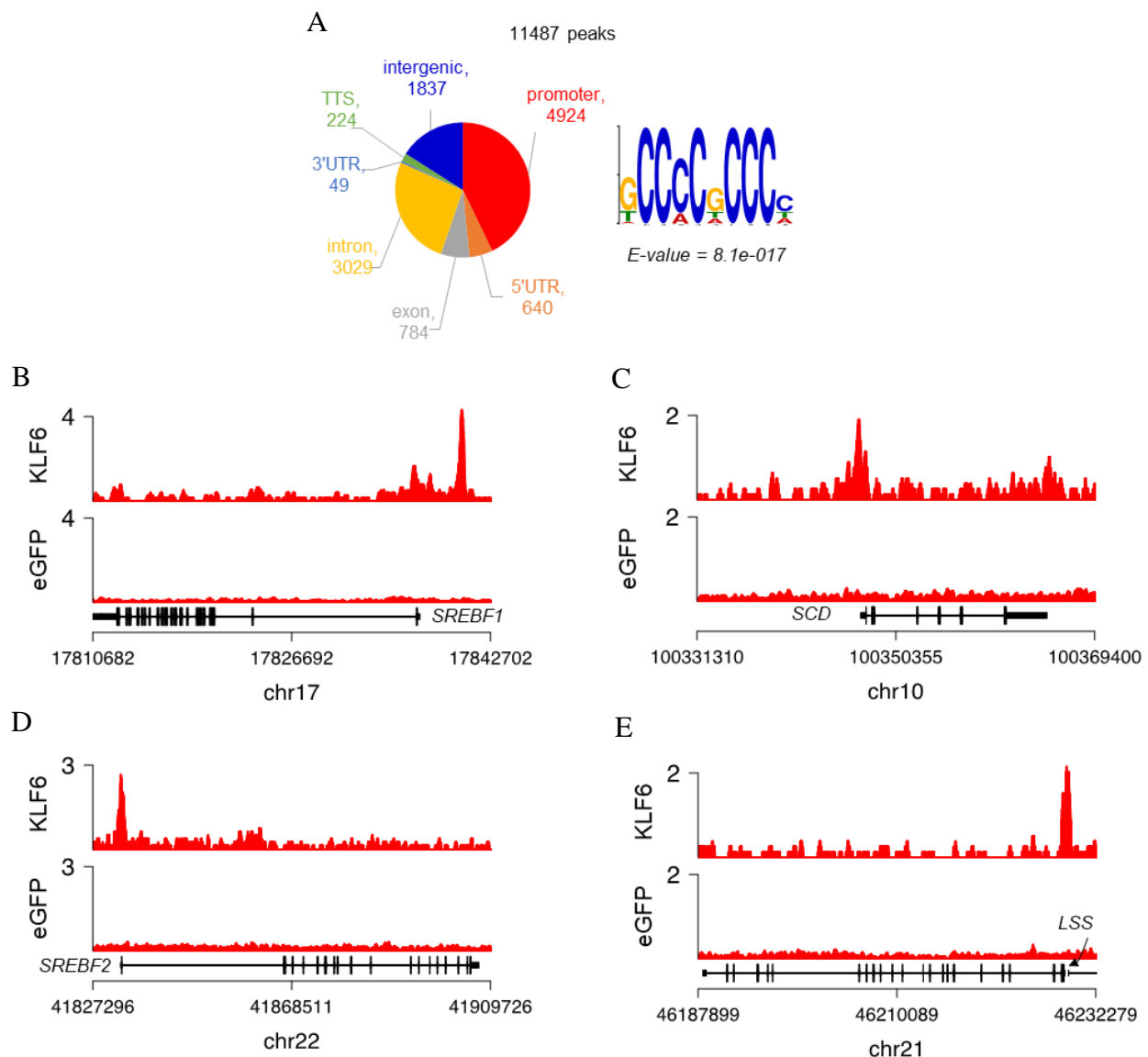


Figure 55: Genomic regions bound by the flag-KLF6. **(A)** (*Left*) Genomic distribution of the 11487 KLF6 peaks relative to known transcripts. (*Right*) The most significant DNA motif detected using MEME *de novo* motif discovery on the 500 most significant KLF6 peaks. **(B-E)** Enrichment of flag-KLF6 signal in the genomic regions of **(B)** *SREBF1*, **(C)** *SCD*, **(D)** *SREBF2* **(E)** and *LSS*. Arrows indicate the direction of transcription.

5.2.6 Impaired mTORC1 activity in the *KLF6*-targeted ccRCC cell lines

I have demonstrated that KLF6 directly regulates the expression of lipid metabolism genes as well as possible involvement of the mTORC1 complex in modulating the lipid homeostasis pathways in ccRCC. To further investigate the contributing role of mTORC1 complex to the observed phenotypes, the level of mTORC1 activity in the *KLF6*-depleted and control 786-M1A cells was assessed. I hypothesised that KLF6 inhibition could have an effect on the cells mTORC1 activity that would consequently lead to the deregulation of lipid homeostasis pathways. Hence, to test this hypothesis, the expression level of P-p70 S6 kinase and P-S6, read-out for mTORC1 activity, were assessed in the *KLF6*-depleted and control cells upon serum starvation overnight.

In line with the hypothesis, I found that the mTORC1 activity of the *KLF6*-depleted cells was attenuated after an overnight serum starvation, demonstrated by significant reduction in the expression of P-p70 S6 kinase and P-S6. In contrast, the control cells were able to sustain the expression of these phosphorylated proteins even under the serum-starved condition (Figure 56A). This could possibly be due to either the higher basal level of mTORC1 activity or the presence of unknown factor that was able to sustain the mTORC1 activity in these 786-M1A control cells. I further validated this finding by examining the effect of KLF6 inhibition on the

mTORC1 activity of other VHL-mutant ccRCC cell lines, the OS-LM1 and UOK101. I observed that the *KLF6*-depleted OS-LM1 and UOK101 cells also had reduced expression of P-S6 (Figure 56B-C), thus confirming the hypothesis that *KLF6* inhibition in ccRCC cells led to mTORC1 activity impairment in these cells. Collectively, these findings revealed *KLF6* dual roles in modulating lipid homeostasis in ccRCC; 1) *KLF6* directly regulates the expression of lipid homeostasis genes and 2) *KLF6* modulates mTORC1 activity in ccRCC in which the mTORC1 complex plays a role in SREBF1 and SREBF2 activation and subsequent regulation of the lipid homeostasis pathway.

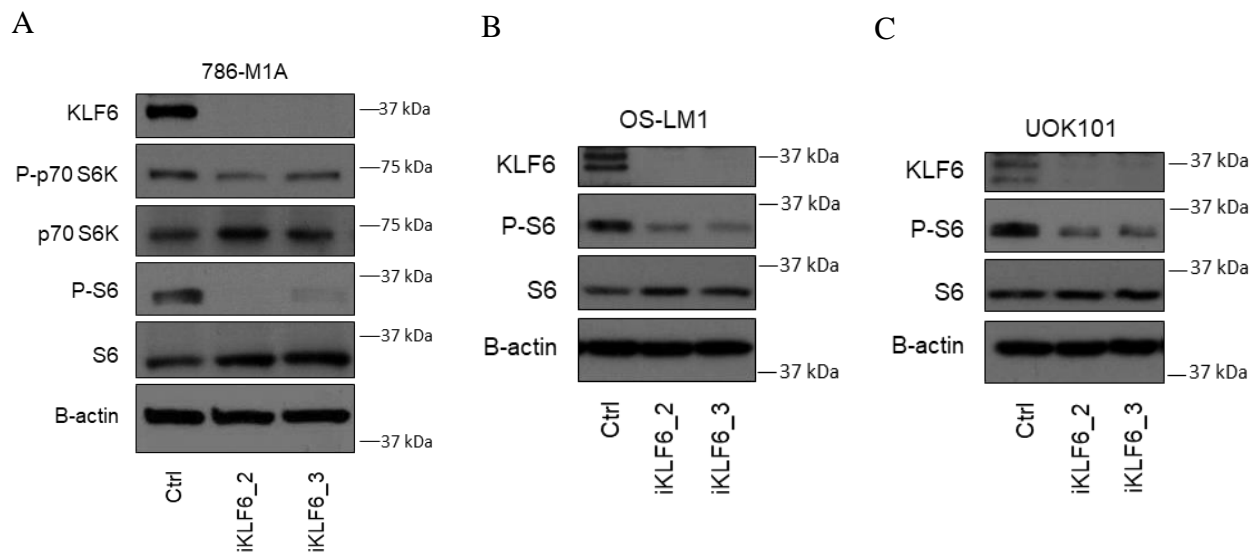


Figure 56: Impaired mTORC1 activity in *KLF6*-depleted ccRCC cell lines. (A-C) mTORC1 activity in *KLF6*-depleted (A) 786-M1A, (B) OS-LM1 and (C) UOK101 cells.

5.2.7 mTORC1 activity supports ccRCC growth *in vitro* and *in vivo*.

Impaired mTORC1 activity was possibly another contributing factors that led to the reduced proliferation rate of these *KLF6*-targeted cells. To further validate the role of mTORC1 complex in supporting ccRCC growth, the effect of treating the 786-M1A cells with everolimus, a mTORC1 complex inhibitor, on the cells growth was assessed. I first checked the expression of P-p70 S6 kinase and P-S6 in the 786-M1A cells 48 hours post-everolimus treatment. The mTORC1 activity was attenuated in the everolimus-treated 786-M1A cells in a dose-dependent manner (Figure 57A). It was observed that the everolimus-treated 786-M1A cells grew slower compared to the cells treated with the vehicle control (Figure 57B), thus validating the role of mTORC1 complex in supporting the growth of these cells *in vitro*.

I also investigated the effect of everolimus treatment on the ccRCC tumour growth *in vivo*. The 786-M1A cells were subcutaneously injected into each flank of athymic nude mice as previously described in Chapter 3. After the tumours had become palpable, the mice were separated into two groups; the experimental and control groups. Mice in the experimental group were orally treated with everolimus (5mg/kg) while the control group mice were administered with vehicle control. The assay was performed daily for 21 days where the tumours growth were monitored via calliper measurement. At the end of the assay, I found that the tumours of the everolimus-treated mice were smaller compared to tumours of vehicle-treated mice, indicating the tumours impaired growth upon the treatment with everolimus (Figure 57C). Collectively, these findings confirmed the role of mTORC1 complex in supporting the 786-M1A cells growth both *in vitro* and *in vivo*.

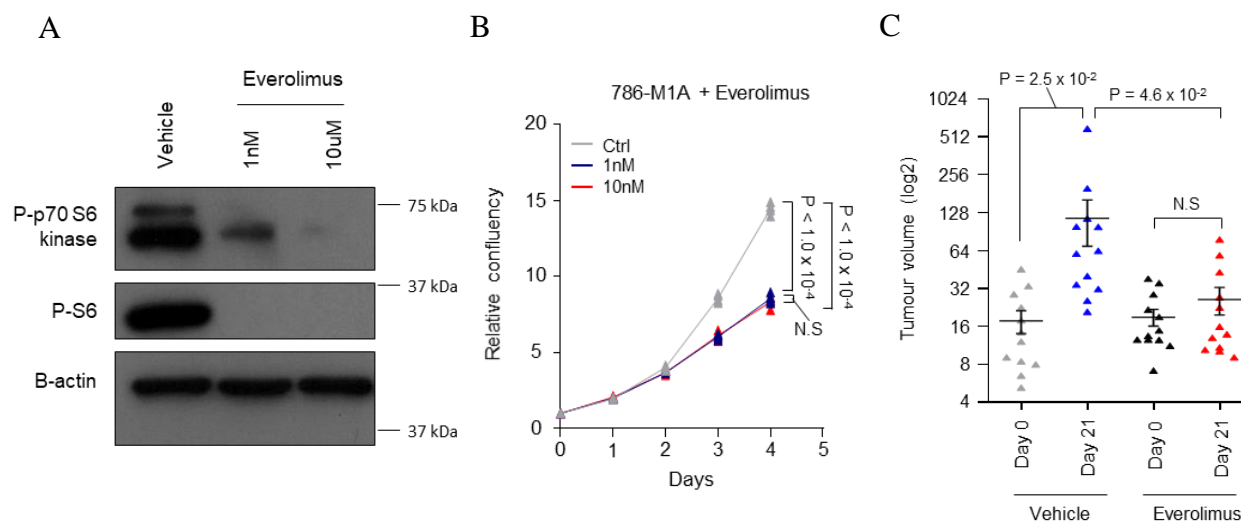


Figure 57: mTORC1 complex perturbation impairs ccRCC cells growth *in vitro* and *in vivo*. **(A)** mTORC1 activity in the everolimus-treated 786-M1A cells. **(B)** Proliferation of 786-M1A cells treated with either vehicle or indicated concentrations of everolimus. Average of four technical replicates. Two-way ANOVA with Tukey's range test. **(C)** Tumours volume from 786-M1A cells in mice fed with everolimus or vehicle pre- and 21 days post treatment. N=12 tumours/group. One-way ANOVA with Tukey's range test.

5.2.8 KLF6 modulates mTORC1 activity via transcriptional regulation of *PDGFB*

Next, I sought to investigate how KLF6 would involve in promoting mTORC1 activity in ccRCC. As previously speculated, there might be the presence of unknown factors that would contribute to the sustained mTORC1 activity in the 786-M1A control cells under the serum-starved condition. This could possibly explain the difference in the level of mTORC1 activity between the control and *KLF6*-depleted cells. However, to our knowledge, there has been no report linking KLF6 and the mTORC1 signalling pathway. Thus, in order to identify the potential mediator between KLF6 and mTORC1 signalling pathway, I re-examined the RNA-Seq data of the *KLF6*-depleted 786-M1A cells. I specifically looked for the downregulated genes that

were either known mTORC1 agonist or have been linked with mTORC1 signalling pathway in general. From the RNA-Seq data, there was a significant downregulation of *PDGFB* expression, a known activator of the mTORC1 signalling pathway, in the *KLF6*-depleted cells. Moreover, previous report has shown that PDGFB was able to modulate the SREBF1 and SREBF2 expression and activity²⁰¹. Based on these evidences, I hypothesised that KLF6 potentially modulates mTORC1 activity in ccRCC by transcriptionally regulating the expression of its agonist *PDGFB*.

I then validated this RNA-Seq finding by checking the expression of *PDGFB* in the independent set of *KLF6*-depleted 786-M1A cells. On top of this, I also assessed *PDGFB* expression level in the *KLF6* knockdown OS-LM1 and UOK101 cells. In line with the RNA-Seq data, the qPCR analysis confirmed that there was downregulation in the expression of *PDGFB* in the *KLF6*-depleted 786-M1A, OS-LM1 and UOK101 cells (Figure 58A-C). Importantly, the reintroduction of either exogenous KLF6 or flag-KLF6 into the *KLF6*-depleted 786-M1A cells was able to rescue the *PDGFB* expression (Figure 58D and 59A). This data seemed to suggest that the impaired mTORC1 activity upon KLF6 inhibition in ccRCC cells was potentially due to the downregulation of *PDGFB* expression in these cells.

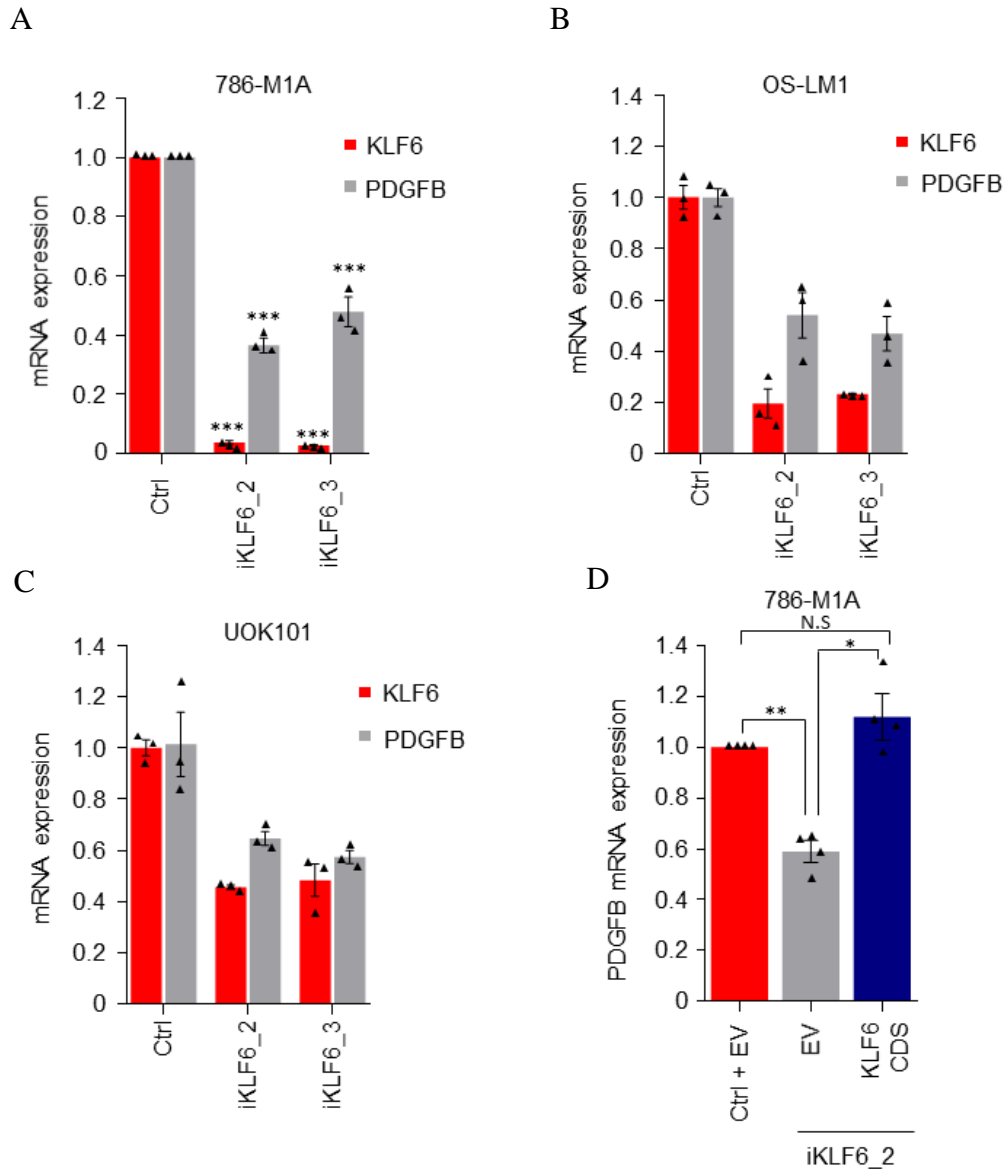
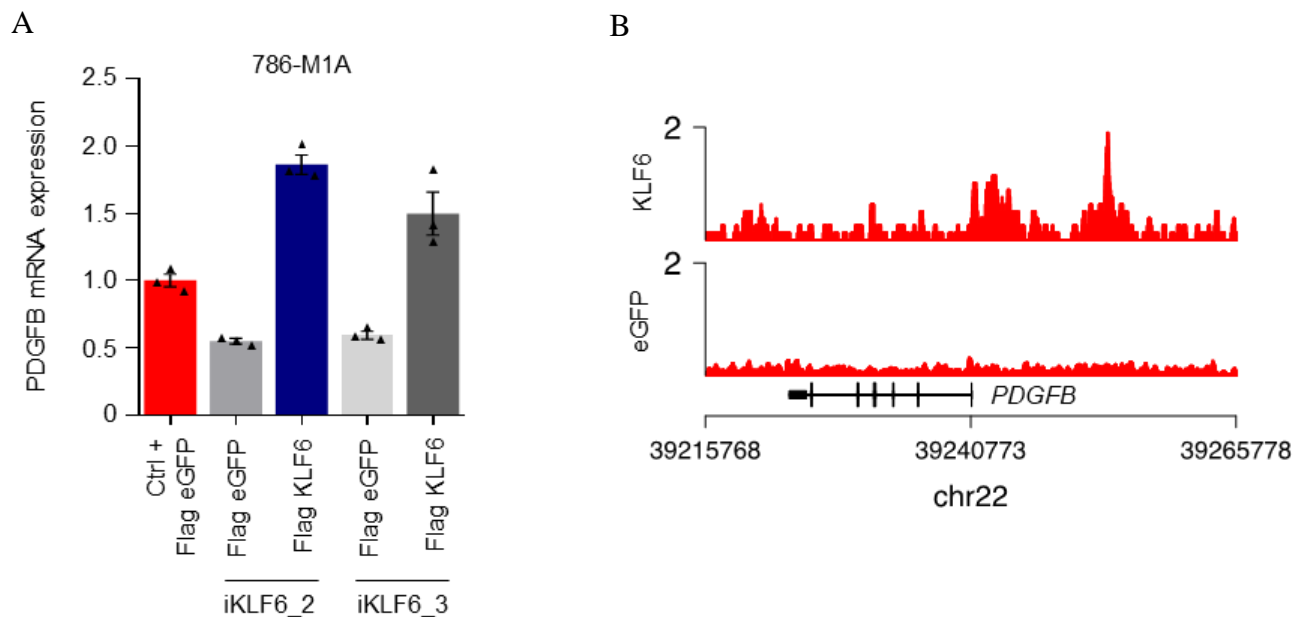


Figure 58: Downregulation of mTORC1 agonist *PDGFB* in the *KLF6*-depleted ccRCC cell lines. **(A)** *PDGFB* expression in *KLF6*-depleted 786-M1A cells as measured by qPCR. Average of three experiments. Error bars, SEM. One-way ANOVA with Dunnett's test. **(B-C)** *PDGFB* expression in *KLF6*-depleted **(B)** OS-LM1 and **(C)** UOK101 cells. Average of three technical replicates. Error bars, SEM. **(D)** *PDGFB* expression in the *KLF6*-depleted 786-M1A cells, with the reintroduction of either empty vector or exogenous *KLF6*. Average of four experiments. Error bars, SEM. One-way ANOVA with Tukey's range test. * $P < 0.05$, ** $P < 0.005$ and *** $P < 0.0005$

The RNA-Seq and qPCR data as well as the exogenous KLF6 rescue experiment indicated that KLF6 potentially operated upstream of *PDGFB* in ccRCC. I next wanted to determine whether *PDGFB* was a direct KLF6 downstream target. To investigate this, I examined the previously generated flag-KLF6 ChIP-Seq data and found that the *PDGFB* proximal regulatory region contained KLF6 peaks, signifying KLF6 binding at this region (Figure 59B). The corresponding ChIP-qPCR analysis showed the enrichment of flag-KLF6 at the *PDGFB* proximal regulatory region, thus validating the ChIP-Seq finding (Figure 59C). In sum, the *PDGFB* qPCR as well as the flag-KLF6 ChIP-Seq and ChIP-qPCR data strongly demonstrated that KLF6 directly regulates the expression of mTORC1 signalling agonist *PDGFB* in ccRCC cells. Sakari Vanharanta and I subsequently tested whether these *in vitro* findings were clinically relevance and reflected in the actual ccRCC clinical samples. Analysis of the ccRCC TCGA RNA-Seq data revealed that ccRCC patients with high level of *KLF6* expression also expressed higher levels of *PDGFB* (Figure 59D), which was aligned with our *in vitro* findings that KLF6 transcriptionally regulated *PDGFB* expression in ccRCC.



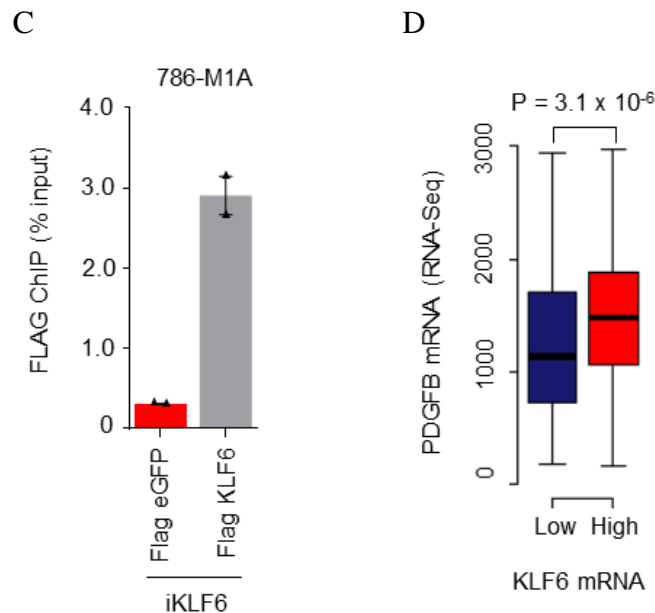


Figure 59: KLF6 directly regulates the expression of *PDGFB* in ccRCC. **(A)** *PDGFB* expression in *KLF6*-depleted 786-M1A cells, reintroduced with either exogenous flag-KLF6 or flag eGFP. Average of three technical replicates. Error bars, SEM. **(B)** Flag ChIP-Seq signal at the *PDGFB* proximal regulatory region. **(C)** Flag ChIP-qPCR of the *PDGFB* proximal regulatory region. Average of two of experiments. Error bars, SEM **(D)** *PDGFB* expression (RSEM normalised counts) in clinical ccRCC samples with either high (top 50%) or low (bottom 50%) *KLF6* expression. Mann Whitney U test.

5.2.9. *PDGFB* activates mTORC1 signalling pathway in ccRCC

I have thus far provided evidences that 1) KLF6 directly regulates *PDGFB* expression and 2) the impaired mTORC1 activity in the *KLF6*-targeted cells was the consequence of *PDGFB* downregulation in these cells. Nonetheless, to further consolidate these findings, the role of *PDGFB* in regulating the mTORC1 signalling pathway in ccRCC was directly tested. To address this, *PDGFB* was targeted in the 786-M1A cells using the CRISPRi approach, followed

by checking the expression of mTORC1 activity surrogate markers in these cells. *PDGFB* was targeted using the single sgRNA targeting approach where two sgRNA constructs were designed, iPDGFB_1 and iPDGFB_2. Downregulation of *PDGFB* was confirmed in the iPDGFB-transduced 786-M1A cells (Figure 60A). The mTORC1 activity of these cells were assessed after an overnight serum starvation. It was found that *PDGFB* inhibition impaired the mTORC1 activity of these cells (Figure 60B), phenocopying the effect of KLF6 inhibition in ccRCC cell lines (Figure 56A-C). This finding validated the role of PDGFB in regulating the mTORC1 signalling pathway in ccRCC.

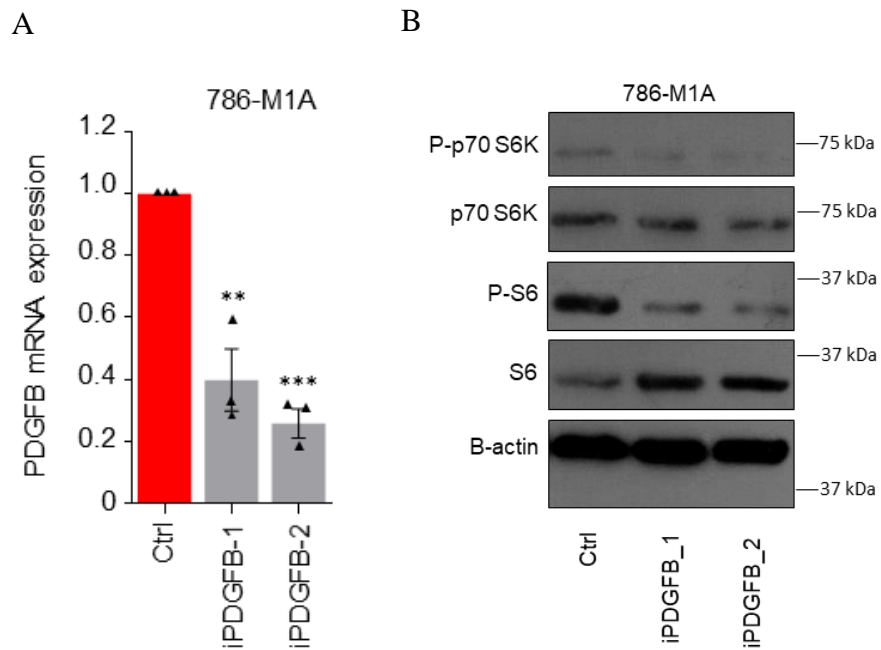
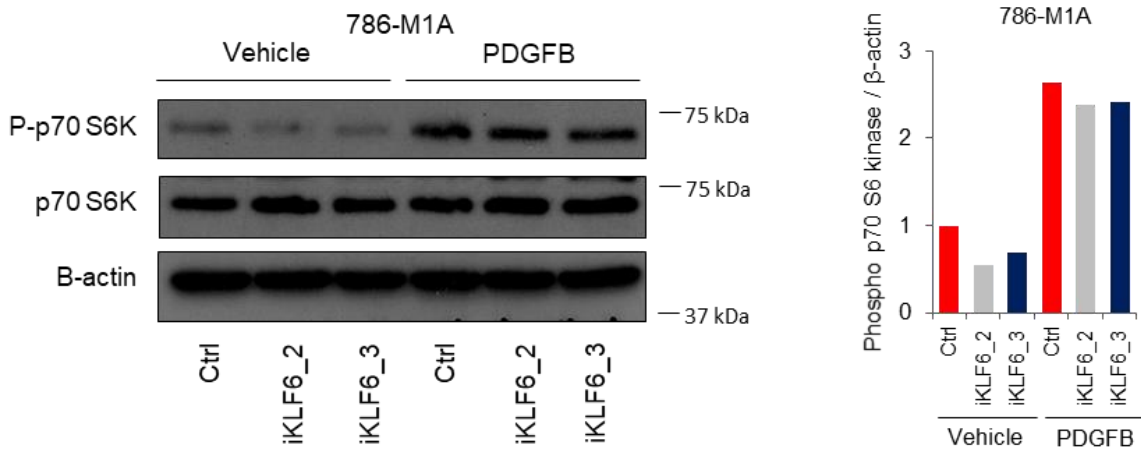


Figure 60: PDGFB regulates mTORC1 signalling pathway in ccRCC. **(A)** *PDGFB* expression in *PDGFB*-depleted 786-M1A cells. Average of three experiments. Error bars, SEM. One-way ANOVA with Dunnett's test. **(B)** mTORC1 activity in *PDGFB*-depleted 786-M1A cells.

Finally, I tested the effect of supplementing the *KLF6*-targeted 786-M1A cells with human recombinant PDGFB. Based on the previous findings, I postulated that the recombinant PDGFB supplementation would be able to re-stimulate the mTORC1 signalling pathway in these

KLF6-targeted cells under the serum-starved condition. Hence, the *KLF6*-targeted and control 786-M1A CRISPRi cells were serum-starved overnight and treated with 10ng/mL human recombinant PDGFB for an hour on the following day. Then, I assessed these cells mTORC1 activity. In line with the hypothesis, supplementation with recombinant PDGFB was able to re-stimulate the mTORC1 signalling pathway in these *KLF6*-targeted cells, demonstrated by an increased expression of P-p70 S6 kinase and P-S6 in these cells as compared to the vehicle-treated cells (Figure 61A-B). This validated the role of KLF6-PDGFB axis in supporting the mTORC1 activity in ccRCC.

A



B

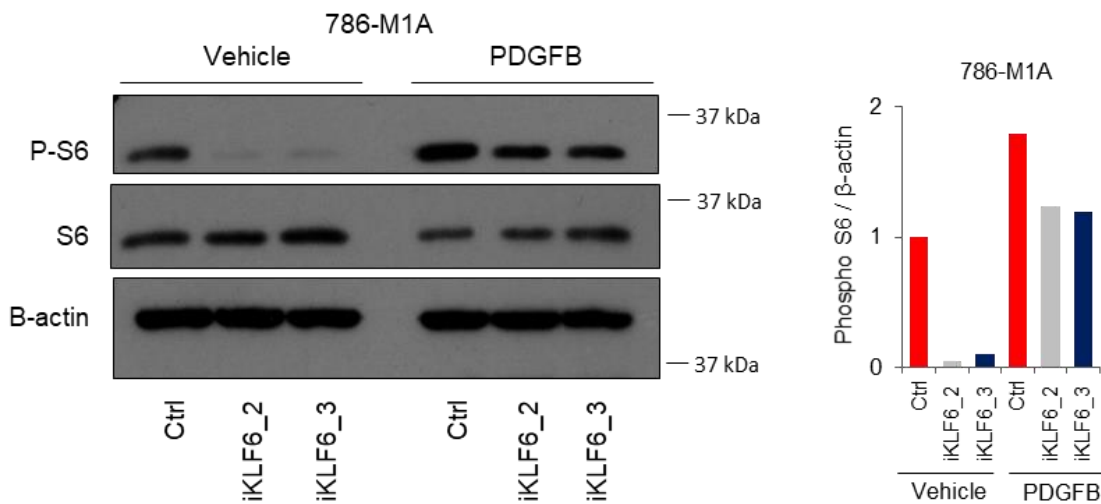


Figure 61: Recombinant PDGFB supplementation re-stimulates mTORC1 activity in the *KLF6*-depleted cells. **(A and B)** Expression of **(A)** P-p70 S6 kinase and **(B)** P-S6 in the *KLF6*-depleted 786-M1A cells supplemented with either human recombinant PDGFB or vehicle control for 1 hour. Graph on the right shows quantification of the immunoblot bands.

5.3 Summary

Through transcriptomic profiling and subsequent functional assays, I unraveled a network of transcriptional programs linking the super enhancer-regulated transcription factor *KLF6* with the modulation of lipid homeostasis and mTORC1 signalling pathways in ccRCC. These data suggested that the proliferative defect observed upon *KLF6* inhibition was the consequence of impaired lipid homeostasis and mTORC1 signalling pathways in these cells. This was supported by the findings that direct perturbation of lipid homeostasis as well as the mTORC1 signalling pathways reduced ccRCC cells growth, phenocopied the effect of targeting *KLF6* in ccRCC cells (discussed in Chapter 3).

Further investigations into the mechanism on how *KLF6* could be involved in modulating the lipid homeostasis pathways in ccRCC revealed that *KLF6* regulates the expression of some lipid homeostasis genes that include the *SREBF1* and *SREBF2*, two critical transcriptional regulators of lipid metabolism. Then I discovered that the mTORC1 signalling pathway also contributed to the deregulation of lipid homeostasis pathways in the *KLF6*-targeted cells. I had first prompted to check the involvement of the mTORC1 signalling pathway based on previous reports^{81,82} that have demonstrated the role of mTORC1 complex in modulating lipid metabolism via the regulation of *SREBF1* and *SREBF2* activity. In line with the previous reports^{81,82}, impaired mTORC1 activity was observed in the *KLF6*-targeted cells in which these cells were

more sensitive to serum-starvation as compared to the control cells. Taken these observations together, deregulation of lipid homeostasis pathways in the KLF6-targeted cells were due to downregulation of some lipid homeostasis genes, whose expression were directly regulated by KLF6, as well as impaired mTORC1 signalling pathway.

In this chapter, the question on how KLF6 was linked to the mTORC1 signalling pathway was also investigated. I found that KLF6 inhibition led to the downregulation of *PDGFB* which is a known activator of the mTORC1 signalling pathway. Via exogenous KLF6 rescue and flag-KLF6 ChIP-Seq and ChIP-qPCR experiments, *PDGFB* was demonstrated to be a direct KLF6 downstream target. Reintroduction of exogenous KLF6 into the *KLF6*-targeted cells was able to restore *PDGFB* expression in these cells. The flag-KLF6 ChIP-Seq and ChIP-qPCR experiments revealed that KLF6 bound to the proximal regulatory region of *PDGFB*. Importantly, supplementing the overnight serum-starved, *KLF6*-depleted cells with human recombinant PDGFB was able to re-activate the mTORC1 signalling pathway in these cells. In sum, KLF6 promotes the mTORC1 signalling pathway in ccRCC by transcriptionally regulating the expression of one of its agonist *PDGFB*.

In addition to the transcriptional networks described above, the gene set enrichment analysis performed by our collaborator found a significant association between *KLF6* inhibition and downregulation of the canonical hypoxia-response gene signature. This data suggested that KLF6 was involved in regulating the expression of some of the known HIF2A downstream targets. I tested this by checking whether KLF6 reintroduction into the VHL-expressing ccRCC cells was able to restore the expression of several HIF2A downstream targets. It was observed that KLF6 reintroduction was able to restore the expression of *BHLHE40* to the level seen in the control cells. Slight upregulation in the expression of *VEGFA* and *CCND1* was also observed,

but the expression level of these genes was still fairly low. Interestingly, it has been shown previously that HIF2A drove the expression of *KLF6* in ccRCC by acting through the *KLF6* super enhancer locus. Hence, these findings further indicated that some of the HIF2A downstream targets are secondary targets that were activated by KLF6. Collectively, through the works presented in this chapter, I discovered several transcriptional networks that were regulated by KLF6 of which some of these transcriptional programs were essential in supporting ccRCC pathogenesis

Chapter 6

Discussion

6.1 Introduction

The purpose of this study was to identify a novel transcriptional network that plays a role in supporting ccRCC pathogenesis with the hope that the gained knowledge could potentially be useful for diagnostic and/or therapeutic development. As discussed in Chapter 1, the current clinically-approved therapeutic strategies for ccRCC have been those targeting the angiogenesis and the frequently hyper-activated mTOR signalling pathways. Nevertheless, objective patients' response rates especially in patients with advanced stage ccRCC towards these treatment options are still low. One factor that contributes to the lack of efficient therapies developed for ccRCC is the incomplete understanding on ccRCC cellular dependencies or the underlying mechanisms that support its progression. Therefore, to address this problem, a better understanding on ccRCC pathogenesis is urgently needed given the high mortality and poor prognosis of the advanced stage ccRCC.

6.2 *KLF6* expression regulation by a robust super enhancer

By utilising previously generated active chromatin ChIP-Seq data, a large enhancer cluster with enriched H3K27ac signal was identified encompassing the *KLF6* locus. As demonstrated in Chapter 4, *KLF6* expression in ccRCC was found to be regulated by this nearby super enhancer. Comprehensive *in vitro* and *in vivo* functional assays showed that this super enhancer-regulated transcription factor KLF6 was functionally important in supporting ccRCC growth. KLF6 inhibition resulted in reduced ccRCC cells proliferation rate both *in vitro* and *in vivo*. This was in line with reports linking super enhancers and the regulation of critical genes including those that support cancer phenotypes^{149,150}.

Targeting cancer-associated super enhancers is actively being explored as a potential therapeutic strategy in several different cancer types due to reports demonstrating that they may be particularly sensitive to perturbations¹⁶⁵⁻¹⁶⁷. However, in contrast to what others have suggested, I found that this *KLF6* super enhancer tolerated the perturbations in the activity of its constituent enhancers fairly well. These findings seemed to imply that targeting *KLF6* super enhancer and its subsequent development as an alternative approach for treating ccRCC could potentially be challenging. Yet, this speculation was solely based on several CRISPRi enhancer inactivation experiments, thus I cannot eliminate the possibility that this *KLF6* super enhancer could still remain an attractive therapeutic target for ccRCC. Further interrogation into this super enhancer region could possibly lead to the identification of machineries or co-factors that upon its targeting would perturb this *KLF6* super enhancer landscape and therefore would constitute a potential therapeutic avenue. Also, it is appealing to test in the future study whether this *KLF6* super enhancer locus is sensitive to BRD4 or CDK7 inhibition by JQ1 or THZ1, respectively.

Furthermore, I discovered that this super enhancer locus functions in a modular fashion to drive *KLF6* expression in ccRCC. Significant reduction in the *KLF6* mRNA level was only achieved when several constituent enhancers were simultaneously inactivated or large segment of this enhancers cluster was deleted. The tight regulation of *KLF6* expression by the super enhancer was in line with *KLF6* high expression in ccRCC clinical samples and its important role in supporting ccRCC growth. Moreover, the redundancy and robustness in the regulation of *KLF6* expression in ccRCC are well-aligned with the fact that most critical biological processes and developmental transcriptional programmes are insensitive to environmental and other incoming variations^{133,202}.

6.3 Identification of *KLF6* upstream transcriptional regulators

Interestingly, HIF2A was discovered to act through this *KLF6* enhancers cluster in modulating *KLF6* expression in ccRCC. Thus, it is plausible that the accumulation of HIF2A due to VHL inactivation in ccRCC consequently contributes to the relatively high expression of *KLF6* in ccRCC clinical samples as compared to other tumour types. This might also explain the observed upregulation of *KLF6* expression in ccRCC as compared to normal kidney tissues. Through previously generated p300 ChIP-Seq data, several distinct p300 peaks were identified at the valley of this super enhancer H3K27ac signals. This region is known to be the transcription factor binding site. Thus, in addition to HIF2A, there could be several other important transcription factors that bind to this super enhancer region and drive the expression of *KLF6* in ccRCC. The identification of these transcription factors would give us better insight on how *KLF6* expression is regulated as well as explaining its upregulation in ccRCC samples as compared to the normal kidney tissues. This could also possibly lead to the discovery of factors that support the formation and maintenance of this *KLF6* super enhancer landscape. The discovery of such factor might be beneficial if targeting this *KLF6* super enhancer to be further explored and developed as an alternative treatment strategy for ccRCC.

One approach to identify these transcription factors is by performing DNA motif discovery within this *KLF6* super enhancer locus using the available online tools such as MEME and FIMO. These putative transcription factors role in driving *KLF6* expression can be assessed by perturbing the function of these transcription factors by either CRISPR-Cas9 or CRISPRi, followed by assessing the *KLF6* mRNA level. Luciferase reporter assay can subsequently be employed to confirm the binding of these putative transcription factors to the super enhancer locus if they are found to drive *KLF6* expression. A very preliminary DNA motif discovery

analysis was performed on the iSE-2 revealed a DNA motif known to be bound by the transcription factor FOXJ3 at this enhancer region (Figure 62). Also, the *FOXJ3* expression was found to be highly expressed in ccRCC as compared to other tumour types in the TCGA RNA-Seq data set. Thus, it is worth to follow-up on this finding in the future as well as identifying other transcription factors that bind to this *KLF6* super enhancer using the DNA motif discovery approach described previously.

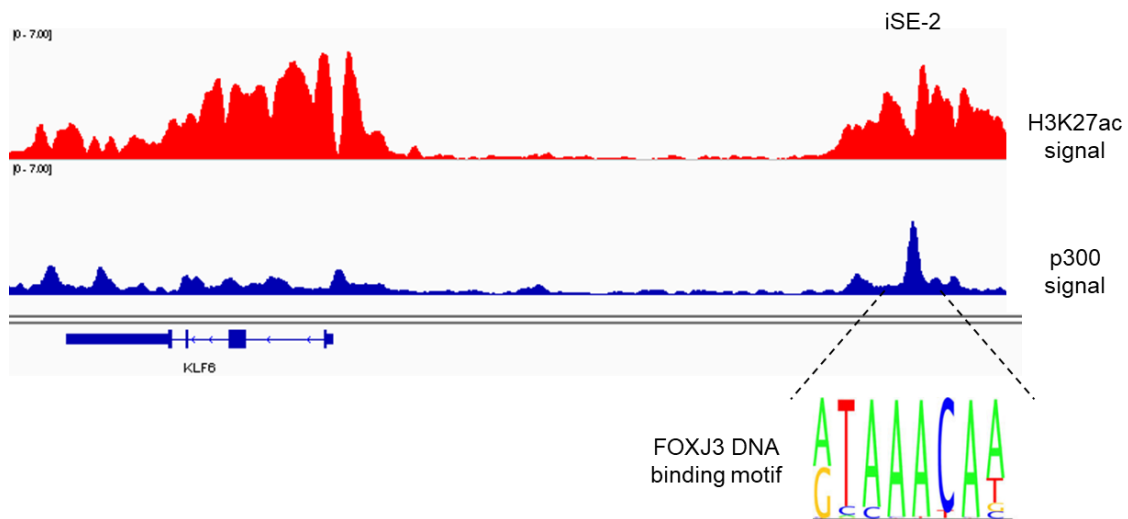


Figure 62: FOXJ3 DNA binding motif at the iSE-2 enhancer region.

In addition to the DNA motif discovery analysis, the candidate transcription factors can also be shortlisted by looking into previous studies that have reported or identified any upstream regulators of *KLF6*. For instance, there were studies that demonstrated the role MEF2 family transcription factor in regulating *KLF6* expression in which this MEF2-KLF6 axis acted as a pro-survival factor in hippocampal neurons and cardiomyocytes^{203,204}. Therefore, it is interesting to test whether this family of MEF2 transcription factors are also involved in regulating *KLF6* expression and functionally relevance in supporting ccRCC pathogenesis.

6.4 The pro-tumourigenic role of KLF6 in ccRCC

There have been opposing reports on the role of KLF6 in different type of cancers^{183,187,189,205}. In this present study, KLF6 was discovered to have a pro-tumourigenic role in ccRCC. KLF6 inhibition in several VHL-deficient ccRCC cell lines impaired cell growth which resulted in the formation of smaller tumours *in vivo*. Also, the KLF6-targeted 786-M1A cells had reduced metastatic lung colonisation capability, which could be the consequence of impaired cells growth. Overall, this was an interesting finding because the 786-M1A cells are the metastatic sub-population of the 786-O cells, which are aggressive and characterised by a significantly enhanced lung colonisation capability¹⁷³. Nonetheless, these present findings contradicted those of Gao *et al*, who have reported that KLF6 possesses a growth suppressive function in ccRCC²⁰⁶. We are not certain of the reasons behind this discrepancy. Technical-wise, KLF6 was targeted in this study by utilising both CRISPR-Cas9 and CRISPRi approaches in which two independent sgRNA constructs were designed for each targeting approach. I also demonstrated that the reintroduction of exogenous KLF6 into these CRISPR-Cas9 and CRISPRi KLF6-targeted cells was able to alleviate the cells proliferative defect. These comprehensive interrogations on KLF6 function in our model system were to ensure the robustness and reliability of our findings. On the other hand, the study that has demonstrated the growth suppressive function of KLF6 rely solely on a single siRNA construct²⁰⁶, thus making it difficult to exclude any possible off-target effects.

Also, due to *KLF6* high expression and regulation by one of the strongest super enhancer in ccRCC, it may possibly be difficult to target and achieve significant reduction in the *KLF6* expression level. Nonetheless, by employing the *state-of-the-art* CRISPRi in conjunction with tandem sgRNAs targeting approaches, I was able to obtain 95% reduction in the *KLF6*

expression level. Thus, I believe that our CRISPR-Cas9 and CRISPRi-based gene inactivation strategies might be more efficient and robust in targeting *KLF6* compared to the RNAi approach employed by Gao *et al*²⁰⁶. I also attempted to reproduce one of their main findings which has suggested that *KLF6* suppressed ccRCC cells growth by repressing the expression of *E2F1*²⁰⁶. I first examined the *KLF6*-depleted 786-M1A cells RNA-Seq data to check the *E2F1* expression level in these cells. In contrast to the effect seen by Gao *et al*²⁰⁶, *KLF6* inhibition led to the downregulation of *E2F1* expression in these cells. This RNA-Seq finding was validated by performing *E2F1* qPCR analysis on two independent *KLF6*-depleted 786-M1A cells validation sets (Figure 63).

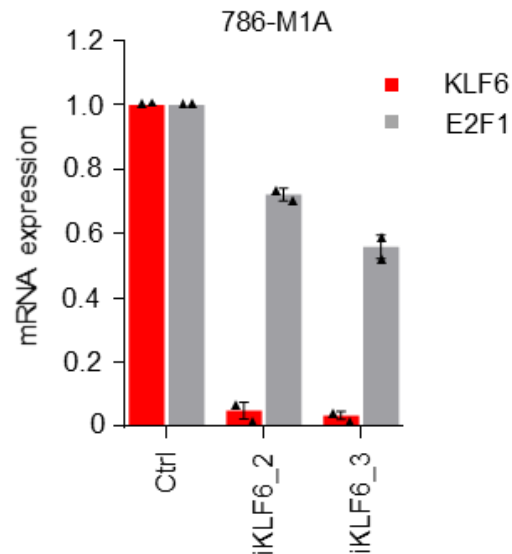


Figure 63: *KLF6* and *E2F1* expression in *KLF6*-targeted 786-M1A CRISPRi cells. Average of two experiments. Error bars, SEM.

The same group who had initially discovered the *KLF6* inactivation and its tumour suppressive function in prostate cancer subsequently reported about the presence of several *KLF6* transcript isoforms in this tumour type^{181,183}. The presence of these isoforms, *KLF6*-SV1, -SV2 and SV3, are the consequence of alternative splicing that occurs due to a germ line single

nucleotide polymorphism (SNP) in the *KLF6* intron 1 (IVS1 -27 G/A). The *KLF6*-SV1 in particular has been linked to tumour progression and poor prognosis in breast and ovarian cancer^{190,191}. However, it has been confirmed that the observed phenotypic defect in this present study was due to the inhibition of full length *KLF6*, not the presumably “*oncogenic*” *KLF6*-SV1. This was because these ccRCC cell lines predominantly expressed the full length *KLF6*, with little evidence showing these *KLF6* transcript isoforms were being expressed in these cells (Figure 19). Furthermore, to my knowledge, there has been no report describing the presence of the aforementioned *KLF6* intronic polymorphism in ccRCC.

Despite the discrepancy between my findings and those reported by Gao *et al*, as well as the possible contribution of *KLF6*-SV1 isoform, I am convinced that *KLF6* is a pro-tumourigenic transcription factor that supports ccRCC pathogenesis. This was because *KLF6* expression was high in ccRCC clinical samples as compared to normal kidney tissues. In theory, I would not have expected the expression of *KLF6* to become upregulated in ccRCC samples if it possesses a tumour suppressive function. Moreover, *KLF6* expression was robustly regulated by one of the strongest super enhancers in ccRCC, signifying the *KLF6* functional relevance in ccRCC pathogenesis. Last but not least, I also discovered that *KLF6* was partially activated by the ccRCC-initiating VHL-HIFA pathway, which has been widely-established as the hallmark gatekeeper of renal tumourigenesis. These evidences were indeed well-aligned and supportive of a pro-tumourigenic role for *KLF6* in ccRCC.

6.5 Dual *KLF6* roles in modulating lipid homeostasis pathways in ccRCC

It was discovered that *KLF6* inhibition in ccRCC cell lines led to the deregulation of lipid homeostasis pathways. Direct genetic and pharmacological perturbations of lipid homeostasis

pathways impaired ccRCC cells growth *in vitro*, thus implying that the reduction in the KLF6-targeted cells proliferation rate was due to the deregulation of the lipid homeostasis pathways in these cells. Mechanistically, I identified a dual role for KLF6 in modulating lipid homeostasis pathways in ccRCC. First, KLF6 was discovered to directly regulate the expression of several lipid homeostasis genes in ccRCC, which include the lipid metabolism master transcriptional regulator SREBF1 and SREBF2. Through flag-KLF6 ChIP-Seq experiment, we provided a clear evidence that KLF6 binds at the proximal regulatory region and drive the expression of these lipid homeostasis genes. Secondly, KLF6 was found to modulate the lipid homeostasis pathways in ccRCC by supporting the activity of mTORC1 complex. Evidences from the literatures have demonstrated that mTORC1 complex is a critical regulator of lipid homeostasis pathways in which it involves in regulating SREBF1 and SREBF2 activation^{81,82}. In line with the previous reports, I found that the inhibition of mTORC1 complex impaired SREBF1 and SREBF2 activation in our model system. Taken these together, these data revealed that impaired mTORC1 activity in the KLF6-targeted cells also contributed to the observed lipid homeostasis pathways deregulation in these cells.

Metabolic rewiring that includes alterations in the lipid metabolism has been described as the emerging hallmarks of cancer^{136,207}. Increased lipid biosynthesis is frequently observed in different cancer types as rapidly proliferating cancer cells require lipids for the synthesis of new cell membrane¹⁹⁹. Lipids are the cells membrane main building block in which the fatty acid forms the membrane phospholipid bilayer whereas the membrane lipid rafts are enriched with cholesterol and sphingolipids. Lipid rafts play important roles in modulating the membrane fluidity and molecules trafficking as well as providing the structural base for the assembly of receptor signalling complex. In addition to its structural role, lipids could serve as source of

energy as well as functioning as signalling molecules¹⁹⁹. A known example of lipid signalling molecule is phosphoinositide, a second messenger, which upon phosphorylation relays the transduced cellular signals. Despite the established roles of lipid metabolism in promoting tumourigenesis, it is of interest to investigate in future studies on how the deregulation of lipid homeostasis pathways would specifically contribute to the impaired ccRCC growth.

6.6 Cholesterol biosynthesis role in supporting cells fitness and survival

The cholesterol biosynthesis pathway was among the top most significantly downregulated pathways upon KLF6 inhibition in ccRCC cells. On top of this, there was a highly significant association between genes that were downregulated upon *KLF6* depletion and those participated in cholesterol homeostasis pathways. In line with these findings, I observed a reduction in total cholesterol level in the KLF6-targeted cells. Furthermore, inhibiting the activity of mTORC1 complex in ccRCC cell line phenocopied the effect of KLF6 inhibition on the total cholesterol level in these cells. Therefore, these data corroborated the KLF6 dual roles in modulating the lipid homeostasis pathway, which in this case I provided the evidence of KLF6 involvement in regulating the cholesterol biosynthesis pathway in ccRCC.

Also, it is important to highlight that one of ccRCC prominent features are the accumulation of glycogen and cytoplasmic lipid, predominantly in the form of cholesteryl ester, which give the ccRCC distinct clear cell morphology. Recent studies have performed lipidomic profiling and found high level of cholesteryl ester and triacylglycerol in ccRCC tissues, suggesting lipid biosynthesis rewiring in ccRCC in order to support its growth and progression^{208,209}. In line with this observation, cholesterol accumulation has been shown to drive tumourigenesis in prostate cancer whereby targeting the cholesterol pathway in this cancer

impairs the cells growth^{210,211}. Several studies have shown statins efficiency in inhibiting the growth of several different cancer cells²¹²⁻²¹⁴, an effect that I also observed upon treating the 786-M1A cells with fatostatin and simvastatin (Figure 52). In addition, I also found that the treatment with high concentration of simvastatin led to complete cells death. Based on these observations and reports demonstrating the importance of cholesterol in driving tumourigenesis, the cholesterol-lowering drug statins are currently being explored for use as cancer therapeutic agent²¹⁵.

As suggested by others, cholesterol could involve in increasing the cancer cells fitness as well as protecting the cells from apoptosis^{210,212,216}. In line with this, I have a very preliminary data showing that the KLF6-targeted cells were more sensitive towards camptothecin-induced apoptosis (Figure 64). This observation was consistent with several studies that demonstrated the role of KLF6 as a pro-survival factor that protect podocytes²¹⁷, hippocampal neuronal²⁰⁴ and hepatocellular carcinoma cells¹⁸⁷ from apoptosis and stress. However, it remains unknown whether the increased in *KLF6*-targeted ccRCC cells sensitivity to induced apoptosis was due to downregulation of cholesterol biosynthesis in these cells in which this could potentially be tested in future studies.

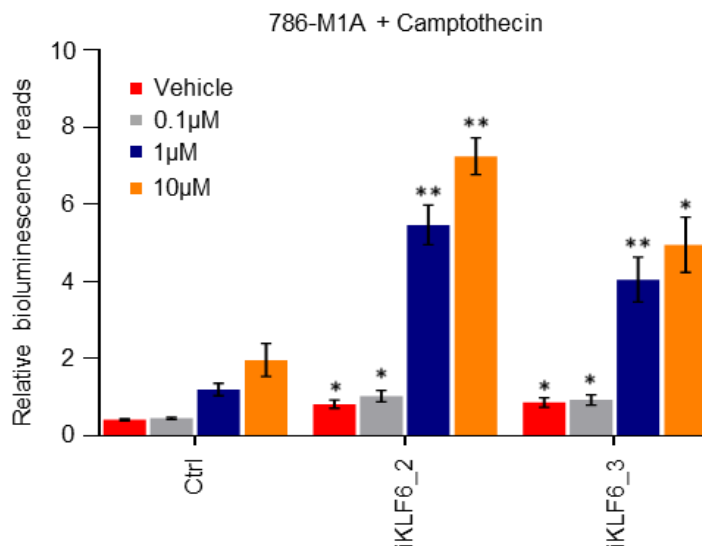


Figure 64: Increased *KLF6*-depleted 786-M1A CRISPRi cells sensitivity towards camptothecin-induced apoptosis. Relative bioluminescence reads of caspase 3/7 in the *KLF6*-targeted and control 786-M1A cells treated with indicated concentration of camptothecin. Average of three experiments. Error bars, SEM. Two-tailed Student's t-test. P values were calculated comparing the bioluminescence reads of the *KLF6*-targeted cells and control cells of the same condition. * P < 0.05, ** P < 0.005 and *** P < 0.0005.

6.7 Cytoplasmic lipid accumulation and ccRCC clear cell phenotype

As discussed previously, abundant accumulation of cytoplasmic lipid is a distinctive feature of ccRCC. However, the molecular mechanism that leads to this phenotype remains elusive. Also, it has not yet been fully elucidated how this accumulation of lipid contributes to ccRCC growth and progression. Therefore, these have been among the areas of active investigation in the field of kidney cancer. In ccRCC, the accumulated cholesteryl ester and triacylglycerides are stored in the form of lipid droplets in which these lipid droplets serve as source of energy as well as lipid species for membrane synthesis and signal transduction. A study found an overexpression of HIF2A-regulated *PLIN2* (Adipophilin/Adipose Differentiation Related Protein) in ccRCC clinical samples in which *PLIN2* encodes for lipid droplet coat protein and involves in mediating the lipid storage in ccRCC²¹⁸. In addition, the HIF2A-*PLIN2*-modulated lipid storage plays a role in supporting ccRCC fitness by maintaining the integrity of endoplasmic reticulum.

To check whether the findings of this present study have any relevance or link to this existing data, I re-examined the *KLF6*-depleted 786-M1A cells RNA-Seq data and found that *PLIN2* was downregulated in these cells. This suggested that *KLF6* could possibly modulate

PLIN2 expression in ccRCC, based on the evidences shown that a part of HIF2A downstream genes are secondary targets activated by KLF6. However, further investigation to address the functional links between KLF6, *PLIN2* and regulation of lipid accumulation and storage in ccRCC are necessary.

Furthermore, another study has demonstrated that lipid accumulation in ccRCC could be mediated by HIF1A regulation of *very low-density lipoprotein receptor* gene in which upregulation of this gene would increase the extracellular lipid uptake²¹⁹. In addition, study by Tun *et al.* has shown that renal cancer cells may exhibit a mesenchymal-like stem cell state and can undergo adipogenic transdifferentiation upon supplementation with the adipocyte differentiation cocktail²²⁰. In general, adipocyte differentiation is marked by the formation of lipid droplet as well as an increase in the expression of adipogenic differentiation markers such as *PPARG*. Consistent with this, gene expression analyses conducted by Tun *et al.* have found that *PPARG* was upregulated in early stage ccRCC, suggesting its potential role in mediating lipid accumulation in ccRCC. Nevertheless, recent study by Sanchez *et al.* has performed *PPARG* loss-of-function analyses and found that *PPARG* perturbation neither effect the lipid accumulation nor ccRCC progression *in vitro* and *in vivo*²²¹. Overall, it still remains an open yet interesting *to-be-solved* puzzles on the molecular determinants that facilitate the ccRCC cytoplasmic lipid accumulation and the rise of “clear cell” phenotype. Also, it is encouraging to test in the future studies whether KLF6 could directly involve in contributing to the lipid accumulation in ccRCC.

6.8 KLF6 and the mTORC1 signalling pathway in ccRCC

The mTOR signalling pathway is frequently hyper-activated in ccRCC^{92,93}. However, the molecular mechanisms leading to its hyper activation is less understood. Others have suggested genetic alterations in the components of this signalling pathway such as *PTEN* and *mTOR* gene contributed to this phenotype, however, there is only a fraction of ccRCC patients who actually harbour these mutations^{35,36}, suggesting the involvement of additional molecular players. Indeed, recent studies on generating novel ccRCC mouse model demonstrated that concomitant loss of *VHL* and either *PBRM1* or *BAP1* could directly lead to increased mTORC1 activity in the course of ccRCC development^{104,106}. KLF6 was found in this present study to promote mTORC1 activity in ccRCC which could lead to the speculation that the high expression of this super enhancer-driven transcription factor KLF6 may contribute to mTORC1 signalling pathway hyperactivation observed in ccRCC patients. In my point of view, this is interesting as I unravelled a link between one of the strongest super enhancers and the regulation of frequently hyper-activated mTORC1 signalling pathway in ccRCC. Since *KLF6* is also partially regulated by HIF2A, these data established a novel link between the ccRCC-initiating VHL-HIF axis and the modulation of mTORC1 signalling pathway.

It was discovered in this study that KLF6 supported the mTORC1 signalling pathway by directly regulating the expression of its activator *PDGFB*. It is important to point out that the 786-M1A cells used in this study carry a homozygous truncating *PTEN* mutation²²², which would contribute to the mTORC1 activation in these cells. However, my findings seemed to suggest that despite this mutation, the KLF6-regulated PDGFB activating signal was still required. CRISPRi-mediated *PDGFB* targeting impaired the mTORC1 activity in 786-M1A cells upon overnight serum starvation, which phenocopied the effect of targeting *KLF6* in these cells. I

observed that the *KLF6*-depleted cells had more profound reduction in their mTORC1 activity after an overnight serum starvation compared to control cells, whereby recombinant human PDGFB supplementation reactivated the mTORC1 signalling pathway in these cells. Thus, cues to activate this signalling pathway are still required and this was in line with study by Xu *et al.* who have reported that mTOR-activating mutated HeLa cells remained dependent on the activation by its upstream regulators RHEB⁹⁶. Also, a previous report has shown an increased in the mTORC1 activity of the metastatic renal cancer in the absence of *PTEN* deletion⁹⁸, thus further highlighting the important role of upstream activating signals such to stimulate the mTORC1 signalling pathway in ccRCC.

Since PDGFB is a secreted factor, it can then act in both autocrine and paracrine manners to activate the PDGF receptor and its downstream effectors. Autocrine signalling is defined by the activation of hormones or growth factors on the same cells that secrete them. The paracrine signalling, on the other hand, is denoted by the binding and acting of these secreted factors on the neighbouring cells. As described in chapter 3, competitive proliferation assay was employed to assess the proliferation rate of the *KLF6*-targeted ccRCC cells. In this approach, the *KLF6*-targeted cells were pooled and competed either against the control cells (CRISPR-Cas9 approach) or untransduced parental cells (CRISPRi approach). Therefore, one limitation with this strategy was the control/parental cells or maybe the *KLF6*-targeted cells could secrete factors that might affect their counterpart growth in a paracrine manner. Despite of this possibility, the findings of the *in-vivo* assays, where the *KLF6*-targeted and control cells were individually inoculated into the mice, were in line with the competitive proliferation assays observations. The *KLF6*-targeted cells grew slower that resulted in the formation of smaller

subcutaneous tumours compared to the control cells. Also, targeting KLF6 reduced the cells capability to metastasize and colonize the lungs.

Moreover, it still remains to be investigated whether ccRCC cells actually secrete PDGFB into the extracellular environment. This could hence be another potential follow-up experiment in the future, testing whether ccRCC cells could secrete PDGFB extracellularly and activate the mTORC1 signalling pathway in the autocrine or paracrine manner. If ccRCC cells do secrete PDGFB, there was possibility during the competitive proliferation assay that the PDGFB secreted by the control cells could activate the mTORC1 signalling pathway in the KLF6-targeted cells. To investigate this possibility in the future study, the KLF6-targeted ccRCC cells can be supplemented with conditioned media from the control or parental ccRCC cells, followed by assessing the mTORC1 activity of these supplemented cells. Even if PDGFB acts in the paracrine manner, the KLF6-targeted cells were still depleted from the competitive proliferation assay, which seemed to suggest that the “*secreted PDGFB*” might not be sufficient to promote the growth of the KLF6-targeted cells. One explanation to this observation was KLF6 depletion also resulted in the downregulation of genes that were associated with lipid homeostasis pathways and hypoxia responsive transcriptional program in which these pathways were also important in supporting ccRCC cells growth.

PDGFB is also a known pro-angiogenic factor and therefore, it is also appealing to examine in a follow-up study whether PDGFB perturbation would affect ccRCC growth both *in vitro* and *in vivo* and importantly the ccRCC tumours “*hyper-vascular*” morphology. In addition to several molecular signalling loops that I have discussed previously, the findings of this study also revealed a functional link between the pro-angiogenic PDGFR and mTORC1 signalling pathways, which are the two main clinically-approved therapeutic targets for ccRCC^{111,116}. I have

highlighted in the Chapter 1 that targeting this pathway individually did not particularly result in a satisfactory overall patients' response rate¹²⁰. However, a recent clinical trial testing the combinatorial treatment approach using mTOR inhibitor everolimus and lenvatinib (a multi-target RTKs inhibitor that include PDGFRA and PDGFRB²²³) demonstrated that the combined therapies resulted in a superior median progression-free survival and overall survival as compared to treatment with each of these drugs alone¹²⁴. Therefore, the functional link that I discovered between these two molecular pathways could explain the favourable effect of this combinatorial treatment strategy in ccRCC.

6.9 Targeting KLF6 as a novel ccRCC treatment strategy

In term of the therapeutic benefit of this present study, it is still premature to speculate whether KLF6 could be targeted for ccRCC therapeutic purpose, at least based on the current available knowledge on this transcription factor. Also, reports have suggested that transcription factors are difficult to drug due to lack of region or site that could be exploited for designing the small molecule inhibitor²²⁴. Nonetheless, there are several transcription factors such as HIF2A^{127,130}, PPARG²²⁵ and SREBF^{200,226} in which inhibitors targeting them have been successfully developed. Therefore if pursued, further studies on KLF6 are necessary especially on its 3-dimensional structure and interaction with DNA or other proteins. This could potentially reveal the KLF6 "*Achilles heel*" that could subsequently be exploited for the development of its inhibitor. However, one concern about potentially targeting this transcription factor is specificity as it is still unknown what other pathways or downstream targets that are regulated by KLF6. It would pose a problem if KLF6 function is also somewhat needed in normal cells, thus it is crucial to develop drug against KLF6 that will specifically target the cancer cells. At this stage, I am not certainly sure on the feasibility of targeting KLF6 as a novel therapeutic approach for

ccRCC. Therefore, targeting KLF6 super enhancer as discussed in section 6.2 could potentially be a more viable option if only key factors that involve in establishing and maintaining the robustness of super enhancer landscape are identified.

Despite the predicted challenges to target KLF6 in ccRCC, a number of inhibitors have been developed to target the KLF6-modulated pathways identified in this study. Even some of these drugs have been clinically approved to treat ccRCC patients such as the aforementioned mTOR and angiogenic inhibitors. Also, the statin class family targeting the SREBF1 and SREBF2 transcription factors and/or the lipid biosynthesis pathways have been shown to efficiently inhibit the growth of different cancer types including ccRCC in which I have demonstrated in this study. Therefore, KLF6 could potentially be utilised as a biomarker to predict patients' sensitivity towards these inhibitors targeting the mTORC1 signalling and the lipid homeostasis pathways.

6.10 Summary and model

In conclusion, I identified a cellular signalling loop that links the super enhancer-driven transcription factor KLF6 to the modulation of lipid metabolism and mTORC1 activity that supports ccRCC growth. Furthermore, these findings demonstrated a central role for KLF6 in regulating two important pathways in ccRCC, which was well-aligned with its high expression and robust regulation by one of the strongest super enhancer in ccRCC. Also, I found that *KLF6* expression is partially activated by the ccRCC-initiating VHL-HIF2A pathway, which could explain the relatively high KLF6 mRNA levels observed in human ccRCC. Importantly, KLF6 plays a dual role in modulating the lipid homeostasis pathways in ccRCC; 1) KLF6 directly regulates the expression of several important lipid homeostasis genes including the lipid

metabolism master transcription factors SREBF1 and SREBF2, 2) KLF6 enhances the activation of SREBF1 and SREBF2 by promoting the mTORC1 activity. KLF6 supports the mTORC1 signalling pathway by directly regulates the expression of its upstream activator PDGFB. The overall findings of this study is summarized in the model shown in figure 65.

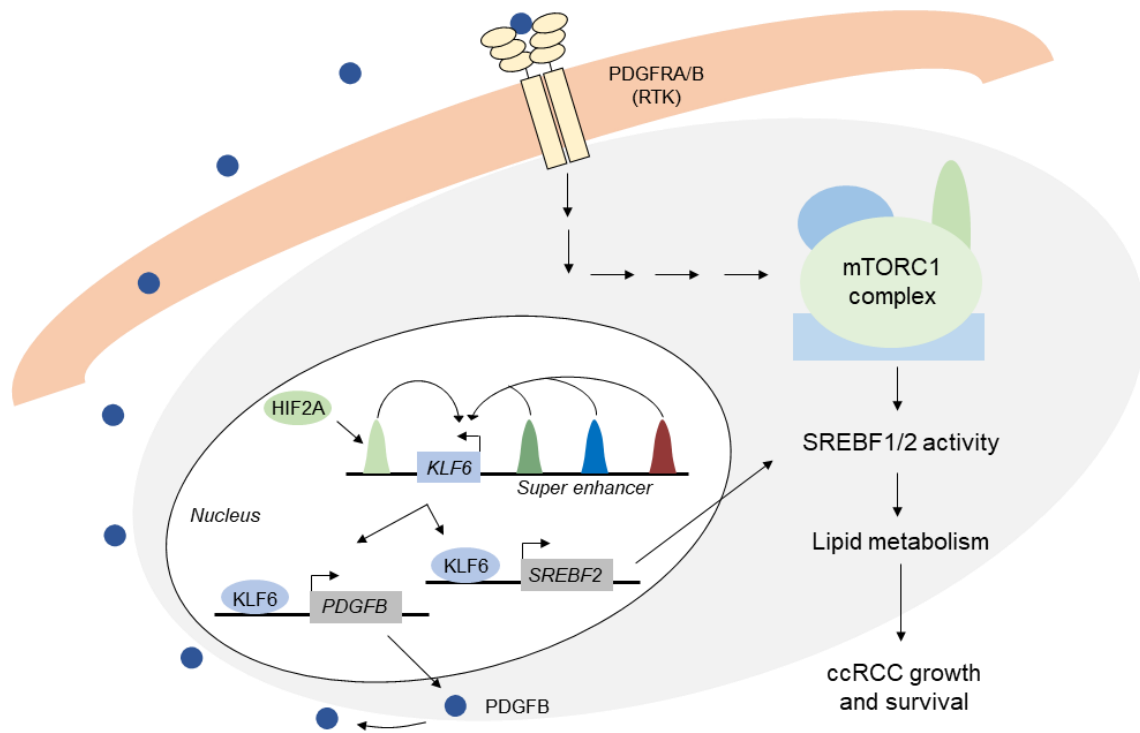


Figure 65: The model of lipid metabolism modulation by the super enhancer-driven KLF6 in supporting ccRCC growth and survival.

REFERENCES

- 1 *University of Rochester Medical Center Rochester. Anatomy and function of the urinary system,* <<https://www.urmc.rochester.edu/encyclopedia/content.aspx?ContentTypeID=85&ContentID=P01468>> (
- 2 *Kidney Research UK. The kidneys-a basic guide,* <<https://www.kidneyresearchuk.org/health-information/resources/the-kidneys-a-basic-guide>> (
- 3 *Health Pages. Kidney anatomy and function,* <<https://www.healthpages.org/anatomy-function/kidney/>> (
- 4 Fitzmaurice, C. *et al.* Global, Regional, and National Cancer Incidence, Mortality, Years of Life Lost, Years Lived With Disability, and Disability-Adjusted Life-years for 32 Cancer Groups, 1990 to 2015: A Systematic Analysis for the Global Burden of Disease Study. *JAMA Oncol* 3, 524-548, doi:10.1001/jamaoncol.2016.5688 (2017).
- 5 *World Cancer Research Fund. Kidney cancer: How diet, nutrition and physical activity affect kidney cancer risk,* <<https://www.wcrf.org/dietandcancer/kidney-cancer>> (
- 6 *Cancer Research UK. Kidney cancer statistics,* <<https://www.cancerresearchuk.org/health-professional/cancer-statistics/statistics-by-cancer-type/kidney-cancer>> (
- 7 *American Cancer Society. Key statistics about kidney cancer,* <<https://www.cancer.org/cancer/kidney-cancer/about/key-statistics.html>> (
- 8 Hsieh, J. J. *et al.* Renal cell carcinoma. *Nat Rev Dis Primers* 3, 17009, doi:10.1038/nrdp.2017.9 (2017).
- 9 Escudier, B. *et al.* Renal cell carcinoma: ESMO Clinical Practice Guidelines for diagnosis, treatment and follow-up. *Ann Oncol* 27, v58-v68, doi:10.1093/annonc/mdw328 (2016).
- 10 Moch, H., Cubilla, A. L., Humphrey, P. A., Reuter, V. E. & Ulbricht, T. M. The 2016 WHO Classification of Tumours of the Urinary System and Male Genital Organs-Part A: Renal, Penile, and Testicular Tumours. *Eur Urol* 70, 93-105, doi:10.1016/j.eururo.2016.02.029 (2016).
- 11 Rini, B., Campbell, S., & Escudier, B. Renal cell carcinoma. *The Lancet* 373, 14 (2009).

- 12 Gebhard, R. L. *et al.* Abnormal cholesterol metabolism in renal clear cell carcinoma. *Journal of lipid research* 28, 1177-1184 (1987).
- 13 Rezende, R. B. *et al.* Differential diagnosis between monomorphic clear cell adenocarcinoma of salivary glands and renal (clear) cell carcinoma. *Am J Surg Pathol* 23, 1532-1538 (1999).
- 14 Linehan, W. M., Srinivasan, R., & Schmidt, L. S. The genetic basis of kidney cancer: a metabolic disease. *Nature reviews. Urology* 7, 277-285, doi:10.1038/nrurol.2010.47 (2010).
- 15 Hakimi, A. A. *et al.* An epidemiologic and genomic investigation into the obesity paradox in renal cell carcinoma. *J Natl Cancer Inst* 105, 1862-1870, doi:10.1093/jnci/djt310 (2013).
- 16 Hakimi, A. A. *et al.* An Integrated Metabolic Atlas of Clear Cell Renal Cell Carcinoma. *Cancer Cell* 29, 104-116, doi:10.1016/j.ccell.2015.12.004 (2016).
- 17 Turajlic, S. *et al.* Deterministic Evolutionary Trajectories Influence Primary Tumor Growth: TRACERx Renal. *Cell* 173, 595-610 e511, doi:10.1016/j.cell.2018.03.043 (2018).
- 18 Young, A. C. *et al.* Analysis of VHL Gene Alterations and their Relationship to Clinical Parameters in Sporadic Conventional Renal Cell Carcinoma. *Clin Cancer Res* 15, 7582-7592, doi:10.1158/1078-0432.CCR-09-2131 (2009).
- 19 Kaelin, W. G. Von Hippel-Lindau disease. *Annu Rev Pathol* 2, 145-173, doi:10.1146/annurev.pathol.2.010506.092049 (2007).
- 20 Turajlic, S. *et al.* Tracking Cancer Evolution Reveals Constrained Routes to Metastases: TRACERx Renal. *Cell* 173, 581-594 e512, doi:10.1016/j.cell.2018.03.057 (2018).
- 21 Gerlinger, M. *et al.* Genomic architecture and evolution of clear cell renal cell carcinomas defined by multiregion sequencing. *Nat Genet* 46, 225-233, doi:10.1038/ng.2891 (2014).
- 22 Kibel, A., Iliopoulos, O., DeCaprio, J. A. & Kaelin, W. G., Jr. Binding of the von Hippel-Lindau tumor suppressor protein to Elongin B and C. *Science* 269, 1444-1446 (1995).
- 23 Greer, S. N., Metcalf, J. L., Wang, Y. & Ohh, M. The updated biology of hypoxia-inducible factor. *EMBO J* 31, 2448-2460, doi:10.1038/emboj.2012.125 (2012).

- 24 Ema, M. *et al.* A novel bHLH-PAS factor with close sequence similarity to hypoxia-inducible factor 1alpha regulates the VEGF expression and is potentially involved in lung and vascular development. *Proceedings of the National Academy of Sciences of the United States of America* 94, 4273-4278 (1997).
- 25 Chen, L., Endler, A. & Shibasaki, F. Hypoxia and angiogenesis: regulation of hypoxia-inducible factors via novel binding factors. *Exp Mol Med* 41, 849-857, doi:10.3858/emmm.2009.41.12.103 (2009).
- 26 Wood, S. M., Gleadle, J. M., Pugh, C. W., Hankinson, O. & Ratcliffe, P. J. The role of the aryl hydrocarbon receptor nuclear translocator (ARNT) in hypoxic induction of gene expression. Studies in ARNT-deficient cells. *The Journal of biological chemistry* 271, 15117-15123 (1996).
- 27 Pugh, C. W. & Ratcliffe, P. J. Regulation of angiogenesis by hypoxia: role of the HIF system. *Nat Med* 9, 677-684, doi:10.1038/nm0603-677 (2003).
- 28 Maxwell, P. H. *et al.* The tumour suppressor protein VHL targets hypoxia-inducible factors for oxygen-dependent proteolysis. *Nature* 399, 271-275, doi:10.1038/20459 (1999).
- 29 Jaakkola, P. *et al.* Targeting of HIF-alpha to the von Hippel-Lindau ubiquitylation complex by O₂-regulated prolyl hydroxylation. *Science* 292, 468-472, doi:10.1126/science.1059796 (2001).
- 30 Ivan, M. *et al.* HIFalpha targeted for VHL-mediated destruction by proline hydroxylation: implications for O₂ sensing. *Science* 292, 464-468, doi:10.1126/science.1059817 (2001).
- 31 Wenger, R. H., Stiehl, D. P. & Camenisch, G. Integration of oxygen signaling at the consensus HRE. *Sci STKE* 2005, re12, doi:10.1126/stke.3062005re12 (2005).
- 32 Majmundar, A. J., Wong, W. J. & Simon, M. C. Hypoxia-inducible factors and the response to hypoxic stress. *Mol Cell* 40, 294-309, doi:10.1016/j.molcel.2010.09.022 (2010).
- 33 Gnarra, J. R. *et al.* Mutations of the VHL tumour suppressor gene in renal carcinoma. *Nat Genet* 7, 85-90, doi:10.1038/ng0594-85 (1994).
- 34 Knudson, A. G., Jr. Hereditary cancer, oncogenes, and antioncogenes. *Cancer Res* 45, 1437-1443 (1985).

- 35 Cancer Genome Atlas Research, N. Comprehensive molecular characterization of clear cell renal cell carcinoma. *Nature* 499, 43-49, doi:10.1038/nature12222 (2013).
- 36 Sato, Y. *et al.* Integrated molecular analysis of clear-cell renal cell carcinoma. *Nat Genet* 45, 860-867, doi:10.1038/ng.2699 (2013).
- 37 Herman, J. G. *et al.* Silencing of the VHL tumor-suppressor gene by DNA methylation in renal carcinoma. *Proceedings of the National Academy of Sciences of the United States of America* 91, 9700-9704 (1994).
- 38 Kaelin, W. G., Jr. The von Hippel-Lindau tumour suppressor protein: O₂ sensing and cancer. *Nature reviews. Cancer* 8, 865-873, doi:10.1038/nrc2502 (2008).
- 39 Goel, H. L. & Mercurio, A. M. VEGF targets the tumour cell. *Nature reviews. Cancer* 13, 871-882, doi:10.1038/nrc3627 (2013).
- 40 Liberti, M. V. & Locasale, J. W. The Warburg Effect: How Does it Benefit Cancer Cells? *Trends Biochem Sci* 41, 211-218, doi:10.1016/j.tibs.2015.12.001 (2016).
- 41 Zatyka, M. *et al.* Identification of cyclin D1 and other novel targets for the von Hippel-Lindau tumor suppressor gene by expression array analysis and investigation of cyclin D1 genotype as a modifier in von Hippel-Lindau disease. *Cancer Res* 62, 3803-3811 (2002).
- 42 Staller, P. *et al.* Chemokine receptor CXCR4 downregulated by von Hippel-Lindau tumour suppressor pVHL. *Nature* 425, 307-311, doi:10.1038/nature01874 (2003).
- 43 Raval, R. R. *et al.* Contrasting properties of hypoxia-inducible factor 1 (HIF-1) and HIF-2 in von Hippel-Lindau-associated renal cell carcinoma. *Mol Cell Biol* 25, 5675-5686, doi:10.1128/MCB.25.13.5675-5686.2005 (2005).
- 44 Keith, B., Johnson, R. S. & Simon, M. C. HIF1alpha and HIF2alpha: sibling rivalry in hypoxic tumour growth and progression. *Nature reviews. Cancer* 12, 9-22, doi:10.1038/nrc3183 (2011).
- 45 Shen, C. *et al.* Genetic and functional studies implicate HIF1alpha as a 14q kidney cancer suppressor gene. *Cancer Discov* 1, 222-235, doi:10.1158/2159-8290.CD-11-0098 (2011).
- 46 Gordan, J. D., Bertout, J. A., Hu, C. J., Diehl, J. A. & Simon, M. C. HIF-2alpha promotes hypoxic cell proliferation by enhancing c-myc transcriptional activity. *Cancer Cell* 11, 335-347, doi:10.1016/j.ccr.2007.02.006 (2007).

- 47 Koshiji, M. *et al.* HIF-1alpha induces cell cycle arrest by functionally counteracting Myc. *EMBO J* 23, 1949-1956, doi:10.1038/sj.emboj.7600196 (2004).
- 48 Gordan, J. D. *et al.* HIF-alpha effects on c-Myc distinguish two subtypes of sporadic VHL-deficient clear cell renal carcinoma. *Cancer Cell* 14, 435-446, doi:10.1016/j.ccr.2008.10.016 (2008).
- 49 Kondo, K., Kim, W. Y., Lechpammer, M. & Kaelin, W. G., Jr. Inhibition of HIF2alpha is sufficient to suppress pVHL-defective tumor growth. *PLoS Biol* 1, E83, doi:10.1371/journal.pbio.0000083 (2003).
- 50 Maranchie, J. K. *et al.* The contribution of VHL substrate binding and HIF1-alpha to the phenotype of VHL loss in renal cell carcinoma. *Cancer Cell* 1, 247-255 (2002).
- 51 Varela, I. *et al.* Exome sequencing identifies frequent mutation of the SWI/SNF complex gene PBRM1 in renal carcinoma. *Nature* 469, 539-542, doi:10.1038/nature09639 (2011).
- 52 Pawlowski, R. *et al.* Loss of PBRM1 expression is associated with renal cell carcinoma progression. *Int J Cancer* 132, E11-17, doi:10.1002/ijc.27822 (2013).
- 53 Dalgliesh, G. L. *et al.* Systematic sequencing of renal carcinoma reveals inactivation of histone modifying genes. *Nature* 463, 360-363, doi:10.1038/nature08672 (2010).
- 54 Pena-Llopis, S. *et al.* BAP1 loss defines a new class of renal cell carcinoma. *Nat Genet* 44, 751-759, doi:10.1038/ng.2323 (2012).
- 55 Gerlinger, M. *et al.* Intratumor heterogeneity and branched evolution revealed by multiregion sequencing. *N Engl J Med* 366, 883-892, doi:10.1056/NEJMoa1113205 (2012).
- 56 Mitchell, T. J. *et al.* Timing the Landmark Events in the Evolution of Clear Cell Renal Cell Cancer: TRACERx Renal. *Cell* 173, 611-623 e617, doi:10.1016/j.cell.2018.02.020 (2018).
- 57 Laplante, M. & Sabatini, D. M. mTOR signaling in growth control and disease. *Cell* 149, 274-293, doi:10.1016/j.cell.2012.03.017 (2012).
- 58 Saxton, R. A. & Sabatini, D. M. mTOR Signaling in Growth, Metabolism, and Disease. *Cell* 168, 960-976, doi:10.1016/j.cell.2017.02.004 (2017).
- 59 Laplante, M. & Sabatini, D. M. mTOR signaling at a glance. *J Cell Sci* 122, 3589-3594, doi:10.1242/jcs.051011 (2009).

- 60 Yang, H. *et al.* mTOR kinase structure, mechanism and regulation. *Nature* 497, 217-223, doi:10.1038/nature12122 (2013).
- 61 Zoncu, R., Efeyan, A. & Sabatini, D. M. mTOR: from growth signal integration to cancer, diabetes and ageing. *Nat Rev Mol Cell Biol* 12, 21-35, doi:10.1038/nrm3025 (2011).
- 62 Jacinto, E. *et al.* Mammalian TOR complex 2 controls the actin cytoskeleton and is rapamycin insensitive. *Nat Cell Biol* 6, 1122-1128, doi:10.1038/ncb1183 (2004).
- 63 Loewith, R. *et al.* Two TOR complexes, only one of which is rapamycin sensitive, have distinct roles in cell growth control. *Mol Cell* 10, 457-468 (2002).
- 64 Kim, D. H. *et al.* GbetaL, a positive regulator of the rapamycin-sensitive pathway required for the nutrient-sensitive interaction between raptor and mTOR. *Mol Cell* 11, 895-904 (2003).
- 65 Peterson, T. R. *et al.* DEPTOR is an mTOR inhibitor frequently overexpressed in multiple myeloma cells and required for their survival. *Cell* 137, 873-886, doi:10.1016/j.cell.2009.03.046 (2009).
- 66 Hara, K. *et al.* Raptor, a binding partner of target of rapamycin (TOR), mediates TOR action. *Cell* 110, 177-189 (2002).
- 67 Sarbassov, D. D. *et al.* Rictor, a novel binding partner of mTOR, defines a rapamycin-insensitive and raptor-independent pathway that regulates the cytoskeleton. *Curr Biol* 14, 1296-1302, doi:10.1016/j.cub.2004.06.054 (2004).
- 68 Inoki, K., Li, Y., Zhu, T., Wu, J. & Guan, K. L. TSC2 is phosphorylated and inhibited by Akt and suppresses mTOR signalling. *Nat Cell Biol* 4, 648-657, doi:10.1038/ncb839 (2002).
- 69 Zhang, H. *et al.* PDGFRs are critical for PI3K/Akt activation and negatively regulated by mTOR. *J Clin Invest* 117, 730-738, doi:10.1172/JCI28984 (2007).
- 70 Razmara, M., Heldin, C. H. & Lennartsson, J. Platelet-derived growth factor-induced Akt phosphorylation requires mTOR/Rictor and phospholipase C-gamma1, whereas S6 phosphorylation depends on mTOR/Raptor and phospholipase D. *Cell Commun Signal* 11, 3, doi:10.1186/1478-811X-11-3 (2013).
- 71 Stokoe, D. *et al.* Dual role of phosphatidylinositol-3,4,5-trisphosphate in the activation of protein kinase B. *Science* 277, 567-570 (1997).

- 72 Chalhoub, N. & Baker, S. J. PTEN and the PI3-kinase pathway in cancer. *Annu Rev Pathol* 4, 127-150, doi:10.1146/annurev.pathol.4.110807.092311 (2009).
- 73 Potter, C. J., Pedraza, L. G. & Xu, T. Akt regulates growth by directly phosphorylating Tsc2. *Nat Cell Biol* 4, 658-665, doi:10.1038/ncb840 (2002).
- 74 Inoki, K., Li, Y., Xu, T. & Guan, K. L. Rheb GTPase is a direct target of TSC2 GAP activity and regulates mTOR signaling. *Genes Dev* 17, 1829-1834, doi:10.1101/gad.1110003 (2003).
- 75 Yu, J. S. & Cui, W. Proliferation, survival and metabolism: the role of PI3K/AKT/mTOR signalling in pluripotency and cell fate determination. *Development* 143, 3050-3060, doi:10.1242/dev.137075 (2016).
- 76 Laplante, M. & Sabatini, D. M. Regulation of mTORC1 and its impact on gene expression at a glance. *J Cell Sci* 126, 1713-1719, doi:10.1242/jcs.125773 (2013).
- 77 Inoki, K., Zhu, T. & Guan, K. L. TSC2 mediates cellular energy response to control cell growth and survival. *Cell* 115, 577-590 (2003).
- 78 Hara, K. *et al.* Regulation of eIF-4E BP1 phosphorylation by mTOR. *The Journal of biological chemistry* 272, 26457-26463 (1997).
- 79 Gingras, A. C. *et al.* Regulation of 4E-BP1 phosphorylation: a novel two-step mechanism. *Genes Dev* 13, 1422-1437 (1999).
- 80 Holz, M. K., Ballif, B. A., Gygi, S. P. & Blenis, J. mTOR and S6K1 mediate assembly of the translation preinitiation complex through dynamic protein interchange and ordered phosphorylation events. *Cell* 123, 569-580, doi:10.1016/j.cell.2005.10.024 (2005).
- 81 Porstmann, T. *et al.* SREBP activity is regulated by mTORC1 and contributes to Akt-dependent cell growth. *Cell Metab* 8, 224-236, doi:10.1016/j.cmet.2008.07.007 (2008).
- 82 Duvel, K. *et al.* Activation of a metabolic gene regulatory network downstream of mTOR complex 1. *Mol Cell* 39, 171-183, doi:10.1016/j.molcel.2010.06.022 (2010).
- 83 Peterson, T. R. *et al.* mTOR complex 1 regulates lipin 1 localization to control the SREBP pathway. *Cell* 146, 408-420, doi:10.1016/j.cell.2011.06.034 (2011).
- 84 Horton, J. D., Goldstein, J. L. & Brown, M. S. SREBPs: activators of the complete program of cholesterol and fatty acid synthesis in the liver. *J Clin Invest* 109, 1125-1131, doi:10.1172/JCI15593 (2002).

- 85 Horton, J. D. *et al.* Combined analysis of oligonucleotide microarray data from transgenic and knockout mice identifies direct SREBP target genes. *Proceedings of the National Academy of Sciences of the United States of America* 100, 12027-12032, doi:10.1073/pnas.1534923100 (2003).
- 86 Guertin, D. A. & Sabatini, D. M. Defining the role of mTOR in cancer. *Cancer Cell* 12, 9-22, doi:10.1016/j.ccr.2007.05.008 (2007).
- 87 Populo, H., Lopes, J. M. & Soares, P. The mTOR signalling pathway in human cancer. *Int J Mol Sci* 13, 1886-1918, doi:10.3390/ijms13021886 (2012).
- 88 Yuan, T. L. & Cantley, L. C. PI3K pathway alterations in cancer: variations on a theme. *Oncogene* 27, 5497-5510, doi:10.1038/onc.2008.245 (2008).
- 89 Cancer Genome Atlas, N. Comprehensive molecular portraits of human breast tumours. *Nature* 490, 61-70, doi:10.1038/nature11412 (2012).
- 90 Cancer Genome Atlas Research, N. *et al.* Integrated genomic characterization of endometrial carcinoma. *Nature* 497, 67-73, doi:10.1038/nature12113 (2013).
- 91 Dillon, L. M. & Miller, T. W. Therapeutic targeting of cancers with loss of PTEN function. *Curr Drug Targets* 15, 65-79 (2014).
- 92 Pantuck, A. J. *et al.* Prognostic relevance of the mTOR pathway in renal cell carcinoma: implications for molecular patient selection for targeted therapy. *Cancer* 109, 2257-2267, doi:10.1002/cncr.22677 (2007).
- 93 Robb, V. A., Karbowiczek, M., Klein-Szanto, A. J. & Henske, E. P. Activation of the mTOR signaling pathway in renal clear cell carcinoma. *J Urol* 177, 346-352, doi:10.1016/j.juro.2006.08.076 (2007).
- 94 Chung, J., Grammer, T. C., Lemon, K. P., Kazlauskas, A. & Blenis, J. PDGF- and insulin-dependent pp70S6k activation mediated by phosphatidylinositol-3-OH kinase. *Nature* 370, 71-75, doi:10.1038/370071a0 (1994).
- 95 Pullen, N. & Thomas, G. The modular phosphorylation and activation of p70s6k. *FEBS Lett* 410, 78-82 (1997).
- 96 Xu, J. *et al.* Mechanistically distinct cancer-associated mTOR activation clusters predict sensitivity to rapamycin. *J Clin Invest* 126, 3526-3540, doi:10.1172/JCI86120 (2016).

- 97 Kucejova, B. *et al.* Interplay between pVHL and mTORC1 pathways in clear-cell renal cell carcinoma. *Mol Cancer Res* 9, 1255-1265, doi:10.1158/1541-7786.MCR-11-0302 (2011).
- 98 Abou Youssif, T. *et al.* The mammalian target of rapamycin pathway is widely activated without PTEN deletion in renal cell carcinoma metastases. *Cancer* 117, 290-300, doi:10.1002/cncr.25402 (2011).
- 99 Hou, W. & Ji, Z. Generation of autochthonous mouse models of clear cell renal cell carcinoma: mouse models of renal cell carcinoma. *Exp Mol Med* 50, 30, doi:10.1038/s12276-018-0059-4 (2018).
- 100 Gnarra, J. R. *et al.* Defective placental vasculogenesis causes embryonic lethality in VHL-deficient mice. *Proceedings of the National Academy of Sciences of the United States of America* 94, 9102-9107 (1997).
- 101 Rankin, E. B., Tomaszewski, J. E. & Haase, V. H. Renal cyst development in mice with conditional inactivation of the von Hippel-Lindau tumor suppressor. *Cancer Res* 66, 2576-2583, doi:10.1158/0008-5472.CAN-05-3241 (2006).
- 102 Frew, I. J. *et al.* pVHL and PTEN tumour suppressor proteins cooperatively suppress kidney cyst formation. *EMBO J* 27, 1747-1757, doi:10.1038/emboj.2008.96 (2008).
- 103 Schietke, R. E. *et al.* Renal tubular HIF-2 α expression requires VHL inactivation and causes fibrosis and cysts. *PLoS One* 7, e31034, doi:10.1371/journal.pone.0031034 (2012).
- 104 Gu, Y. F. *et al.* Modeling Renal Cell Carcinoma in Mice: Bap1 and Pbrm1 Inactivation Drive Tumor Grade. *Cancer Discov* 7, 900-917, doi:10.1158/2159-8290.CD-17-0292 (2017).
- 105 Kapur, P. *et al.* Effects on survival of BAP1 and PBRM1 mutations in sporadic clear-cell renal-cell carcinoma: a retrospective analysis with independent validation. *Lancet Oncol* 14, 159-167, doi:10.1016/S1470-2045(12)70584-3 (2013).
- 106 Nargund, A. M. *et al.* The SWI/SNF Protein PBRM1 Restrains VHL-Loss-Driven Clear Cell Renal Cell Carcinoma. *Cell Rep* 18, 2893-2906, doi:10.1016/j.celrep.2017.02.074 (2017).
- 107 Dabestani, S. *et al.* Renal cell carcinoma recurrences and metastases in primary non-metastatic patients: a population-based study. *World J Urol* 34, 1081-1086, doi:10.1007/s00345-016-1773-y (2016).

- 108 Wirth, M. P. Immunotherapy for metastatic renal cell carcinoma. *Urol Clin North Am* 20, 283-295 (1993).
- 109 Law, T. M. *et al.* Phase III randomized trial of interleukin-2 with or without lymphokine-activated killer cells in the treatment of patients with advanced renal cell carcinoma. *Cancer* 76, 824-832 (1995).
- 110 Fyfe, G. *et al.* Results of treatment of 255 patients with metastatic renal cell carcinoma who received high-dose recombinant interleukin-2 therapy. *J Clin Oncol* 13, 688-696, doi:10.1200/JCO.1995.13.3.688 (1995).
- 111 Motzer, R. J. *et al.* Sunitinib versus interferon alfa in metastatic renal-cell carcinoma. *N Engl J Med* 356, 115-124, doi:10.1056/NEJMoa065044 (2007).
- 112 Escudier, B. *et al.* Sorafenib in advanced clear-cell renal-cell carcinoma. *N Engl J Med* 356, 125-134, doi:10.1056/NEJMoa060655 (2007).
- 113 Sternberg, C. N. *et al.* Pazopanib in locally advanced or metastatic renal cell carcinoma: results of a randomized phase III trial. *J Clin Oncol* 28, 1061-1068, doi:10.1200/JCO.2009.23.9764 (2010).
- 114 Escudier, B. *et al.* Phase III trial of bevacizumab plus interferon alfa-2a in patients with metastatic renal cell carcinoma (AVOREN): final analysis of overall survival. *J Clin Oncol* 28, 2144-2150, doi:10.1200/JCO.2009.26.7849 (2010).
- 115 Hudes, G. *et al.* Temsirolimus, interferon alfa, or both for advanced renal-cell carcinoma. *N Engl J Med* 356, 2271-2281, doi:10.1056/NEJMoa066838 (2007).
- 116 Motzer, R. J. *et al.* Efficacy of everolimus in advanced renal cell carcinoma: a double-blind, randomised, placebo-controlled phase III trial. *Lancet* 372, 449-456, doi:10.1016/S0140-6736(08)61039-9 (2008).
- 117 Efeyan, A. & Sabatini, D. M. mTOR and cancer: many loops in one pathway. *Curr Opin Cell Biol* 22, 169-176, doi:10.1016/j.ceb.2009.10.007 (2010).
- 118 Yu, K. *et al.* Biochemical, cellular, and in vivo activity of novel ATP-competitive and selective inhibitors of the mammalian target of rapamycin. *Cancer Res* 69, 6232-6240, doi:10.1158/0008-5472.CAN-09-0299 (2009).
- 119 Thoreen, C. C. *et al.* An ATP-competitive mammalian target of rapamycin inhibitor reveals rapamycin-resistant functions of mTORC1. *The Journal of biological chemistry* 284, 8023-8032, doi:10.1074/jbc.M900301200 (2009).

- 120 Choueiri, T. K. & Motzer, R. J. Systemic Therapy for Metastatic Renal-Cell Carcinoma. *N Engl J Med* 376, 354-366, doi:10.1056/NEJMra1601333 (2017).
- 121 Rini, B. I. & Atkins, M. B. Resistance to targeted therapy in renal-cell carcinoma. *Lancet Oncol* 10, 992-1000, doi:10.1016/S1470-2045(09)70240-2 (2009).
- 122 Negrier, S. *et al.* Temsirolimus and bevacizumab, or sunitinib, or interferon alfa and bevacizumab for patients with advanced renal cell carcinoma (TORAVA): a randomised phase 2 trial. *Lancet Oncol* 12, 673-680, doi:10.1016/S1470-2045(11)70124-3 (2011).
- 123 Rini, B. I. *et al.* Randomized phase III trial of temsirolimus and bevacizumab versus interferon alfa and bevacizumab in metastatic renal cell carcinoma: INTORACT trial. *J Clin Oncol* 32, 752-759, doi:10.1200/JCO.2013.50.5305 (2014).
- 124 Motzer, R. J. *et al.* Lenvatinib, everolimus, and the combination in patients with metastatic renal cell carcinoma: a randomised, phase 2, open-label, multicentre trial. *Lancet Oncol* 16, 1473-1482, doi:10.1016/S1470-2045(15)00290-9 (2015).
- 125 Brahmer, J. R. *et al.* Safety and activity of anti-PD-L1 antibody in patients with advanced cancer. *N Engl J Med* 366, 2455-2465, doi:10.1056/NEJMoa1200694 (2012).
- 126 Leach, D. R., Krummel, M. F. & Allison, J. P. Enhancement of antitumor immunity by CTLA-4 blockade. *Science* 271, 1734-1736 (1996).
- 127 Cho, H. *et al.* On-Target Efficacy of a HIF2alpha Antagonist in Preclinical Kidney Cancer Models. *Nature*, doi:10.1038/nature19795 (2016).
- 128 Wallace, E. M. *et al.* A Small-Molecule Antagonist of HIF2alpha Is Efficacious in Preclinical Models of Renal Cell Carcinoma. *Cancer Res* 76, 5491-5500, doi:10.1158/0008-5472.CAN-16-0473 (2016).
- 129 Scheuermann, T. H. *et al.* Allosteric inhibition of hypoxia inducible factor-2 with small molecules. *Nat Chem Biol* 9, 271-276, doi:10.1038/nchembio.1185 (2013).
- 130 Chen, W. *et al.* Targeting Renal Cell Carcinoma with a HIF-2 antagonist. *Nature*, doi:10.1038/nature19796 (2016).
- 131 Courtney, K. D. *et al.* Phase I Dose-Escalation Trial of PT2385, a First-in-Class Hypoxia-Inducible Factor-2alpha Antagonist in Patients With Previously Treated Advanced Clear Cell Renal Cell Carcinoma. *J Clin Oncol* 36, 867-874, doi:10.1200/JCO.2017.74.2627 (2018).

- 132 Lee, T. I. & Young, R. A. Transcriptional regulation and its misregulation in disease. *Cell* 152, 1237-1251, doi:10.1016/j.cell.2013.02.014 (2013).
- 133 Spitz, F. & Furlong, E. E. Transcription factors: from enhancer binding to developmental control. *Nat Rev Genet* 13, 613-626, doi:10.1038/nrg3207 (2012).
- 134 Ong, C. T. & Corces, V. G. Enhancer function: new insights into the regulation of tissue-specific gene expression. *Nat Rev Genet* 12, 283-293, doi:10.1038/nrg2957 (2011).
- 135 Kagey, M. H. *et al.* Mediator and cohesin connect gene expression and chromatin architecture. *Nature* 467, 430-435, doi:10.1038/nature09380 (2010).
- 136 Hanahan, D. & Weinberg, R. A. Hallmarks of cancer: the next generation. *Cell* 144, 646-674, doi:10.1016/j.cell.2011.02.013 (2011).
- 137 Bradner, J. E., Hnisz, D. & Young, R. A. Transcriptional Addiction in Cancer. *Cell* 168, 629-643, doi:10.1016/j.cell.2016.12.013 (2017).
- 138 Dang, C. V. MYC on the path to cancer. *Cell* 149, 22-35, doi:10.1016/j.cell.2012.03.003 (2012).
- 139 Gabay, M., Li, Y. & Felsher, D. W. MYC activation is a hallmark of cancer initiation and maintenance. *Cold Spring Harb Perspect Med* 4, doi:10.1101/cshperspect.a014241 (2014).
- 140 Kasthuber, E. R. & Lowe, S. W. Putting p53 in Context. *Cell* 170, 1062-1078, doi:10.1016/j.cell.2017.08.028 (2017).
- 141 Zheng, J. Oncogenic chromosomal translocations and human cancer (review). *Oncol Rep* 30, 2011-2019, doi:10.3892/or.2013.2677 (2013).
- 142 Sankar, S. & Lessnick, S. L. Promiscuous partnerships in Ewing's sarcoma. *Cancer Genet* 204, 351-365, doi:10.1016/j.cancergen.2011.07.008 (2011).
- 143 Osborne, C. S. *et al.* Myc dynamically and preferentially relocates to a transcription factory occupied by Igh. *PLoS Biol* 5, e192, doi:10.1371/journal.pbio.0050192 (2007).
- 144 Sanchez-Vega, F. *et al.* Oncogenic Signaling Pathways in The Cancer Genome Atlas. *Cell* 173, 321-337 e310, doi:10.1016/j.cell.2018.03.035 (2018).
- 145 Sur, I. & Taipale, J. The role of enhancers in cancer. *Nature reviews. Cancer* 16, 483-493, doi:10.1038/nrc.2016.62 (2016).

- 146 Soshnev, A. A., Josefowicz, S. Z. & Allis, C. D. Greater Than the Sum of Parts: Complexity of the Dynamic Epigenome. *Mol Cell* 69, 533, doi:10.1016/j.molcel.2018.01.015 (2018).
- 147 Baxter, E., Windloch, K., Gannon, F. & Lee, J. S. Epigenetic regulation in cancer progression. *Cell Biosci* 4, 45, doi:10.1186/2045-3701-4-45 (2014).
- 148 Creyghton, M. P. *et al.* Histone H3K27ac separates active from poised enhancers and predicts developmental state. *Proceedings of the National Academy of Sciences of the United States of America* 107, 21931-21936, doi:10.1073/pnas.1016071107 (2010).
- 149 Whyte, W. A. *et al.* Master transcription factors and mediator establish super-enhancers at key cell identity genes. *Cell* 153, 307-319, doi:10.1016/j.cell.2013.03.035 (2013).
- 150 Hnisz, D. *et al.* Super-enhancers in the control of cell identity and disease. *Cell* 155, 934-947, doi:10.1016/j.cell.2013.09.053 (2013).
- 151 Loven, J. *et al.* Selective inhibition of tumor oncogenes by disruption of super-enhancers. *Cell* 153, 320-334, doi:10.1016/j.cell.2013.03.036 (2013).
- 152 Hnisz, D. *et al.* Convergence of developmental and oncogenic signaling pathways at transcriptional super-enhancers. *Mol Cell* 58, 362-370, doi:10.1016/j.molcel.2015.02.014 (2015).
- 153 Chen, X. *et al.* Integration of external signaling pathways with the core transcriptional network in embryonic stem cells. *Cell* 133, 1106-1117, doi:10.1016/j.cell.2008.04.043 (2008).
- 154 Saint-Andre, V. *et al.* Models of human core transcriptional regulatory circuitries. *Genome Res* 26, 385-396, doi:10.1101/gr.197590.115 (2016).
- 155 Sengupta, S. & George, R. E. Super-Enhancer-Driven Transcriptional Dependencies in Cancer. *Trends Cancer* 3, 269-281, doi:10.1016/j.trecan.2017.03.006 (2017).
- 156 Wong, R. W. J. *et al.* Enhancer profiling identifies critical cancer genes and characterizes cell identity in adult T-cell leukemia. *Blood* 130, 2326-2338, doi:10.1182/blood-2017-06-792184 (2017).
- 157 Jiang, Y. *et al.* Co-activation of super-enhancer-driven CCAT1 by TP63 and SOX2 promotes squamous cancer progression. *Nat Commun* 9, 3619, doi:10.1038/s41467-018-06081-9 (2018).

- 158 Mansour, M. R. *et al.* Oncogene regulation. An oncogenic super-enhancer formed through somatic mutation of a noncoding intergenic element. *Science* 346, 1373-1377, doi:10.1126/science.1259037 (2014).
- 159 Drier, Y. *et al.* An oncogenic MYB feedback loop drives alternate cell fates in adenoid cystic carcinoma. *Nat Genet* 48, 265-272, doi:10.1038/ng.3502 (2016).
- 160 Zhang, X. *et al.* Identification of focally amplified lineage-specific super-enhancers in human epithelial cancers. *Nat Genet* 48, 176-182, doi:10.1038/ng.3470 (2016).
- 161 Gryder, B. E. *et al.* PAX3-FOXO1 Establishes Myogenic Super Enhancers and Confers BET Bromodomain Vulnerability. *Cancer Discov* 7, 884-899, doi:10.1158/2159-8290.CD-16-1297 (2017).
- 162 Tomazou, E. M. *et al.* Epigenome mapping reveals distinct modes of gene regulation and widespread enhancer reprogramming by the oncogenic fusion protein EWS-FLI1. *Cell Rep* 10, 1082-1095, doi:10.1016/j.celrep.2015.01.042 (2015).
- 163 Kennedy, A. L. *et al.* Functional, chemical genomic, and super-enhancer screening identify sensitivity to cyclin D1/CDK4 pathway inhibition in Ewing sarcoma. *Oncotarget* 6, 30178-30193, doi:10.18632/oncotarget.4903 (2015).
- 164 Lin, L. *et al.* Super-enhancer-associated MEIS1 promotes transcriptional dysregulation in Ewing sarcoma in co-operation with EWS-FLI1. *Nucleic Acids Res*, doi:10.1093/nar/gky1207 (2018).
- 165 Chipumuro, E. *et al.* CDK7 inhibition suppresses super-enhancer-linked oncogenic transcription in MYCN-driven cancer. *Cell* 159, 1126-1139, doi:10.1016/j.cell.2014.10.024 (2014).
- 166 Christensen, C. L. *et al.* Targeting transcriptional addictions in small cell lung cancer with a covalent CDK7 inhibitor. *Cancer Cell* 26, 909-922, doi:10.1016/j.ccell.2014.10.019 (2014).
- 167 Chapuy, B. *et al.* Discovery and characterization of super-enhancer-associated dependencies in diffuse large B cell lymphoma. *Cancer Cell* 24, 777-790, doi:10.1016/j.ccr.2013.11.003 (2013).
- 168 Bhagwat, A. S. *et al.* BET Bromodomain Inhibition Releases the Mediator Complex from Select cis-Regulatory Elements. *Cell Rep* 15, 519-530, doi:10.1016/j.celrep.2016.03.054 (2016).

- 169 Kwiatkowski, N. *et al.* Targeting transcription regulation in cancer with a covalent CDK7 inhibitor. *Nature* 511, 616-620, doi:10.1038/nature13393 (2014).
- 170 Wang, Y. *et al.* CDK7-dependent transcriptional addiction in triple-negative breast cancer. *Cell* 163, 174-186, doi:10.1016/j.cell.2015.08.063 (2015).
- 171 Vanharanta, S. & Massague, J. Origins of metastatic traits. *Cancer Cell* 24, 410-421, doi:10.1016/j.ccr.2013.09.007 (2013).
- 172 Luo, J., Solimini, N. L. & Elledge, S. J. Principles of cancer therapy: oncogene and non-oncogene addiction. *Cell* 136, 823-837, doi:10.1016/j.cell.2009.02.024 (2009).
- 173 Vanharanta, S. *et al.* Epigenetic expansion of VHL-HIF signal output drives multiorgan metastasis in renal cancer. *Nat Med* 19, 50-56, doi:10.1038/nm.3029 (2013).
- 174 Wang, T., Wei, J. J., Sabatini, D. M. & Lander, E. S. Genetic screens in human cells using the CRISPR-Cas9 system. *Science* 343, 80-84, doi:10.1126/science.1246981 (2014).
- 175 Sanjana, N. E., Shalem, O. & Zhang, F. Improved vectors and genome-wide libraries for CRISPR screening. *Nat Methods* 11, 783-784, doi:10.1038/nmeth.3047 (2014).
- 176 Gilbert, L. A. *et al.* Genome-Scale CRISPR-Mediated Control of Gene Repression and Activation. *Cell* 159, 647-661, doi:10.1016/j.cell.2014.09.029 (2014).
- 177 Koike-Yusa, H., Li, Y., Tan, E. P., Velasco-Herrera Mdel, C. & Yusa, K. Genome-wide recessive genetic screening in mammalian cells with a lentiviral CRISPR-guide RNA library. *Nat Biotechnol* 32, 267-273, doi:10.1038/nbt.2800 (2014).
- 178 Schmittgen, T. D. & Livak, K. J. Analyzing real-time PCR data by the comparative C(T) method. *Nat Protoc* 3, 1101-1108 (2008).
- 179 Tetreault, M. P., Yang, Y. & Katz, J. P. Kruppel-like factors in cancer. *Nature reviews. Cancer* 13, 701-713, doi:10.1038/nrc3582 (2013).
- 180 Andreoli, V., Gehrau, R. C. & Bocco, J. L. Biology of Kruppel-like factor 6 transcriptional regulator in cell life and death. *IUBMB Life* 62, 896-905, doi:10.1002/iub.396 (2010).
- 181 Narla, G. *et al.* A germline DNA polymorphism enhances alternative splicing of the KLF6 tumor suppressor gene and is associated with increased prostate cancer risk. *Cancer Res* 65, 1213-1222, doi:10.1158/0008-5472.CAN-04-4249 (2005).

- 182 Kremer-Tal, S. *et al.* Frequent inactivation of the tumor suppressor Kruppel-like factor 6 (KLF6) in hepatocellular carcinoma. *Hepatology* 40, 1047-1052, doi:10.1002/hep.20460 (2004).
- 183 Narla, G. *et al.* KLF6, a candidate tumor suppressor gene mutated in prostate cancer. *Science* 294, 2563-2566, doi:10.1126/science.1066326 (2001).
- 184 Reeves, H. L. *et al.* Kruppel-like factor 6 (KLF6) is a tumor-suppressor gene frequently inactivated in colorectal cancer. *Gastroenterology* 126, 1090-1103 (2004).
- 185 Cerami, E. *et al.* The cBio cancer genomics portal: an open platform for exploring multidimensional cancer genomics data. *Cancer Discov* 2, 401-404, doi:10.1158/2159-8290.CD-12-0095 (2012).
- 186 Gao, J. *et al.* Integrative analysis of complex cancer genomics and clinical profiles using the cBioPortal. *Sci Signal* 6, pl1, doi:10.1126/scisignal.2004088 (2013).
- 187 Sirach, E. *et al.* KLF6 transcription factor protects hepatocellular carcinoma-derived cells from apoptosis. *Cell Death Differ* 14, 1202-1210, doi:10.1038/sj.cdd.4402114 (2007).
- 188 D'Astolfo, D. S., Gehrau, R. C., Bocco, J. L. & Koritschoner, N. P. Silencing of the transcription factor KLF6 by siRNA leads to cell cycle arrest and sensitizes cells to apoptosis induced by DNA damage. *Cell Death Differ* 15, 613-616, doi:10.1038/sj.cdd.4402299 (2008).
- 189 Gehrau, R. C., D'Astolfo, D. S., Dumur, C. I., Bocco, J. L. & Koritschoner, N. P. Nuclear expression of KLF6 tumor suppressor factor is highly associated with overexpression of ERBB2 oncoprotein in ductal breast carcinomas. *PLoS One* 5, e8929, doi:10.1371/journal.pone.0008929 (2010).
- 190 DiFeo, A. *et al.* Roles of KLF6 and KLF6-SV1 in ovarian cancer progression and intraperitoneal dissemination. *Clin Cancer Res* 12, 3730-3739, doi:10.1158/1078-0432.CCR-06-0054 (2006).
- 191 Hatami, R. *et al.* KLF6-SV1 drives breast cancer metastasis and is associated with poor survival. *Sci Transl Med* 5, 169ra112, doi:10.1126/scitranslmed.3004688 (2013).
- 192 Narla, G. *et al.* Targeted inhibition of the KLF6 splice variant, KLF6 SV1, suppresses prostate cancer cell growth and spread. *Cancer Res* 65, 5761-5768, doi:10.1158/0008-5472.CAN-05-0217 (2005).
- 193 Ran, F. A. *et al.* Genome engineering using the CRISPR-Cas9 system. *Nat Protoc* 8, 2281-2308, doi:10.1038/nprot.2013.143 (2013).

- 194 Shalem, O., Sanjana, N. E. & Zhang, F. High-throughput functional genomics using CRISPR-Cas9. *Nat Rev Genet* 16, 299-311, doi:10.1038/nrg3899 (2015).
- 195 Larson, M. H. *et al.* CRISPR interference (CRISPRi) for sequence-specific control of gene expression. *Nat Protoc* 8, 2180-2196, doi:10.1038/nprot.2013.132 (2013).
- 196 Rodrigues, P. *et al.* NF-kappaB-Dependent Lymphoid Enhancer Co-option Promotes Renal Carcinoma Metastasis. *Cancer Discov*, doi:10.1158/2159-8290.CD-17-1211 (2018).
- 197 Fellmann, C. *et al.* An optimized microRNA backbone for effective single-copy RNAi. *Cell Rep* 5, 1704-1713, doi:10.1016/j.celrep.2013.11.020 (2013).
- 198 Yao, X. *et al.* VHL Deficiency Drives Enhancer Activation of Oncogenes in Clear Cell Renal Cell Carcinoma. *Cancer Discov* 7, 1284-1305, doi:10.1158/2159-8290.CD-17-0375 (2017).
- 199 Baenke, F., Peck, B., Miess, H. & Schulze, A. Hooked on fat: the role of lipid synthesis in cancer metabolism and tumour development. *Dis Model Mech* 6, 1353-1363, doi:10.1242/dmm.011338 (2013).
- 200 Kamisuki, S. *et al.* A small molecule that blocks fat synthesis by inhibiting the activation of SREBP. *Chem Biol* 16, 882-892, doi:10.1016/j.chembiol.2009.07.007 (2009).
- 201 Demoulin, J. B. *et al.* Platelet-derived growth factor stimulates membrane lipid synthesis through activation of phosphatidylinositol 3-kinase and sterol regulatory element-binding proteins. *The Journal of biological chemistry* 279, 35392-35402, doi:10.1074/jbc.M405924200 (2004).
- 202 Felix, M. A. & Barkoulas, M. Pervasive robustness in biological systems. *Nat Rev Genet* 16, 483-496, doi:10.1038/nrg3949 (2015).
- 203 Hashemi, S., Salma, J., Wales, S. & McDermott, J. C. Pro-survival function of MEF2 in cardiomyocytes is enhanced by beta-blockers. *Cell Death Discov* 1, 15019, doi:10.1038/cddiscovery.2015.19 (2015).
- 204 Salma, J. & McDermott, J. C. Suppression of a MEF2-KLF6 survival pathway by PKA signaling promotes apoptosis in embryonic hippocampal neurons. *J Neurosci* 32, 2790-2803, doi:10.1523/JNEUROSCI.3609-11.2012 (2012).
- 205 Kremer-Tal, S. *et al.* Downregulation of KLF6 is an early event in hepatocarcinogenesis, and stimulates proliferation while reducing differentiation. *J Hepatol* 46, 645-654, doi:10.1016/j.jhep.2006.10.012 (2007).

- 206 Gao, Y. *et al.* KLF6 Suppresses Metastasis of Clear Cell Renal Cell Carcinoma via Transcriptional Repression of E2F1. *Cancer Res* 77, 330-342, doi:10.1158/0008-5472.CAN-16-0348 (2017).
- 207 Beloribi-Djefafli, S., Vasseur, S. & Guillaumond, F. Lipid metabolic reprogramming in cancer cells. *Oncogenesis* 5, e189, doi:10.1038/oncsis.2015.49 (2016).
- 208 Saito, K. *et al.* Lipidomic Signatures and Associated Transcriptomic Profiles of Clear Cell Renal Cell Carcinoma. *Sci Rep* 6, 28932, doi:10.1038/srep28932 (2016).
- 209 Zhang, Y. *et al.* Addressing metabolic heterogeneity in clear cell renal cell carcinoma with quantitative Dixon MRI. *JCI Insight* 2, doi:10.1172/jci.insight.94278 (2017).
- 210 Yue, S. *et al.* Cholesteryl ester accumulation induced by PTEN loss and PI3K/AKT activation underlies human prostate cancer aggressiveness. *Cell Metab* 19, 393-406, doi:10.1016/j.cmet.2014.01.019 (2014).
- 211 Thysell, E. *et al.* Metabolomic characterization of human prostate cancer bone metastases reveals increased levels of cholesterol. *PLoS One* 5, e14175, doi:10.1371/journal.pone.0014175 (2010).
- 212 Zhuang, L., Kim, J., Adam, R. M., Solomon, K. R. & Freeman, M. R. Cholesterol targeting alters lipid raft composition and cell survival in prostate cancer cells and xenografts. *J Clin Invest* 115, 959-968, doi:10.1172/JCI19935 (2005).
- 213 Cho, S. J. *et al.* Simvastatin induces apoptosis in human colon cancer cells and in tumor xenografts, and attenuates colitis-associated colon cancer in mice. *Int J Cancer* 123, 951-957, doi:10.1002/ijc.23593 (2008).
- 214 Liu, Y. *et al.* Lovastatin enhances adenovirus-mediated TRAIL induced apoptosis by depleting cholesterol of lipid rafts and affecting CAR and death receptor expression of prostate cancer cells. *Oncotarget* 6, 3055-3070, doi:10.18632/oncotarget.3073 (2015).
- 215 Nielsen, S. F., Nordestgaard, B. G. & Bojesen, S. E. Statin use and reduced cancer-related mortality. *N Engl J Med* 367, 1792-1802, doi:10.1056/NEJMoa1201735 (2012).
- 216 Guo, D. *et al.* An LXR agonist promotes glioblastoma cell death through inhibition of an EGFR/AKT/SREBP-1/LDLR-dependent pathway. *Cancer Discov* 1, 442-456, doi:10.1158/2159-8290.CD-11-0102 (2011).
- 217 Mallipattu, S. K. *et al.* Kruppel-like factor 6 regulates mitochondrial function in the kidney. *J Clin Invest* 125, 1347-1361, doi:10.1172/JCI77084 (2015).

- 218 Qiu, B. *et al.* HIF2alpha-Dependent Lipid Storage Promotes Endoplasmic Reticulum Homeostasis in Clear-Cell Renal Cell Carcinoma. *Cancer Discov* 5, 652-667, doi:10.1158/2159-8290.CD-14-1507 (2015).
- 219 Sundelin, J. P. *et al.* Increased expression of the very low-density lipoprotein receptor mediates lipid accumulation in clear-cell renal cell carcinoma. *PLoS One* 7, e48694, doi:10.1371/journal.pone.0048694 (2012).
- 220 Tun, H. W. *et al.* Pathway signature and cellular differentiation in clear cell renal cell carcinoma. *PLoS One* 5, e10696, doi:10.1371/journal.pone.0010696 (2010).
- 221 Sanchez, D. J., Steger, D. J., Skuli, N., Bansal, A. & Simon, M. C. PPARgamma is dispensable for clear cell renal cell carcinoma progression. *Mol Metab* 14, 139-149, doi:10.1016/j.molmet.2018.05.013 (2018).
- 222 Jacob, L. S. *et al.* Metastatic Competence Can Emerge with Selection of Preexisting Oncogenic Alleles without a Need of New Mutations. *Cancer Res* 75, 3713-3719, doi:10.1158/0008-5472.CAN-15-0562 (2015).
- 223 Matsui, J. *et al.* E7080, a novel inhibitor that targets multiple kinases, has potent antitumor activities against stem cell factor producing human small cell lung cancer H146, based on angiogenesis inhibition. *Int J Cancer* 122, 664-671, doi:10.1002/ijc.23131 (2008).
- 224 Fontaine, F., Overman, J. & Francois, M. Pharmacological manipulation of transcription factor protein-protein interactions: opportunities and obstacles. *Cell Regen (Lond)* 4, 2, doi:10.1186/s13619-015-0015-x (2015).
- 225 Seargent, J. M., Yates, E. A. & Gill, J. H. GW9662, a potent antagonist of PPARgamma, inhibits growth of breast tumour cells and promotes the anticancer effects of the PPARgamma agonist rosiglitazone, independently of PPARgamma activation. *Br J Pharmacol* 143, 933-937, doi:10.1038/sj.bjp.0705973 (2004).
- 226 Tang, J. J. *et al.* Inhibition of SREBP by a small molecule, betulin, improves hyperlipidemia and insulin resistance and reduces atherosclerotic plaques. *Cell Metab* 13, 44-56, doi:10.1016/j.cmet.2010.12.004 (2011).

APPENDICES

Supplementary table 1. PCR conditions for amplifying the tandem oligonucleotides

| Steps | Temperature (°C) | Time | |
|----------------------|------------------|-------|--------------------|
| Initial denaturation | 95 | 5 min | |
| Denaturation | 95 | 15 s | } 35 cycles |
| Annealing | 65 | 25 s | |
| Extension | 68 | 30 s | |
| Final extension | 68 | 5 min | |

Supplementary table 2. PCR conditions for amplifying the shRNA oligonucleotide

| Steps | Temperature (°C) | Time | |
|----------------------|------------------|-------|--------------------|
| Initial denaturation | 95 | 5 min | |
| Denaturation | 95 | 25 s | } 25 cycles |
| Annealing | 56 | 25 s | |
| Extension | 72 | 30 s | |
| Final extension | 72 | 5 min | |

Supplementary table 3. PCR conditions for amplifying the *KLF6* coding sequence

| Steps | Temperature (°C) | Time | |
|----------------------|------------------|-------|--------------------|
| Initial denaturation | 95 | 5 min | |
| Denaturation | 95 | 15 s | } 35 cycles |
| Annealing | 68 | 30 s | |
| Extension | 72 | 60 s | |
| Final extension | 72 | 8 min | |

Supplementary table 4. PCR conditions for generating flag-KLF6

| Steps | Temperature (°C) | Time | |
|----------------------|-------------------------|-------------|--------------------|
| Initial denaturation | 95 | 5 min | |
| Denaturation | 95 | 15 s | } 35 cycles |
| Annealing | 65 | 25 s | |
| Extension | 72 | 60 s | |
| Final extension | 72 | 10 min | |

Supplementary table 5. PCR conditions for generating flag-eGFP

| Steps | Temperature (°C) | Time | |
|----------------------|-------------------------|-------------|--------------------|
| Initial denaturation | 95 | 5 min | |
| Denaturation | 95 | 15 s | } 35 cycles |
| Annealing | 65 | 30 s | |
| Extension | 72 | 60 s | |
| Final extension | 72 | 10 min | |

Supplementary table 6. PCR conditions for TOPO-TA cloning

| Steps | Temperature (°C) | Time | |
|----------------------|-------------------------|-------------|--------------------|
| Initial denaturation | 95 | 5 min | |
| Denaturation | 95 | 15 s | } 35 cycles |
| Annealing | 56 | 15 s | |
| Extension | 72 | 30 s | |
| Final extension | 72 | 8 min | |

Supplementary table 7. Recipe for SDS-PAGE resolving gel

| Reagent | Gel percentage (%) | |
|-------------------------------|--------------------|---------|
| | 8 | 10 |
| dH ₂ O | 6.5 mL | 5.1 mL |
| 10% SDS | 320 µL | 320 µL |
| Buffer (1.5 M Tris pH 8.8) | 7.68 mL | 7.68 mL |
| 30% Acrylamide/Bis-acrylamide | 5.3 mL | 6.7 mL |
| 10% APS | 150 µL | 150 µL |
| TEMED | 15 µL | 10 µL |

Supplementary table 8. Recipe for SDS-PAGE stacking gel

| Reagent | |
|-------------------------------|---------|
| dH ₂ O | 2.87 mL |
| 10% SDS | 50 µL |
| Buffer (0.5 M Tris pH 8.8) | 1.2 mL |
| 30% Acrylamide/Bis-acrylamide | 830 µL |
| 10% APS | 100 µL |
| TEMED | 5 µL |

Supplementary table 9. Recipe for resolving gel buffer

| Reagent | |
|-------------------|--------|
| Tris | 91 g |
| SDS | 2 g |
| dH ₂ O | 500 mL |

Supplementary table 10. Recipe for stacking gel buffer

| Reagent | |
|-------------------|---------|
| Tris | 6.057 g |
| SDS | 0.4 g |
| dH ₂ O | 100 mL |

Supplementary table 11. Recipe for 10x running buffer

| Reagent | |
|-------------------|--------|
| Tris | 15.1 g |
| Glycine | 93.8 g |
| SDS | 5 g |
| dH ₂ O | 500 mL |

Supplementary table 12. Recipe for 10x transfer buffer

| Reagent | |
|-------------------|--------|
| Tris | 30.3 g |
| Glycine | 140 g |
| dH ₂ O | 1 L |

** 1 x transfer buffer: 100 mL 10x stock + 200 mL methanol + 800 mL dH₂O